THE UNIVERSITY *of* EDINBURGH

Tephrochronology, landscape and population: impacts of plague on medieval Iceland

Richard T. Streeter

Doctor of Philosophy

The University of Edinburgh

December 2011

Declaration of Originality

All the work included in this thesis is original and my own, unless otherwise stated. The research presented in this thesis has not been submitted for any other degree or professional qualification.

Signed

Abstract

This thesis examines the extent to which geomorphological change in sub-arctic landscapes may be driven by rapid declines in population over timescales of decades to centuries. Demographic decline driven by disease in pastoral agricultural systems is expected to alter patterns of land use. Using a chronology with 20 visible dated tephra layers from AD 870 to present, 2625 tephra layers were identified in 200 sediment profiles. Rates of sediment accumulation dated by tephra provide a record of erosion in Skaftártunga, South Iceland. The scale of enquiry is that of individual landholdings (5–10 km^2) over decades to centuries; in order to tackle questions of resilience and change within coupled socio-ecological systems larger and smaller spatial scales (regions of 400 km^2 and individual sediment profiles) and longer and shorter temporal scales (2.6 ka and years to decades) are also considered. The novel application of photogrammetric techniques to recording stratigraphic sections increases the frequency of measurement from tens to hundreds per stratigraphic unit and the resolution from ±2.5 mm to ±1 mm. This technique improves the accuracy of representative measures of sediment accumulation and their use in measuring landscape change. Two little known 15^{th} century AD Grímsvötn tephras are mapped and dated to AD 1432±5 and AD 1457± 5 using sediment accumulation rates. A period of landscape stability from AD 1389–1597 is consistent with reduced grazing pressure due to population declines of more than 30% after plague in AD 1402–1404 and AD 1494. Climatic deterioration from AD 1450-1500 does not increase erosion as much as expected; this may be due to decreased grazing pressure after population decline in the 15^{th} century. Increased erosion from AD 935–1262 is related to woodland clearance and increases in sediment accumulation post AD 1625 are related to climatic cooling during the Little Ice age and the migration of erosion fronts into deep lowland sediments.

Acknowledgements

Many people have helped me in the process of completing this PhD. Firstly I would like to thank the farmers at Búland and Snæblýi for their permission to dig (lots of!) holes in their fields, especially Eliń Þorgeirsdóttir and Borgor Þorsteinsson at Hrífunes farm who were always helpful, and provided accommodation either in their house or at their campsite.

This project would not have been possible without financial support from the Natural Environment Research Council, and I also benefited from the US National Science Foundation International Polar Year project. Fieldwork is not possible on your own and I'm very grateful to Will Hiscock, Martin Ball, Anna Brookfield, Dave Sinclair, Neil Thompson, Duncan MacGregor and Kirsty Maclean for putting up with rain, mud and cold in the pursuit of tephra. I've made many friends in fellow graduate students and post-docs at Edinburgh, especially those who shared the fun of demonstrating (and cooking) on the undergraduate field course in Iceland at Heimaland over 2008–2011 (Kate Briggs, Laura Comeau, Andy Casley, Andy Hein) and all those in the Lower Lewis office which has been my home over the past four years. Thankyou to Clare who manage to put up with me at every stage of the PhD, from fieldwork to the write up.

Many colleagues helped formulate my ideas, but particular mention must go to Tom McGovern, Orri Véstiensson (who provided translations of livestock census data) and Christian Keller. Colleagues at *Fornleifastofnun Íslands* (The Institute of Archaeology of Iceland) were very helpful with logistics, particularly Hildur Gestsdóttir with whom I helped with some archeology work in Skaftártunga. Thanks also goes to those in NABO and the graduate students at City University New York (CUNY). Thanks to Chris Hayward who helped with the EMPA analysis, and Anthony Newton for many ideas and help with preparing the samples. Thanks also to William Mackaness who provided helpful suggestions at the beginning of the project.

Lastly I would like to to thank my supervisor Andy Dugmore who was a constant source of ideas and inspiration. I am grateful for his tireless enthusiasm and his seemingly limitless knowledge of Iceland. It was a real privilege to work with him.

Nomenclature

Terms are used in this thesis as follows. Tephra layers are referred to by a letter denoting their volcanic origin, followed by the calendar year (AD) of the eruption; for instance H 1104 is tephra from the eruption of Hekla in AD 1104. The volcanic systems are H : Hekla, K : Katla, V : Veiðivötn, G : Grímsvötn, Ö : Öræfjajökull, E : Eldgjá, L : Laki.

The following abbreviations and terms are used in the text.

EMPA Electron microprobe analysis

Landnám The settlement of Iceland by the Norse in AD ∼870, can also refer to the Landnám tephra, which is from an eruption at approximately the same time as settlement

LIA The Little Ice Age

MWP The Medieval Warm period

rofabard An erosion escarpment, which is common in Iceland

SeAR Sediment accumulation rates

SILK Silicic Katla tephra, after Larsen *et al.,* 2001.

SST Sea surface temperatures

Tephra Volcanic ash, after Þórarinsson (1944)

Contents

List of Figures

List of Tables

Chapter 1

Introduction

1.1 Overall aim of the project

The overall aim of this project is to investigate the effects of depopulation on landscape stability in pastoral farming economies and enhance our understanding of the environmental consequences of periods of sudden population reduction after disease, famine or volcanic events. This is important because human populations have both waxed and waned through time, and we need to know what happens to the environment both when population increases (the subject of many studies), and when populations decline.

Human and environmental systems are interlinked and cannot be considered in isolation, therefore effective approaches consider coupled socio-ecological systems (Crumley, 1994). The overall approach to this research is grounded in geography, meaning the processes of the earth and human society, spatial patterns of change and the relationship between humans and their physical surroundings (Cutter *et al.*, 2002). The work is informed by resilience thinking (Gunderson & Holling, 2002; Walker *et al.*, 2004) and tephrochronology is applied to a case study. A key motivation for this research is the idea that the past is a valuable source of 'completed' experiments in how integrated human-environmental systems have responded to both natural and social changes. This deep time understanding provides essential understanding for sustainability science and responses to contemporary challenges posed by global change (Kates *et al.*, 2001; Costanza *et al.*, 2007a).

Pastoral societies are found in all regions of the world from the tropics to the arctic. The implications of declining population in pastoralist societies may differ substantially from those supported by arable agriculture because here the environmental impacts of cultivation are closely linked to continued human activities. Domestic livestock can have a continued (and even increasing)

impact without continued human involvement. As a result population decline in pastoral systems may have a range of different effects from; no change in impact to the environment to increased impact to the environment or a reduced impact on the environment. It is not immediately obvious which outcome is most likely and so that is the focus for this research.

1.2 Population decline and environmental change

Population decline and 'collapse' is usually approached from the perspective of unsustainable human exploitation of a fragile environment (e.g. Diamond, 2005), but relatively little attention has been paid to what happens to the environment when population declines independently through disease. Over the past 2000 years large areas of the world have experienced significant population decline after pandemics of bubonic plague, smallpox, measles and influenza. These large, sudden population declines are of interest because environmental responses to demographic change may be non-linear and a lower population may not necessarily mean a reduced environmental impact. Episodes of disease which reduce population create change which is effectively instantaneous over large areas when considered over century timescales, thus providing a 'natural experiment' (Diamond & Robinson, 2010) for the environmental impact of population decline.

Pandemics can have global environmental consequences. Settlement in the 15^{th} century by Europeans brought influenza, measles and smallpox to the Americas, killing ∼95% of the native population who had no natural immunity (Denevan, 1992). This reduced a pre-contact population of ∼60 million to less than 10 million (Denevan, 1992; Dull *et al.*, 2010) — the most rapid and widespread population decline in the late Holocene (Lovell, 1992). Cultivated clearings in forests were abandoned and there may have been ∼5 million km^2 of forest regeneration (Nevle & Bird, 2008). Charcoal records also show declines in biomass burning (Nevle & Bird, 2008), although this can also be explained by climatic change (Marlon *et al.*, 2008). It is debated whether the resultant afforestation and carbon sequestration contributes to a ∼5 ppm decline in global CO_2 levels observed in Antarctic ice cores from AD 1500–1750 (e.g. Ruddiman, 2003; Nevle & Bird, 2008; Dull *et al.*, 2010). The land cover change impact of post-Colombian epidemics in the Americas therefore provides a key test on the early Anthropocene hypothesis, which argues that the anthropogenic impact on the climate was significant before the Industrial revolution (Ruddiman, 2003; 2005). It is therefore important that we improve the understanding of how landscapes react to demographic collapse, and how it

appears in environmental records.

The medieval pandemic of AD 1347–1352 ('the Black Death') probably killed 30–50% of Europe's population (Platt, 1996; Benedictow, 2004) and repeated pandemics and demographic stagnation meant population levels did not recover in many areas for over 150 years (Hatcher, 1977; Wrigley & Schofield, 1981). Its impact on economic and social systems was profound, and in contrast to post-Colombian epidemics in the Americas, well documented (Platt, 1996; Bolton, 1996). Proxy records of vegetation (pollen) show increases in woodland cover and a decline in arable farming across most of Europe, with large spatial variation (Yeloff & van Geel, 2007). Estimates of forest regeneration of 25–45%, based on an inferred biospheric carbon sequestration caused by afforsetation reducing global CO_2 levels (e.g. Ruddiman 2003), would appear to be too high, as continued browsing by livestock of tree species such as *Betula spp.* limited the potential for forest re-growth (Yeloff & van Geel, 2007). Probably the biggest environmental change was caused by the switch from intensive to extensive agriculture, as shown by changing ratios of arable to pasture land (Poos, 1991).

The focus of most research into 'landscapes of depopulation' has been in tropical or temperate areas where arable farming is practised and there is extensive forest cover. This study extends the scope of this research to pastoral societies in sub-arctic areas marginal for agriculture. These are areas where the natural forest cover is low, and unlikely to respond quickly to reductions in grazing pressure. The environmental impact of population decline has been examined using palynological records (Yeloff & van Geel, 2007) and charcoal records (Nevle & Bird, 2008): a geomorphological approach provides a spatially distributed record of change and may provide new insights.

1.3 Research approach

This research is informed by hypothesis which are tested through a case study approach. The following requirement's were used to determine the appropriate case study, which had to have the following attributes:

- A written record of discrete episodes of plague
- A well understood pastoral system
- An accumulated record of change across large proportions of the landscape
- Good chronological control which is precise to years-decades and spatially ubiquitous

Based on these criteria the best place in the world to tackle this problem is Skaftártunga, south Iceland.

1.3.1 Iceland

Iceland was settled very rapidly by the Norse in AD ∼870 (Landnám). Much of its history is recorded in contemporaneous written records and there is a clearly defined pre-settlement period allowing the creation of long-term reconstructions of natural changes. The farming system during the medieval period was almost exclusively based on pastoralism, with limited arable cultivation practised in the south (mainly for beer production), and limited development of fishing until the 17^{th} century (Adalsteinsson, 1990; Karlsson, 2000). Iceland's comparative isolation means that episodes of plague only occur twice, in AD 1402–1404 and AD 1494, each killing around 30–40% of the population (Karlsson, 1996).

Iceland's location on the mid-Atlantic ridge means it is subject to frequent volcanic activity, and on average there is a volcanic eruption every 5 years (Figure 1.1, Larsen & Eiríksson, 2008b). The volcanic ash (tephra) from these eruptions can be identified, correlated and dated (Section 1.3.5), which provides excellent chronological control for episodes of landscape change (Dugmore *et al.*, 2009).

Iceland's landscape has been extensively modified by human activity since settlement in AD ∼870. Of significant environmental impact has been the introduction of grazing livestock who have created extensive areas of soil erosion. Total vegetation cover has been estimated to decline from 54% (Ólafsdóttir *et al.*, 2001) prior to Landnám to the current 28% (LMI, 1993). The main driver of erosion in this period is probably grazing by sheep and goats (and to a lesser extent pigs, cattle and horses) compounded by climate deterioration. Changes, either in the intensity of grazing or its spatial patterns, may be inferred from patterns of sediment accumulation (e.g. Dugmore & Buckland 1991; Simpson *et al.* 2001; 2004; Dugmore *et al.* 2009). These records of sediment accumulation are sensitive to changes over both local (<250 m) and regional (> 1 km) scales, so can be used to reconstruct spatial patterns of landscape change (Dugmore & Erskine, 1994). Iceland could therefore be considered a 'model system' (*sensu* Kirch 2007) for analysing the environmental impact of depopulation on a pastoral agricultural system.

1.3.2 The past as a 'natural experiment'

In effect, environmental records provide the results of past 'experiments' on natural systems (Diamond & Robinson, 2010). Plague can be considered an

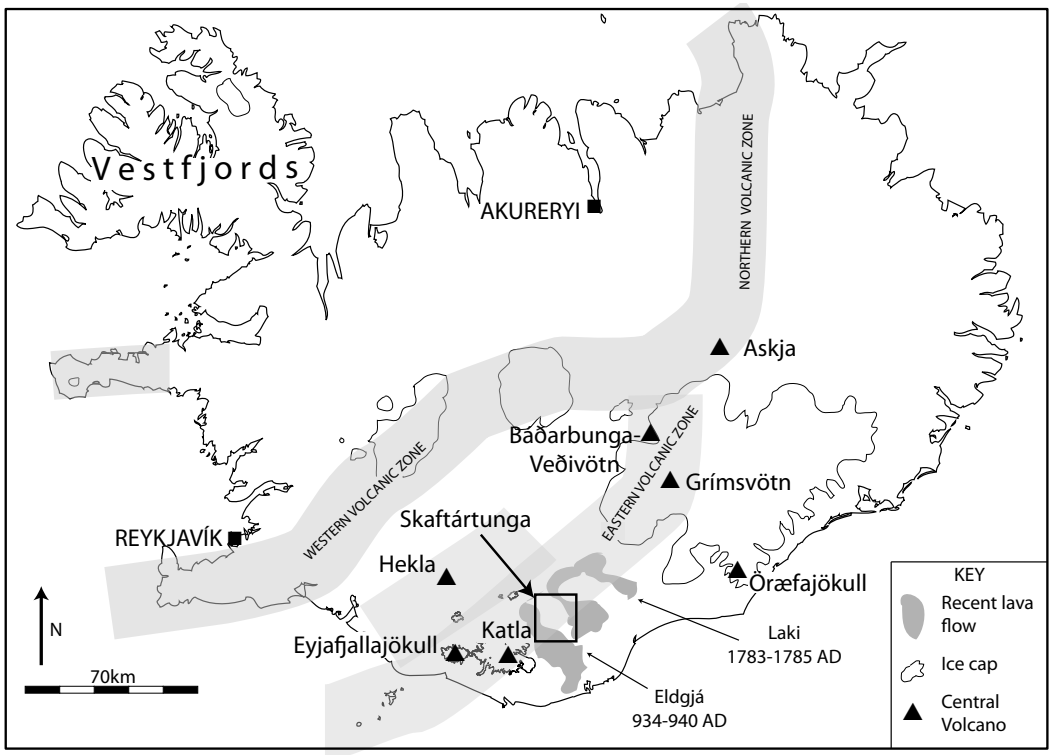

Figure 1.1: Map of Iceland indicating the main volcanic zones and the most active central volcanoes. Eruptions from these frequently deposit tephra across the landscape. Volcanic zones from Larsen & Eiríksson, 2008b.

homogeneous perturbation as its impact on human populations is similar across societies, therefore differences in its impact are due to differences in the environments and societies it affects. In order to be able to use these 'completed' experiments, paleo-environmental records are needed. In order for paleo-environmental records to provide context to current global change and provide insights into coupled socio-natural systems, they need to be of high resolution, be able to provide socially relevant proxies and the records need to be integrated with archaeological and historical records (Oldfield & Alverson, 2003; Caseldine & Turney, 2010).

Deterministic approaches can be used to simplistically correlate past social change with past environmental change (e.g. Patterson *et al.*, 2010), however better insights come from considering human societies as responding in complex and unpredictable ways to environmental change, and as part of integrated socio-ecological systems (Crumley, 1994; Coombes & Barber, 2005; O'Sullivan, 2008; Caseldine & Turney, 2010). This is the basis for the evolving human-ecodynamic interdisciplinary approach which is used in this study (Costanza *et al.*, 2007b).

1.3.3 Scale of research

The focus of this research covers multiple spatial and temporal scales. The main scale is change over decades to centuries following episodes of population decline in AD 1402 and AD 1494, and over a spatial scale of 5–10 km^2, approximately the size of individual landholdings (Figure 1.2). However in order to provide context, larger and smaller temporal and spatial scales are also investigated (Figure 1.2). At it widest scope this study investigates changes in sediment flux over the past 2.6 ka over an area of ∼400 km^2, and at its smallest scope; yearly changes in sediment accumulation over individual slopes and erosion features (areas of ∼0.2 km^2, based on local sediment sources originating from within a 250 m radius from a stratigraphic section, Dugmore & Erskine 1994).

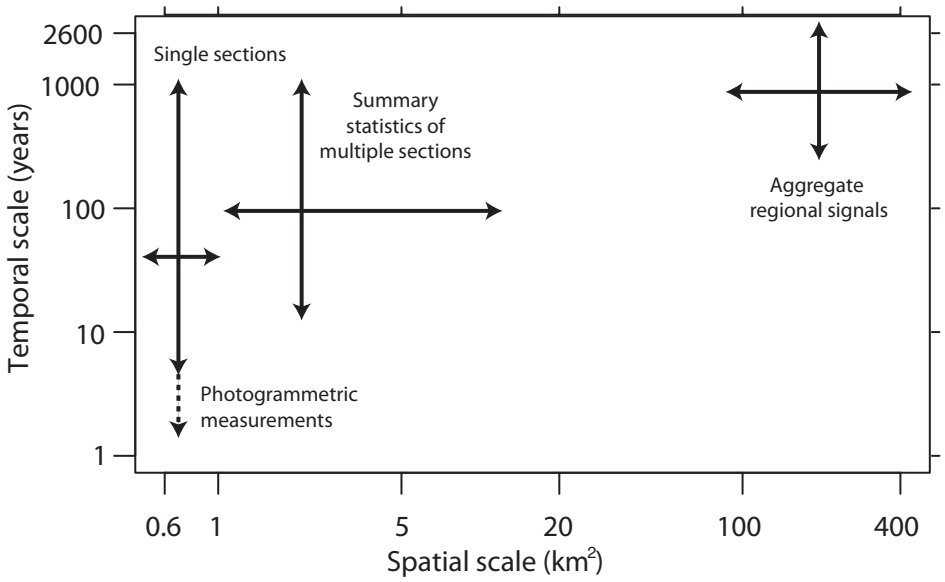

Figure 1.2: Multiple scales of research underpin this study. The main focus is on temporal scales of decades-centuries and spatial scale of landholdings (5–10 km^2), but scales larger and smaller spatial and temporal scales are also considered.

1.3.4 The geomorphic record

The geomorphic record available in Skaftártunga allows for the investigation of this case study because:

- there are high rates of sediment accumulation, in the order of 0.3–0.5 mm yr^{-1} in south Iceland. This means relatively small changes in sediment accumulation are easily measured.

- Soil erosion proceeds through loss of area which means that the record is spatially heterogenous and there is a mosaic of both eroding spots where the record is lost located near areas where a record of erosion is created through sediment accumulation.

- Within soil sections two components can be distinguished, aeolian (from the wider area) and non-aeolian sediments (principally derived from upslope of the profile).

1.3.5 Tephrochronology

Tephrochronology is the use of layers of volcanic ash (tephra) as age-equivalent marker horizons, and was pioneered in Iceland by Sigurður Þórarinsson (1944, 1958, 1967). It has worldwide application in dating palaeo-environmental records (Lowe, 2011). Tephra layers can be identified by both their macro scale features and their geochemical composition, which allows them to be correlated in both terrestrial and marine sediments, lakes and ice cores.

A key advantage of tephrochronology is the correlation of layers with historic volcanic events, which allows precise (to the year, month or day) dating control. Older tephra may be aged through radiocarbon dating of associated organic material (Dugmore *et al.*, 1995a; Larsen *et al.*, 1999; Church *et al.*, 2007), the constriction of age-depth models in sediment sequences (Óladóttir *et al.*, 2005) and by correlation to ice core records (Gronvöld *et al.*, 1995; Vinther *et al.*, 2006). Where background sediment accumulation rates are high, multiple tephra that are chronologically close may be preserved in sediments. This spatial and precise record allows for a wide range of applications to problems in geology, geomorphology, archaeology and palaeo-enviromental research in general.

The correlation of multiple tephra across a landscape can be used to reconstruct spatial patterns of environmental change. In Iceland this has been applied to reconstructions of glacial extent (Dugmore, 1987; Casely & Dugmore, 2004; Bradwell *et al.*, 2006; Kirkbride & Dugmore, 2006; 2008), the impact of jökulhlaups (Smith & Dugmore, 2006; Dugmore *et al.*, 2000) and the investigation of landscape change since Landnám (Dugmore & Buckland, 1991; Dugmore & Erskine, 1994; Dugmore *et al.*, 2009). Tephra has also been used in Iceland to date pollen cores (Lawson *et al.*, 2007; Erlendsson *et al.*, 2009) and archaeological sites (McGovern *et al.*, 2007). It offers both the chronological precision and the ability to define spatial patterns of change that are required to address questions of resilience in human-environment systems. Rates of sediment accumulation have been related to rates of erosion (Thórarinsson,

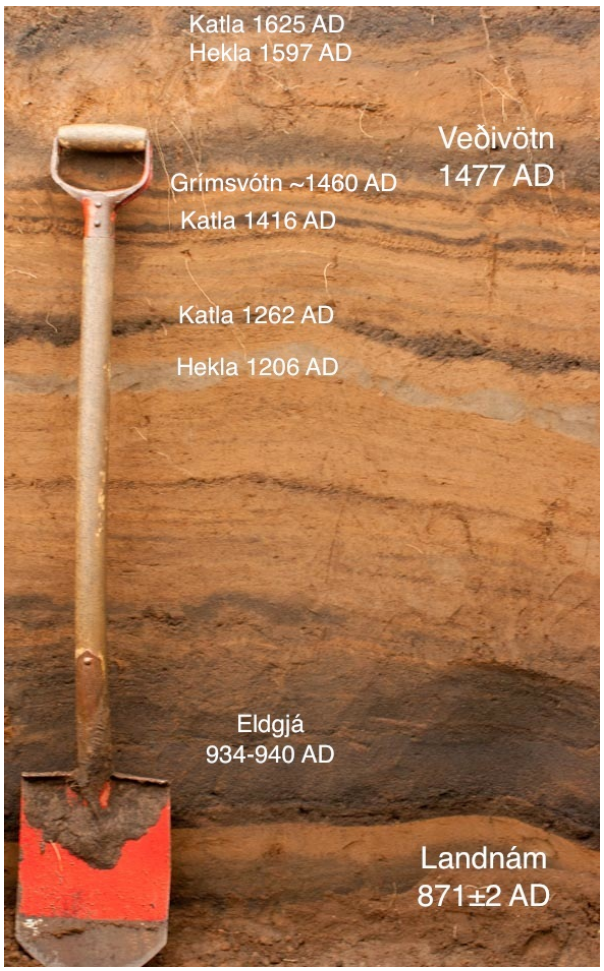

Figure 1.3: Stratigraphic section illustrating tephra layers in an aeolian sediment sequence. Tephra layers vary in colour and texture, allowing field identification. Correlation with historical records of eruptions allows for precise dating. Information about past environmental change is contained both in the sediment between tephra and in the morphology of the tephra itself (Dugmore & Buckland, 1991; Dugmore *et al.*, 2009).

1961; Dugmore & Buckland, 1991; Dugmore *et al.*, 2009). This makes it possible to see trends in landscape change through time, at a greater resolution than where sediments need to be radiocarbon dated. Once a chronology is well known tephras can be field identified which means that dating of sections can be more accurate, faster and cheaper than radiocarbon dating of sediments. As many records can be collected, detailed spatial patterns of change to be examined.

Skaftártunga's (Figure 1.1) proximity to Iceland's four most active volcanic systems, Grimsvötn, Katla, Hekla, and Veiðivötn-Bárðarbunga, (Larsen & Eiríksson, 2008b), means that 20 post-Landnám tephras occur in sediments here (Larsen, 2000; Óladóttir *et al.*, 2005). High background sediment accumulation rates (on average 0.55 mm yr^{-1} post-Landnám) ensure that tephras can be

readily distinguished within the stratigraphy. These tephras provide a high resolution of chronological control, as of the 20 tephra layers observed in the stratigraphy over the past 1200 years 15 are dated to the year (Thórarinsson, 1958; 1967; 1975; Einarsson *et al.*, 1980; Larsen, 1984; 2000).

1.3.6 Improved measurement of sedimentary sequences

In order to enhance current methodologies for recording and understanding past landscape change in Iceland higher resolution records of thickness are required. Current measurements of thickness in sedimentary sequences are based on single or fewer than ten manual measurements, which may have a precision of ±1 mm (e.g. Óladóttir *et al.* 2011b), however mm-cm scale variations in the thickness of both tephra and aeolian sediment means that the accuracy of mean measures of thickness based on small numbers of measurements is probably lower, around ±2.5 mm. This has been sufficient for tackling fundamental issues of tephrochronology such as the source of a tephra, its dispersal patterns, volume estimates and its visible extent. Within sequences where the chronology is already established however higher resolutions may be able to resolve more detailed changes over smaller spatial and temporal scales. The use of photogrammetric techniques to measure 3-D surfaces in geomorphology (Chandler, 1999), and the improved accuracy of commercially available cameras (Chandler *et al.*, 2005; Wackrow *et al.*, 2007; Rieke-Zapp *et al.*, 2009) means that photogrammetric measurement techniques can be considered for field measurements of tephra stratigraphies.

This thesis applies photogrammetric techniques to the problem of recording large numbers of measurements within a stratigraphic section. The novel application of this technique to the field recording of stratigraphic sections increases not only the precision of measurements to ±1 mm, but also increases the number of measurements possible, which improves estimates of mean sediment and tephra depth. This increases the utility of tephrochronology as a dating tool to to tackle wider questions (e.g. McGovern *et al.* 2007).

1.4 Key questions to be addressed

This thesis assess the geomorphic impact of 15^{th} century plagues in Iceland. Two overall research objectives drive the research:

(a) to enhance methodologies for assessing the rates of landscape change at annual to decadal resolutions over century timescales using tephrochronology

(b) to assess landscape change in Skaftártunga, south Iceland, over two periods of population contraction in the 15^{th} century in the context of landscape change through the settlement period (after AD 870) and the late Holocene (2.6 ka).

In order to achieve the research objective (b) the following questions and associated hypotheses are tested.

(1) What are the geomorphic consequences of population decline in pastoral farming systems? Four hypothesis are proposed:

   (i) There is a decline in landscape impact *because reductions in population are related to commensurate reductions in livestock*

   (ii) There is no change in landscape impact *because livestock are not directly affected by plague grazing continues as before*

   (iii) There is an increase in landscape impact *because reduced labour means less fodder collection and more winter grazing; or there is a switch from more labour demanding livestock (cows) to less labour demanding but more environmentally damaging livestock (sheep/goats); or there are feral sheep which graze unmanaged.*

   (iv) There is a change in spatial patterns of landscape impact *(i.e. a combination of the above)*

(2) Do plague driven modifications of geomorphology have subsequent effects on landscape resilience in the face of climate change? The hypothesis are:

   (i) It does not change resilience

   (ii) It changes resilience, by either:

      (a) Increasing landscape resilience to climatic change

      (b) Decreasing landscape resilience to climate change

(3) At what scales are patterns of landscape change related to population decline visible? Three hypothesis are tested:

   (i) visible only at the scale of the region ($\sim$400 km^2)

   (ii) visible only at the scale of landholdings (5–10 km^2)

   (iii) visible only at the scale of slopes ($<$ 1km^2)

1.5 Outline of thesis

This chapter has provided a broad overview of the topic, and introduced key terms and concepts. The rest of the thesis is organised along the following structure.

Chapter 2 expands on the theoretical framework on which this study is based, examing Malthusianism, methodological problems in linking change in environmental records to changes in human societies, and the concepts of thresholds and resilience.

Chapter 3 provides background context to plague driven population change in Europe and Iceland, summarises relevant aspects of climate change in the North Atlantic for the period AD 500–2000 and gives an overview of existing models and physical processes of land degradation.

Chapter 4 summarises the methodologies used to gather environmental data. These are: field mapping of tephra, geochemical analysis of tephra samples and the procedures used to measure sedimentary sequences. It presents a new photogrammetric method for recording soil sections to ± 1 mm precision.

Chapter 5 presents the data. Firstly an improved tephrochronology for Skaftártunga. The chronology includes mapping, geochemical analysis and age estimates based on sediment accumulation rates for two Grímsvötn tephras in the 15^{th} century. This is followed by identifying key geomorphological features, summarising profiles and the presentation of 200 stratigraphic sections with 2625 identified tephra.

Chapter 6 uses measured rates of sediment accumulation to synthesise existing models of landscape change over the settlement period and adds a new model based on the impact of the plague in the 15^{th} century, in the context of rapid climatic decline. It then assesses landscape change over the 15^{th} century at multiple scales.

Chapter 7 provides an overall synthesis and conclusions, and recommendations for further work.

Chapter 2

Theory

2.1 Introduction

This chapter examines existing approaches to the environmental effects of population change and the concepts of thresholds and resilience. In order to evaluate the impact of human actions on the environment there are methodological issues in linking short duration events in human populations to paelao-environmental records which do not directly record the event. In addition this chapter examines the geomorphological concepts relevant to natural systems, and how systems may exhibit a range of different responses to change.

2.2 Population and the environment

This section describes applications of Malthusian ideas to pre-industrial societies, criticisms of Malthusian approaches, and considers how Malthusian ideas contribute to understanding environmental change as a result of externally driven population declines.

2.2.1 Malthusian Approaches

A theory of how demographic increase is limited by environmental constraints was proposed by Thomas Malthus (1766–1834) in his AD 1798 essay 'An Essay on the Principle of population'. Geometric increases in resources are unable to match exponential growth rates in population — therefore as population increases it will outstrip available resources. Famine, warfare and disease then reduce population until it is within its resource limits. A population can therefore be considered to be 'Malthusian' if its growth is density-dependant (Lee, 1987). Malthusian ideas have been used in the study of pre-industrial societies, for instance in the case of Easter Island (Brander & Taylor, 1998).

An application of the Malthusian population model to pre-industrial societies is described in Wood (1998), Figure 2.1. The concept of demographic saturation replaces carrying capacity, and is a function of the available resources, level of technology and the organisation of production (Wood, 1998). Pre-industrial societies reach equilibrium on "the edge of misery", where population is the maximum resources can sustain unless there are social or economic checks on population (Wood, 1998). Coombes and Barber (2005) apply this model to the retreat of societies at the margins; declines in resource availability driven by environmental change result in reduced levels of buffering, increasing vulnerability. Based on Wood's (1998) model three possible responses to externally forced population decline can be hypothesised (Figure 2.1). Firstly a population may move away from demographic saturation and increase its surplus and buffering against environmental change. Alternatively population decline may decrease surpluses and increase vulnerability to environmental change, because a population moves further away from its optimum level. Finally population may decline below a minimum population threshold for that particular system of production and may either 'collapse' or be forced to change its system of production (Figure 2.1, part c).

Empirical studies of population in Iceland have found that marriage rules kept population levels lower than could have been supported in most years, creating a buffer against poor harvests (Vasey, 1996). The implication of this is that scenario two or three (Figure 2.1) may be more realistic than scenario one. Less productive but less labour intensive production methods in Iceland could involve a greater use of wild food resources, increased sheep grazing relative to cattle and increased winter grazing rather than fodder production. These changes in land use may produce a different landscape impact.

2.2.2 Modifications and alternatives to Malthusianism

Malthusian type approaches to population have been critiqued in two basic ways. A formal theory of population and resource use represents an idealised system and ignores institutional, economic or social pressures. This limits the applicability of any sort of partially deterministic model for those who argue that the political-economic system is integral to a society (Cowgill, 1998). However, with modifications Malthusian ideas are still useful.

A key modification of Malthusian concepts is the idea that innovation, system reorganisation and technological progress — leading to the increase of total system output — may be triggered by environmental stresses, avoiding the regulation of population by famine (Boeserup, 1965). Empirical data and

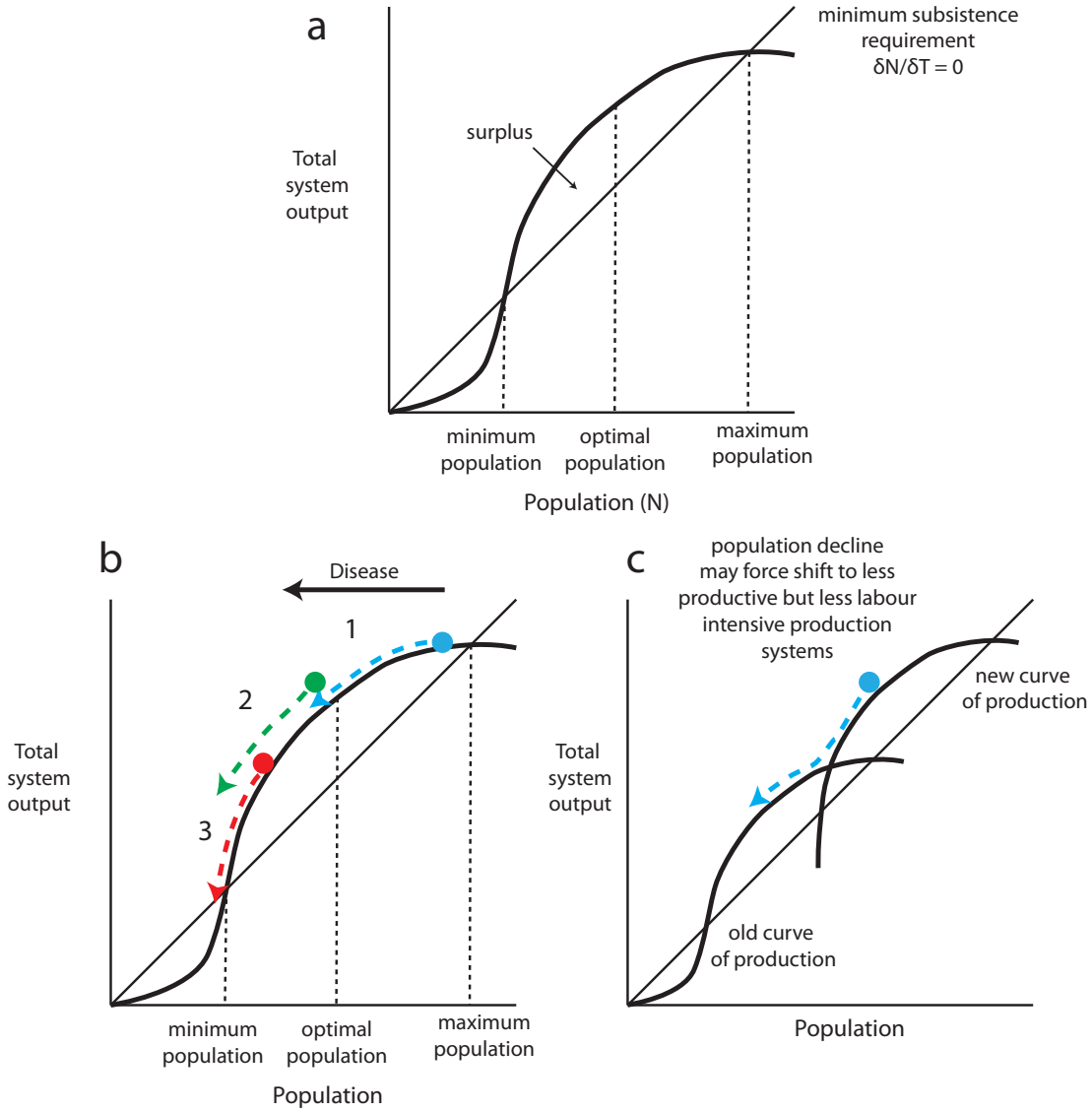

Figure 2.1: A Malthusian model of pre-industrial population, diagrams redrawn from Wood (1998). (a) shows a hypothetical system where the curve of production (thick line) goes above the linear minimum subsistence requirements. Areas where the curve is above the line (i.e. system output is above the minimum required) is the total range of possible populations. (b) illustrates three possible scenarios for the impact of exogenous population decline on total system output and increase in surplus and therefore buffering, which would correspond to either a overall decline in environmental impact (1) or force a reorganisation of the system because it has crossed a threshold (3), or at least reduce surplus and consequentially system buffering (2). (c) shows a more realistic model with multiple curves of production, and hypothesis a switch to a lower output but less labour intensive system.

models of changing land use appear to support this view even in pre-Industrial societies, with a much greater per-capita land use in Europe in the early historical era than in the later, pre-industrial era (Kaplan *et al.*, 2009). A greater per-capita impact in earlier human societies has implications for interpreting environmental records, particularly in relation to pre-historic land cover changes (Ruddiman & Ellis, 2009). For instance, in Europe modelled woodland cover declines more rapidly from AD 0–1350, after this period it declines at a slower rate despite an increasing rate of population increase (Figure 2.2, Kaplan *et al.*, 2009). Models based on declining per-capita forest clearance are a better fit to empirical records of forest cover than models based on constant per-capita woodland clearance (Kaplan *et al.*, 2009).

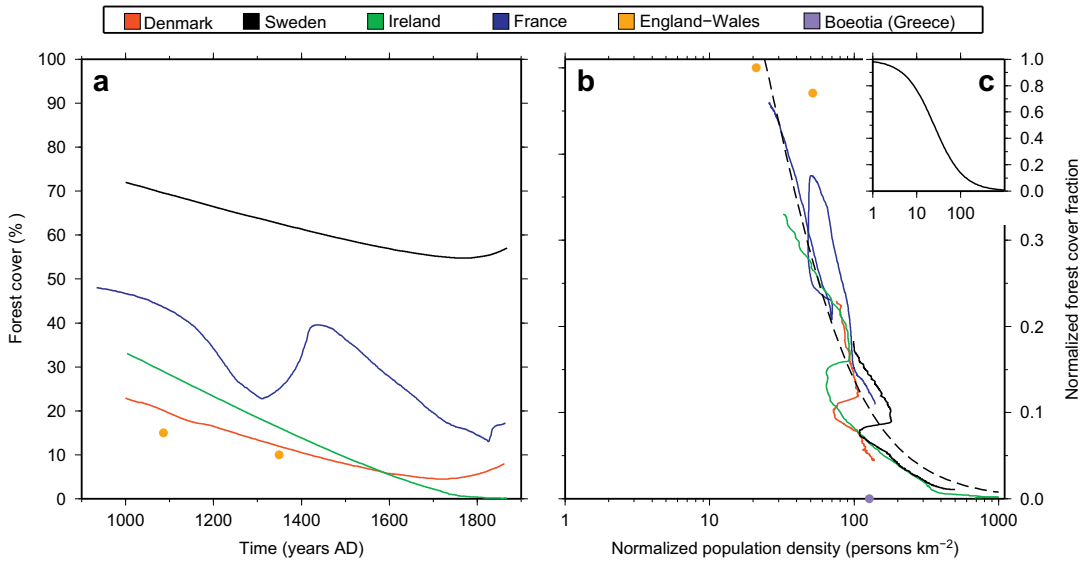

Figure 2.2: The relationship between forest cover and population, after Kaplan *et al.* (2009). (a) shows historical data from 6 areas, while (b) shows the data in (a) plotted against normalized population density (persons per km^2 of cultivatable land) versus normalized forest cover fraction. There is a declining per capita impact in terms of forest area cleared through time.

This argument can be taken further and population can be seen as a 'limitless resource' and not a cost on the environment (Simon, 1996). This 'cornucopian' view of the natural resources is driven by the idea that increasing human ingenuity will always outpace drawdown of resources. This viewpoint is mostly used in reference to modern capitalist societies — however it can provide an alternative viewpoint to the consequences of depopulation in pre-capitalist societies.

The relationship between environmental impact and population is therefore not straightforward. The application of Malthusianism to understanding past

environmental change depends on knowing the per capita impact of any given population — which reflects both the social organisation of the society and the available technology, therefore the per-capita impact can change rapidly. It is apparent that a declining population does not inevitably lead to a reduced environmental impact and that less labour intensive subsistence approaches may be more damaging to the environment. In Iceland winter grazing is used as a substitute for fodder when there is not enough labour capacity available to collect sufficient fodder to last the winter (Adalsteinsson, 1990; Simpson *et al.*, 2004), and could be one way in which a declining or smaller total population would have a larger per-capita impact. In addition population decline may not be evenly spread and key actors and skills may be lost producing a disruption out of proportion to the pro-rata decline.

2.3 Linking historical and environmental records

Linking a visible environmental change in a proxy record to short-lived, infrequent events such as disease, that leave no direct signal in environmental records requires that three conditions are met. Firstly is theory: there needs to be a plausible mechanism for environmental change to be related to the change being tested. Secondly the temporal resolution of the environmental record needs to be such that we can be sure that changes observed are truly synchronous with the event. Lastly the spatial scale of the record must match the scale of the change observed, and should ideally be able to spot local trends and regional shifts. However even when all these conditions causality cannot be implied. Detecting partial declines in settlement is particularly hard because rarely will anthropogenic pressures on the landscape be removed entirely, this is likely to be especially true in pastoralist systems, where much lower populations are likely to be able to sustain higher livestock numbers than are needed for direct subsistence (Coombes & Barber, 2005).

2.3.1 System complexity

There are two characteristics of large, complex societies which means they are not considered for this study. Firstly, for any signal in environmental records, larger societies will have a greater frequency of possible perturbations which could generate that signal. At the levels of chronological resolution available it may not be possible to discriminate between multiple possible causes. A second, more fundamental epistemological problem is that complex systems are more likely to respond in a non-linear way to minor perturbations (Coombes &

Barber, 2005). Major changes (such as 'collapse' or migration) seen in societies may be driven by perturbations which leave a signal in environmental records, such as climatic change. Alternatively they may have a political or social cause, which would not necessarily leave a record. Therefore it is hard to ascertain to what extent large scale changes visible in past societies may in fact be independent of contemporaneous changes in external variables.

Many studies have correlated social change with climatic change (Weiss *et al.*, 1993; deMenocal, 2001; Patterson *et al.*, 2010), and this is perhaps because, especially in the case of large successful societies such as the Akkadian empire, collapse is considered hard to explain by cultural means (Coombes & Barber, 2005). However, complex systems, both natural and social, can exhibit properties of 'self-organised criticality' (Brunk, 2002). In systems that have the properties of 'self-organised criticality' change can be non-linear, and without a detailed knowledge of the internal dynamics external change appears random. If, as some have argued, human societies can be considered systems that display signs of self-organised criticality (Brunk, 2002), then it becomes extremely difficult to predict how societies will react to environmental, social or economic change (Coombes & Barber, 2005).

2.3.2 Chronological resolution

Many palaeo-environmental datasets offer great potential in answering questions about how interlinked human-environmental systems respond to change over long timescales, and the temptation is to correlate them with human records of change. This may not be appropriate if the resolution of the environmental record is not the same as the resolution of change observed in human societies. Ultimately the chronological resolution control determines what sort of questions can be answered using palaeo-environmental records (Blaauw, 2011).

Uncertainty in the dating of environmental records may lead to two phenomenomena - the 'sucking in' and the 'smearing' of events (Baillie, 1991; Blaauw, 2011, Figure 2.3). Events that may in reality be asynchronous appear to be correlated. Blaauw (2010; 2011) argues that even when events have been dated as being asynchronous the temptation is still there to invoke 'lags' and 'leads' without questioning whether in fact the records are correlated at all.

2.3.3 Spatial Resolution

Although disease is able to affect populations nearly simultaneously over large areas, the impact of disease is likely to be spatially differentiated. This is a problem because while in aggregate the overall picture may be appear to be of

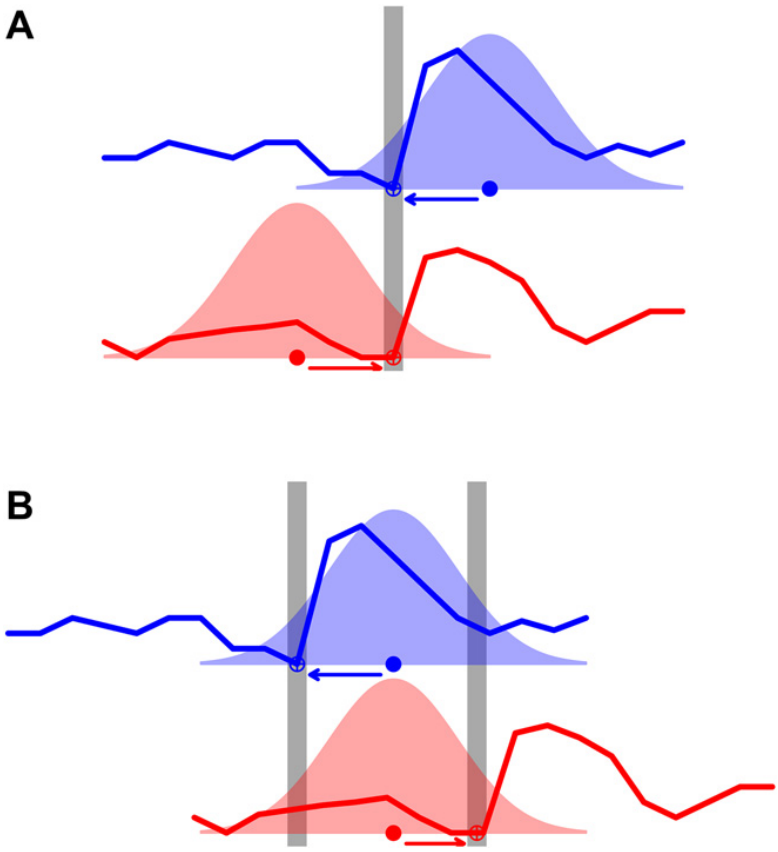

Fig. 3. Schematic of "sucking in" (A) and "smearing" (B) of proxy events (open circles with crosses on grey bars) owing to chronological uncertainties (bell-shaped distributions). In panel A, the proxy events in two time series are separate in time (filled dots). However, chronological uncertainties allow for some flexibility in the assigned timing of the events (arrows), in this case sucking the separate events into an illusionary single synchronous event (grey bar). In panel B, the two proxy series in reality reacted synchronously to a single event (filled dots), but chronological errors caused imperfect dating of the proxy changes, smearing out the single event into two separate events (grey bars). Time on arbitrary horizontal axis.

Figure 2.3: How short term events may become 'sucked in' and 'smeared' with poor chronological control, after Blaauw, in press

no change, particular locations may experience a great deal of change. Population decline as a result of plague in medieval Sweden resulted in a heterogenous pattern of abandonment, with high levels of abandonment in marginal areas (70%) but only low levels (∼10%) in productive areas (Lagerås, 2007). Therefore while regional pollen chronologies from large lakes show a pattern of no or little change a combination of local pollen diagrams show a clear signal of agricultural abandonment (Lagerås, 2007).

2.4 Thresholds and critical transitions

Systems — either natural systems, or coupled social-ecologial systems (SES) —may exhibit several possible responses to an external perturbation (Figure 2.4). There may be a short, ramped disturbance, before returning to previous levels (Figure 2.4, a). Alternatively a perturbation may cause a threshold change within a system, and the change in response to the perturbation is non-linear (Figure 2.4, b) . Threshold change may be non-catastrophic (reversible) or catastrophic (non-reversible). Systems have been observed to undergo catastrophic threshold changes in a wide range of natural and social systems, and they can also be referred to as a critical transitions (Scheffer *et al.*, 2009), Figure 2.4. Threshold crossing may be triggered by changes in both external or internal variables. The concept of threshold change has been applied to explain a range of transitions observable in geomorphic systems (Brunsden & Thornes, 1979; Schumm, 1979; Phillips, 2003).

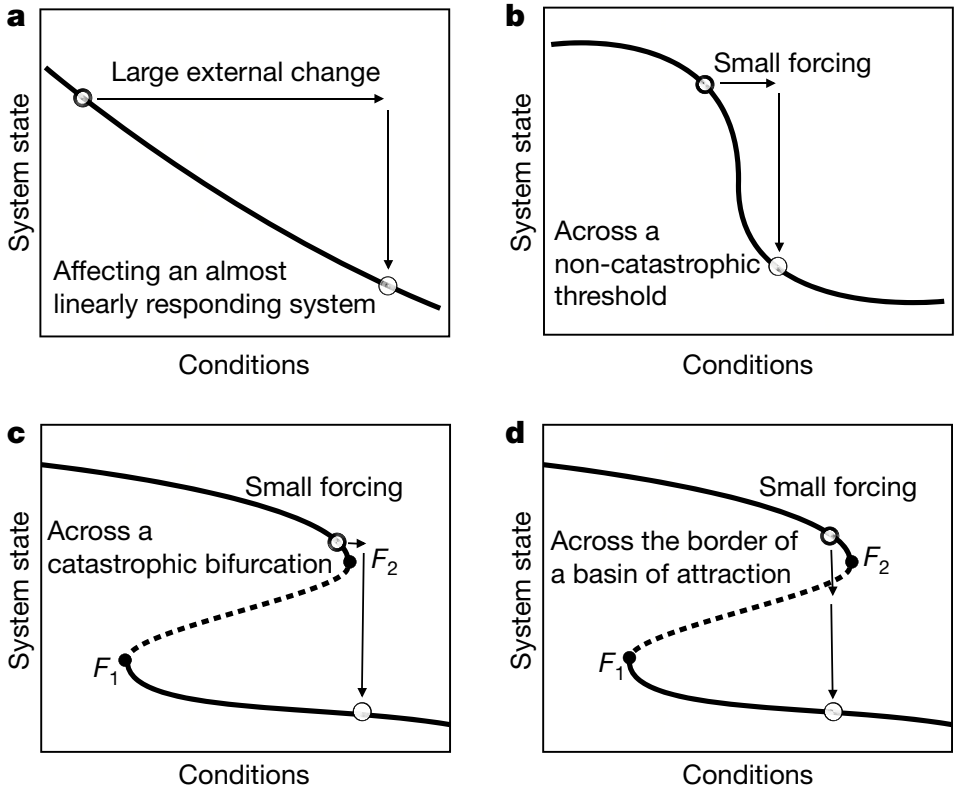

Figure 2.4: After Scheffer *et al.*, 2009. The state of a system may respond in four basic ways to a forcing, the bold line indicates a systems potential 'equilibrium curve'. In (a) the system responds linearly, in (b) it is a non-linear change but reversible. In (c) and (d) the 'equilibrium curve' is folded backwards, so when a system had moved to the lower state change is not reversible.

In addition to aspatial models of system change, the threshold concept can

also be applied spatially (Figure 2.5). Initial linear responses to increasing aridity end when the spatial geometry of patches of vegetation reaches a critical threshold and vegetation suddenly disappears completely, and cannot return (Scheffer *et al.*, 2009). This concept may be applied to landscape change in Iceland because erosion has a strong spatial pattern, with a patchwork of fully vegetated areas and barren areas. Erosion may respond linearly to climatic or grazing changes, until the ratio of eroding slope to area reaches a threshold, and erosion may rapidly increase, and the soil cover rapidly disappears (Figure 2.5). The likelihood of a threshold being crossed depends not only on the magnitude of perturbation and spatial patterns but also on the resilience of a system.

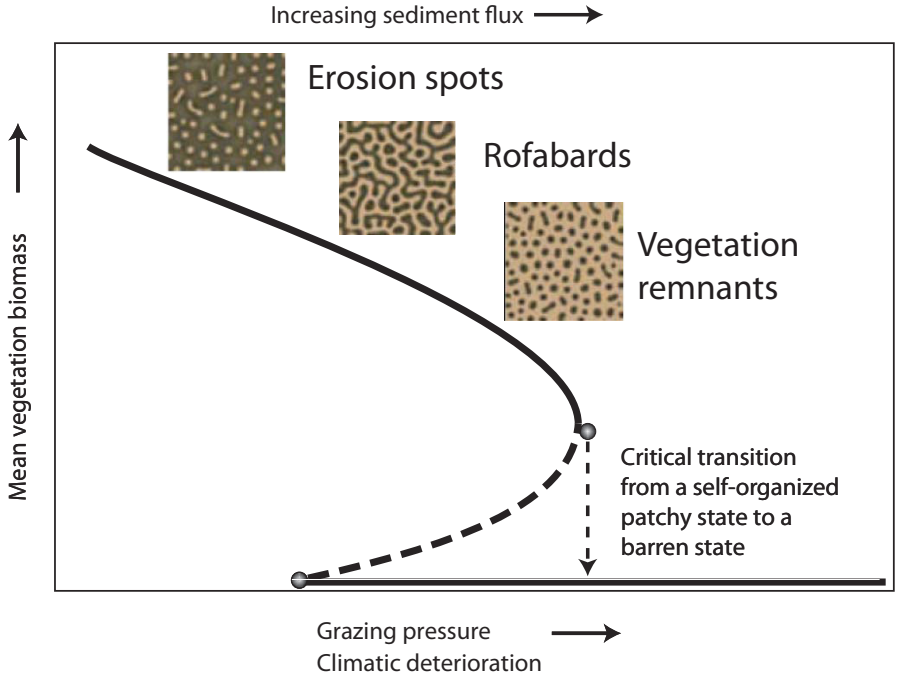

Figure 2.5: Modelling of vegetation transitions in a progressively drier climate show a linear response until the spatial pattern reaches a threshold and there is a sudden system change to no vegetation, from which it is hard to recover. Black line is equilibrium biomass densities. Modifications show how this model could apply to soil erosion in south Iceland, where there is a strong spatial pattern to erosion. Modified from Scheffer *et al.,* 2009.

2.4.1 Resilience

Resilience is a term which has proved difficult to define (Walker *et al.*, 2004). Central to the concept is the idea that systems may have multiple, alternative stable states or domains, within which systems show small variations but remain

essentially the same. Resilience therefore describes how difficult the transition between alternative multiple stable states is. More resilient systems tend to be:

(a) more adaptable to change (i.e. able to absorb larger perturbations without moving to a different stable state)

(b) not close to a threshold

(c) resistant to change (i.e. it takes a larger perturbation to cause change)

(Walker *et al.*, 2004).

The relevance of the concept is that it can be used to understand why some systems may undergo radical change in response to a perturbation, yet the same system at a different time may show no response to a perturbation of similar size. The differences in response are related to the different resilience of the system at different times, even if the system may not have appeared to have changed. The concept has been applied in studies of natural systems, human societies and coupled socio-ecological systems (Gunderson & Holling, 2002).

Studies of a wide range of natural systems have found empirical evidence of signals indicating that a system is close to a threshold change to an alternative stable state (Scheffer *et al.*, 2009). These signals appear to be a result of phenomenon called 'critical slowing down', which means that the system becomes increasingly slow at responding to perturbations. One of the effects of this is increased variability within the system, which indicates that the effect of perturbations persists and potentially begins to accumulate (Figure 2.6). Systems close to thresholds will have low resilience and are vulnerable to small perturbations causing a change in state.

Pre-cursers of impending threshold crossing could potentially be identified in geomorphological signals of landscape change in Iceland. Increased spatial variability in sediment accumulation rates or tephra thickness may indicate a slower response time to small perturbations (for instance small breaches in vegetation take longer to heal). Tephra fall is a perturbation to the landscape, so the length of time it takes tephra to stabilise on a surface may indicate overall (landscape) system resilience, with larger larger variations in the thickness of a tephra over small areas indicating a landscape close to a critical transition.

2.5 Key Points

- Deterministic and Malthusian approaches to human-environment interactions see population as having a direct and linear impact on the environment, however populations tend to have changing per-capita

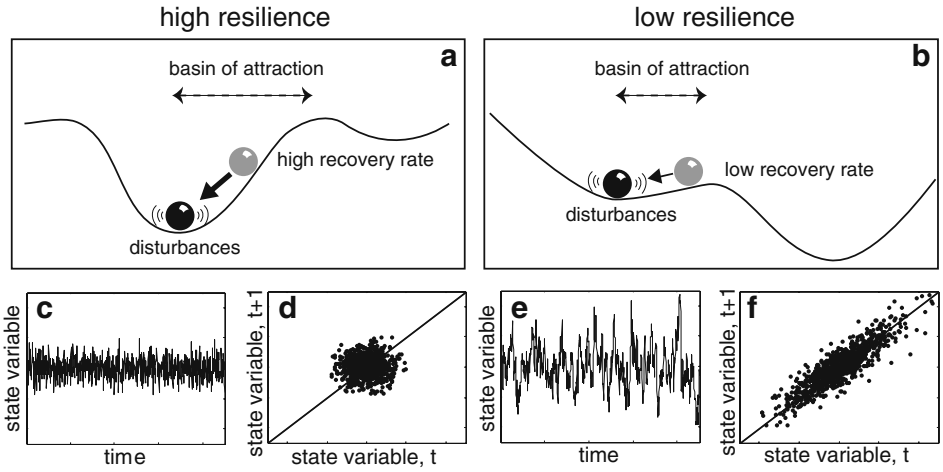

Figure 2.6: Tipping points and leading indicators. Systems which are not close to thresholds (a) respond quickly to perturbations, compared to systems with low resilience (b) which show greater variability as the system is slow to respond to perturbations. After Dakos *et al.* (2010).

impacts, and reductions in population may not reduce environmental impact.

- In order to link historical events and environmental records appropriate chronological control and spatial resolution is key, otherwise little can be said about how a particular event impacts on the environmental record
- Geomorphological approaches, especially tephrochronology can be used to define spatial patterns of change through time and provide appropriate environmental records for investigating change in pastoral agricultural societies.
- The concepts of landscape sensitivity, resilience, threshold crossing are central to understanding change. Systems close to to critical transitions or threshold change (i.e. systems with low resilience) can be identified by a range of signals, the most robust of which are a increased response time to perturbations and therefore increased variability in a system.
- Testable ideas and putative mechanisms of how different elements of social-ecological systems may be related provide an essential theoretical framework.

Chapter 3

Context: Population and Environment

3.1 Introduction

This chapter provides wider context and chronology to the plagues in Europe and Iceland during AD 1300-1500 and their social, economic and environmental effects. It also introduces the region of Skaftártunga, south Iceland, as the case study, providing background on the physical environment, land degradation, climate, land use and history over the past 1500 years.

3.2 The 'Black Death'

The plagues between AD 1350-1600 were the most significant population reductions experienced in Europe since the Justinian plagues of AD 541–542, 810 years previously (Hays, 2005). Population declined simultaneously across a large area, with a range of environments and agricultural practices. The plagues can be considered a natural experiment (*sensu* Diamond & Robinson, 2010) on the environmental consequences of declining population. Good written records survive from England and continental Europe which detail demographic, economic and land use changes, allowing comparisons with changes seen in the environmental record.

Whilst we know something of the environmental impact of plague in mixed arable and pastoral farming systems (van Hoof *et al.*, 2006; Lagerås, 2007), its impact on predominately pastoralist landscapes is less clear. Pastoralist areas on the northern margins of agriculture include areas of northern England, Scotland, Norway, Sweden and Iceland, and these are all areas that the plague reached at least twice (Danielsen, 1995; Karlsson, 1996; Herlihy, 1997). These

are areas where late medieval settlement and environmental change is associated with the climatic deterioration of the Little Ice Age (LIA) from AD 1300 (e.g. Parry, 1981), but to fully evaluate the impact of the LIA it is important to identify the probable effects of the plague years. To complicate matters further these areas were also affected by frequent livestock epidemics, such as cattle murrains [1] and sheep liver fluke (Spinage, 2003). Therefore while the Black Death is a significant event which could be expected to be visible in environmental records, it must be considered in the context of other events which could also be visible (Figure 3.1).

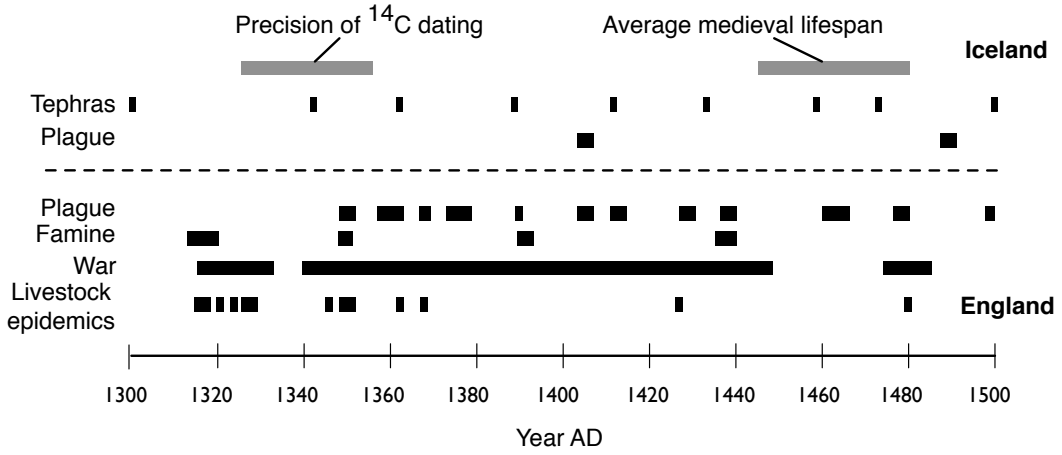

Figure 3.1: Summary diagram of relevant social and demographic events in Iceland and England, with indicators of dating precision of radiocarbon and tephras available for environmental reconstruction. Note there are far fewer documentary records from Iceland than England. The complexity of change in England makes it almost impossible to separate out events with the available resolution of environmental records. Plague and famine years from Herlihy, 1997 and Kershaw, 1973. Livestock epidemics refers to periods when large numbers of sheep and cattle were recorded as dying — some of these outbreaks were epidemics (rinderpest for cattle and liver fluke for sheep) whereas other periods are probably when poor weather or lack of food affected livestock numbers, but these events were still recorded as disease. Data from Spinage, 2003.

3.2.1 Population AD 1200-1350

It has been argued that by AD 1300 European population levels had reached their Malthusian limits as population levels stagnated in the early 14^{th} century (Herlihy, 1997). Alternatively increases in wage-labour may have decreased the

[1] An outbreak of the viral disease of rinderpest which affects cattle. Rinderpest is highly infectious and produces high mortality rates. At this period the term murrain was applied to all incidences of high mortality in livestock, however subsequently most of these events have been identified as epidemics of rinderpest (Spinage, 2003).

optimum family size, reducing overall fertility rates and stalling continued population expansion (Gummer, 2009). The Great Famine of AD 1315–1317, where mortality is estimated to have reached 10% (Kershaw, 1973), was caused by successive failures of the wheat harvest due to poor weather (Aberth, 2001). This was followed by an especially severe outbreak of both sheep and cattle murrains which reduced livestock populations, so that in some areas by AD 1321 arable agriculture had to be given up because of a lack of oxen to pull ploughs (Spinage, 2003). After the famine population recovered quickly and remained stable until the middle of the century.

3.2.2 Chronology and Population

The Black Death (also known as the 'Great Death') is one of a series of pandemics which affects Europe and the regions surrounding the Mediterranean in the mid 14^{th} century. The initial pandemic spread from Italy in the winter of AD 1347, reaching England by the winter of AD 1349 and persisted for about two years (Herlihy, 1997; Gummer, 2009). This particular pandemic is what is commonly referred to as the 'Black Death' and it reached from Italy and Spain in the south to Scotland, Norway and Sweden in the north. It is the first of dozens of incidences of plague over the next 200 years in Britain and continental Europe (Figure 3.1). There is a wealth of literature based on contemporary records that deals with its impact in Europe (Bolton, 1996; Platt, 1996; Herlihy, 1997; Cohn, 2002).

Although DNA analysis of plague victims has shown the modern plague bacillus *Yersinia pestis* was responsible (Haensch *et al.*, 2010) there is still some debate about whether these plagues were the same as the modern plague spread by fleas on the black rat *Rattus rattus*. Mortality rates from bubonic plague in the 19^{th} century in India were less than 1%, which does not match with historical evidence that at least 30% of the population perished between AD 1348–1350. Twigg (1984) argues that the black rat was not widespread in Britain at this stage and Karlsson (1996) demonstrates that it was not present in Iceland at all at this time, despite the plague occurring twice here. When the symptoms described by medieval chroniclers are compared with the modern plague bacillus there are clear inconsistencies (Cohn, 2002) and the speed at which it spread is hard to reconcile with our knowledge of how bubonic plague spreads (Duncan & Scott, 2005). Alternative theories have centred on the idea that it was not *Yersinia pestis*, but some other, unspecified, virulent infection which could spread rapidly (up to 5 km a day, Gummer, 2009) and directly from person to person (Duncan & Scott, 2005).

Mortality varied spatially from rural to urban areas. There is a broad consensus that mortality was much higher than recent pandemics, with estimates for England ranging from 20% (Russell, 1948) to 60% (Benedictow, 2004). Evidence is limited to somewhat unreliable written records and urban areas experienced continual inwards migration which increases the apparent mortality rate, but it seems population declined by at least 30% within two years. Population seemed to recover soon after the first outbreak (Bolton, 1996), but repeated episodes (with mortality rates of 10-15%) acted to depress the lower population and stop it returning to pre-plague levels (Platt, 1996). However repeated plagues cannot fully explain the length of demographic stagnation — population levels in England, which may have been 6 million in AD 1350, did not reach this level again until AD 1700 (Hatcher, 1977; Wrigley & Schofield, 1981). This counters Malthusian interpretations which would see increasing birth rates as a result of land becoming easily available which creating opportunities for marriage at a younger age as farm tenancies became easier to obtain.

In addition to repeated occurrences of plague, prolonged population stagnation was caused by changes to demographic variables due to the plague itself, and changes caused by longer term economic trends (Bolton, 1996). This model of demographic change argues that fertility rates before and after the Black Death were generally low (a low pressure demographic regime) and one explanation is that greater female independence and work opportunities meant that women had fewer children (Poos, 1991). There was also an increase in the proportion of wage-labourers relative to smallholders, who married later and did not benefit from having large numbers of children. It is argued that this change in demographic variables had started before the Black Death and was due to the transition from a feudal agricultural system to a wage dominated system (Bailey, 1996).

3.2.3 Social and economic effects

The Black Death is either seen as having directly transformative effects on society and economics (Herlihy, 1997) or as acting as a catalyst for longer term trends (Karlsson, 2000). The immediate effect was price inflation as production fell more rapidly than population (Herlihy, 1997). In the longer term labour became more expensive, which acted to raise living standards for the poorest (Kitsikopoulos, 2002) but made it hard for land owners to maintain their wealth (Bolton, 1996). Changes to the system made to try to reduce labour costs contributed to the peasants revolt of AD 1381 (Bolton, 1996). The decline in

oxen population during murrains at this time made arable cultivation harder (Spinage, 2003). The link between land and family became less pronounced which increased mobility as tenancies became easier to obtain (Bolton, 1996).

3.2.4 Plague in Iceland

Although the plague originated in trading ports around the Mediterranean it spread to the margins of Europe, affecting Iceland, Sweden and Norway. In Norway, which ruled Iceland during this period, there was long term economic and population decline and farm abandonment of up to 40% (Gissel *et al.*, 1981; Danielsen, 1995). Sweden also experienced population decline and extensive farm abandonment, mostly from recently colonised marginal areas (Lagerås, 2007). In Iceland documentary evidence shows that the plague occurs twice, in AD 1404-1402 and AD 1494 (Karlsson, 1996). Records of farm abandonment and contemporary accounts show that the first epidemic may have killed 50–60% of the population, and 30–40% in the second epidemic (Karlsson, 1996, 2000). In general the north of the country was more severely hit, although the Westfjords escaped the second epidemic entirely. Population levels between the epidemics are unclear, although farm occupation rates suggest that by the time of the second epidemic 95% of farm systems were in use again, but not necessarily occupied (Karlsson, 1996). Because having access to land was a pre-requisite for marriage, high rates of population growth could be expected after plagues as land became available. After the second plague, landowners who saw increased labour costs added additional labour demands to tenant leases. This may have limited the labour available at key periods of the year for tenant farms, which are the majority of farms in Iceland by this period (Bolender, 2006).

3.2.5 Environmental Impact of plague

This section summarises biotic (palynological) and abiotic (geomorphological and CO_2) evidence of environmental change in Europe associated with the demographic decline the 14^{th} century. Population decline as a result of the Black Death caused environmental change by altering land use patterns and land abandonment (Figure 3.2). Legal *post-mortum* data from Essex shows that the ratio of pasture and meadow to arable went from 0.08 in AD 1272–1309 to 0.32 by AD 1461–1485 (Poos, 1991), and this shift to pastoralism is also seen in Ireland and Sweden (Hall, 2003; Lagerås, 2007). Reduced labour availability may have driven this switch to less intensive agriculture, however better living standards as a result of the pandemics (Kitsikopoulos, 2002) increased demand

for meat and wool products, which could partially account for this shift (Gummer, 2009). A synthesis by Yeloff & van Geel (2007) shows that environmental changes were not universal, and probably related to the severity of disease in a particular area.

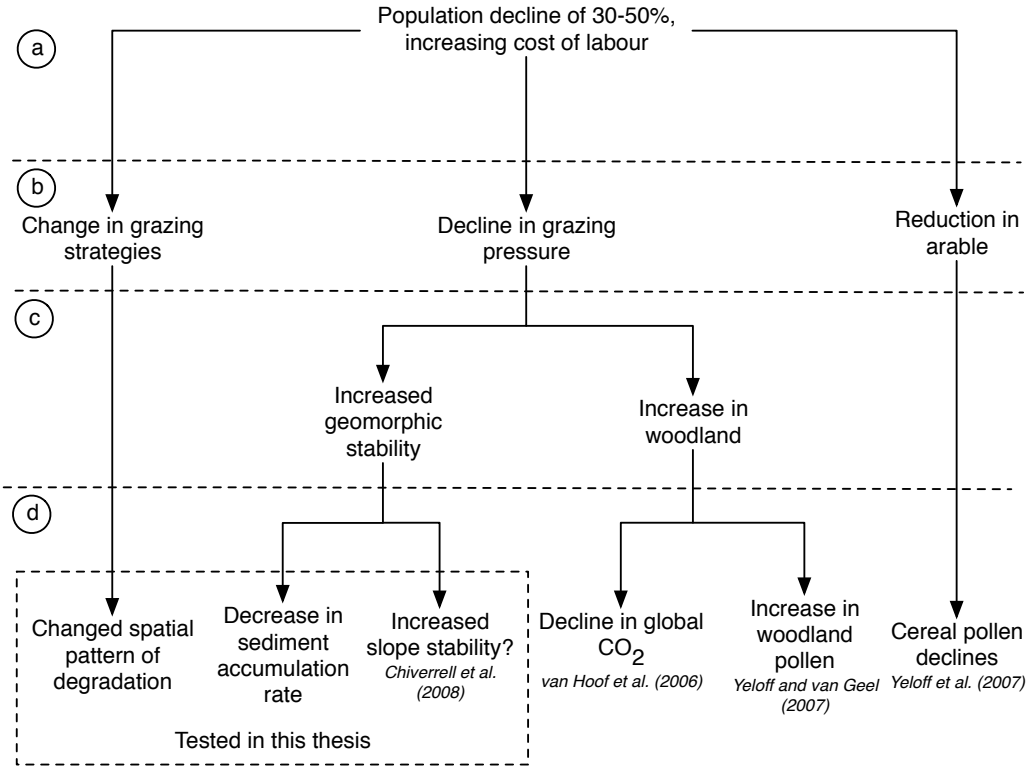

Figure 3.2: Mechanisms linking population decline and change identifiable in environmental records. (a) There is a social and economic change associated with population decline. (b) This results in changes in land use, which produces an environmental response (c). (d) Changes caused by population decline may be recorded in a range of palaeo-environmental records. Environmental records tested in this thesis are shown in the box.

Biotic

Environmental indicators of late medieval decline have been found in pollen assemblages across Europe. Changing land use is indicated by a decline or cessation in the occurrence of cereal pollen (rye, *Secale cereale L.*) and other indicators of arable farming such as nettle (*Urtica*) and dock (*Rumex obtusifolius*). This is seen in sites in northern England, Ireland, southern Sweden, France and the Netherlands (Yeloff & van Geel, 2007; Yeloff *et al.*, 2007; van Hoof *et al.*, 2006; Lagerås, 2007). In Moneyveagh Bog in western Ireland the cessation in cereal cultivation is dated to within a decade of AD ∼1350 by Hall (2003) using the the AD 1362 Öræfjajökull tephra. Other cereal

declines are dated using wiggle-matching radiocarbon techniques to AD ∼1350 in south east Netherlands (Figure 3.3, van Hoof *et al.*, 2006) and after AD 1350 in Northumberland, England (Yeloff *et al.*, 2007). This evidence matches with documentary evidence of a shift in land use from arable to grazing (Poos, 1991).

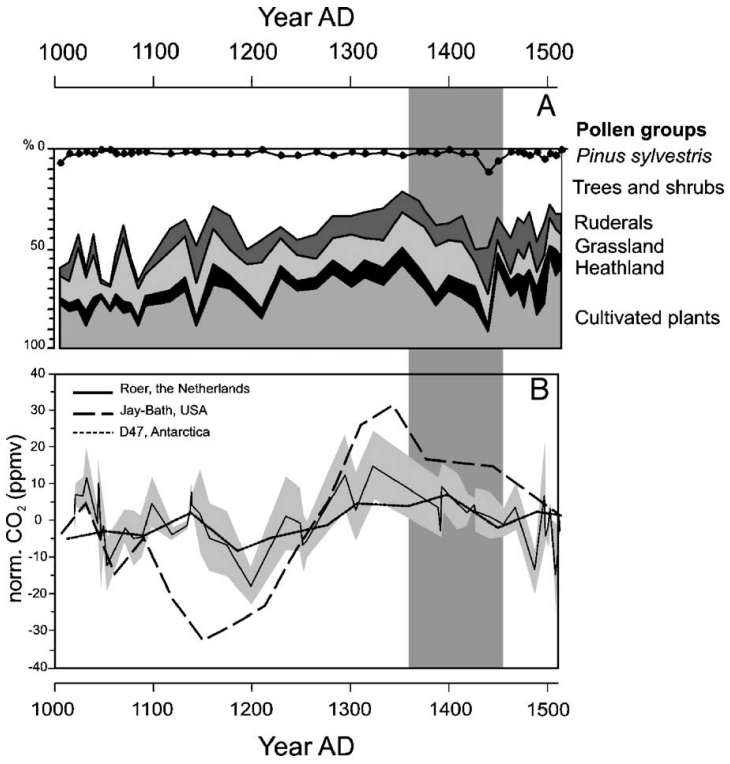

Figure 3.3: Regional vegetation development from pollen analysis, after (van Hoof *et al.*, 2006). B shows three different atmospheric CO_2 records. vanHoof *et al.* , (2006) argue that although declining CO_2 levels indicated by stomatal frequency are coeval with increases in forest density this change can be explained by other mechanisms.

In addition there is a rise in palynological indicators of land abandonment and forest re-growth, indicated by increases in pollen from pioneer tree species such as birch (*Betula*) and willow (*Salix*). Sites in the north of England experienced a rise in secondary woodland (*Betula*) after ∼AD 1350 (Yeloff *et al.*, 2007) and areas in southern Sweden also saw forest re-growth (Lagerås, 2007; Gustavsson *et al.*, 2009). Woodland cover across Europe increased to reach a maximum in AD ∼1400 (Yeloff & van Geel, 2007). By combining cereal cultivation, woodland and pasture indicators using 20 local pollen assemblages in southern Sweden, Lagerås (2007) forms a regional picture of late medieval land abandonment (Figure 3.4). Where farms are known to be abandoned indicators of arable stop, however indicators of grazing continue, suggesting the land was still used but in a less intensive way. Additional indicators show that

grasslands changed from hay meadows (which requires considerable labour input) to grassland, indicated by a cessation in *Rhianthus* type (yellow-rattle) pollen (Lagerås, 2007). The lack of increase in *Calluna* type vegetation precludes the argument that abandonment was a result of soil exhaustion. Signals indicating regrowth in woodland are weaker than indicators of a declines in intensive arable agriculture. An increased emphasis on pastoralist agriculture would have suppressed forest re-growth, leading to limited and short lived changes in woodland cover relative to a population decline of ∼30% (Yeloff & van Geel, 2007). To summarise, in most areas there was a switch from intensive agriculture to extensive agriculture, with some loss of marginal land to forest regrowth for a short period (around 50 years).

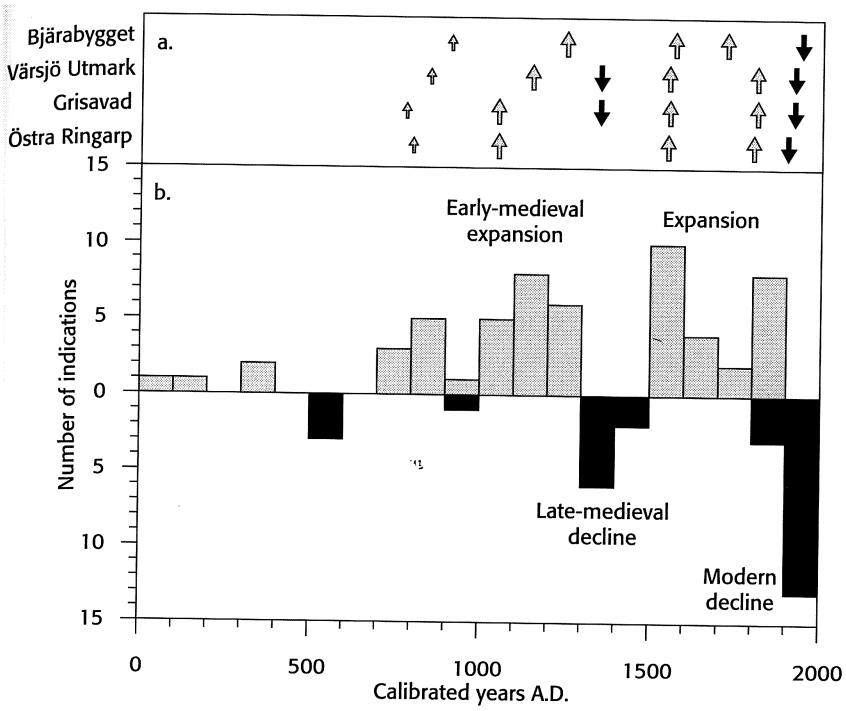

Figure 3.4: Aggregate indicators of changing land use for two areas in southern Sweden, after Lagerås, 2007

Abiotic

A geomorphic indicator of grazing intensity is slope stability. Radiocarbon dated evidence of channel incision and alluvial fan development in northern England and southern Scotland suggests that the 14^{th} and 15^{th} centuries had relatively stable landscapes (Chiverrell *et al.*, 2007). It is suggested that this is due to reduced grazing pressure after population decline caused by the Black Death and also population reduction and dislocation associated with the cross

border warfare prevalent through this area at the time (Chiverrell *et al.*, 2007). This period of relative stability is against a longer term trend of increasing instability due to the effects of climatic deterioration in the LIA.

Ruddiman (2003; 2005) has suggested that the human influence on climate started before the Industrial revolution with the development of agriculture and that major regressions in agriculture leading to forest re-growth and carbon sequestration decreased global CO_2 levels. However van Hoof *et al.* (2006) tested this using stomatal frequency data in oak leaves from an oxbow lake in the Netherlands and found that although declining CO_2 levels corresponded with increases in woodland pollen in the late 14^{th} century, these declines could be explained by other mechanisms (Figure 3.3).

3.3 Iceland

3.3.1 Population

Episodes of plague in Iceland need to be considered in the context of a range other episodes of increased mortality. Until the 19^{th} century the population of Iceland frequently experienced famines due to bad harvests (Karlsson, 2000). A summary of population is presented in Figure 3.5. The first census of Iceland in AD 1703 records a population of 50,538, prior to this point population figures are estimates. This census was commissioned as a result of famine and hardship late 17^{th} century, suggesting that population was larger prior AD 1703 (Thórarinsson, 1961; Karlsson, 2000).

Indeed most estimates put medieval population at a higher level than that recorded in the first census in AD 1703 (Karlsson, 2000; Thórarinsson, 1961). Using precise population records from the 18^{th} century Vasey (1996) argues that the property requirement for marriage acted to suppress population levels and in effect provided a buffer against poor harvests. Vasey also notes the contrasting population recovery times between smallpox in AD 1707–1709 and after the 'haze' famine in AD 1783 (Figure 3.5), which were due to different age cohorts within the population being affected. Only 13.3% of women of child-bearing age were killed in the 'haze' famine versus their 27.7% proportion of the overall population allowing the population to quickly recover (Vasey, 1996). In contrast the smallpox epidemic of AD 1707 killed an unusually high proportion of young adults which can explain the slow population recovery time after this event. Subsequent smallpox epidemics (such as in AD 1742) had mortality rates of 2–3%.

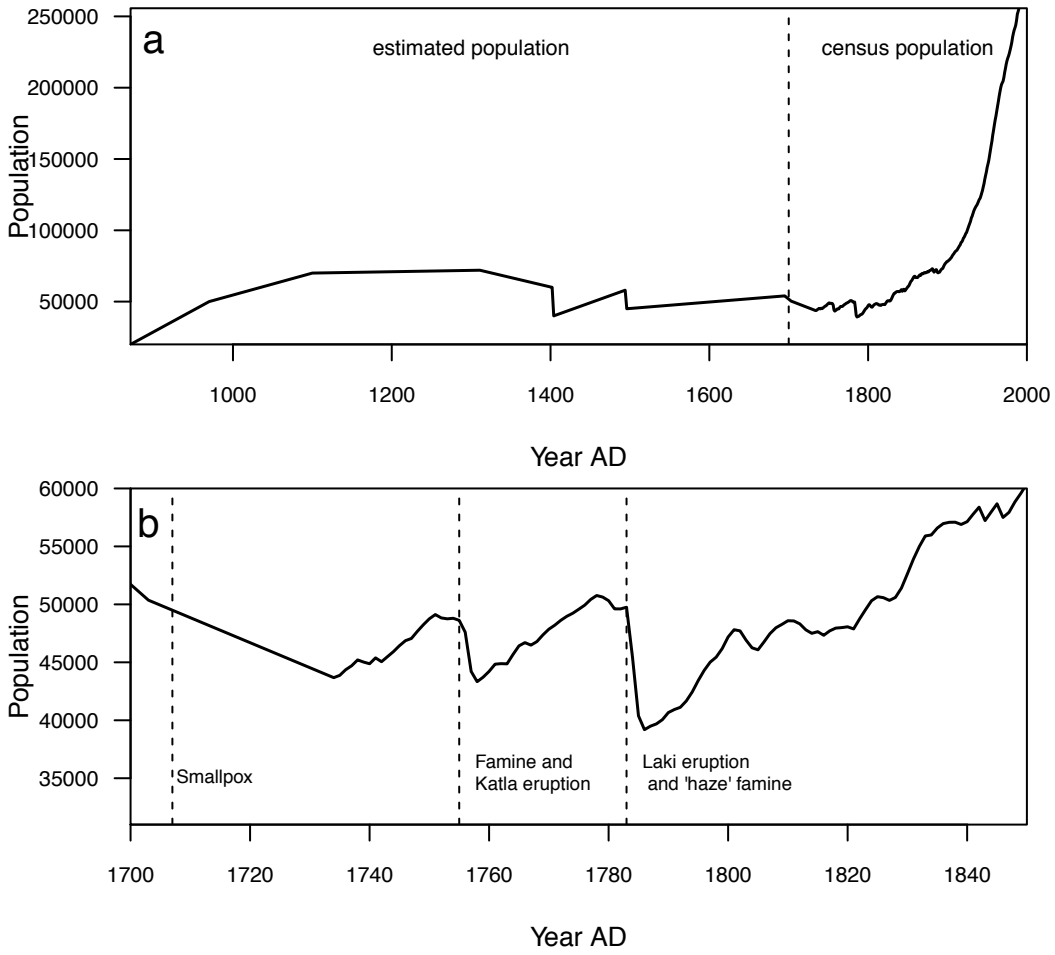

Figure 3.5: Population of Iceland (a) AD 870–2000. Prior to AD 1703 population is estimated based on tax records (After Thorarinsson 1961; Karlsson, 2000). A key point to note is the medieval population was probably higher prior to the population recorded in the 18^{th} century. (b) Population of Iceland AD 1700–1850. A census in AD 1703 and regular censuses after show population declines caused by smallpox in AD 1707–1709, a famine caused by cold weather after the eruption of Katla in AD 1755 and the 'haze' famine caused by the eruption of Laki in AD 1783.

3.3.2 Agriculture

Until the 20^{th} century lowland grasslands would be used for milking stock and the home fields were of vital importance to produce fodder to sustain animals through the long winter, although the grazing of animals in lowland areas in winter was also common (Adalsteinsson, 1990; Simpson *et al.*, 2004). Rangelands (areas of common grazing, known as *afréttir* and extending up to 500–600 m) are grazed from April to October and are primarily for fattening meat animals, which are rounded up in the autumn for slaughter (Adalsteinsson, 1990). The best fodder was reserved for cattle, with sheep

having to make do with the minimum and supplement with winter grazing; in some years adult wethers may have needed no fodder supplement (Adalsteinsson, 1990). It has been suggested that during times of low population and livestock pressure (for example after plague or famine) farmers would not graze the highland pastures as there was sufficient grazing in lowland pastures (Júliusson (1995), cited in Ólafsdóttir, 2001).

At Landnám settlers brought with them cattle, pigs, sheep, horses and goats but goats and pigs were found to be too damaging so numbers were reduced quickly (Dugmore *et al.*, 2000). A major change over the settlement period has been the increase in the relative numbers of sheep compared to cattle. By the AD 1703 census there were nine sheep per head of cattle; zooarchaeological evidence from Mývatnsveitt, north Iceland shows that prior to 12^{th} century sheep were less common (McGovern *et al.*, 2007). This change may be related to the increasing importance of wool as a cash crop for export (Karlsson, 2000). However it is not known exactly how this ratio varied across the country, and areas in the south may have kept relatively more cattle until a much wider shift towards relatively more sheep in the 19^{th} century (Orri Vésteinsson, personal communication). The implications of a switch to wool production and increased sheep numbers would have been to increase pressure on outfield and rangeland grazing.

3.3.3 Skaftártunga

Icelandic regions are separated into community based areas called *hreppurs* which are on average 30 farms in size. The size of these units has its origin in communal grazing units and also of units of sufficient size to be able to provide poor relief (Vasey, 1996). The area of Skaftártunga forms half of the hreppur Leiðvallahreppur which is in the region of Vestur-Skaftáfellsýsla (Figure 3.6 and 3.7). Skaftártunga has natural barriers which prevent easy livestock movement on all sides. In the south Mýrdalssandur prevents livestock movement, and the fast flowing glacial river Hólmsá prevents movement to the west. In the east the river Skaftá prevents easy movement to the adjoining grasslands. The coast is 30 km away and has no shelter for harbours, limiting the extent to which diets could be supplemented by fishing or other wild foods, although long distance transport would have been common. There is communal rangeland grazing to the north, extending into the uninhabited interior. The land rises from an altitude of around 60 m in the southern part to 725 m in the north, with most of the area being below 400 m. Lava flows from the Eldgjá (AD 934–940) and Laki (AD 1783) eruptions flowed along the eastern, western and southern

boundaries of the area.

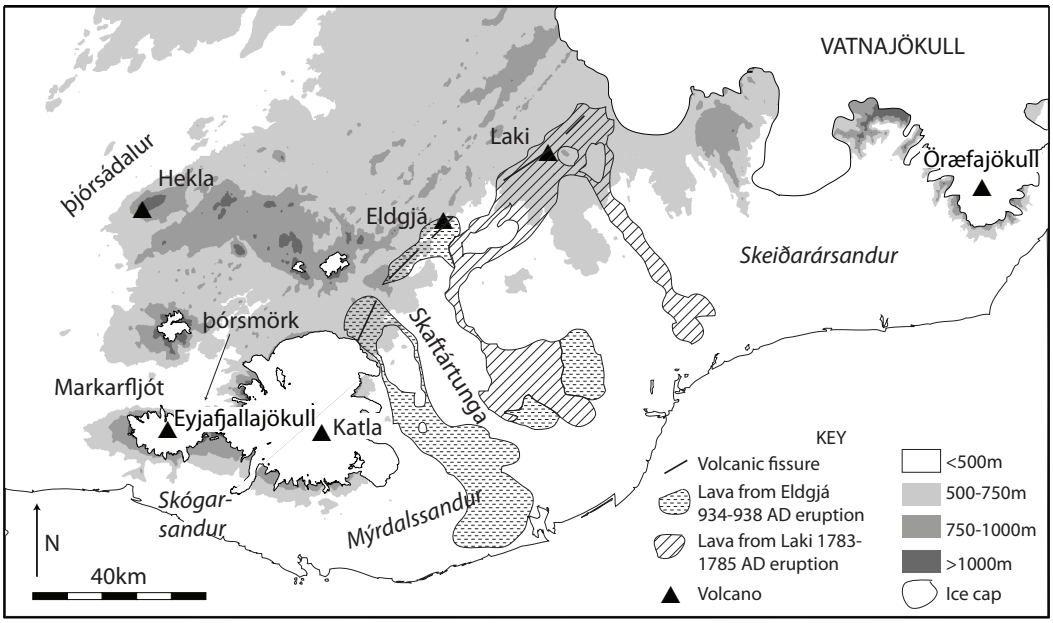

Figure 3.6: Skaftártunga, south Iceland. Extent of lava from Larsen (2000)

This size of area (∼400 km^2) is large enough to provide a good approximation of changes at the regional scale. The population was 106 in the AD 1703 census, and the number of livestock (especially cattle) compared to the number of residents gives an indication of the relative wealth of each landholding (Table 3.1). The mean temperature is 0°C in January and 10°C in July, higher than average for Iceland, and snow cover is only occasional in winter and rainfall is high, on average 2000–2500 mm per year (Einarsson, 1984). The area has 14 landholdings, of which most are mentioned in the 1703 AD census. Also presented are the current boundaries of landholdings (Figure 3.7). These follow natural features and the location of farms has not changed since Landnám. It is therefore assumed that historic landholding boundaries are broadly represented by the current boundaries. Historically farms had multiple owners and it was possible that you could own multiple, non-adjacent farms so it is unlikely that physical landholdings were combined.

3.4 Environmental change

3.4.1 Impact of volcanism

Skaftártunga are has been affected by frequent volcanic eruptions over the past 1200 years. The tephrochronology of this region is covered in section 5.2, here

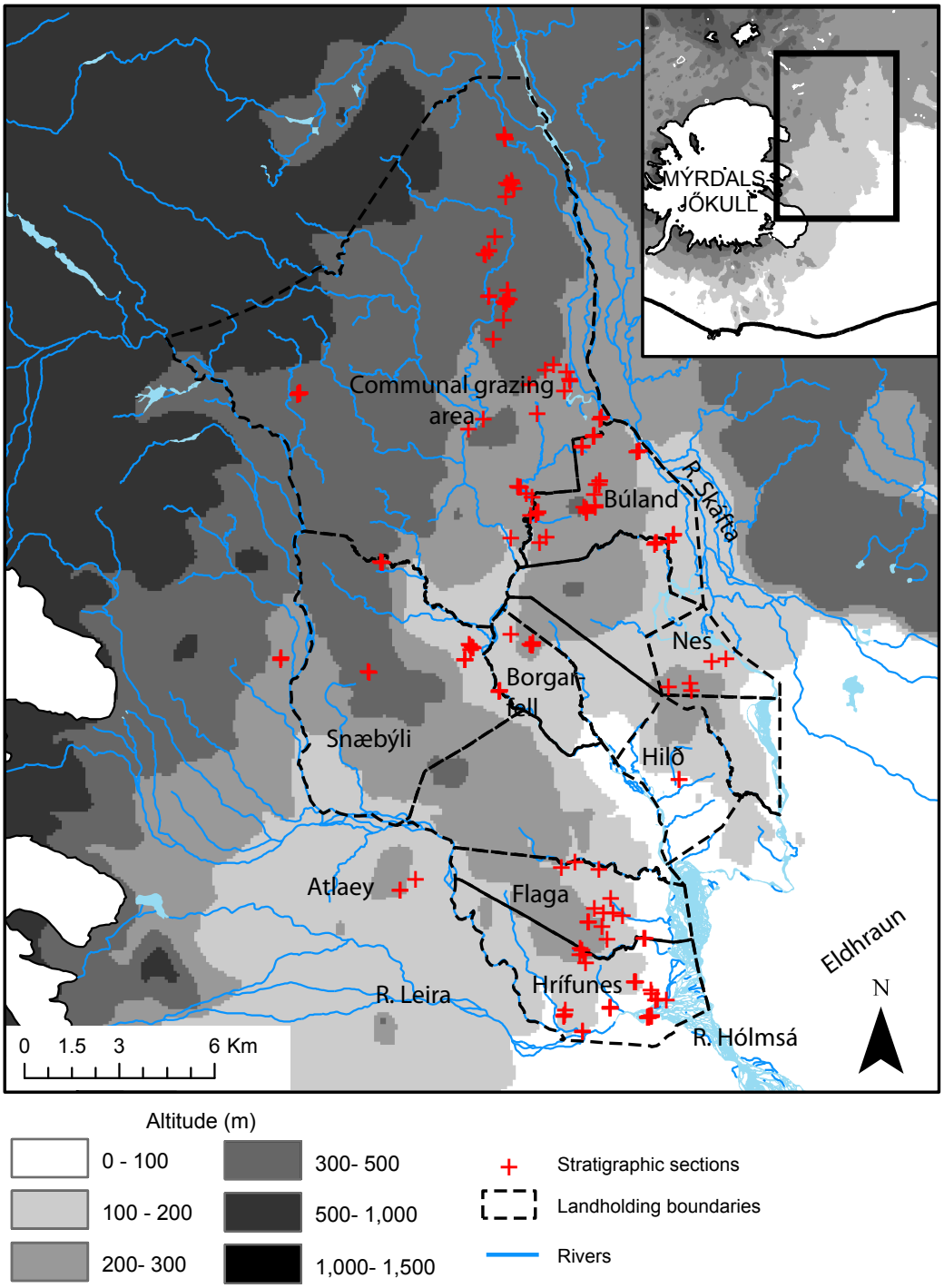

Figure 3.7: Names and boundaries of landholdings where stratigraphic sections were recorded.

Table 3.1: Results of Jarðabók AD 1703 census for Skaftártunga. Translation from Icelandic provided by Orri Vésteinsson from (Census, 1703). Note there are usually multiple households on a landholding. Landholdings which form part of this study are indicated by an *. Although Snæbýli and Ljótarstaðir were not recorded in the Jarðabók survey they are recorded in an AD 1695 tax survey (Lárasson, 1967).

	Household	People	Cattle	Sheep	Horses
Eystri Ásar	1	8	13	53	8
Ytri Ásar	1	6	13	53	7
	2	6	11	35	6
Hrífunes*	1	6	12	19	5
Flaga*	2	15	23	173	15
Hemra	1	7	11	71	6
Hílð*	1	7	12	36	7
	2	7	16	128	13
Gröf	1	4	5	22	3
Borgarfell*	1	6	7	26	4
Búland*	1	7	14	60	9
Hvammur	1	7	9	80	7
Svínadalur	1	5	10	54	7
	2	5	9	51	3
	3	4	6	2	3
Nes	1	6	14	70	10
Snæbýli*	-	-	-	-	-
Ljótarstaðir*	-	-	-	-	-
Total		106	185	933	113

eruptions thought to have had a significant impact on agriculture area considered (Table 3.2). Two eruptions which would have had major impacts are the Eldgjá eruption in AD 934–940 and the 'Skaftár fires' eruption of Laki in AD 1783.

The eruption in the Eldgjá fissure (which is 70 km long and at its closest 35 km from Skaftártunga) has been dated to AD 935±2 (Zielinski *et al.*, 1995) and also AD 933±1 (Vinther *et al.*, 2006), but the eruption is thought to have taken place over a period of several years (Larsen, 2000). It deposited 2.7 km^3 of tephra over an area of 20,000 km^2 and erupted 18 km^2 of lava, the largest known flood lava deposit in the historical period (Larsen, 2000). The depth of tephra deposited in Skaftártunga was ranges from 25 cm in the north to 12–15 cm in the south. This would have been damaging to vegetation due to smothering and wind abrasion. Some areas have never recovered from the impact of this eruption as the tephra never stabilised (Larsen, 2000).

The basaltic fissure eruption of Laki in AD 1783–1785 AD had major impacts on populations in both Iceland and Europe (Karlsson, 2000; Grattan

Table 3.2: Major eruptions affecting Skafártunga since Landnám

Volcanic origin	Age (AD)	Local impact
Eldgjá	934–940	Lava flows along course of Hólmsá river on the western edge of Skaftártunga, destroying grazing areas. Deep tephra fall (20–50 cm) kills vegetation by smothering and wind abrasion. Destruction of 600 km^2 land which has never recovered (Larsen, 2000).
Katla	1625	Coarse black tephra fall, mean thickness 40 mm.
Katla	1755	Coincides with poor summer and bad winter. Widespread famine kills 15% of the population
Laki	1783	Lava flow down Skafta river destroying pasture. Chronic fluorosis kills $>$ 60% livestock in Iceland (Thordarson & Self, 1993) and famine kills 25% of total population. Acidic rain killed trees, shrubs and grasses which did not recover for 3–10 years.

et al., 1995). The eruption produced 14.7±1km^2 of lava and 120 Mt of SO_2 (Thordarson & Self, 1993). The impact from sulphur emissions may have caused up to 30,000 deaths in in England and mainland Europe (Grattan *et al.*, 1995). Ten fissures spread over 27 km and are located 20 km to the north east of Skaftártunga. Lava flowed south following the course of the river Skaftá, destroying areas of lowland grazing in Skaftártunga (Figure 3.6). Arguably the biggest impact was caused by the high fluorine levels in the tephra. The deposition of ∼500 mg of fluorine per km^2, caused chronic dental and skeletal fluorosis in the human population and it also killed an estimated 80% of sheep and 50% of cattle within 2–14 days of the eruption starting (Thordarson & Self, 2003). This initiated a severe famine which ultimately killed 20–25% of the total population of Iceland (Vasey, 1996). The famine was made worse by poor weather — the winter of AD 1782–83 was long and harsh, as was the summer and winter of AD 1783–84 (Ogilvie, 1986). Population recovered relatively quickly in the country as a whole, approaching pre-famine levels by AD 1800 (Figure 3.5).

This event provides some analogues to population change in the 15^{th} century. Differences are that this event killed livestock first — whereas disease killed people and reductions in livestock numbers were not inevitable. However if maintaining livestock numbers is reliant on having sufficient labour, for instance to produce fodder which is needed to sustain livestock through winter, then disease may act to limit livestock numbers. This is especially true for cattle

which cannot survive without supplementary fodder through winter. Sheep can be overwintered outside but this can be damaging to the landscape as vegetation is more sensitive outside the growing season (Simpson *et al.*, 2001).

3.4.2 Climatic change

While climate over the Holocene has been relatively stable, high resolution records show that on century and decadal time scales it has at times been highly variable. Iceland lies close to the atmospheric polar and oceanic front, and its climate is marginal for pastoralism (Dugmore *et al.*, 2000). The key climatic periods in Iceland since Landnám can be broadly characterised as the Medieval Warm period (MWP) lasting from around AD 800–1300 and the Little Ice Age (LIA) lasting from AD 1300–1920 (Grove, 2001). These terms are used in the context of the entire North Atlantic region, even though the exact timing and differences between the MWP and LIA was spatially variable and it is very difficult to define start and end points. Ogilvie and Jónsson (2001) argue the use of these terms is unhelpful as both periods were variable, and Grove (2001) argues that it should exclusively refer to glacial advances. However multiple proxy based reconstructions (e.g. Mann *et al.*, 2009) do show broad trends: the MWP had a similar climate to current conditions and was relatively stable, whereas the LIA can be categorised as cooler and stormier with more variability than current conditions.

Iceland's position in the North Atlantic on the boundary of two weather systems means it is sensitive to changes in atmospheric circulation and changes in the frequency and extent of sea ice (Ogilvie & Jonsson, 2001). A key phenomenon that dictates Iceland's weather is the North Atlantic Oscillation (NAO), an index of the pressure difference between Iceland and the Azores, which has either a positive or a negative state (Figure 3.8, Dawson *et al.*, 2004). When the NAO index is positive Iceland has warmer winters and the north coast is minimally affected by drift ice. When the NAO is in a negative phase Iceland experiences colder, wetter conditions and drift ice is frequent off the north coast and occasionally occurs on the southern and eastern coasts. Climatic changes over the last 2000 years have been related to changes in the strength of the NAO, with a change to a higher frequency of negative NAO conditions occurring around AD 1400–1420 (Dawson *et al.*, 2004; 2007). This climatic change is notable because it occurs coincidentally with the impact of the first episode of plague in AD 1402.

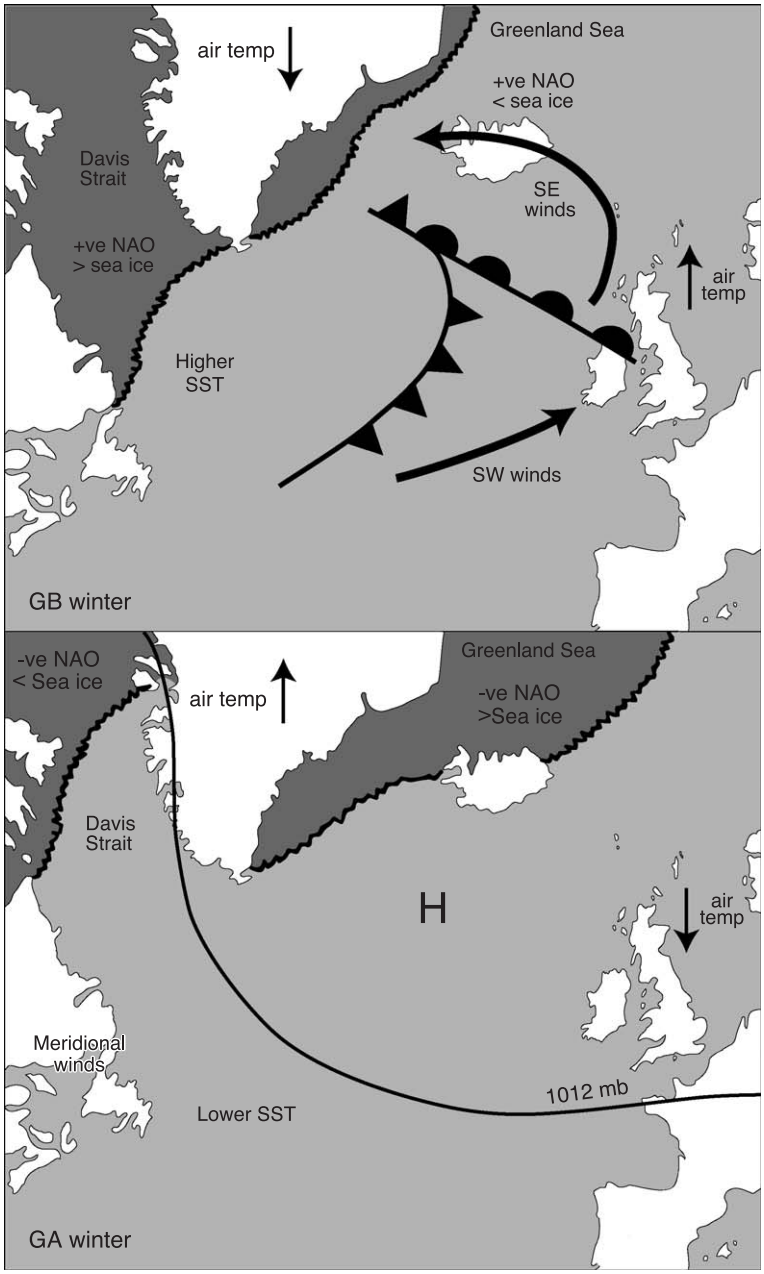

Figure 3.8: After Dawson *et al.*, 2004, showing the North Atlantic 'see-saw'. Note the very different extents of sea ice cover around Iceland between positive and negative NAO index states.

3.4.3 AD 870–1300

Multiple proxy records of temperature in the North Atlantic for the period AD 500–2000 are summarised in Figure 3.9. During the first four centuries of settlement (AD 870–1300) Iceland experienced a relatively stable and warm climate. There was still considerable variability however and several periods of colder than usual temperature. Documentary sources show that harsh periods were experienced in AD 1180–1210, 1280–1290 (Ogilvie, 1984), while diatom proxies indicate cooler summer temperatures in AD 1050–1100 and ∼1150 (Geirsdottir *et al.*, 2009). However before AD 1300 sea surface temperatures (SST) were consistently above the 2000 year mean of 2.8°C (Jiang *et al.*, 2005). Major changes in climate and indications of the LIA appear around AD 1250–1300 (Geirsdottir *et al.*, 2009) and AD 1300 can be considered the start of LIA type conditions. Records of glacial advance broadly show a period of low ice extent although more sensitive lowland glaciers such as Gígjökull show signs of advance between the 10^{th} and 12^{th} centuries (Kirkbride & Dugmore, 2006; 2008).

Evidence for climatic deterioration after AD 1300 has been found by dating glacial re-advance (Kirkbride & Dugmore, 2001), diatom proxies (Jiang *et al.*, 2005; Geirsdottir *et al.*, 2009; Gathorne-Hardy *et al.*, 2009; Ran *et al.*, 2011), documentary evidence (Ogilvie, 1992; Ogilvie & Jonsson, 2001), sea ice proxies (Massé *et al.*, 2008) and terrestrial sediment aeolian proxies (Jackson *et al.*, 2005). The late AD 1300s sees a large negative deviation in SST (Jiang *et al.*, 2005; Mann *et al.*, 2009; Ran *et al.*, 2011) and increased sea ice frequency (Ogilvie, 1984; 1992; Massé *et al.*, 2008).

3.4.4 AD 1400–1500

From around AD 1420 the NAO cycle strengthens increasing the frequency and intensity of winter storms (Meeker & Mayewski, 2002; Dawson *et al.*, 2004; 2007). The 15^{th} century therefore seems to mark the boundary between the warmer positive NAO conditions and cooler, wetter, stormier negative NAO conditions which predominate until AD 1920. Cumulative deviations from the mean can be indicators of changes in trajectories of climate, and based on the cumulative deviation from the mean Na^+ storminess proxy from the GISP Greenland ice core conditions deteriorate from AD ∼1425 (Dugmore *et al.*, 2007b). Documentary evidence from this century is poor (Ogilvie & Jonsson, 2001), but a range of proxies indicate it was one of the coldest periods of the LIA. Sea ice incidence is high from AD 1467–1494 (Massé *et al.*, 2008), in the period AD 1450–1500 summer temperatures as recorded in Haukadalsvatn lake,

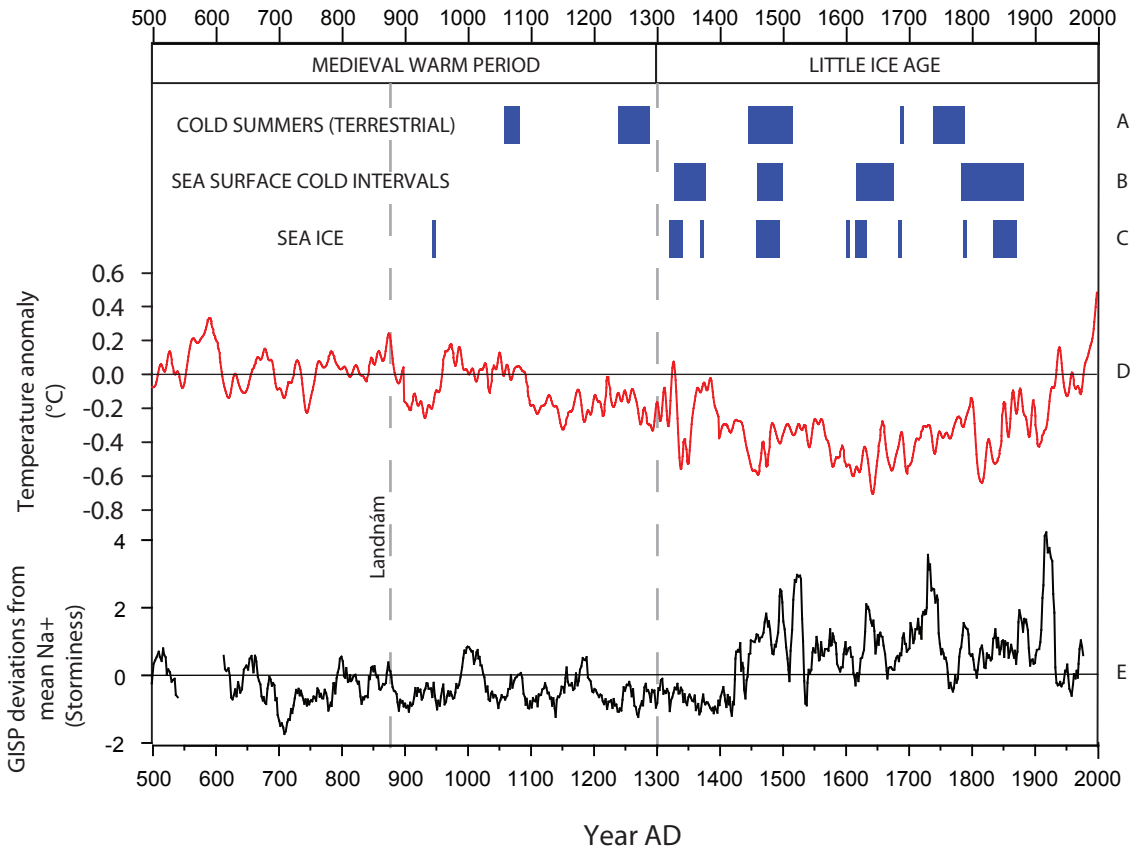

Figure 3.9: Multi-proxy summary of climatic changes over the past 1500 years. (a) Periods with especially cool summer temperatures from Haukadalsvatn lake, western Iceland (Geirsdottir *et al.*, 2009). (b) Cold intervals from diatom reconstructed summer SST, north Iceland, (Ran *et al.*, 2011). (c) Heavy sea ice periods from an IP25 proxy, marine core, north Iceland, Massé et al. 2008. (d) Multi-proxy weighted reconstructed SST in the North Atlantic region, (Mann *et al.*, 2009). (e) Records of North Atlantic storminess (Na^{+}) from the GISP ice core.

west Iceland decline by the largest amount in 2000 years (Geirsdottir *et al.*, 2009), AD 1460–1500 is a particularly cold interval recorded in marine diatom records from north of Iceland (Ran *et al.*, 2011), and the regional signal shows a decline in average temperatures between AD 1380–1450 (Mann *et al.*, 2009).

3.4.5 AD 1500–2000

The period AD 1500–1900 is variable but includes decades which are probably the coldest during the LIA, as well as periods that were almost as warm as the MWP. The 16^{th} century is relatively mild compared to the periods AD 1350–1400 and AD 1450–1500, with low indicators of sea ice (Massé *et al.*,

2008). After AD 1600 the record becomes more variable with extremes more common (Jiang *et al.*, 2005). Documentary sources improve and harsh decades are recorded in AD 1630–1640, 1690–1700, 1740–1760 and 1780–1790 (Ogilvie & Jonsson, 2001). Sea ice is severe in AD 1560–1570, 1590–1640, 1690–1720 and 1740–1790, with the AD 1780s probably having the most sea ice in the last 500 years (Ogilvie & Jonsson, 2001). The 19^{th} century is cold (Ran *et al.*, 2011) but by the end of the century temperatures rise. Records of glacial advance from south eastern Iceland (Bradwell *et al.*, 2006; McKinzey *et al.*, 2005), south Iceland (Kirkbride & Dugmore, 2008) and central Iceland (Kirkbride & Dugmore, 2006) all show increased glacial extent in this period, in particular the periods AD 1690–1740 and the late 19^{th} century (Kirkbride & Dugmore, 2006).

3.4.6 Impact of climate change

Climate, especially the incidence of sea ice, has long been considered key to the success and failure of agriculture and the fortunes of Iceland as a whole, even more so than volcanic eruptions (Ogilvie, 2001, from Thoroddsen, (1914), page 215). Since Iceland is climatically marginal for agriculture any cooling would have had a significant impact — Bergthorsson (1985) calculated that the potential livestock carrying capacity declines by 30% for a 1°C reduction on the AD 1901–1930 mean temperature of 3.2°C. The cessation of growing barley in the north of Iceland by the 12^{th} century, and in the south of Iceland by the 15^{th} century has been explained solely as a factor of climatic deterioration (Grove, 2004) although soil erosion could also have contributed to the decline (Amorosi *et al.*, 1997). Soil modelling indicates that yield increases from manuring largely compensate for the loss of yield due to temperature declines, suggesting socio-economic reasons were more important (Simpson *et al.*, 2002). Evidence from a high status farm at Reykholt supports this, with no apparent link between climate deterioration and cessation of growing barley (Sveinbjarnardottir *et al.*, 2007).

The key question in studies of climate and history is not why a wet autumn resulted in the loss of a fodder crop but why no barns were built to protect the harvest (McGovern *et al.*, 2007). Critical to the climates impact on agriculture was the frequency and timing of unfavourable weather, rather than the intensity of change (McGovern *et al.*, 2007). Prediction of (and preparation for) future change may have been just as important as the magnitude of change (Figure 3.10). Cool winters could be more damaging than cool summers because this was a critical time when stocks from the previous year were running low, and there was a need to graze sheep while the grass was not growing, potentially

triggering soil erosion and leading to irreversible land degradation (Simpson *et al.*, 2001). Because population was socially limited by access to property; to some extent this created a buffer against the impact of bad years (Vasey, 1996).

The cumulative deviation from the mean of climatic records highlights periods where climate changed trajectory — a potential period where past experience is not a guide to the future (Figure 3.10, Dugmore *et al.*, 2007b). In particular a change to increasing sea ice extent around AD 1450 and increasing storminess AD 1425, could have been significant, even though the LIA was not yet at its coldest (Dugmore *et al.*, 2007b). Periods where climate change did not match past experiences of climate (15 years) may have been particularly challenging to cope with, so may have been a time when previous management techniques could not cope (Simpson *et al.*, 2001, Figure 3.10). Modelling of total vegetation production indicates a reduction in capacity of up to 40% as a result of declining temperatures throughout the LIA (Haraldsson & Ólafsdóttir, 2006). However this reduction in vegetation production is mainly in upland areas, and may not be as important as declines in production from lowland areas as there is more than sufficient biomass production in the summer (Thomson, 2003; Thomson & Simpson, 2007).

3.5 Soil and erosion

The majority of Icelandic soils are derived from recently weathered volcanic material. Tephra and pumice are porous and have a high surface to volume ratio which means they weather rapidly, forming allophane, Al-humus complexes and additional colloidal materials (Wada, 1985). The most frequent soil type is Andisols (Andosls) of recent volcanic origin. Andisols are defined as having a high organic mineral content, low bulk density and a high water holding capacity (Arnalds, 1990). Andisols make up 76 % of the soil cover in Iceland by area and 5% of the world's coverage (Arnalds, 2004). Other soils types common in Iceland are Vitrisols ($\sim$20%) and Histisols ($< 5\%$). All Icelandic soils are subject to frequent tephra falls, active eolian deposition of between $<$0.0001 mm yr $^{-1}$ to $>$ 1 mm yr^{-1} and regular freeze-thaw cycles (Arnalds, 2008).

Soil properties which influence the likelihood of erosion are the texture and density of soil grains and aggregates, tephra layers within the soil profile and the thickness of aeolian deposits (Arnalds, 1990). In these respects Icelandic soils, and especially andisols, are particularly vulnerable to erosion. Andisols are poorly cohesive making them susceptible to wind and water transport and a high water content increases susceptibility to cryoturbation (Arnalds, 2004). Because the soil particles have low density (0.9–1.3 g cm^{-3}) they are susceptible

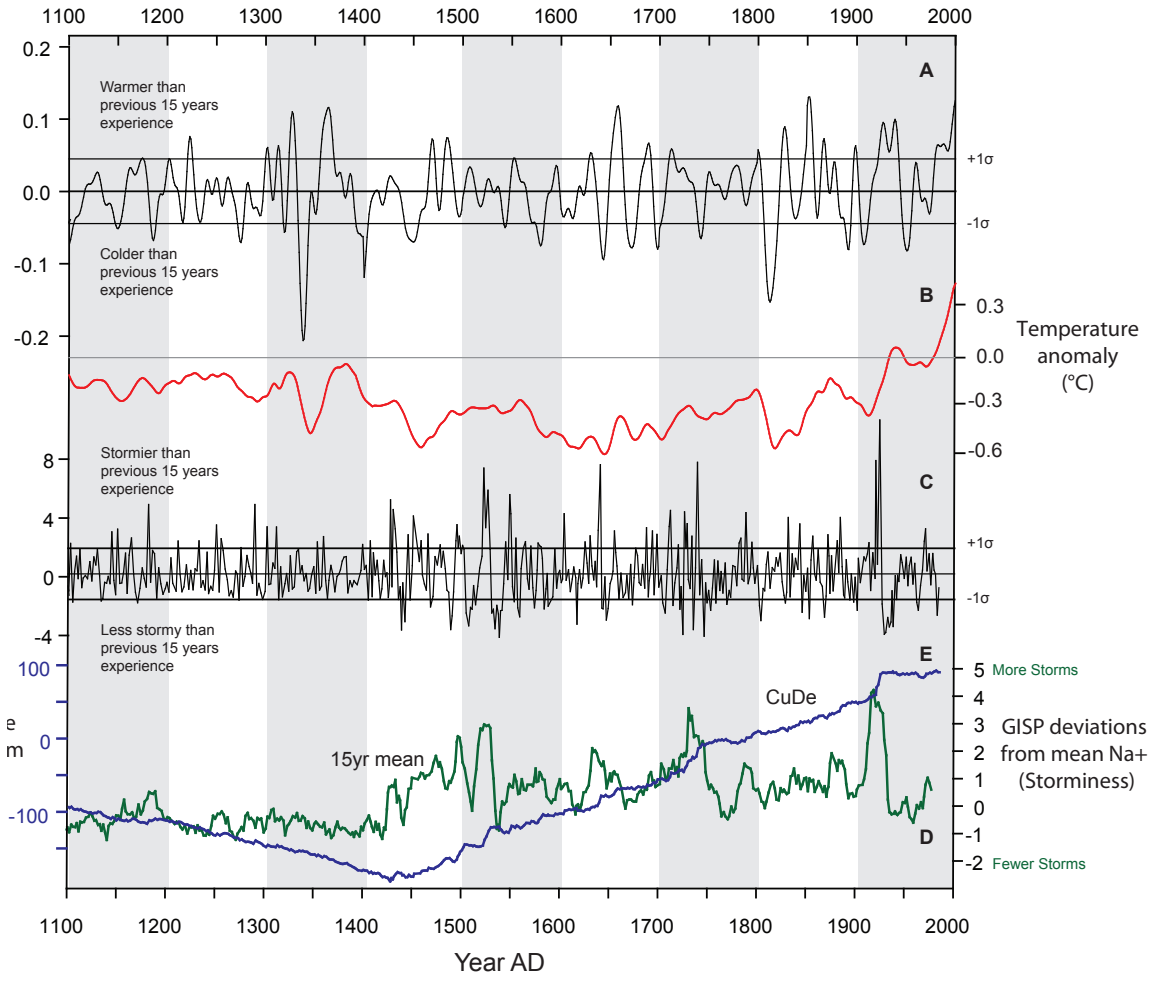

Figure 3.10: Deviations from the 15 year mean for (a) multi-proxies temperature reconstruction from Mann et al. 2009 (shown in (b)). (c) is deviations in storminess from mean of previous 15 years of storminess. These highlight periods of climate that were significantly different from previous experience, periods where past experience would not be a good proxy for current change. (e) is cumulative deviations in storminess from Dugmore *et al.*, 2007b.

to saltation at low wind speeds, and even coarse tephra particles of >1 mm may saltate in relatively low wind speeds (Arnalds, 1990). Poor cohesion also means the soils are susceptible to rain-splash and running water. High levels of water retention and the cool climate means that cryoturbation is very active.

All Icelandic soils have formed in the Holocene (Arnalds, 2004), however sediment sequences can be more than 7 m deep reflecting high rates of accumulation over the past 8.7 ka (Óladóttir *et al.*, 2007). If vegetation cover is breached this provides a large supply of sediment which can be blown considerable distances (Figure 3.11). Where there are thick deposits of unconsolidated tephra within the soil sequence even minor breaches in soil cover may initiate a prolonged period of instability. For example in Þórsmörk, south

Iceland, once the Katla AD 920 tephra was breached many areas experienced several centuries of disturbance (Dugmore *et al.*, 2006). This is especially the case in the volcanically active zones where tephra layers may make up 50–80% of the thickness of postglacial sediment, although the proportion of tephra is lower in post-Landnám sequences, around 20–30%, reflecting the higher rates of accumulation since Landnám. The higher content of tephra within soils in volcanically active areas means these areas are more vulnerable to erosive processes, and this is reflected by generally higher erosion rates in the younger Holocene and Upper Pleistocene bedrock areas and lower erosion rates in older Tertiary bedrock areas (Gísladóttir, 1998).

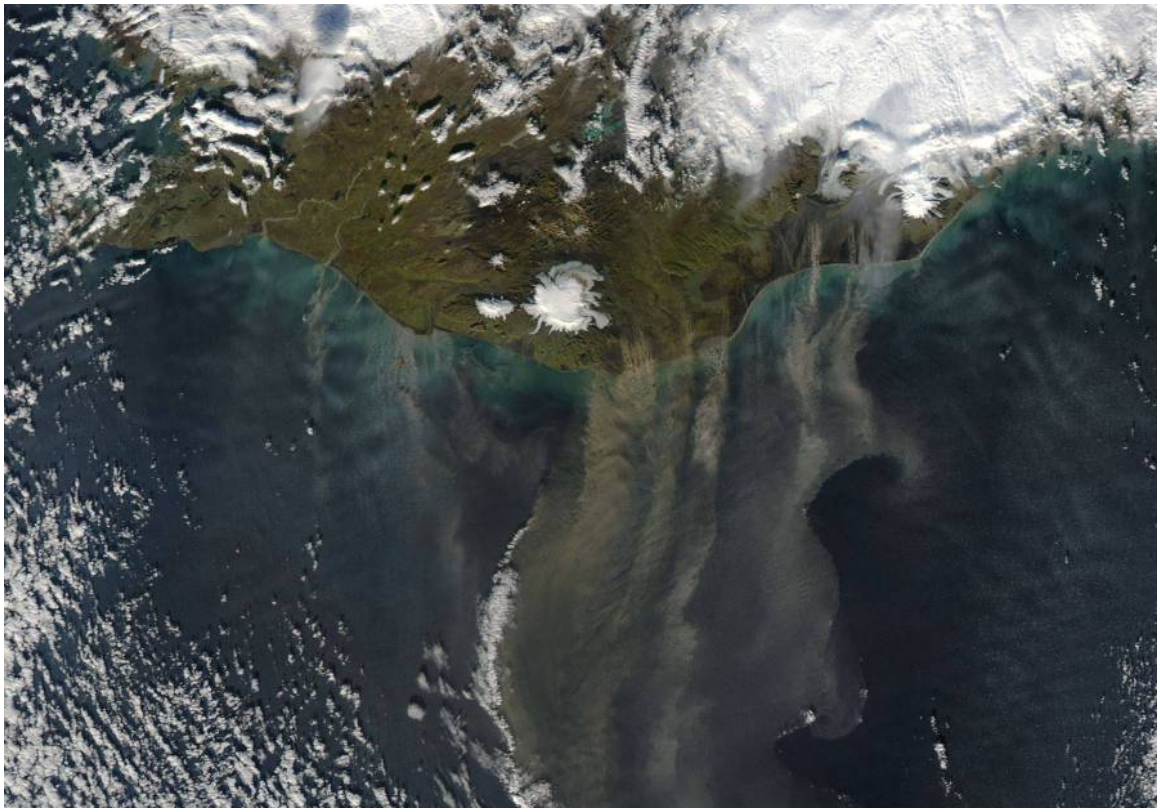

Figure 3.11: A dust storm in October 2004 moves sediment from eroded areas west and east of Myrdalsjökull >150 km south from the coast. Image from NASA Earth Observatory, http://earthobservatory.nasa.gov/

The soil type in south-central Iceland is predominately Brown Andosol, with areas of Arenic and Cambric Vitrisol found on the sandur plains (Arnalds *et al.*, 2001). Vitrisols comprise $< 1\%$ organic carbon and support low levels of vegetation cover (Arnalds, 2004). If vegetation does establish itself the soil can develop into a Brown Andosol within 50–200 years (Arnalds, 2004). Most of the vegetation covered areas in Skaftártunga are Brown Andosol (Arnalds *et al.*, 2001), in which both basaltic and rhyolitic tephra layers are easily distinguished

against the orange-brown colour of the soil. Typically the level of carbon in Brown Andosol is 12–20% and these soils are free draining (Arnalds, 2008), however the oxidisation and lithification of Fe rich tephra layers within the profile can obstruct drainage. Andosols tend to accumulate organic matter and in Iceland the climate allows organic buildup in water saturated situations (Arnalds, 2008), however this tendency is reduced where rates of aeolian sedimentation are high.

3.5.1 Land degradation in Iceland

Since the settlement of Iceland in AD ∼870 vegetation cover has decreased substantially and the landscape has experienced extensive and severe soil erosion. These changes are the result of a combination of factors, including: inherently sensitive vegetation cover and soils, climatic deterioration during the LIA, volcanic impacts and the anthropogenic impact of grazing in a landscape that is marginal for agriculture (Dugmore *et al.*, 2000). Presently ∼40% of Iceland rangelands are classified as severely eroded (Arnalds *et al.*, 2001) and on Eyjafjallajökull, south Iceland an estimated 90% of soil cover has been lost in areas above 300 m (Dugmore & Buckland, 1991). It is important to note however that despite the soil loss there is still some vegetation in these areas and they continue to be grazed.

Prior to Landnám there was no grazing apart from geese and swans, after Landnám the Norse settlers introduced sheep, goats, cattle, horses and pigs (Amorosi *et al.*, 1997; Dugmore *et al.*, 2000). The introduction of grazing by terrestrial mammals initiated erosion and caused an order of magnitude increase in sediment accumulation rates (SeAR), from a pre-Landnám level of 0.2–0.3 mm yr^{-1} to 1–2 mm yr^{-1} in the area around Eyjafjallajökull, as well as increasing the spatial and temporal variability between areas (Dugmore & Buckland, 1991; Dugmore & Erskine, 1994; Dugmore *et al.*, 2000). SeAR rates have remained at high levels throughout settlement, with many areas seeing large increases associated with climatic deterioration from the 15^{th} century onwards. This has been observed in terrestrial records (Dugmore & Buckland, 1991) and offshore records (Jennings *et al.*, 2001). However these changes are mostly observed in south Iceland, a marine core from Reykjarfjördur, north Iceland shows no signs of landscape erosion that can be related to the impact of settlement (Andrews *et al.*, 2001). The increasing sediment supply due to erosion is not necessarily due to increasing rates of areal denudation; the erosion of deeper lowland soils has effectively increased sediment fluxes (Dugmore *et al.*, 2009).

Vegetation changes affected, and were affected by, the soil loss. At the time of settlement, total vegetation cover was around 54% (Ólafsdóttir *et al.*, 2001), it is now 28% (LMI, 1993). Woodlands were particularly affected. Prior to Landnám, birch (*Betula pubescens*) and willow (*Salix*) woodland was widespread in areas below 300 m; the estimated woodland coverage has declined from ∼20% to 1% (Hallsdóttir, 1987). However woodland cover was not ubiquitous at low levels, especially in exposed coastal locations (e.g. Erlendsson *et al.*, 2009): its abundance has fluctuated with climate through the Holocene, and was at a high level prior to Landnám (Erlendsson & Edwards, 2009). Deforestation recorded by a decline in birch pollen occurs soon after Landnám in most areas (Hallsdóttir, 1987; Gathorne-Hardy *et al.*, 2009) but across the landscape in general the decline took place over ∼400 years (Lawson *et al.*, 2007). This fits with archaeological (Church *et al.*, 2007) and geomorphological evidence (Mairs *et al.*, 2006; Dugmore *et al.*, 2007a) that by the 14^{th} century the small areas of woodland that survive today may have been conserved for the production of charcoal. In general cleared woodland may have been replaced with heterogeneous heathland plant communities; this vegetation cover is more vulnerable to the impact of grazing than homogeneous grass sward (Gísladóttir, 2001; Dugmore *et al.*, 2009).

Soil erosion decreased the area of land available for summer grazing, but it is debated how this affected overall livestock production. Haraldsson and Ólafsdóttir (2006) model total vegetation productivity and the impact of erosion through settlement. They conclude that although soil loss did decrease productivity, this loss was not as important as the impact of temperature on fodder productivity in home fields. Rangeland grazing has always been plentiful — the greatest numbers of livestock seen in Iceland were in modern times after the cumulative effects of 1000 years of erosion.

3.5.2 Landforms associated with degradation

Typical landforms associated with landscape degradation in Iceland are erosion spots and rofabards (Figure 3.12 and 3.14). Erosion spots are patches in which the vegetation cover is <5%, leaving soil vulnerable to erosive processes. Over time these may coalesce into rofabards, which are erosional escarpments where vegetation is undercut and the escarpment retreats, leaving no or very little soil cover behind (Arnalds, 2000). This creates a patchwork of fully vegetated and barren areas, separated by active erosion fronts. Measurements of erosion based on tonnes per hectare are of limited use in Iceland, and the most appropriate measurement of degradation is the loss of vegetated mantle, measured by

hectare km yr^{-1} (Arnalds, 2000). Once a rofabard has formed the un-vegetated slopes are extremely vulnerable to erosion processes (Arnalds, 2000). Processes controlling the rate of erosion on the slope are site specific. In north Iceland they are dominated by wind saltation and in south Iceland by water erosion (rills and lateral rain impact) (Arnalds, 2000; Dugmore *et al.*, 2009). Trampling by livestock and needle ice formation also promote erosion (Arnalds, 2000). As the erosion front can be long relative to area (tens of km per km^2), Arnalds *et al.*, 2001) slow rates of front erosion (1–20 cm per year) produce large losses of vegetated area. Of importance is the density of eroding patches; if an area develops many erosion spots that then become rofabards the area will be rapidly stripped of soil. The development of rofabards in deep lowland sediments is a factor in the large increases in sediment flux seen after AD 1500 (Figure 3.13, Dugmore *et al.*, 2009).

Figure 3.12: Rofabard erosion features, Skaftártunga. Note the stripping of $>$ 5 m of Holocene sediments, and areas higher on the slope which now have no soil cover and little productive vegetation

3.5.3 Models and records of soil erosion

Based on rates of erosion gathered from tephrochronological studies in Iceland five main models of erosion have been proposed (Figure 3.15), and are discussed in the following two sections.

Dugmore and Buckland (1991) proposed an altitudinal model of soil erosion. Initially, ecologically sensitive upland areas are the focus of grazing (Figure 3.15). Erosion spots develop where the vegetation cover is breached; aeolian erosion processes rapidly enlarge these and the spots coalesce into erosion fronts which propagate down hill. The increase in exposed soil cover initiates periods of slope wash which are first commonly observed in the sediment record in

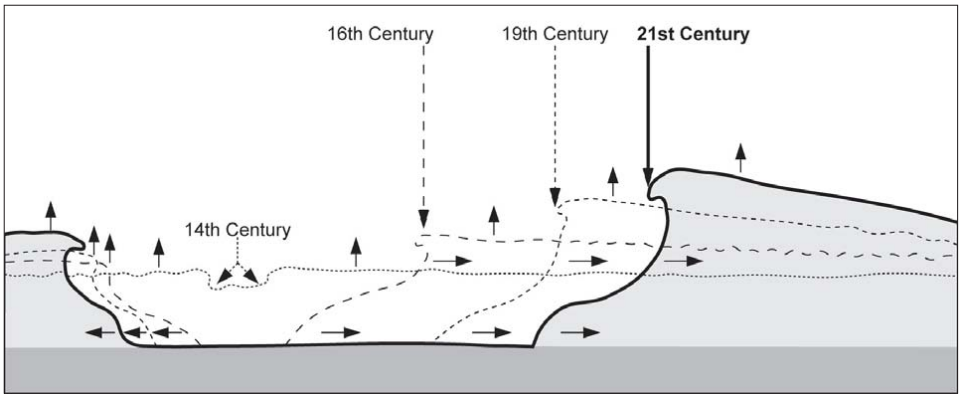

Figure 3.13: After Dugmore *et al.*, 2009. The development of lowland rofabards occurs generally after AD 1500, and due to the depths of sediment, small lateral movements generate large, localised sediment fluxes.

Figure 3.14: A hillside on Búland landholding ($\sim$ 180–240 m) shows a patchwork of areas of continuing accumulation and areas of no accumulation forms, separated by rofabard erosion fronts. This is the result of $\sim$ 500 years of erosion.

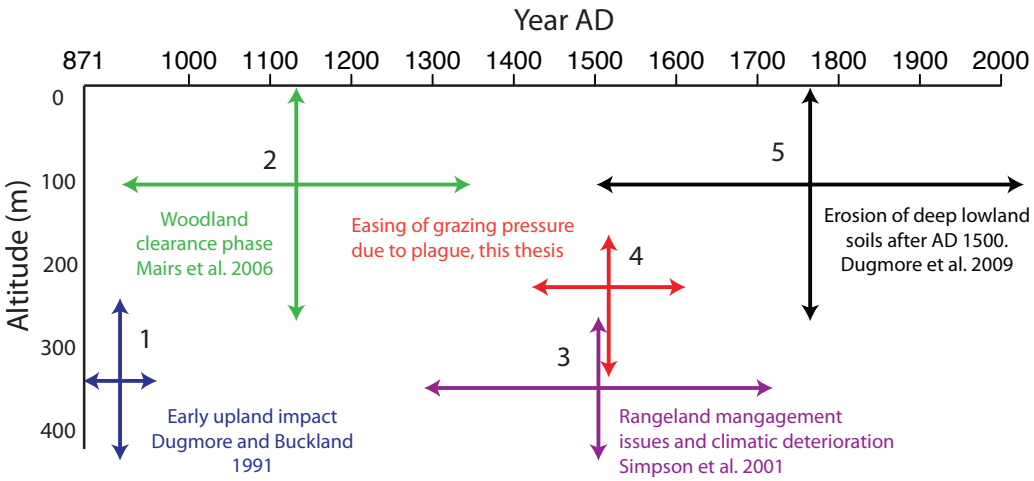

Figure 3.15: Five general models of soil erosion apply to different parts of the historical period. Refer to text for details.

southern Iceland after AD 1341 (Dugmore & Buckland, 1991). Spatial differences in SeAR rates increase from AD 1341 onwards, suggesting that local scale (tens of metres) processes become relatively more important than regional fluxes in sediment (Dugmore & Erskine, 1994). As these 'erosion fronts' reach deeper lowland soils larger volumes of sediment are released, even though the areal change in soil cover is probably similar to or less than earlier periods (Dugmore & Buckland, 1991; Dugmore *et al.*, 2009), Figure 3.16. As erosion progresses it changes the vegetation and hydrological regime at the site. Erosion can continue with low land use pressure until all possible sources of sediment are exhausted.

Gisladóttir (2001) argues that initial vegetation cover is a strong control on erosion. Heterogeneous vegetation, especially heathland dwarf-shrub communities, are more vulnerable to erosion spots forming, the first stage in more extensive erosion. By contrast homogeneous grass sward is able to resist higher grazing pressures.

Dugmore *et al.* (2009) refine the initial model of Dugmore and Buckland (1991) by considering two additional points, the role of erosion triggers and factors that control the propagation of erosion. The implication is that while grazing pressure needs to be high to trigger erosion by breaking through vegetation cover, once this cover is breached low levels of grazing will maintain the exposures of soil, and climatic factors may be more important in determining ongoing erosion rates in these cases (Figure 3.16, Dugmore *et al.*, 2009).

3.5.4 Triggers of erosion

Both climatic deterioration and grazing can trigger erosional episodes. However the relative importance of these mechanisms in the post-Landnám period in Iceland has been a source of debate. Ólafsdóttir and Guóðmundsson (2002) showed that in the area around lake Mývatn, north Iceland there is little geomorphological evidence of erosion prior to the V 1477 tephra, despite 600 years of grazing impact by this point. However climate modelling shows that this area is not marginal so the comparatively late onset of erosion is no real surprise (Casely, 2006). In addition high SeAR levels correspond with two climatically cool periods prior to Landnám, which they suggest shows that climatic deterioration is sufficient to initiate soil erosion. The alternative explanation is that these periods coincide with major tephra forming eruptions and this increased availability of sediment caused the observed increase in SeAR. The formation of turf hummocks formed by cryoturbation, known as

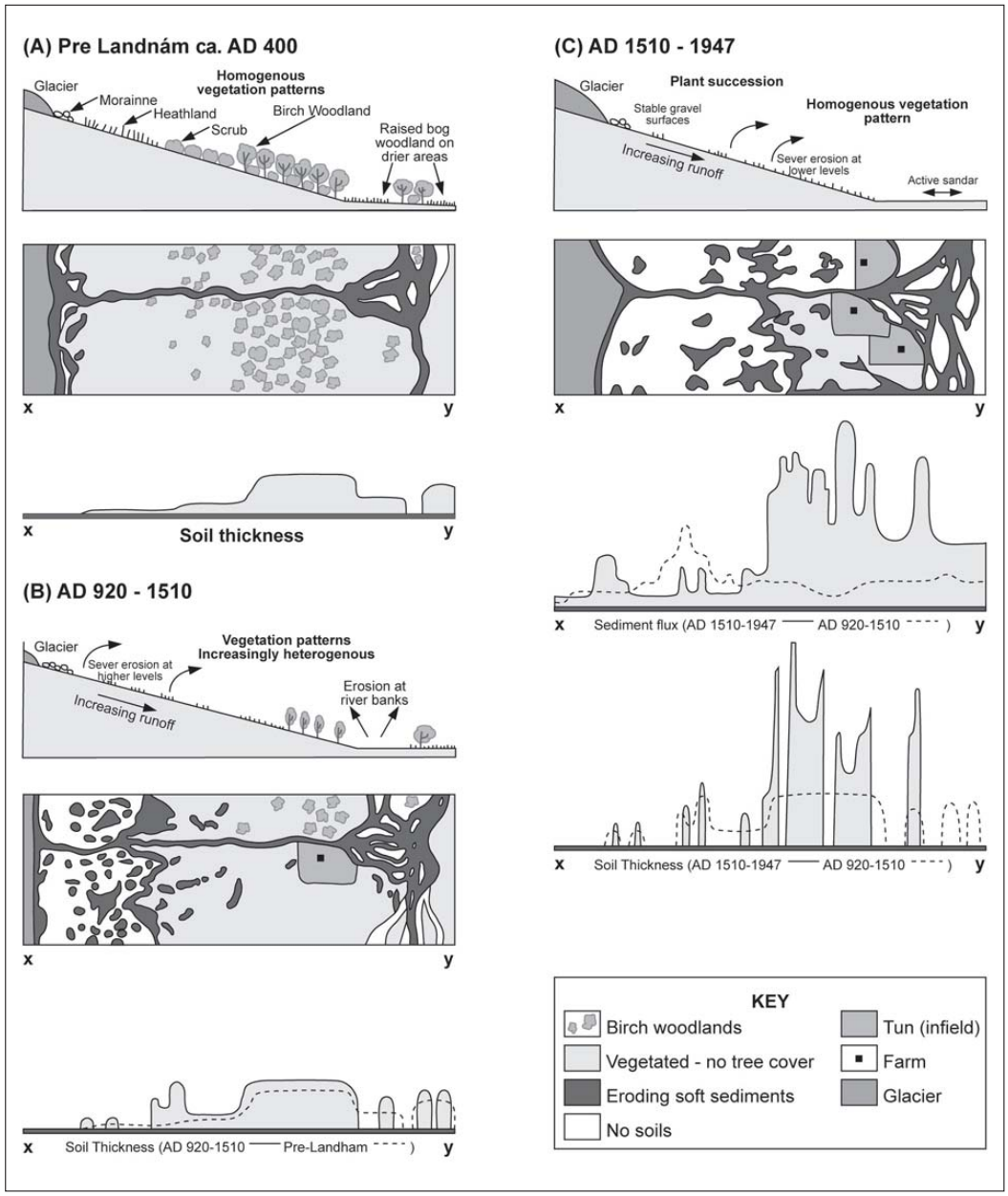

Figure 3.16: A model of post-Landnám landscape change from Dugmore *et al.*, 2009. Initial differences in soil depth are reflected in differences in sediment flux after AD 1500

thufur, in cooler periods, which are potentially vulnerable to erosion is proposed as a mechanism capable of initiating erosion without grazing.

While climatic changes were important in shaping landscape change in the late medieval period in Iceland, modelling work indicates that they alone are inadequate in explaining the pattern and intensity of landscape degradation encountered in Iceland (Simpson *et al.*, 2001; Casely & Dugmore, 2007; Thomson & Simpson, 2007). While tephra fall and bad weather are able to initiate erosion spots without human impact, over the last 1200 years the primary trigger has been grazing — either over grazing or trampling killing vegetation and creating erosion spots. Modelling of vegetation productivity calculates that total biomass productivity in the regions of Eyjafjalljökull and Mývatnssveit would have been sufficient for known livestock stocking densities (Thomson & Simpson, 2007). Therefore the impact of grazing is primarily dependant on livestock management decisions on overall stocking density, grazing duration and timing and livestock type (Dugmore *et al.*, 2009, pg 15). Simpson *et al.*, (2001) show that grazing outside the growing season is highly damaging (Figure 3.15), and although management codes (such as the Grágás law codes) regulate grazing on common land, year on year climate variability made it difficult to prevent overgrazing. The pressure on common land is also dependant on wider management decisions such as the production of sufficient amounts of fodder for livestock over winter. A shortfall in the production of fodder would force farmers to put livestock out to pasture earlier than is prudent.

A key livestock management decision that has consequences for erosion is the widespread practice of winter grazing. The process of winter grazing livestock in order to preserve hay stocks for cattle, is common throughout Iceland, especially in the milder south where rangelands are often snow free for much of the winter (Adalsteinsson, 1990). Winter grazing is potentially very damaging because the grass does not grow in this period. Simpson *et al.,* (2004) specifically look at the impact of winter grazing on SeAR and soil micromorphology in Mývatnssveit, north Iceland. They find that initially after Landnám winter grazing areas have higher SeARs, but that after AD 1200 SeARs decrease as better management techniques are used.

3.5.5 Impact of tephra fall on landscape stability

Tephra fall affects a landscape's susceptibility to erosion. The impact is dependant on the depth of tephra, season of tephra fall, particle size and the underlying vegetation cover. In some cases thick tephra fall coincides with the

stabilisation of landscapes, but this effect is more probably due to the eruption triggering settlement and or land management change (Edwards *et al.*, 2004; Dugmore *et al.*, 2007a). Thórarinsson (1961) noted that in Þjórsárdalur after the Hekla AD 1104 eruption, farms within the 10 cm isopach of tephra fall were permanently abandoned. However tephra fall thinner than vegetation cover may act to promote grass growth, through the smothering of competition, and the insulating effect provided by the tephra. The implication is that tephra falls of < 10 cm do not appear to affect long term settlement or to destabilise slopes, and may in fact benefit taller vegetation. This is supported by data from this study, which shows that where tephra depth is <10 cm, there are signs of post-depositional reworking in 3.7% of stratigraphic units after the tephra, while where tephra depth is >10 cm, there is post-depositional reworking in 42% of stratigraphic units after the tephra.

3.6 Key points

- The 'Black Death' affected most of Europe and altered land use strategies for a period of 200 years. It occurs twice in Iceland in AD 1402–1404 and AD 1494, killing around 30% of the population on each occasion. The plague was one of a series of demographic declines in Iceland, with declines of ∼20% occurring three times in the 18^{th} century.
- Indicators of reforestation of abandoned land and a change from intensive to extensive land use have been observed in palynological records from across Europe in the period AD 1350–1400.
- Skaftártunga is a well constrained geographical area that has been affected by the impact of frequent volcanic eruptions, the most severe of which are Eldgjá in AD 934-940 and Laki in AD 1783.
- Climatic changes in Iceland can be summarised as a relatively warmer and more stable than average climate in AD 500–1300, and a subsequent deterioration into the LIA which occurred over the period of AD 1300–1500. The LIA was on average cooler and stormier, but with high variability on the scale of decades. The 15^{th} century when the plagues take place was a period of rapid climatic deterioration.
- Iceland's vegetation and soil cover has been extensively modified by the impact of grazing over the past 1200 years. Although climate can trigger erosion, over the past 1200 years most erosion has been triggered by the impact of grazing animals.

Chapter 4

Methodology: Environmental Records

4.1 Introduction

Tephrochronology, a method based on the identification, correlation and dating of volcanic ash (tephra), is a powerful tool for chronological control and for investigating past episodes of landscape change (Thórarinsson, 1944; Dugmore *et al.*, 2009; Lowe, 2011). To maximise the information that can be extracted from stratigraphic sections it is important to be able to correctly identify as many tephra isochrones as possible so that the highest resolution sequence is extracted; this is especially important for periods of rapid environmental change. Aeolian sediment accumulation rates (SeAR) can be used as proxy for soil erosion in Iceland (Thórarinsson, 1961; Dugmore *et al.*, 2009), so it is important measurements are as precise as possible and can capture variability in the stratigraphy. Dating multiple sections allows the tracking of variations spatially across a landscape.

This chapter describes methodologies used to collect field data. Primary data was collected in three field seasons: July-August 2008 and 2009 and June 2010. The tephrochronology was established by linking field measurements to chronologies in the literature, major element geochemical analysis of key sequences and the dating of tephra layers of unknown age based on inter-calated sediment accumulations from tephras of known age. Techniques used for recording sediment accumulations are discussed, including the development of a photogrammetric based approach to recording soil sections which increases the number and precision of measurements.

4.2 Establishing a tephrochronology

The first stage of building a tephrostratigraphy is the identification of primary layers within sequences, as opposed to reworked tephra which may be diachronous and therefore of limited utility for dating. This was done by referring to published chronologies, selective geochemical analysis and field mapping of layers in multiple sections (Figure 4.1). Field observations of the tephra provide information which assists in determining if a layer is primary fallout. Primary fallout tephra usually has a distinct colour from surrounding sediment, a sharp contact at its base and no internal bedding features. Geochemical analysis of tephra can also help to distinguish the difference between primary air fall deposits and reworked secondary material. The presence of weathered shards and a heterogenous chemical composition indicates that the layer is probably reworked material, therefore the stratigraphy it defines is not contemporaneous with the tephra forming eruption and the layer is not necessarily an isochrone (Boygle, 1999).

While tephra deposits from large eruptions can be expected to occur in most profiles, tephra from smaller eruptions or tephra at the margin of its contiguous distribution may only be found infrequently in sections. However the identification of these layers is important. Firstly firm identification prevents confusion between these layers and other primary fallout deposits within the sequence, a particular problem where a tephra layer at the margins of its known distribution is well expressed and a similar tephra well within its known distribution is poorly expressed. Secondly if the marginal layer can be positively identified it can be added to the chronology. A particular challenge was the mapping and identification of two tephras from the Grímsvötn volcanic system in the 15^{th} century. These have been published from single sections and in composite chronologies (Larsen, 2000; Óladóttir *et al.*, 2005), but have not been mapped because of the small number of sections where they have been found (Guðrun Larsen, personal communication).

Once primary fallout layers are identified they can then be correlated to a particular volcanic eruption. As the composition of magma varies between volcanic systems major element geochemical analysis of shards of tephra allows the identification of the source volcanic zone. However in most cases major element analysis is unable to distinguish tephra to the specific eruption, as in Iceland many tephras from different eruptions have similar major element compositions (Larsen & Eiríksson, 2008b).

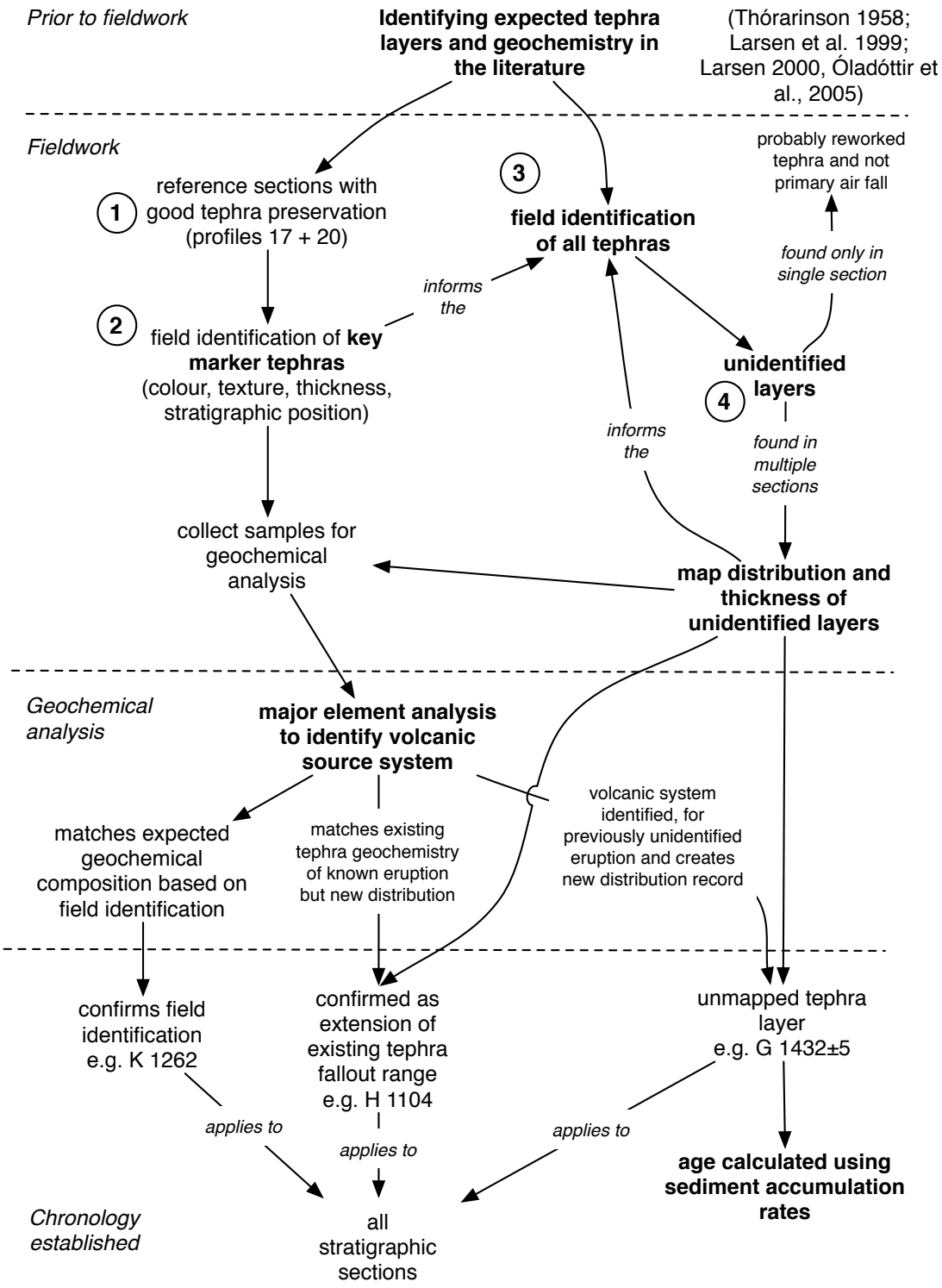

Figure 4.1: Steps to establish a tephrochronology in the field based on an existing tephrochronology. Field identification and selective geochemical analysis is used to correlate tephras to particular eruptions. Tephras which are not in the literature are identified either as extensions of existing distributions, un-mapped tephras or reworked older material.

4.2.1 Mapping of tephras

The tephrochronology of Iceland over the Holocene is well known (Larsen & Eiríksson, 2008b) and for Skaftártunga in particular (Thórarinsson, 1958; Larsen, 1984; 2000; Larsen *et al.*, 2001; Óladóttir *et al.*, 2005). The challenge was to translate the published chronology and reference sections into a wider chronology for the area across a wide range of geomorphic conditions and depositional environments. One approach is to look for reference sections which might be expected to have a particularly complete record of tephra fall (Figure 4.1, step 1). However because of reworking a composite overlapping record is also necessary (Boygle, 1999). Key 'marker horizons' — easily field identifiable tephras that cover the entire study area — were identified from the published chronologies (Figure 4.2 and 4.3). These were L 871±2, E 935, H 1206, K 1262, K 1416, K 1625, K 1755 and K 1918. Tephras were identified on the basis of their grain morphology, colour and stratigraphy.

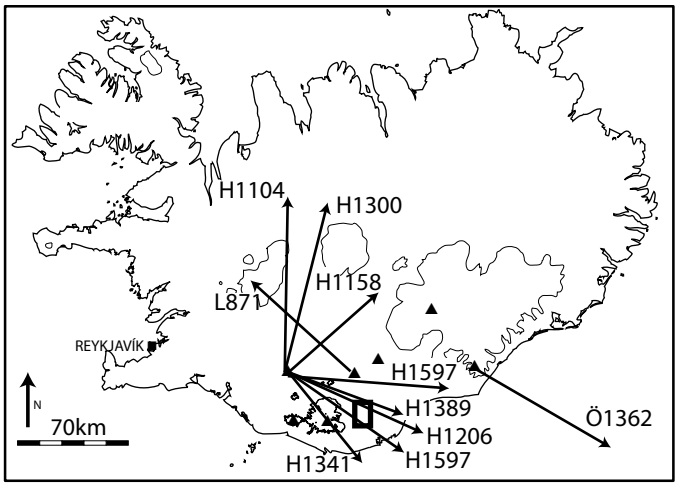

Figure 4.2: Main axis of fallout for post-Landnám silicic and intermediate tephras found in Skaftártunga (boxed region). Based on Larsen *et al.*, 1999; 2001.

4.2.2 Major element geochemical analysis

Major element geochemical analysis is a widely used, relatively low cost technique that makes it possible to distinguish the volcanic provenance of tephras on the basis of their elemental composition (Lowe, 2011). However within Iceland the geochemical composition of source areas overlap (Larsen & Eiríksson, 2008a), and there are often multiple tephras from the same volcano within a sequence, so geochemical analysis alone may not be diagnostic (Westgate & Gorton, 1981). The combination of geochemical analysis and a

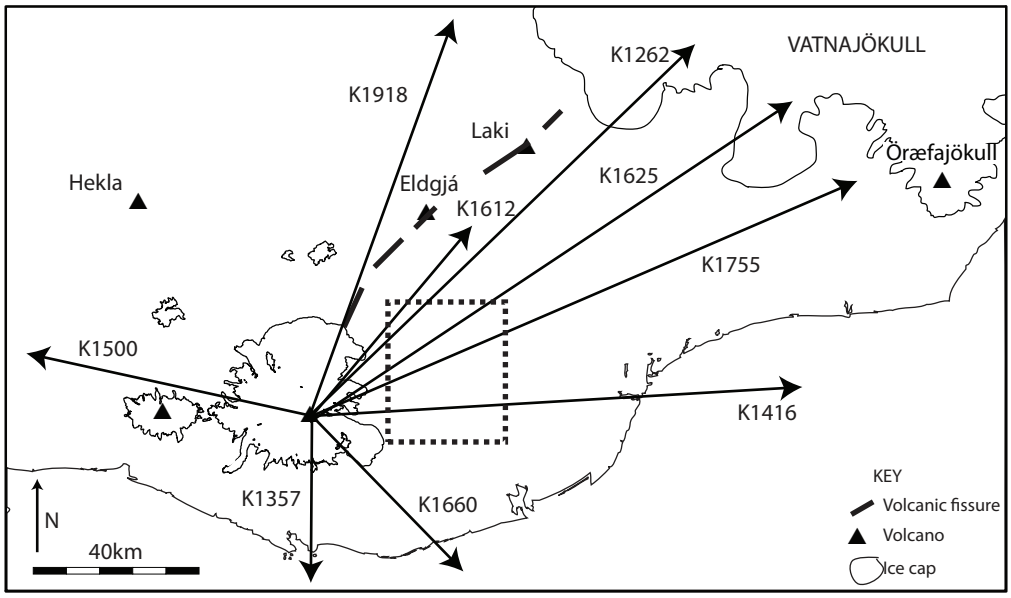

Figure 4.3: Main axis of fallout for basaltic tephras found in Skaftártunga (boxed region) since AD 870. Based on Larsen, 2000.

tephra layer's stratigraphic position gives a better chance of correlating a particular layer with an eruption. The number of profiles recorded (200) and number of tephras identified (2625) means that geochemical analysis was impractical for more than a few tephras from key profiles. It was used here to confirm that field identified stratigraphy in reference sections matched that published by (Larsen, 2000; Larsen *et al.*, 2001; Óladóttir *et al.*, 2005) and to clarify the complex stratigraphy of the 15^{th} century which has five tephra layers.

Sampling locations

Sites for sampling were chosen based on a wide geographical coverage because thin tephra layers can have a patchy distribution, and stratigraphic sections sampled are displayed in Section 5.2, Table 5.2. Sampled sites had high sediment accumulation rates which clearly separates chronologically close layers, and sites that showed signs of fluvial reworking were rejected. Sampling was concentrated on layers which were harder to differentiate based on their field characteristics, especially layers from the 15^{th} century which were sampled over a wider range of sites because this time period was critical to the project. In two reference profiles (profiles 17 and 20) most post-Landnám tephra layers were sampled.

The majority of samples (30) were collected in 2008, with further samples taken in 2009 (6 samples) and 2010 (7 samples) to confirm sequences where the chronology was unclear. Samples were collected using a clean spoon from the base of the tephra layer to ensure only primary air fall tephra was collected.

They were then bagged and labelled along with field interpretation of the tephra.

Slide preparation

Samples were visually checked to see what proportion of tephra they contained. As Skaftártunga is close to the volcanic systems which are the source of the tephras found and samples were only collected from clean stratigraphic sections they all contained nearly 100% tephra, so it was deemed unnecessary to clean them further. Slides were prepared using the techniques outlined in (Dugmore *et al.*, 1995b) and following the guidelines on slide preparation from the Natural Environment Research Council (NERC) Tephra Analytical Unit (http://www.geos.ed.ac.uk/facilities/tephra/). Glass slides were frosted on one side before sample areas were marked out using a pencil. Samples were then floated in water before being placed on the slide using a dropper and dried. Araldite resin and hardener was mixed in with the sample to fix it to the slide and heated to 80 °C for one hour to cure the resin. Once all the samples were fixed they were sanded using progressively finer grade abrasive paper (180, 400, 800, 1200 and 1600), making sure that sample thickness did not go below 0.1 mm. This stage exposes the glass shards for cross section analysis. The slides are then cleaned in a solution of petroleum ether in a beaker in an ultrasonic (USM) bath for 10 minutes to remove any loose material. The slide was then polished for 10 minutes with 6 μm diamond paste, cleaned in the USM for a further 10 minutes, and then polished for 10 minutes with 1 μm diamond paste. At this stage the samples are checked under an optical microscope with both reflected and transmitted light for scratches which can affect analysis totals. If scratches are found the slide is polished until scratches are removed. When this is satisfactory it is cleaned again in the USM bath for 10 minutes. The slides were then carbon coated at the analytical facility in order to distribute the charge during analysis (Reed, 1993).

Microprobe analysis conditions

The samples were analysed in three separate trips to the NERC Tephra Analytical Unit at the University of Edinburgh. They were analysed on a Cameca SX100 electron microprobe using the analytical protocols from Dugmore *et al.* (1995b). Before each batch of analysis the machine was calibrated to known standards (see Appendix C). Each analysis measured the percentage weight of Si, Al, Ti, Fe, Mn, Mg, Ca Na, K and P. The analysing beam used a current of 2 nA, an accelerating voltage of 15 kV and a beam

diameter of 10 μm. 10 shards were selected visually for analysis by selecting for unweathered shards, a lack of crystalline inclusions and a lack of vesicles, although for several samples less than 10 analysis were successful. Raw EMPA totals of < 95 wt% were discarded (Hunt & Hill, 1993). After analysis samples were compared with published geochemical compositions for tephra from Icelandic volcanic systems, using TEPHRABASE (www.tephrabase.org and published analysis Jakobsson, 1979; Larsen *et al.*, 1999; 2001; Óladóttir *et al.*, 2008; 2011a). Binary plots of oxides (TiO_2 vs CaO, FeO vs TiO_2, SiO_2 vs FeO/TiO_2 and K_2O vs TiO_2) were used to compare the measured compositions to known compositions for that tephra. Analysis results are presented in Section 5.2.

4.2.3 Dating tephra layers

The majority of tephra layers found post-Landnám in Iceland are from eruptions which have been correlated to the historic record (Thórarinsson, 1944; 1967, e.g. the eruption of Hekla at 9 am on the 19^{th} of May in AD 1341) but prior to AD 1500 the recording of eruptions is less reliable due to fewer written records — especially for small eruptions located far from habitation. In this area two tephra layers from eruptions at Grímsvötn between AD 1416–1477 were undated. To date tephra layers of unknown age it is possible to use radiocarbon dating of organic material associated with the layer (e.g. Dugmore *et al.*, 1995a; Larsen *et al.*, 2001), radiometric dating (Naeser *et al.*, 1981; Lowe, 2011), the counting of annual layers in ice caps (Steinthorsson, 1977; Gronvöld *et al.*, 1995; Zielinski *et al.*, 1995; Larsen *et al.*, 1998; Vinther *et al.*, 2006) and sediment age-depth models inter-calated from tephras of known age (Óladóttir *et al.*, 2005; 2011b). Radiocarbon analysis is reliant on rapidly accumulating organic deposits which are missing in this field area. Radiocarbon can at best give age uncertainties of $\pm$12 years (i.e. for the Hekla 4 tephra, Dugmore *et al.*, 1995a), which limits its use when tephras are chronologically separated by 20–30 years. Grímsvötn eruptions have been dated with relative precision from tephra within Vatnajökull ice cores (Steinthorsson, 1977; Larsen *et al.*, 1998), but because it is not generally possible to distinguish individual eruptions by their major element geochemistry it is difficult to match these records with stratigraphic sequences surrounding Vatnajökull. Previous applications of sediment age-depth models in Iceland have large uncertainties associated with them ($\pm$250 years, Óladóttir *et al.*, 2005) and are based on small numbers of measurements between radiocarbon dated pre-Landnám tephras. Age-depth dating was selected as the best method because sedimentation rates were high and the collection of large

numbers of measurements of sediment accumulation would reduce uncertainties.

To estimate the age of the undated tephras from Grímsvötn (layers G 1 and G 2) two sediment profiles (Profiles 153 and 179) with undisturbed high rates of aeolian accumulation and even tephra layers were selected. High sedimentation rates (on average 0.55 mm yr^{-1}) ensure the separation of layers which are closely spaced chronologically, and the age gap between known marker horizons was small (61 years). Single measurements of accumulation to relatively poor accuracies (±2.5 mm) have significant errors associated with them. Photogrammetric measurements (Section 4.3.4) were used to collect 985 measures of accumulation between K 1416 and G 1 and 975 measurements between G 2 and V 1477. Measurements were to ±1 mm precision from open sections 1 m wide. Since sediment accumulation rates vary greatly in the historical period (Dugmore & Buckland, 1991; Dugmore *et al.*, 2009) profiles were selected where SeAR showed stability over the period between the tephras of K 1262 and H 1597. An age depth model was constructed based on linear accumulation rates between K 1416 and V 1477. This provided an age estimate for each layer based on its distance from layers of known age (K 1416 and V 1477 for upper and lower Grímsvötn layer respectively). Standard measurements (±2.5 mm, Section 4.3.3) from profiles where all four layers were found were used to provide an independent estimate. This should be less susceptible to changes in sedimentation rates within the profile as measurements are compared between profiles. The accuracy of this technique was tested by dating layers of known age. The K 1262 layer was dated by inter calculating its age from the tephras H 1206 and H 1300. This provided an age of AD 1264 ±10 (mean ±1σ, n=97) which demonstrates that even at low measurement resolutions it is possible to date tephras with SeAR methods at precisions comparable to radiocarbon dating.

The advantages of using multiple measurements is that the statistical robustness of the age estimate can be calculated, a component which is missing from most age depth models used to date tephra layers in sedimentary sequences so far. Although age estimates gathered using this method could be improved in the future, the advantage of tephrochronology is that the relative relationships in the sedimentary sequence still hold if the dating of the layers was improved.

4.3 Measurement of sediment sequences

As sediment accumulation rates have been used extensively to record and quantify landscape change in Iceland (Dugmore & Buckland, 1991; Dugmore & Erskine, 1994; Dugmore *et al.*, 2000; Simpson *et al.*, 2001; Dugmore *et al.*, 2009)

it is important that measurements are made to the highest possible precision and accuracy. In this section the methods used to gather both standard stratigraphic measurements and a new application of photogrammetric techniques to measuring soil sections are described.

In addition to measurements of sediment accumulation other characteristics within stratigraphic sequences can provide additional information. Tephra depth can be used to map primary fallout and also to infer depositional processes. The presence of sand, gravel or reworked tephra layers implies fluvial activity. Structures within the tephra layers themselves such as thufur show periods of high grazing or poor climatic conditions. Gaps in the tephra can indicate the presence of woodland vegetation at the time of tephra fall.

4.3.1 Advantages of measuring to high resolution

The combination of multiple vertical measurements of accumulation from different sections located in both similar and contrasting parts of the landscape has helped to reveal important patterns of landscape change in Iceland (e.g. Dugmore *et al.*, 2009). Although the process of aeolian erosion of soils in Iceland is driven by wind, rain and frost, and the intensities of these natural processes vary across the landscape, it is apparent that major differences in landscape instability are driven by land use (Simpson *et al.*, 2001; Gísladóttir, 2001; Dugmore *et al.*, 2009). Broad patterns can be distinguished using comparatively low resolution measurements, typically ±2.5 mm, if they are considering periods of century-scale duration and accumulations of tens of centimetres of sediment. The frequency of volcanic eruptions in Iceland and the utility of the tephrochronological record mean that more subtle variations taking place at decadal scales may also be considered. At higher resolutions, critical for the examination of human-ecodynamics, a key question is how best to distinguish environmental signals from background 'noise'.

Multiple measurements go some way towards addressing this problem, providing measures of the central tendency of the sediment accumulation data which can be considered representative for the measured sections. Many manual measurements can be recorded to ±1 mm, with typically 50 measurements per layer. This approach gives data more amenable to statistical analysis: however, it is time consuming. Using photogrammetric techniques (Section 4.3.4) thousands of precise (±1 mm) measurements may be collected per profile relatively easily. Typically 200–500 measurements of sediment accumulation rate can be made per layer, compared to one using conventional logging techniques, or 50–200 using labour intensive manual field measurement techniques (Figure

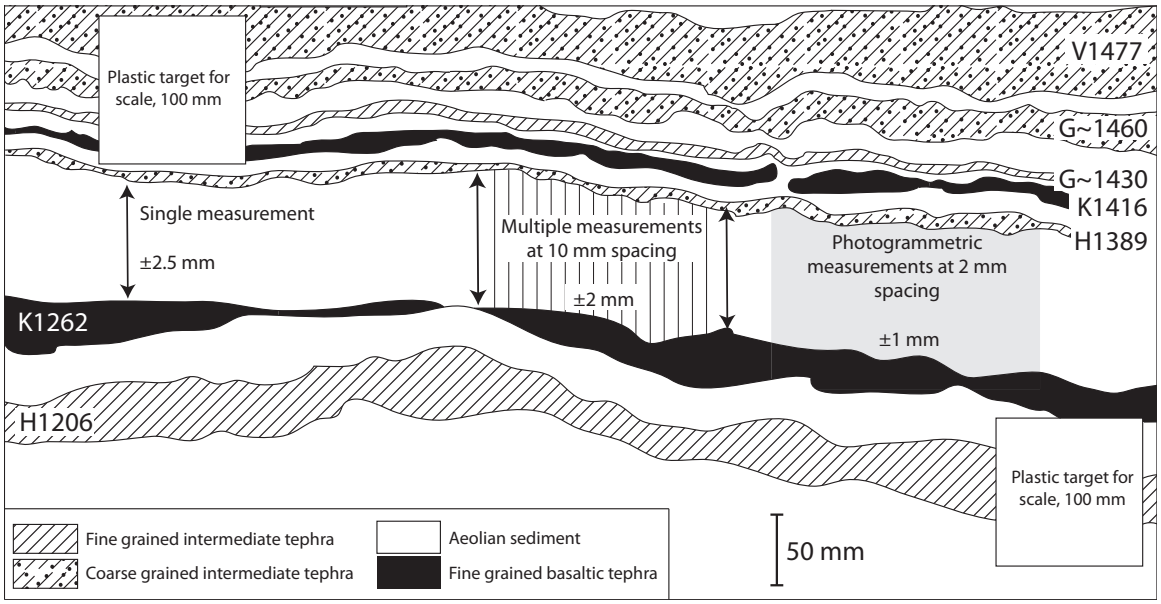

Figure 4.4: Traced photograph of stratigraphic section (profile 179), south Iceland, showing large variations in depths between tephra layers and illustrating different recording techniques used. There is great variability in the thickness of tephra and the sediment between over cm scales, therefore measures of thickness based on small numbers of measurements are unlikely to be representative.

4.4). This expansion in number and density of measurements is highly significant. Summary statistics of sediment accumulation rate can be created that are more representative of actual sediment accumulation rate. This allows greater confidence in identifying subtle variations in landscape trajectories which either go unnoticed or are masked by inaccuracies in manual recording techniques. Better measurements of tephras in sediments may reveal aspects of tephra taphonomy. This could inform the understanding of processes acting on tephras before and after they are incorporated into the stratigraphic record.

4.3.2 Selecting profiles

Once the chronology was resolved profile locations were located in order to investigate specific landholdings, landscape units and altitudes. The landholdings of Hrífunes, Flaga, Hilð, Búland, Snæbýli and the area surrounding the abandoned sheiling site of Búlandssel was targeted, as well as a large area (100 km^2) of communal grazing. Profiles were recorded down to the Landnám tephra where possible, with 12 sections recorded to pre-Landnám tephra layers in order constrain pre-settlement environmental change. Profiles were mostly located on the edge of active eroding soil sections in order to minimise the impact of digging. Where possible two or three profiles were

located within 100 m of each other to try and determine the effect of localised sediment sources on sediment accumulation. Some profiles were recorded in recently dug ditches on the landholdings of Snæbýli and Hilð. These areas are often in home fields which tend to have little exposed soil, so are under represented in the sampling strategy. An additional advantage is that by digging directly into the soil structure these profiles do not have any SeAR increases as a result of their proximity to an eroding front.

4.3.3 Standard measurements

Sections were cleared to a minimum width of 50 cm, but in most cases 100 cm. This was important because the thickness and the presence or absence of tephra layers can vary over short distances due to both depositional effects at the time of the eruption such as vegetation (Dugmore *et al.*, 2009) and also due to post-depositional reworking for instance by cryoturbation processes (Kirkbride & Dugmore, 2005). The section was cleaned to make it as clear as possible. Profiles were logged from the surface down to a resolution of ±2.5 mm. For each tephra and sediment section the particle size, colour and thickness were noted. Particle size was estimated from field characteristics and classified according to Table 4.1. Where thickness varied substantially a representative thickness was selected and the range of depths noted. Tephra layers were identified to source and age as far as possible at this stage (Figure 4.5). In addition, other characteristics were noted such as the presence of erosional surfaces, reworked tephra layers, evidence of fluvial erosion and the presence of cryoturbation features such as thufor. Finally a location using GPS and an altitude for the section was recorded. If the section was suitable for photographic measurements (Section 4.3.4) these were taken in addition to standard measurements in field seasons in 2009 and 2010. In some areas multiple measurements of accumulation were recorded across a section face. Typically 50–100 measurements at ±2 mm were recorded at 1 cm intervals for comparison with and to supplement measurements gathered using photogrammetric techniques.

Table 4.1: Classifying particle size

Grain Size (mm)	Field classification
>2	Very coarse
0.5–2	Coarse
<0.5	Fine

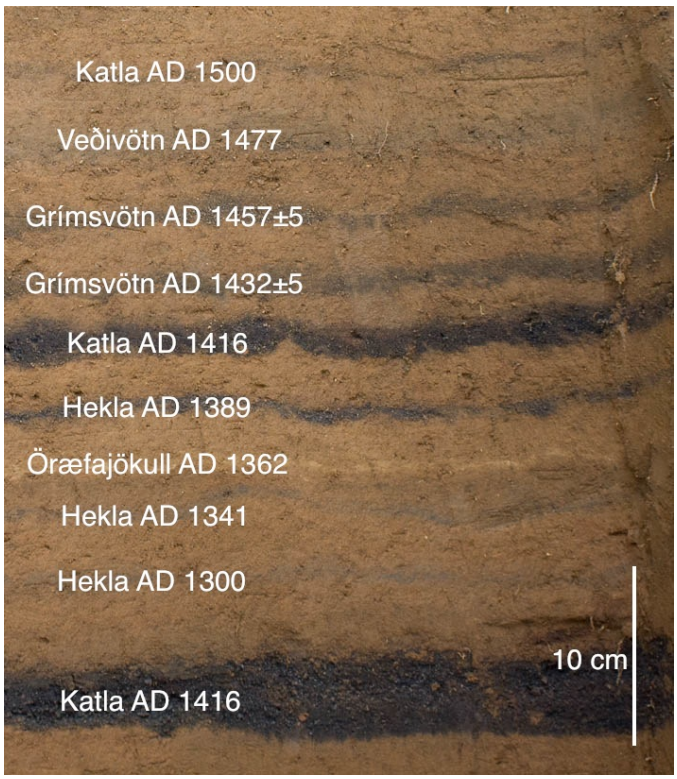

Figure 4.5: Tephra were field identified based on their colour, which changes with increasing SiO_2 content from black (Katla), through brown (Grímsvötn), olive-green (Veiðivötn), blue-grey (Hekla), yellow-white (Hekla) to white (Öræfajökull). Photo from profile 151.

4.3.4 Photogrammetric measurement

Photogrammetric techniques are used to provide accurate spatial 2-D and 3-D measurements in geomorphology at long and close distances (Chandler, 1999; Pike, 2000). The availability of high specification, commercially available digital cameras means that these have replaced the more expensive calibrated cameras for many applications where cost, convenience and portability are issues. Although not as accurate or stable as calibrated metric cameras, commercially available cameras have been used successfully in many scientific applications and as resolution increases and prices decrease their accuracy increases and in some cases matches that of metric cameras (Chandler, 1999; Ahmad A, 1999; Wackrow *et al.*, 2007; Rieke-Zapp *et al.*, 2009). They are also typically smaller and more portable which is useful in remote field areas where large metric cameras and their rigging would be hard to transport (Rieke-Zapp *et al.*, 2009). Self calibration packages allow the quantification of unknown internal camera geometry (Bouguet, 2000). Precision depends on the application but is generally $< \pm 1$ mm for close range images. The use of photogrammetric techniques for geomorphology is an expanding field but most applications so far

have been in capturing 3-D surfaces (Chandler, 1999). 2-D imaging is more straightforward and is of potential use for applications which may previously have dismissed these techniques because of cost or complexity. Cameras are seen as an aid to qualitative approaches, but are not often considered part of the measuring equipment carried in the field (Rieke-Zapp *et al.*, 2009). Here photogrammetric techniques are applied to the problem of collecting many high resolution measurements of sediment thickness at a greater possible accuracy than previously.

Field collection of images

Sections which could be easily widened and had a suitable platform for photographing were selected. The face was cleaned back to present a flat surface and made as vertical as possible. Sections were cleared to a minimum width of 50 cm. Excess roots were trimmed back. The tripod and camera were located 1–2 m away from the face of the profile, and the axes of orientation were perpendicular to the section face (Figures 4.6 and 4.7). A spirit level attached to the top of the camera ensured that it was level. Square 10 cm plastic targets were used to set the scale for each photograph. At least two targets were attached to the face of the profile to check the scale was constant over the image. A sediment log of the profile was made to a resolution of ±2.5 mm, for the identification of tephra layers. For a subset, multiple measurements to a precision of ±2 mm were recorded for direct comparison with measurements obtained from the photographs (Figure 4.4).

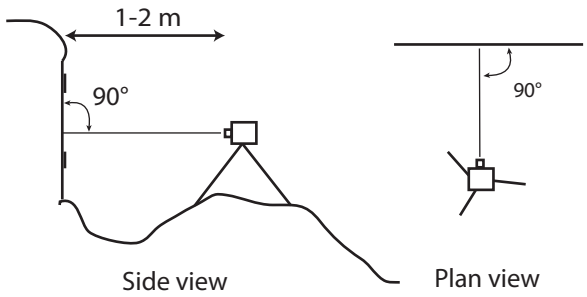

Figure 4.6: Camera orientation for photographing soil sections.

The camera used was a Canon EOS 1000D digital single-reflex (DSLR) camera, used with a Canon EF 28mm f/2.8 lens and mounted on a tripod. DSLR cameras are a suitable choice because they produce high quality photos and can capture more light than compact cameras. This lens allowed the

photographing of a wide section of soil at distances of under 3 m from the profile. This characteristic was essential as erosional faces often slope away sharply so at distances of greater than 3 m away from the section face it would not have been possible to place the tripod. Lenses with a focal length of less than 24 mm should be avoided because of large radial distortion. Fixed focal length lenses are preferable because distortion produced by the lens is more predictable, however zoom lenses can be used if care is taken to quantify the internal geometry (Chandler *et al.*, 2005).

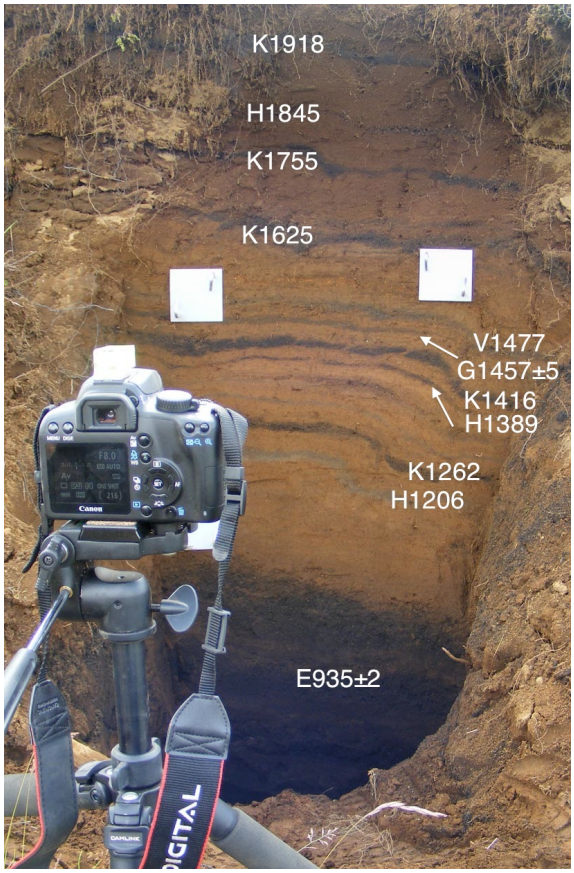

Figure 4.7: Photograph of set up used for photographing stratigraphic sections. White plastic squares attached to section face are markers for scale.

Camera calibration and measurement of sediment accumulation

Non-metric cameras should be calibrated before use in photogrammetric applications (Chandler, 1999; Wackrow *et al.*, 2007). This quantifies distortion caused by the lens (radial distortion) and internal camera geometry, which introduces systematic errors. The Camera Calibration toolbox for the program MATLAB was used to calibrate the camera and lens combination used in the field (Bouguet, 2000). This software runs a form of self-calibrating bundle

adjustment to determine the internal geometry of the camera and the lens distortion, based on a series of calibration images. The average pixel error for this camera and lens combination was x ±1.12, y ± 1.29, with distortion much greater at the edges of the image than the centre (Figure 4.8). At the scales typically used in this study (2–4.5 pixels/mm) this gives a distortion error of x ± 0.26–0.60 mm and y ± 0.27–0.64 mm. The internal characteristics of the camera set up are able to produce results of < ±1 mm at 2 m from the profile face.

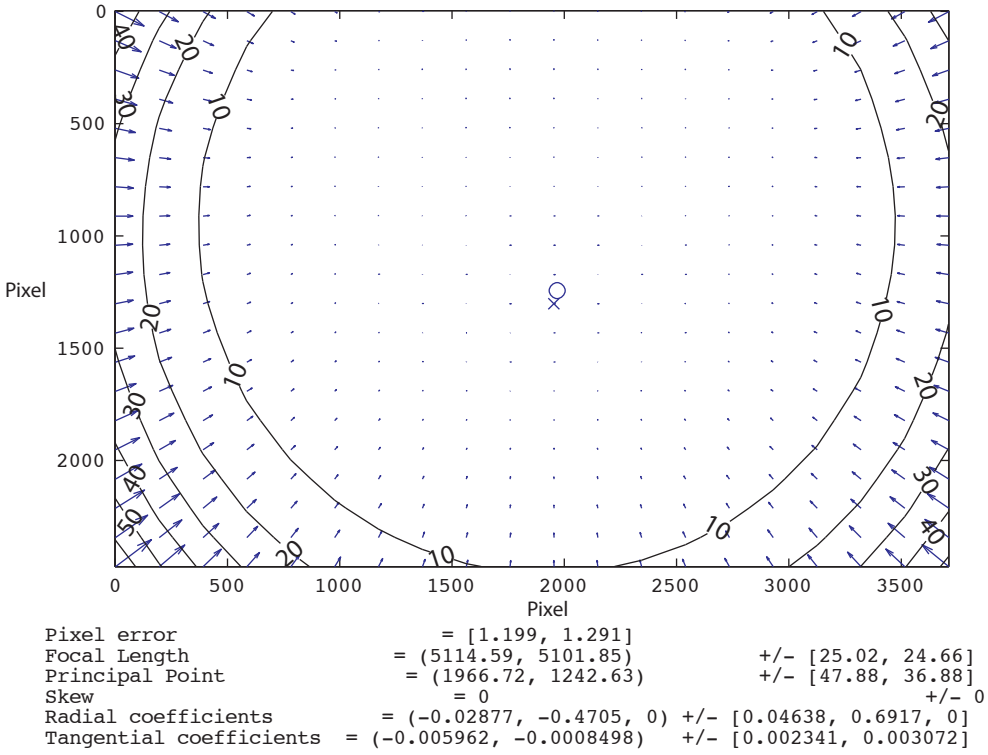

Figure 4.8: Total camera distortion (sum of radial and tangental distortion) from the MATLAB camera calibration toolbox (Bouguet, 2000). Distortion in the centre of pictures is low but significant at the edges. To minimise distortion only measurements > 500 pixels from the image edge should be used.

Photos were taken in RAW format at 3906 x 2602 resolution and adjusted for contrast and white balance using Adobe Photoshop and then converted to JPEG. In some cases the sharpening function was used to enhance the visible contrast between layers. After initial processing measurements were taken using the imaging software ImageJ (http://rsbweb.nih.gov/ij/). A plugin was written for the software which allows the user to trace a layer visible on the photo and the x_1y_1 coordinates are saved for all points along the line. Further details and the source code is in Appendix A. The user then traces the base of the next tephra layer, saving these x_2y_2 coordinates. $y_1 - y_2$ is calculated in pixels where

$x_1 = x_2$. Where values of $x_1 \neq x_2$ no distance is recorded. The scale was determined from the mean of 10 measurements of plastic scale targets in pixels. Scale was calculated individually for each image, as the distance between the camera and section varied dependant on site conditions.

4.3.5 How many measurements are necessary?

The number of measurements required to gain a representative measure of the mean depth of a sediment depends on the variability in depth at the scale of an individual profile (10–100 cm). Measurements of sediment thickness between tephras in this study show that this variability generally increases with the depth of accumulation (Figure 4.9).

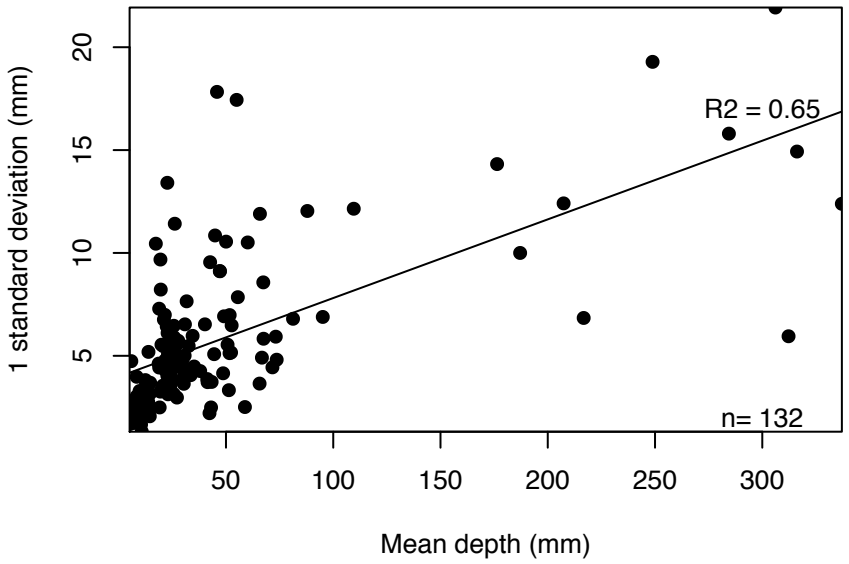

Figure 4.9: Variability in accumulation depths between tephra layers at cm scale increases with increasing depth between tephras.

The number of measurements needed to get representative mean values to a 95% confidence interval for different levels of variance can be calculated simply by using a formula based on central limit theory, which is $n = 16\sigma^2/W^2$, where W is the width of the confidence interval in units (in this case mm). Although the distribution of thicknesses measured is not normally distributed this approach gives an approximation of the number of measurements needed (Figure 4.10). Based on 132 measurements of sediment depth which give a mean standard deviation of 5.8 mm, 22 measurements are needed to have 95% confidence in the mean to ±2.5 mm (Figure 4.11).

In practice single measurements are not randomly selected so accuracy can be higher, but in the samples here 17.5% of single measurements fall outside the

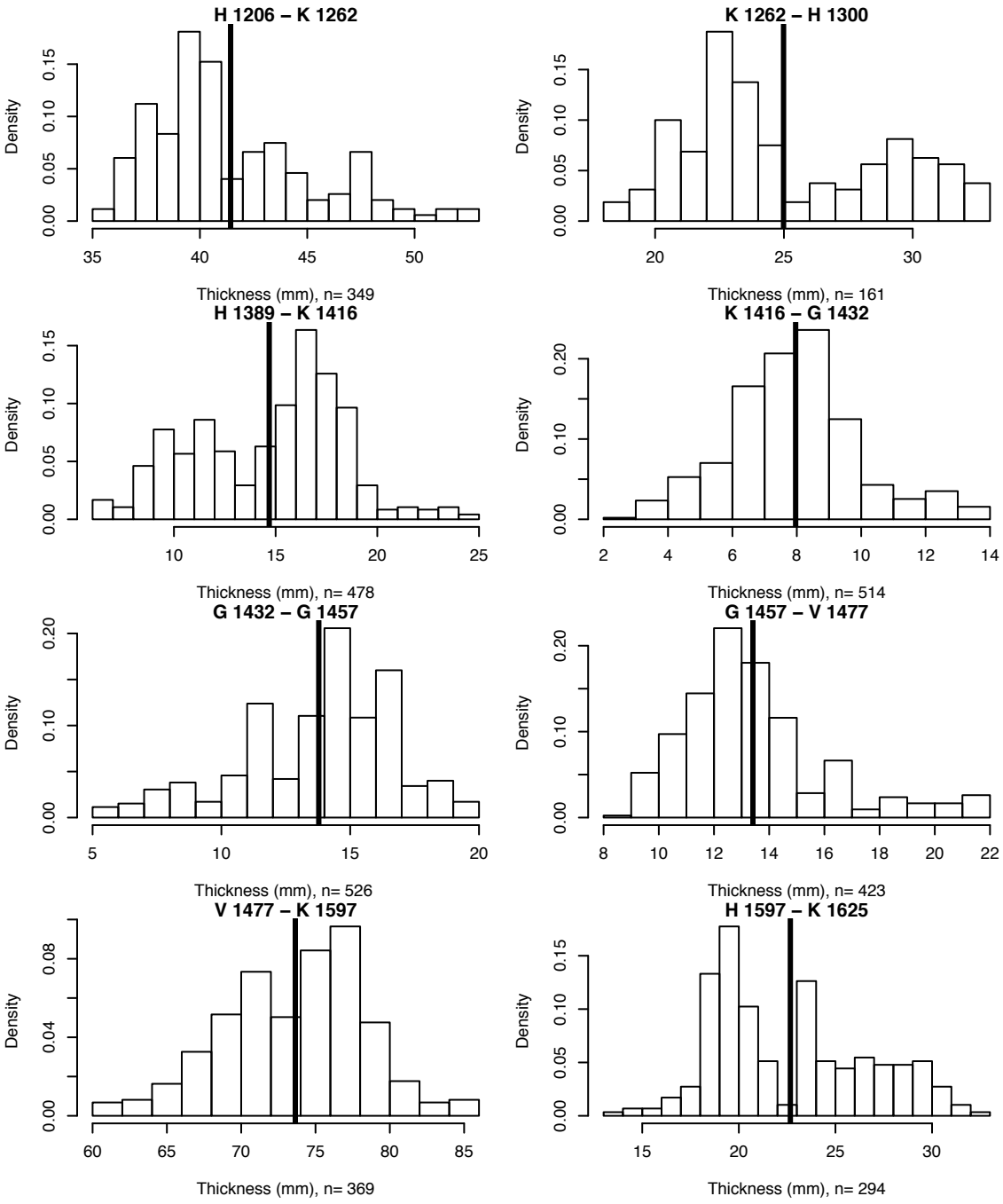

Figure 4.10: Probability density histograms of photogrammetric measurements from Profile 153. Bold vertical lines show the mean of the measurements. Note the wide range of variability that measurements are trying to capture.

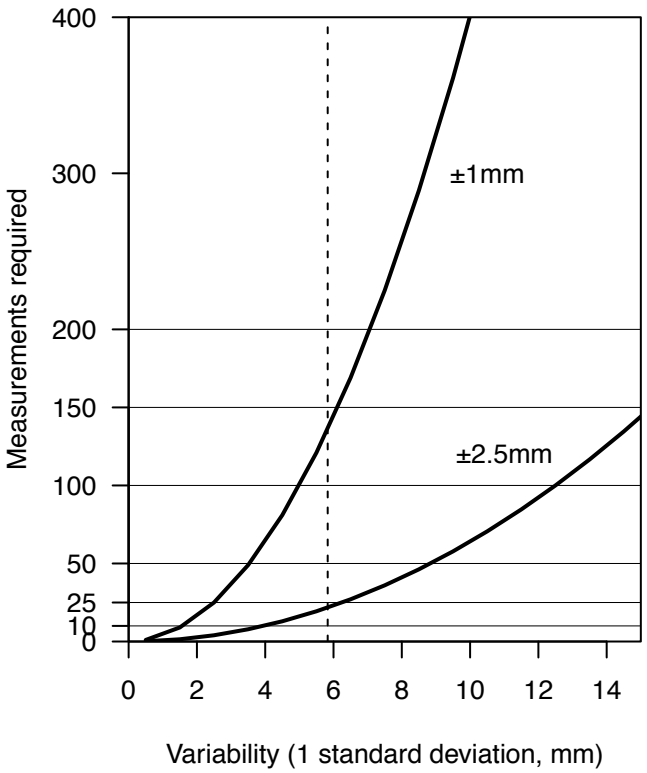

Figure 4.11: Number of measurements required at two levels of accuracy at 95% confidence level for different levels of variability in the thickness of the measured layer. Broken line indicates measured average SD for measurements of sediment accumulation in this study, showing nearly 150 measurements are needed for a 95% CI of 2 mm.

95% confidence interval of the corresponding photographic measurement. This shows the range of variability that the single measurement is trying to measure. If a single measurement is collected with skill it could be representative, however there is a high probability that it is not. Therefore multiple measurements offer a more robust approach.

4.3.6 Comparing measurement techniques in the field

To compare the different measurement techniques 27 stratigraphic sections (Figure 4.12) were recorded using standard single measurement logging techniques, repeated field measurements (typically 15 per layer) and photographic techniques.

An example is presented of measurements of a section of sediment from one profile using three different techniques: a single standard measurement, many detailed measurements and photographic measurement (Table 4.2). Based on over 100 comparisons of measurements between layers using both standard and photographic techniques there is no indication of systematic increases in

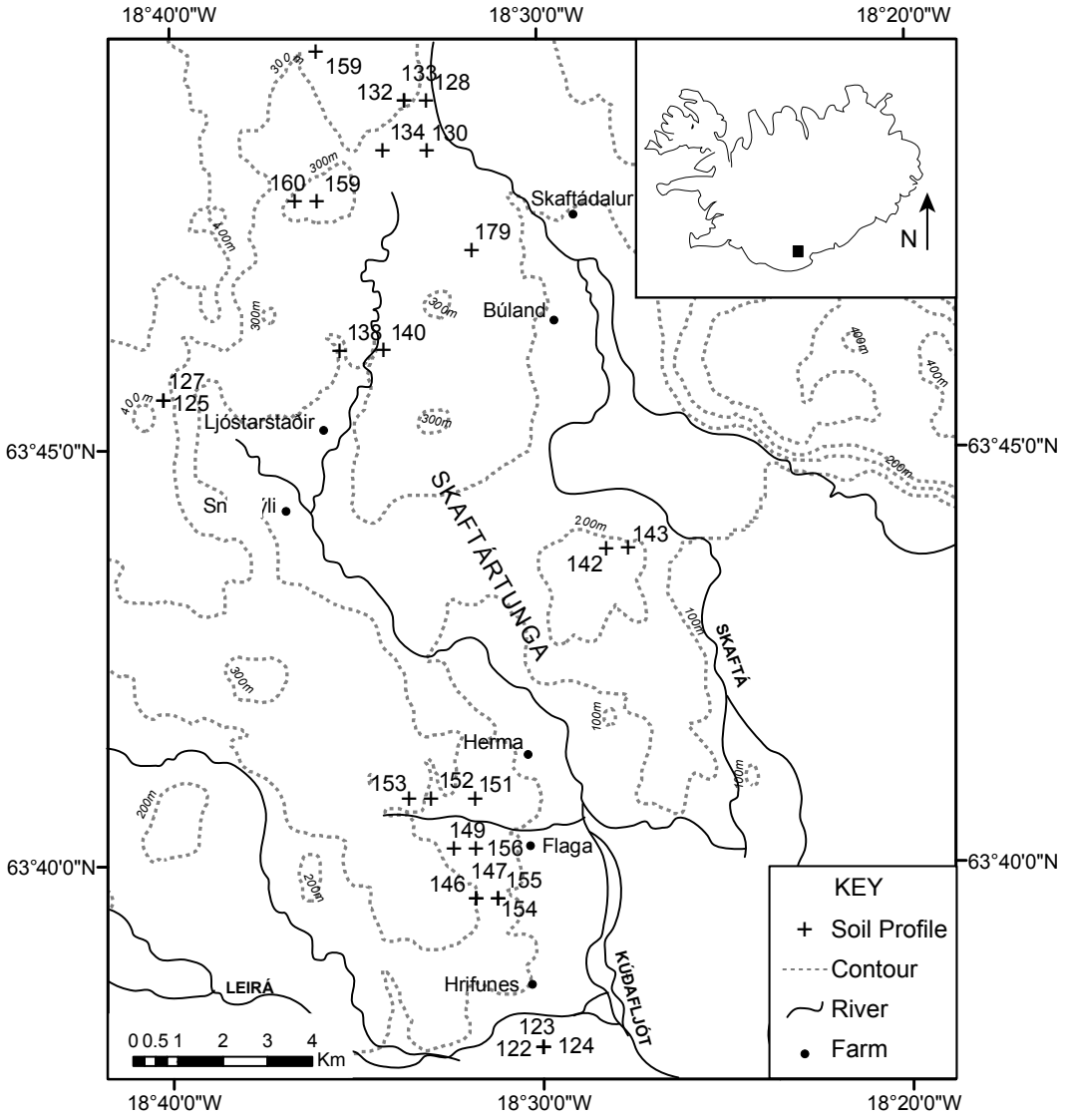

Figure 4.12: Location and profile numbers of stratigraphic sections recorded using photogrammetric techniques.

difference with increasing depth of stratigraphic measurement (Figure 4.13). Increasing variability in sediment accumulation between layers also does not increase differences in the depth recorded by each technique (Figure 4.13). The average difference between standard and photographic measurements was ±22% of the measured distance. The average difference between detailed measurements and photographic measurements is ±15.4% of distance, this decreases to <10% when over 50 measurements were taken. Making many measurements in the field is time consuming but produces figures which are close to those generated using photographic techniques, which indicates that photographic measurement produces results which are close to the true sediment accumulation.

Table 4.2: Comparison of measurements using three different approaches between H 1389 and K 1416, profile 179. Multiple measurements agree closely with photographic techniques.

	n	mean (mm)	resolution (mm)	1σ	2σ	Mean standard error (mm)	SeAR mm yr^{-1}	% MSE error of SeAR
Single	1	15	2.5	-	-	2.19	0.56	29.20
Multiple	141	10.83	2	2.14	4.28	0.18	0.40	1.66
Photo	454	10.82	1	2.19	4.38	0.10	0.40	0.92

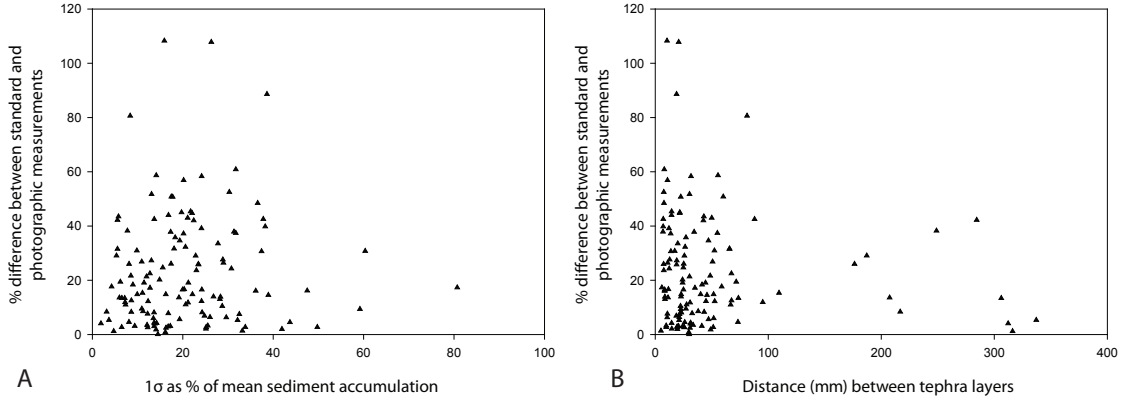

Figure 4.13: The graphs show the percentage difference between standard measurements ($\pm$ 2.5 mm) and photographic measurements ($\pm$1 mm) with (A) increasing variability in thickness defined as 1σ as a % of mean sediment accumulation and (B) mean distance between tephra layers (mm). The graphs show that there is no systematic change in the variation of measurement and thickness measured. Thinner layers are measured to a similar level of certainty as thicker layers.

For short time intervals and depths of 5–50 mm the errors produced by only single measurements have a large enough effect on calculated sediment accumulation rates (SeAR) to change the interpretation (Table 4.2), especially where trying to correlate human events of brief duration with a record that is precise but unevenly spaced. Over greater depths the errors produced by inaccuracies in measurement reduce in relative terms. Detailed measurements reduce the likelihood of measurement artefacts occurring in the data, for example where there are sudden spikes where SeAR changes by more than 25% for short ($<$ 50 year) periods. These spikes were visible in the standard measurements of several profiles but did not exist in the photographic measurements. This is of importance when trying to correlate changes in SeAR

with external events, which may be expected to only produce relatively small changes, compared to the very large landscape changes seen in upland areas in the 16–20th centuries (e.g. Thórarinsson, 1961; Dugmore & Buckland, 1991). By combining measurements across several profiles (e.g. Mairs *et al.*, 2006) it is possible to build up an accurate SeAR regional picture, but for detailed comparisons of relatively small changes across smaller numbers of profiles many measurements per profile are needed.

This technique cannot be applied the recording of all stratigraphic sections because the quality of the tephra record is variable. Some parts of the record are particularly suitable to high resolution analysis (such as the 10th-17th centuries) but other parts are not — in the case of this study the post 17th century record and the pre-Landnám record. This is due to an increasingly variable expression of tephra layers that become patchy and irregular with diffuse margins. In the post 17th century record root penetration can be significant and comprise more than 10% of the profile. Roots create variability in tephra layers that could go in time as profiles aggrade, root frequency reduces and existing roots decay. In pre-Landnám sequences aeolian sediment accumulation rates are lower, sediments exhibit weathering profiles and woody vegetation with substantial roots and stems was more frequent. In these cases representative measurements to within 5 mm are as precise as the record will stand without the generation of a spurious sense of accuracy.

4.4 Key Points

- A combination of field identification of tephras, mapping and selected geochemical analysis are used to apply a known tephrochronology to the field sites.
- Age estimates for tephras based on well constrained age depth models and multiple measurements provide estimates of comparable or better resolution than radiocarbon dating.
- Photogrammetric techniques applied to the collection of measurements of sediment accumulation increase the accuracy and precision of measurements. Variability in sediment accumulation at the cm scale means that multiple measurements are necessary in order to acquire representative measure of thickness.

Chapter 5

Data: Chronology and Geomorphology

5.1 Introduction

This chapter summarises fieldwork data collected in Skaftártunga. Firstly the tephrochronology for Skaftártunga (based on Thórarinsson 1958; Larsen 2000; Larsen *et al.* 2001; Óladóttir *et al.* 2005) including the results of geochemical analysis is presented. Two tephras from Grímsvötn in the 15^{th} century are mapped for the first time and age estimates of AD 1432±5 and AD 1457±5 are calculated from multiple measurements of sediment accumulation rates. The terrestrial isopach of primary fallout for H 1104 is extended and an additional tephra from Grímsvötn is identified and dated to AD 1140–1180. Stratigraphic sections are presented, split into geographical areas based on landholdings. Full locations of profiles are provided in Appendix B, and full geochemical results for sampled tephras are included in Appendix C, while Appendix D contains the sediment accumulation rates for all profiles.

5.2 Chronology

The identification and mapping of all identifiable tephra layers is crucial to building the best possible chronology with sufficient detail to tackle periods of rapid environmental change. The Skaftártunga area to the east of Mýrdalsjökull has one of the most complete terrestrial sediment tephra records found in Iceland, extending back 8.4 ka (Óladóttir *et al.*, 2007). Its proximity to the volcanic system of Katla (27 km) means that Katla is the source of the majority of tephras found here, but there are also tephras from the volcanic systems of Hekla (60 km), Veiðivötn (60 km), Eldjgá, (24 km), Öræfajökull (100 km) and

Grímsvötn (90 km) present (Thórarinsson, 1958; Larsen, 2000; Larsen *et al.*, 2001; Óladóttir *et al.*, 2005; 2008), Table 5.1. The stratigraphy and major element composition of the Katla tephras in Skaftártunga has been explored in detail (Óladóttir *et al.*, 2005; 2008).

The chronology presented develops published chronologies because this study is based on a larger number of profiles and is able to identify four additional tephras. In total 2625 tephra layers are identified from 200 profiles. The mean depth from the surface of the Landnám tephra is 110 cm, and an average of 13 post-Landnám tephras are identified in each section. The summary chronology of post-Landnám tephras and selected key pre-Landnám tephras is shown in Figure 5.1. The following sections describe the profiles sampled and the summary geochemical results. In total 38 samples were analysed during three separate sessions on the EMPA microprobe at the University of Edinburgh Tephra analytical unit. Full results of the geochemical analysis are provided in Appendix C and binary plots of oxides are provided here. Table 5.2 details the profiles from which layers were sampled and provides a reference to the appropriate stratigraphic diagram.

Table 5.1: Volcanic source of post-Landnám tephra

Volcanic system	Percentage of tephra layers
Katla (inc Eldgjá)	45
Hekla	28
Grímsvötn-Laki	12
Veiðivötn	7
Öræfajökull	< 1

5.2.1 Pre-Landnám tephras

In order to constrain pre-settlement SeARs 12 stratigraphic sections were recorded below the Landnám tephra to find distinctive dated tephras (Table 5.3). Most of these sections were recorded as far as two silicic Katla tephras with characteristic needle grain morphology (Larsen *et al.*, 2001). Silicic Katla tephras (SILK) are the least common type of tephra from Katla. They have a SiO_2 content between 63–67% as opposed to basaltic Katla tephras which have a SiO_2 content of 38–43% (Larsen *et al.*, 2001). These layers are found at more than 3 m depth from the surface, and their thickness is 20 mm. Geochemical analysis on two samples from profiles 135 and 147 confirm the tephras sampled are SILK-UN (Figure 5.2, Larsen *et al.*, 2001). The Hekla H-S tephra layer was

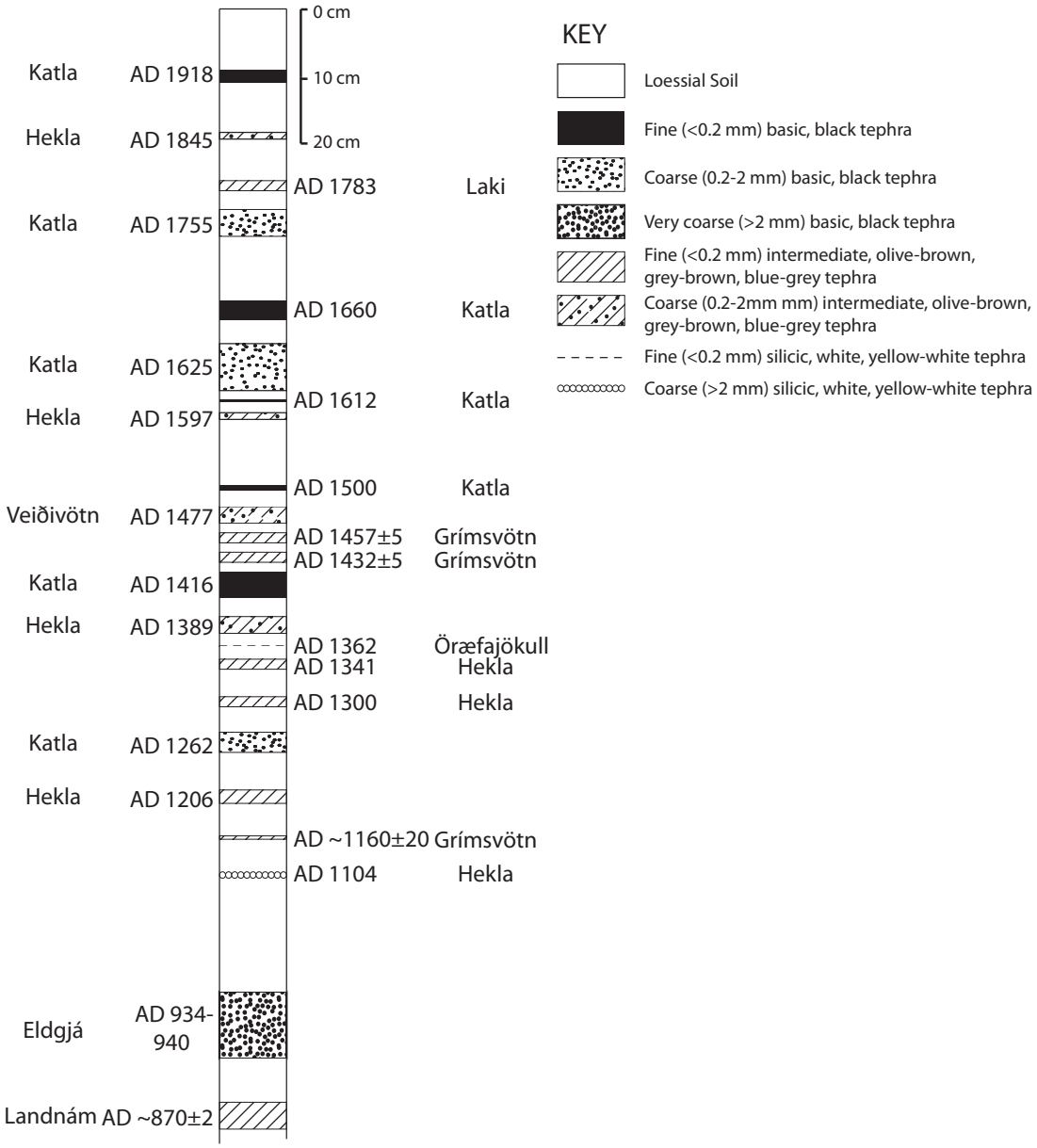

Figure 5.1: Composite post-Landnám tephrochronology of Skaftártunga, modified from Larsen, 2000. Tephra layers on the right hand side were found less frequently while those on the left were found more frequently.

Table 5.2: Tephras sampled

Profile Number	Tephras sampled	Figure reference
17	L 871±2, H 1104, K 1262, G 1457±5, V 1477, H 1845	Figure 5.45
20	H 1104, K 1262, K 1416, G 1457±5, V 1477, H 1597, K 1625, K 1755, H 1845, K 1918	Figure 5.41
27	G 1457±5	Figure 5.22
39	Basaltic Katla tephra, age unknown (originally identified as H 1300)	Figure 5.50
44	H 1300, K 1357	Figure 5.50
49	K 1416, G 1457±5	Figure 5.47
56	G 1457 ±5, H 1597	Figure 5.28
87	G 1432 ±5, G 1457±5	Figure 5.25
112	K 1416, G 1457±5, K 1500	Figure 5.31
130	G 12th C, K 1500	Figure 5.41
135	SILK-UN	Figure 5.24
147	SILK-UN	Figure 5.26
152	G 1432 ±5, G 1457±5, K 1500	Figure 5.26
179	H 1389, K 1416, G 1432±5, G 1457±5, V 1477, K 1500, H 1597	Figure 5.38

found at 6 sites.

Table 5.3: Pre-Landnám tephra identified

Name and volcanic origin	^{14}C date	Reference
SILK-UN (Katla)	2660±50 BP	Larsen *et al.*, 2001
SILK-LN (Katla)	3139±40 BP	Larsen *et al.*, 2001
H-S (Hekla)	3515±55 BP	Larsen *et al.*, 2001
H 4 (Hekla)	3826±12 BP	Dugmore *et al.*, 1995a

5.2.2 Tephras AD 870–1400

A total of nine tephras were found from AD 870–1400 (Table 5.4). The Landnám tephra is dated to AD 871±2 from the GISP ice core in Greenland (Gronvöld *et al.*, 1995). It is important because it coincides with the settlement of Iceland in AD ∼870 and separates the pre- and post- settlement periods. The eruption had two phases, an initial silicic phase and a later basaltic phase (Larsen *et al.*, 1999), the basaltic phase was found here (Figure 5.3).

The Eldgjá fires eruption has been dated to AD 933±1 in three Greenland

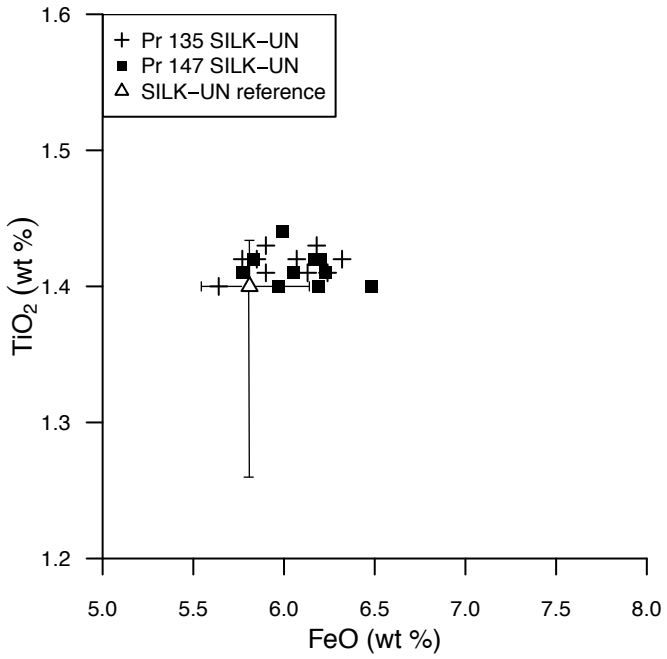

Figure 5.2: Binary plot of FeO against TiO_2 for two samples of SILK-UN tephra layers, plotted against reference data from Larsen *et al.* 2001. Reference shows mean value, error bars shows extent of data.

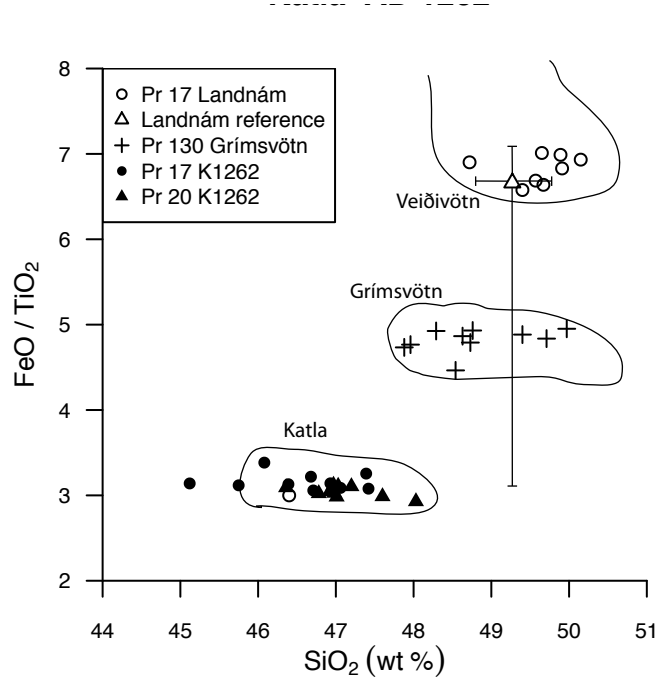

Figure 5.3: Binary plot of SiO_2 against FeO/TiO_2 for four samples plotted against reference data (mean and error bars show extend of data) from Larsen *et al.* (1999). Reference areas are from Jakobsson (1979).

Table 5.4: Tephra layers found in Skaftártunga, AD 870–1400, the reference is for the year of the eruption

Name	Volcanic origin	Calendar year (AD)	Frequency	Mean thickness (mm)	Description	Reference
Landnám (L 871)	Veiðivötn (Vatnödalur)	871 ±2	102	50	Fine to coarse olive-green with crystals	Gronvöld *et al.*, 1995
E 935	Katla (Eldgjá)	934-940, 933±1 in Greenland ice core	139	210	Coarse to very coarse, blue-black	Larsen, 2000; Vinther *et al.*, 2006
H 1104	Hekla	1104	56	5	Coarse yellow-white	Thórarinsson, 1967
G 12^{th}C	Grímsvötn	∼1140–1180	12	5	Fine brown-black	SeAR age, this study
H 1206	Hekla	1206	155	20	Fine blue-grey	Thórarinsson, 1967
K 1262	Katla	1262	161	28	Coarse black	Larsen, 2000
H 1300	Hekla	1300	111	8	Fine-coarse blue-grey	Thórarinsson, 1967
H 1341	Hekla	1341	84	8	Fine blue-grey	Thórarinsson, 1967
K 1357	Katla	1357	9	27	Coarse black	Einarsson *et al.*, 1980
Ö 1362	Öræfajökull	1362	16	5	Fine white	Thórarinsson, 1958
H 1389	Hekla	1389	157	7	Coarse blue-grey	Thórarinsson, 1967

ice cores (DYE-3, GRIP, NGRIP, Vinther *et al.*, 2006), although the eruption took place over several years and has also been dated to to AD 934-940 (Larsen, 2000). The eruption date used for sediment accumulation calculations is AD 935. It is the thickest tephra found in the historic period with a mean thickness of 210 mm and a maximum thickness of 800 mm. Hekla AD 1104 is not present in other published chronologies of this area (e.g., Larsen, 2000; Larsen *et al.*, 2001; Óladóttir *et al.*, 2005) and this finding expands its observed range to the south and east. It is found in 56 profiles north of 63°45'0 N. The eruption of Hekla in AD 1158, of which the main axis of tephra fall was to the north-east (Figure 4.2), was a possible alternative interpretation for this layer based on its stratigraphic position, however the geochemistry determined by geochemical analysis of two samples in profiles 17 and 20 shows this layer is from the H 1104 eruption (Figure 5.4).

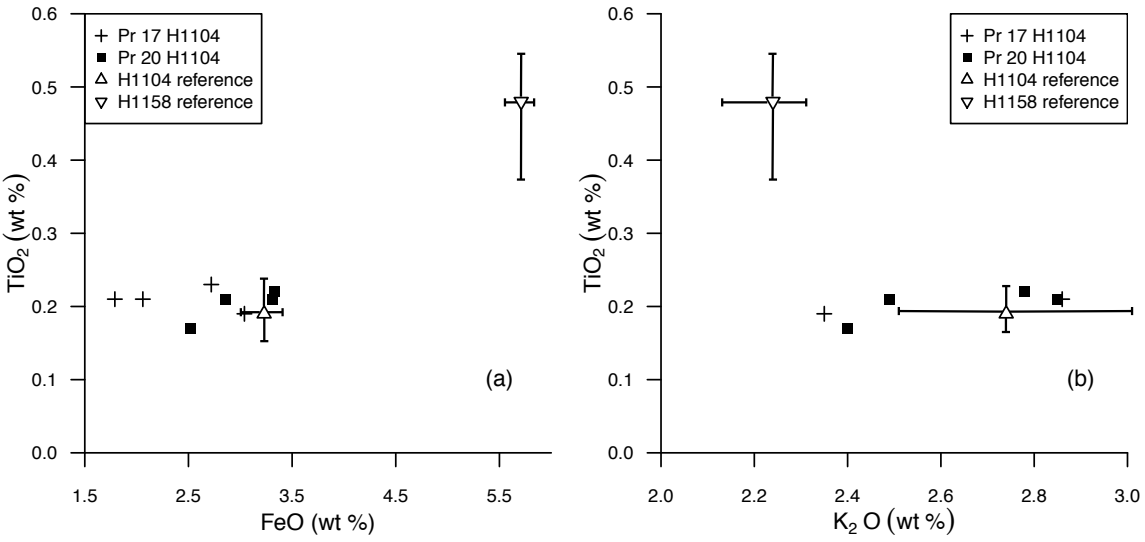

Figure 5.4: Binary plot of samples from H 1104 with reference data for H 1104 and H 1158. (a) FeO vs TiO_2 (b) K_20 vs TiO_2. Reference data for Hekla AD 1158 and Hekla AD 1104 (error bars indicate maximum and minimum values) is from Larsen *et al.* 1999 and shows these samples are not from the H 1158 eruption (H 1158 has a SiO_2 wt% of 67–68% and FeO of 5.5 % wt compared to the sample range of 70–74 SiO_2 and FeO 1.5–3.5 % wt).

A sample of a tephra from Grímsvötn dating to the 12^{th} century was analysed from profile 130 and this tephra appears in 12 profiles. Results from geochemical analysis are presented in Figure 5.3. Based on a limited number of field measurements it is not possible to provide a precise age for this tephra, but its stratigraphic location relative H 1104 and H 1206 indicates it is from an eruption between AD 1140–1180.

Three Hekla tephras from the 14^{th} century are found in this area and samples from H 1300, K 1357, and H 1389 were analysed (Figure 5.5). Hekla AD 1389 is the most widespread, appearing in 157 profiles. K 1357 was not found in Skaftártunga but only in profiles on Mýdralsandur.

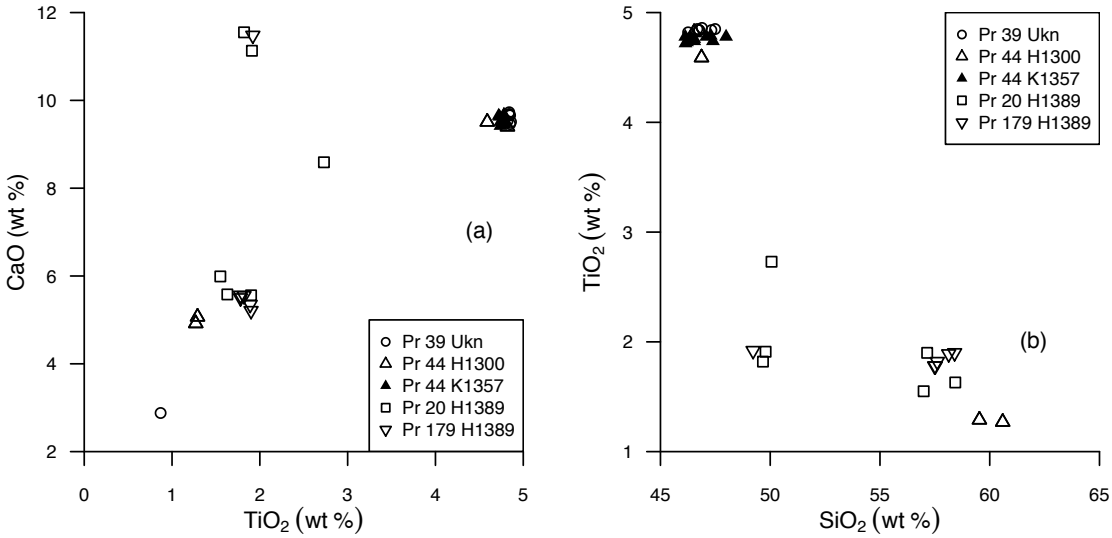

Figure 5.5: Binary plot of samples from H 1300, K1357 and H 1389. The sample from profile 39 is a Katla tephra of unknown age. Mixed geochemistry for samples Pr44 H 1300 and Pr 20 H1389 indicate that these may not be primary airfall tephra.

The eruption of Öræfajókull in AD 1362 was the largest silicic explosive eruption in historical times (Thórarinsson, 1958). The main axis of fallout was to the south east, and tephra here was thin (5 mm) and patchy and it is found in 14 (7%) profiles. Its high SiO_2 composition means it formed a distinctive white tephra in the sequence.

5.2.3 Tephras AD 1400–1500

A total of 5 tephras were found in this period (Table 5.5). Using the stratigraphic framework of field identifiable tephras from eruptions of Katla in AD 1416 (K 1416), Veðvötn in AD 1477 (V 1477), Katla in AD 1500 (K 1500) and tephra characteristics (grain size and colour) it is possible to identify two separate tephra layers (G 1 and G 2) between AD 1416–1477. While these tephras which are from Grïmsvötn have been recorded in individual profiles here previously (Larsen, 2000; Óladóttir *et al.*, 2005) the true extent of their presence in the region was unclear, due to the small number of mapped sections (Guðrun Larsen, personal communication). Their eruption dates are not correlated to

the historic record, but their stratigraphic position indicates they were formed between AD 1416–1477.

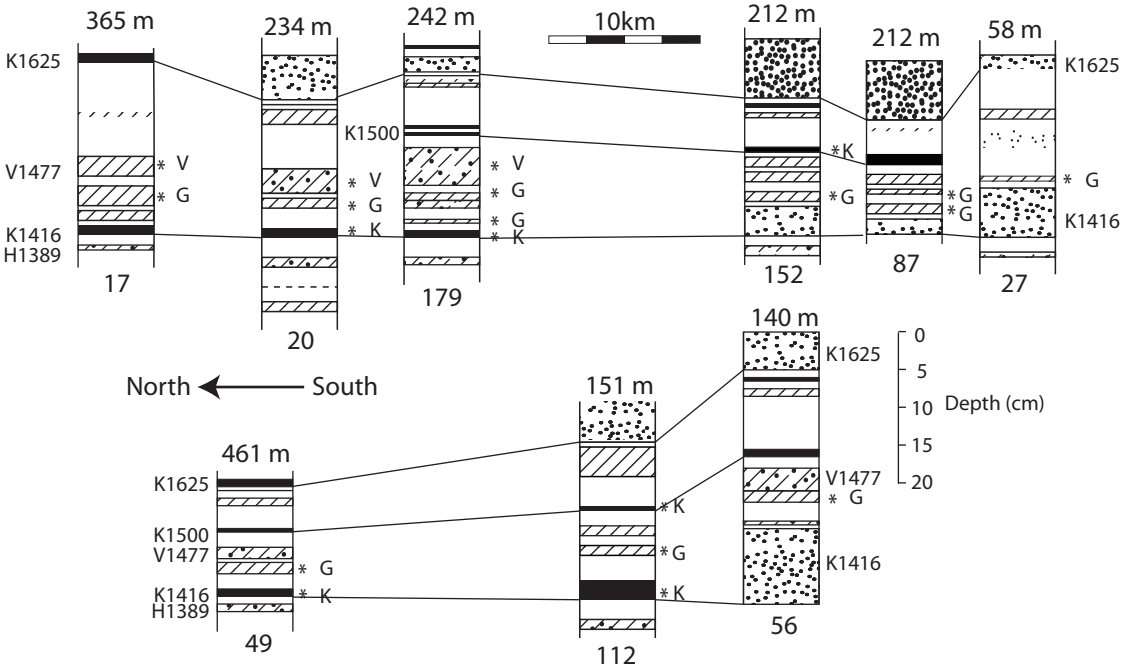

Figure 5.6: Sub-sections from stratigraphic profiles which had samples taken for geochemical analysis of tephras in the period AD 1389–1625. Sections are arranged from north to south (left-right) with the distance in km between profiles shown by the scale bar and the lower profiles are further from Grímsötn. Sampled layers are indicated by * and the letter denotes the volcanic system of origin K: Katla, G: Grímsvötn, V:Veiðivötn, determined from the geochemistry. Profile locations are indicated by profile numbers which match those in Figure 5.7, and the altitude in metres is given above the profile.

Grímsvötn tephras

The Grímsvötn volcanic system is the most active in Iceland, with 64 eruptions since Landnám and seven in the period AD 1400–1480 (Larsen *et al.*, 1998). The majority of tephras from these eruptions have only been found within the ice cap (Steinthorsson 1977; Larsen *et al.,* 1998) and have not produced widespread isopachs suitable for chronological control, although recently the terrestrial record of tephra from volcanic systems beneath Vatnajölkull has been improved (Óladóttir *et al.*, 2011b). Samples of the tephra for geochemical analysis were collected from nine stratigraphic sections (Figure 5.7). In addition samples from tephras bracketing the Grímsvötn tephras in the stratigraphy (K1416, V1477 and K1500) were collected. A total of 113 shards from Grímsvötn, 22 from Veðvötn and 60 from Katla were analysed.

Table 5.5: Tephra layers found in Skaftártunga AD 1400–1500

Name	Volcanic origin	Calendar year (AD)	Frequency	Mean thickness (mm)	Description	Reference
K 1416	Katla	1416	172	18	Fine to coarse black	Larsen, 2000
G 1 or G 1452±5	Grímsvötn	1432±5	89	7	Fine black	brown- SeAR age, this study
G 2 or G 1452±5	Grímsvötn	1457±5	140	10	Fine black	brown- SeAR age, this study
V 1477	Veiðivötn	1477	148	21	Coarse grey	Olive- Larsen, 1984
K 1500	Katla	1500	72	10	Fine black	Larsen, 2000

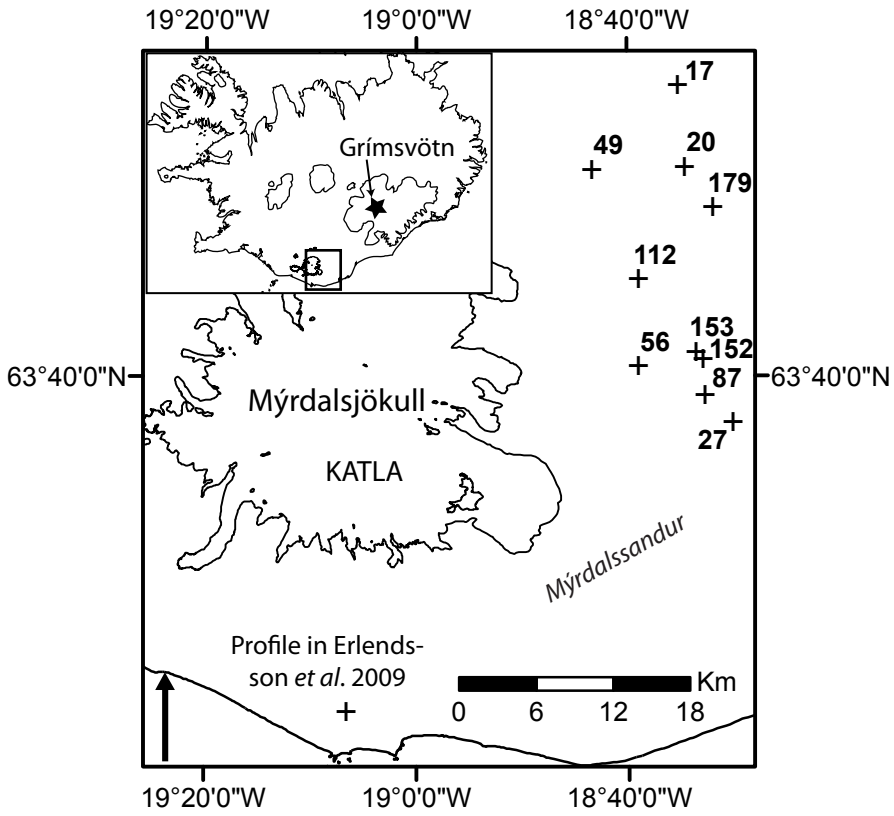

Figure 5.7: Stratigraphic sections where 15^{th} century tephras were sampled, except profile 153 which was only used for SeAR age estimates. Stratigraphic details are in Figure 5.6.

The Grímsvötn samples have uniform geochemistry and individual shards have no signs of weathering, suggesting that both layers are primary air fall and not reworked material. Samples were confirmed to be from Grímsvötn by comparing major element geochemistry against reference data (Figure 5.8, Jakobsson, 1979; TEPHRABASE, www.tephrabase.org). TiO_2 content was in the range 2.6–2.9% wt, lower than Katla (∼4.5% wt) which is the most frequently found tephra in this area. A FeO/TiO_2 ratio of less than six shows the tephra is not from the Bárdarbunga system (Óladóttir *et al.*, 2011a). These analysis confirmed the sequence of primary air fall tephra was Katla (AD 1416), Grímsvötn, Grímsvötn, Veiðivötn (AD 1477) and Katla (AD 1500).

Age estimates

Two sediment profiles (Figure 5.7, profiles 153 and 179) with high rates of aeolian accumulation and where tephra layers were of uniform thickness were selected to calculate the age of the tephras (Section 4.2.3). Based on measurements of sediment accumulation the age lower Grímsvötn layer is AD

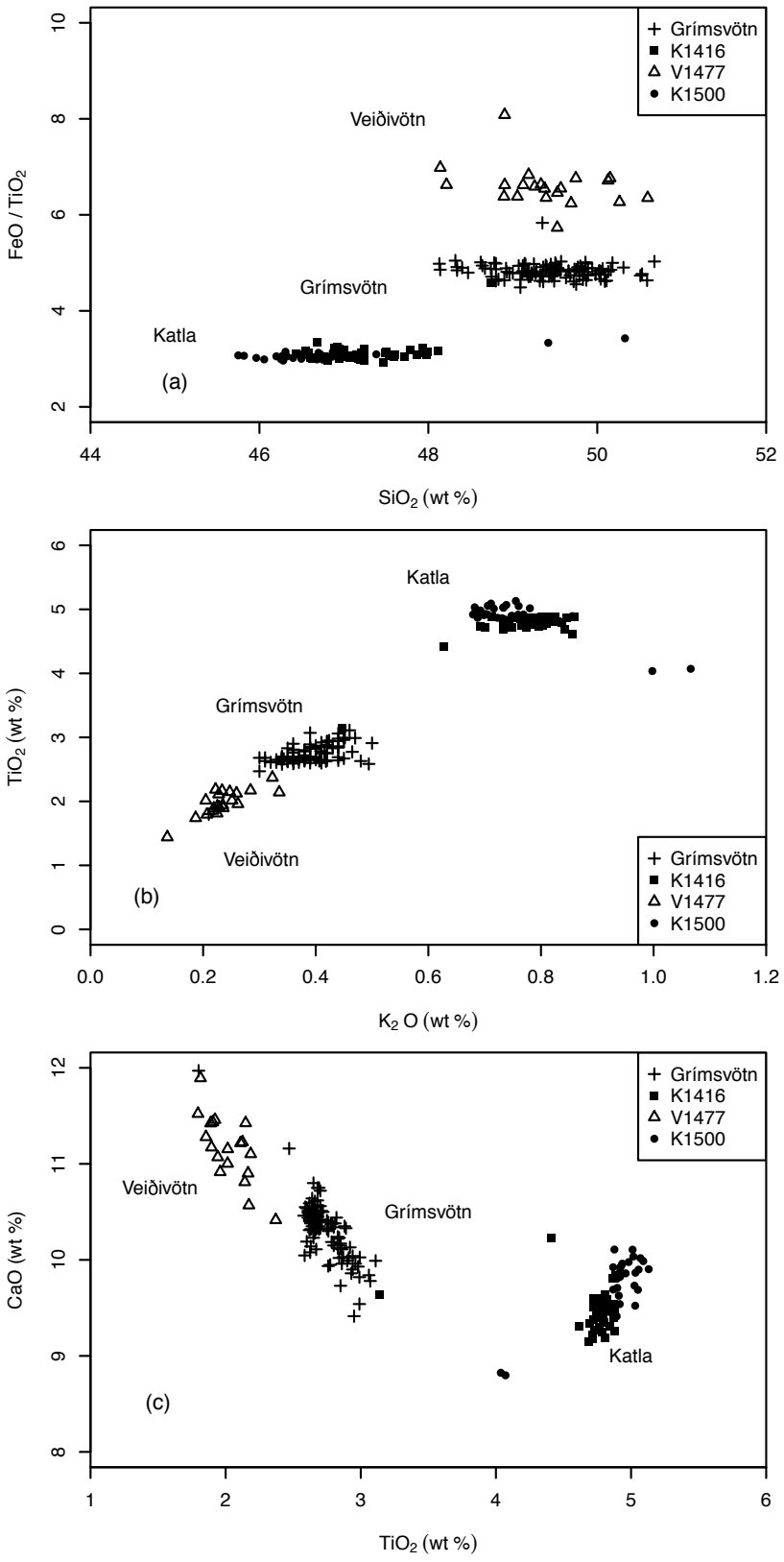

Figure 5.8: Binary major element plots of samples from K 1416, G 1432±5, G 1457±5, V 1477 and K 1500. The samples were located at the sections shown in Figure 5.7, and they were taken from the stratigraphic position indicated by Figure 5.6.

1432 ±5 (mean ±1σ) and the age of upper Grímsvötn layer is is AD 1457 ±5 (mean ±1σ) (Figure 5.9).

Mapping

The distribution and thickness of these Grímsvötn layers has been mapped (Figure 5.10). The lower layer (G1) has a mean thickness of 8 mm and is found in 47% of profiles. It thickens towards the south suggesting that the main axis of fall out was south of Skaftártunga. The upper layer has a uniform depth of 20 mm. It is found in 74% of profiles.

The later G 2 tephra may be correlated with Grímsvötn tephra in two published profiles. This layer also occurs at Ketilsstaðir, Mýrdalur (Figure 5.7) where a tephra layer between K 1416 and K 1500 has the geochemistry of a Grímsvötn tephra (Erlendsson *et al.*, 2009). Its position in the stratigraphy indicates this is most likely to be the later Grímsvötn AD 1457±5 layer, although relatively small changes in accumulation rates would change this interpretation. Identification at Ketilsstaðir would expand the extent visible extent of this layer to over 100 km from Grímsvötn.

Both the G1 and G 2 layers can be correlated with tephra from Grímsvötn found in a profile at 50 km east of Skaftártunga, at Núpsstadarskógar. The Grímsvötn tephra layers are between the K 1417 and V 1477 tephras, which have been dated to ∼ AD 1430 and ∼ AD 1450 based on a SeAR model (Óladóttir *et al.*, 2011b). The thickness of both the upper and lower Grímsvötn layers are 4 cm.

5.2.4 Tephras AD 1500–2010

A total of 10 tephras were found in this period (Table 5.6). In sections recorded in 2010, tephra was found from the eruption on 14^{th} April that year Eyjafjallajökull. It was < 5 mm thick and it is uncertain how it will be incorporated into the stratigraphic section, although layers of similar thickness can be preserved and visible (e.g. Katla AD 1612). Tephra from the Skáftar fires (Laki) eruption in AD 1783 is found in 34 sections in the northern and eastern part of the region. The results of geochemical analysis on Kalta AD 1918 from profile 20 are presented in Figure 5.11. The analysis of Hekla tephras from this period shows that by this stage there was considerable reworking in the landscape as the shard composition was mixed for samples for H 1597 and H 1845, even though field identification was secure (Figure 5.12).

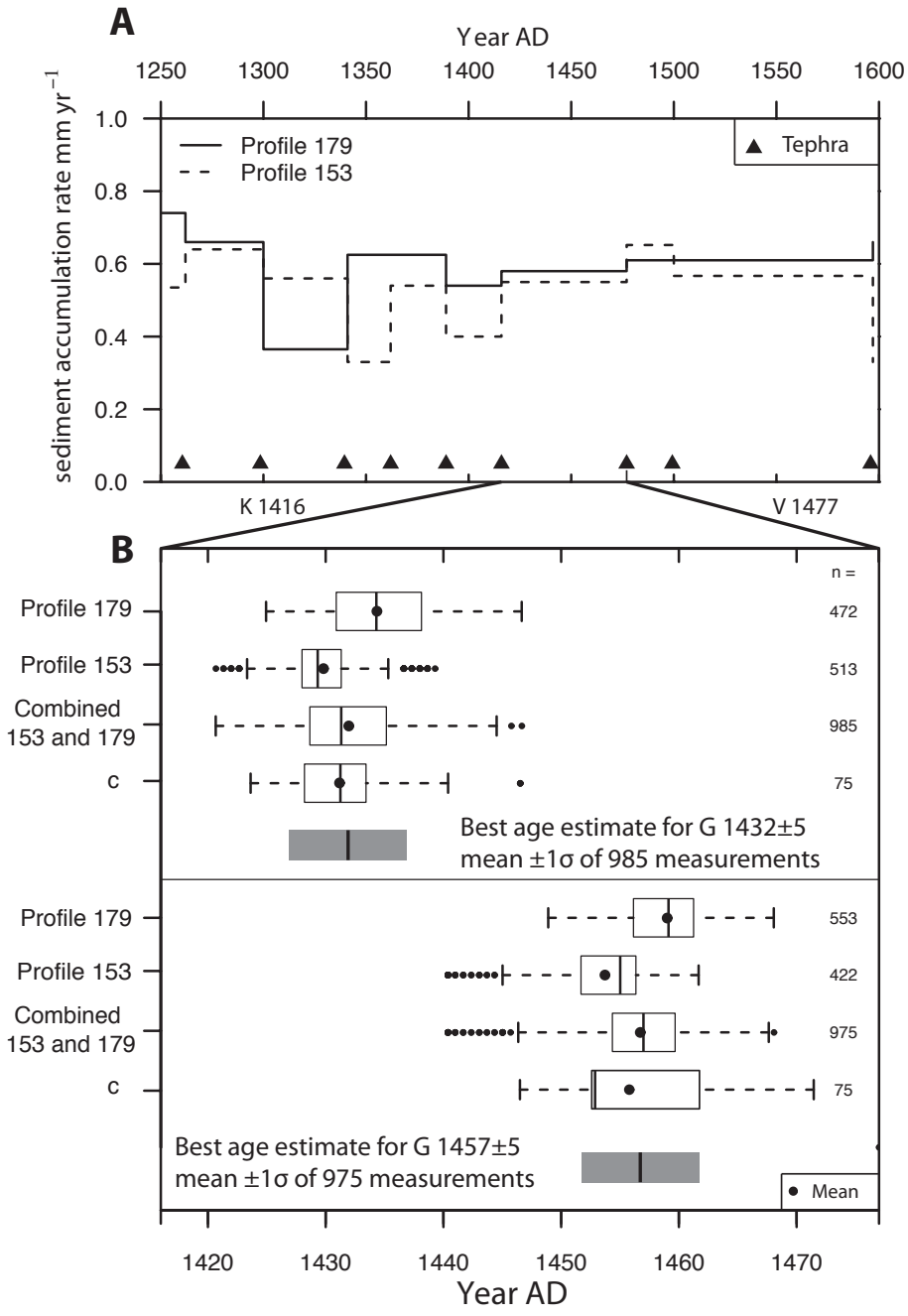

Figure 5.9: Box plots showing estimated age of the Grímsvötn tephras. (A) shows sediment accumulation rates over AD 1250–1600. (B) shows age calculations based on linear sediment accumulation rates between the Katla AD 1416 tephra and the Veiðvötn AD 1477 tephra. (c) is based on single measurements (± 2.5 mm) from 75 profiles where all four tephra layers were present. (c) is included for comparison with the photogrammatically derived data, but is not used in the best age estimates.

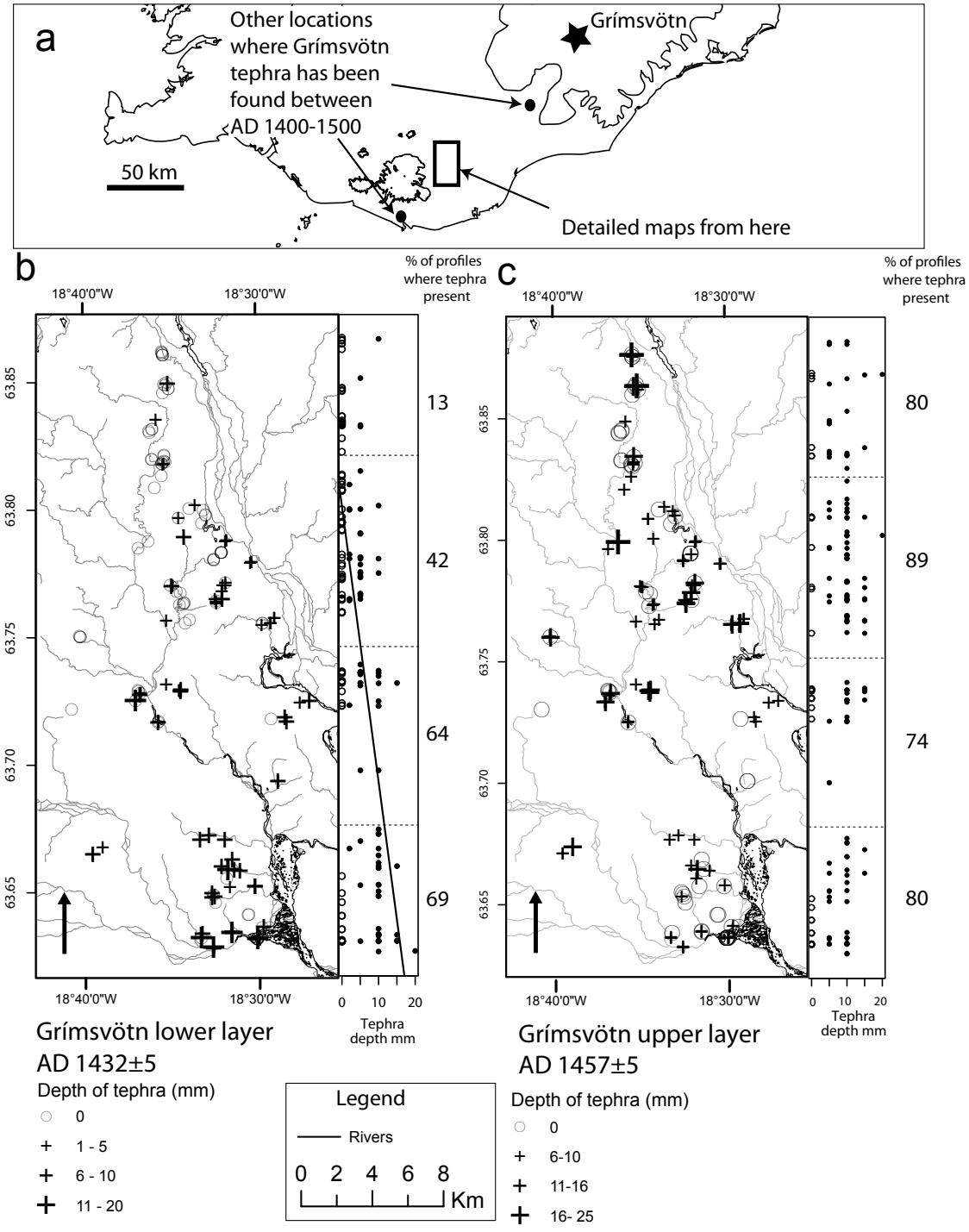

Figure 5.10: Distribution maps for 15^{th} century Grímsvötn tephras. The thickness of each layer of Grímsvötn found is shown at each profile location. A best fit line for G 1 shows the tephra thickness decreasing towards the north whereas G 2 is of uniform depth over Skaftártunga. The markers in section (a) show locations of sections where Grímsvötn tephra which may be from the same eruptions as Grímsvötn tephra mapped here, see Section 5.2.3 for details.

Table 5.6: Tephra layers found in Skaftártunga AD 1500–2010

Name	Volcanic origin	Calendar Year (AD)	Frequency	Mean thickness (mm)	Appearance	Reference
H 1597	Hekla	1597	119	7	Coarse dark grey	Thórarinsson, 1967
K 1612	Katla	1612	66	5	Fine black	Thórarinsson, 1975
K 1625	Katla	1625	167	40	Coarse black, with occasional yellow-white coarse lower section	Thórarinsson, 1975
K 1660	Katla	1660	88	12	Coarse black	Thórarinsson, 1975
K 1721	Katla	1721	9	28	Coarse black	Thórarinsson, 1975
K 1755	Katla	1755	175	24	Coarse black	Thórarinsson, 1975
L 1783	Laki-Grímsvötn	1783	34	8	Fine brown-black	—
H 1845	Hekla	1845	149	10	Coarse grey	Thórarinsson, 1967
K 1918	Katla	1918	175	20	Fine black	Thórarinsson, 1975
Ey 2010	Eyjafjallajökull	2010	20	< 5	Fine light grey	—

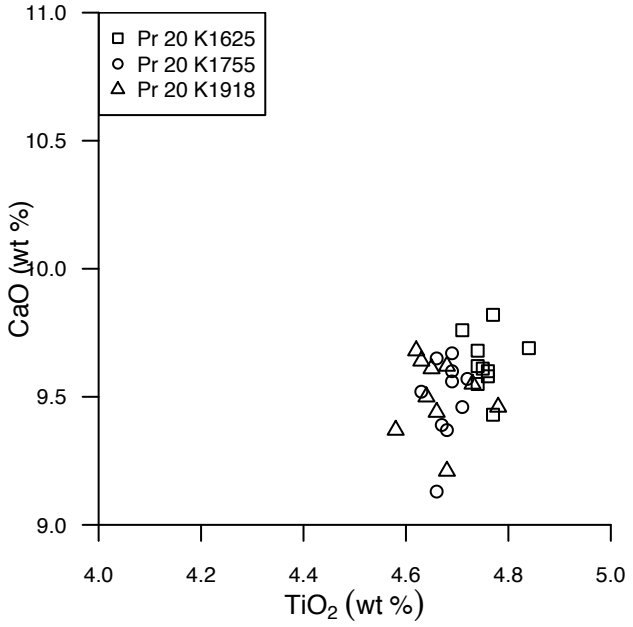

Figure 5.11: Binary plots of five samples of of TiO_2 vs CaO for samples from K 1625, K 1755 and K 1918.

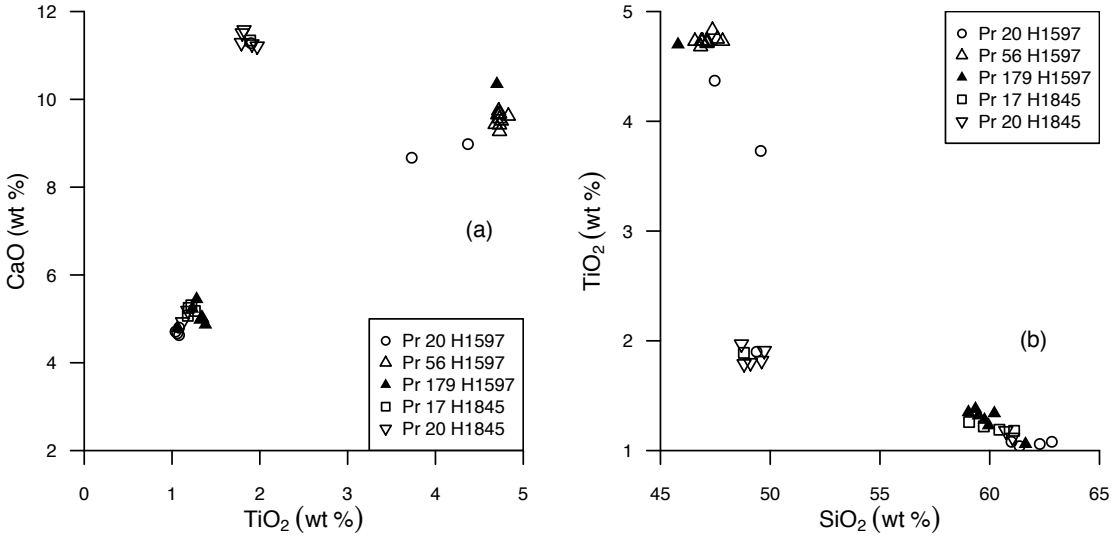

Figure 5.12: Binary plot of (a) TiO_2 vs CaO and (b) SiO_2 and TiO_2 for samples from profiles 17, 20, 56 and 179. H 1597 from profile 56 is shown to be a Katla tephra. All samples showed some signs of reworking and have shards from different volcanic systems within each sample.

5.3 Geomorphology

The geomorphic data collected is presented here. Firstly, the key geomorphic features seen in stratigraphic sections are summarised. Then representative profiles from three different altitudes are described in detail. Finally, all the stratigraphic profiles are presented, separated into four areas.

5.3.1 Summary of geomorphic features

Key geomorphic features found in sections are summarised below.

Reworking caused by thick tephra fall

Instability in sections, indicated by fluvial reworking of tephra and aeolian material, is a common feature and it is related to the depth of tephra deposited (Figure 5.13), with tephra over 100 mm thick greatly increasing the likelihood of fluvial reworking. The E 935 tephra was the thickest tephra in the post-Landnám sequence and it often precedes a period of instability in profiles which may last for several centuries (Figure 5.14). However instability is not inevitable with thick deposits of tephra, as some sections show stability after even $>$ 50 cm thick tephra layers (Figure 5.15, with a sharp upper contact indicating little mixing and rapid stabilisation of the tephra after it was deposited. The depth of tephra needed to destabilise a landscape is related to the vegetation cover at the time; where vegetation is shorter and more likely to be smothered a period of instability is more likely.

Reworking due to local slope instability

Fluvial slope wash, elevated SeARs and other signs of instability occur in sections without the presence of tephra. These indicators were related to local scale slope processes rather than changes in regional ($>$ 250 m) sediment sources (Dugmore & Erskine, 1994).

There may be short periods (decades to centuries) of instability and a return to regional, low SeAR rates, however more common were extended periods of high SeAR levels, up to five times the regional post-Landnám mean and increased signals of instability. This was interpreted as reflecting the proximity of rofabard erosion fronts to the location of the profile.

5.3.2 Summary of stratigraphic sections

The post-Landnám sequences are classified into typical 'summary' sequences which are described in detail. The classification was based on the altitude, the

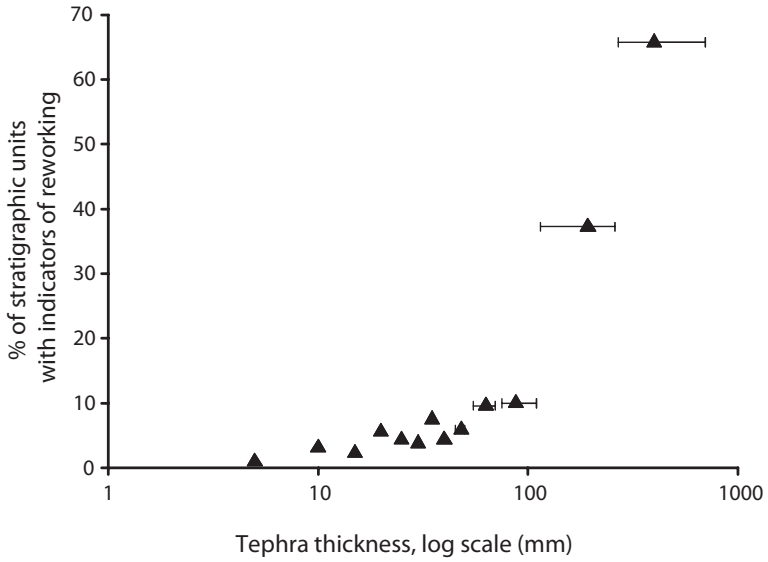

Figure 5.13: Tephra thickness does not cause increased instability until the thickness is more than 100 mm. Above this depth reworking is much more likely. n=> 35 for all points. Tephra thicknesses above 45 mm show the range of depths from which the percentage of instability is calculated from.

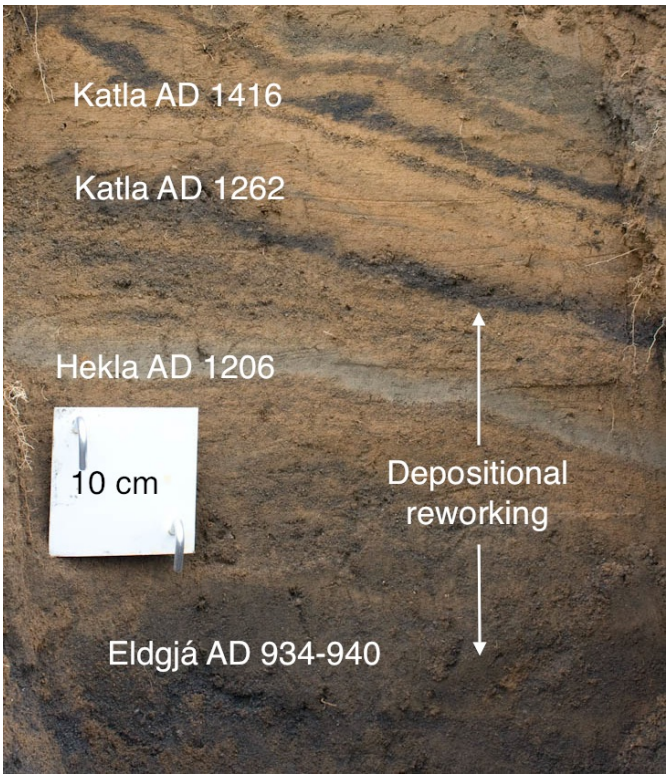

Figure 5.14: A deposit of Eldgjá tephra precedes an extended period of instability (330 years) indicated by continual reworking of E 935. Landscape stability (as indicated by the resumed accumulation of yellow-brown aeolian sediments with limited or no tephra) returns after the K 1262 tephra. Profile 140, Figure 5.36

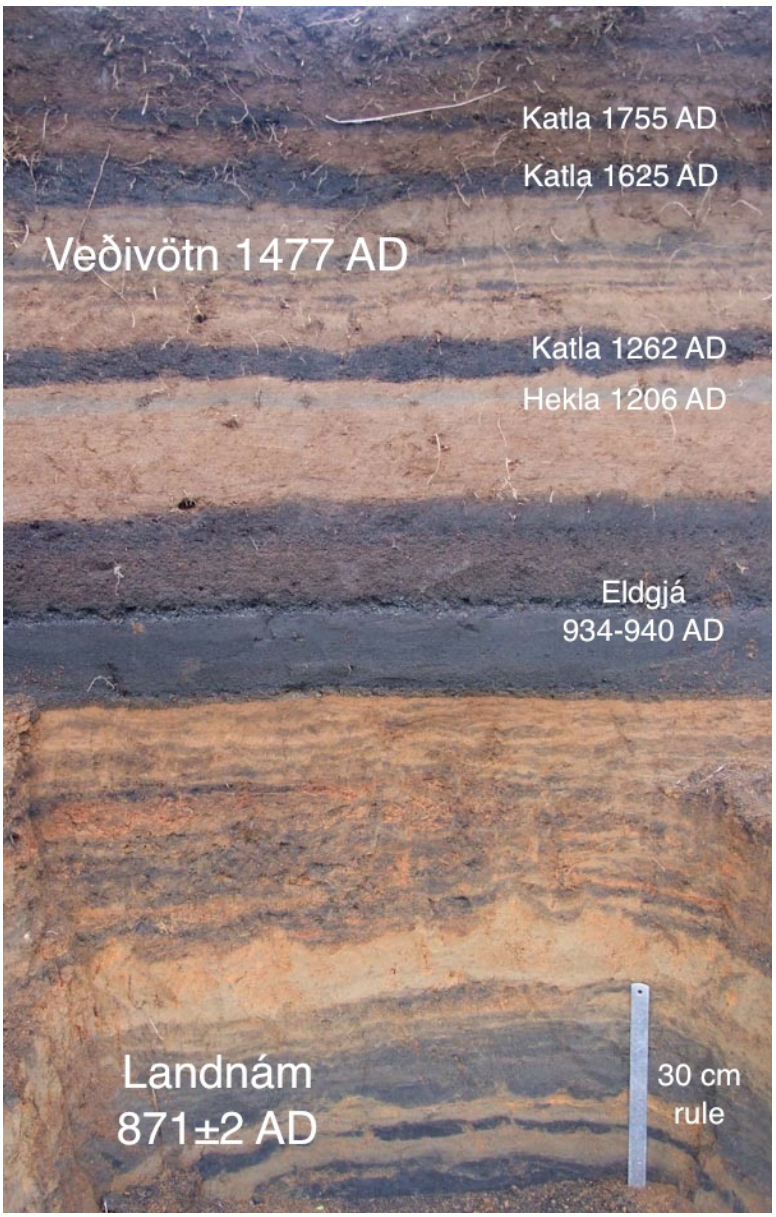

Figure 5.15: Profile 189, 224 m shows signs of slope instability after L 871, however the E 935 tephra is stabilised rapidly.

stratigraphic sections relation to macro scale geomorphic features such as rofabards and slopes, patterns of SeAR through time and indicators of reworking within the section. Characteristics of post-Landnám sequences (ratio of tephra to aeolian sediment, average SeAR over total age of profile, total sediment depth accumulated and total tephra accumulated) are plotted against altitude (Figure 5.16). There is no systematic trend in these variables related to altitude. Large variations in the characteristics of post-Landnám profiles are probably due to differences in local slope morphology and vegetation cover.

Pre-Landnám sequences are less variable than post Landnám sequences.

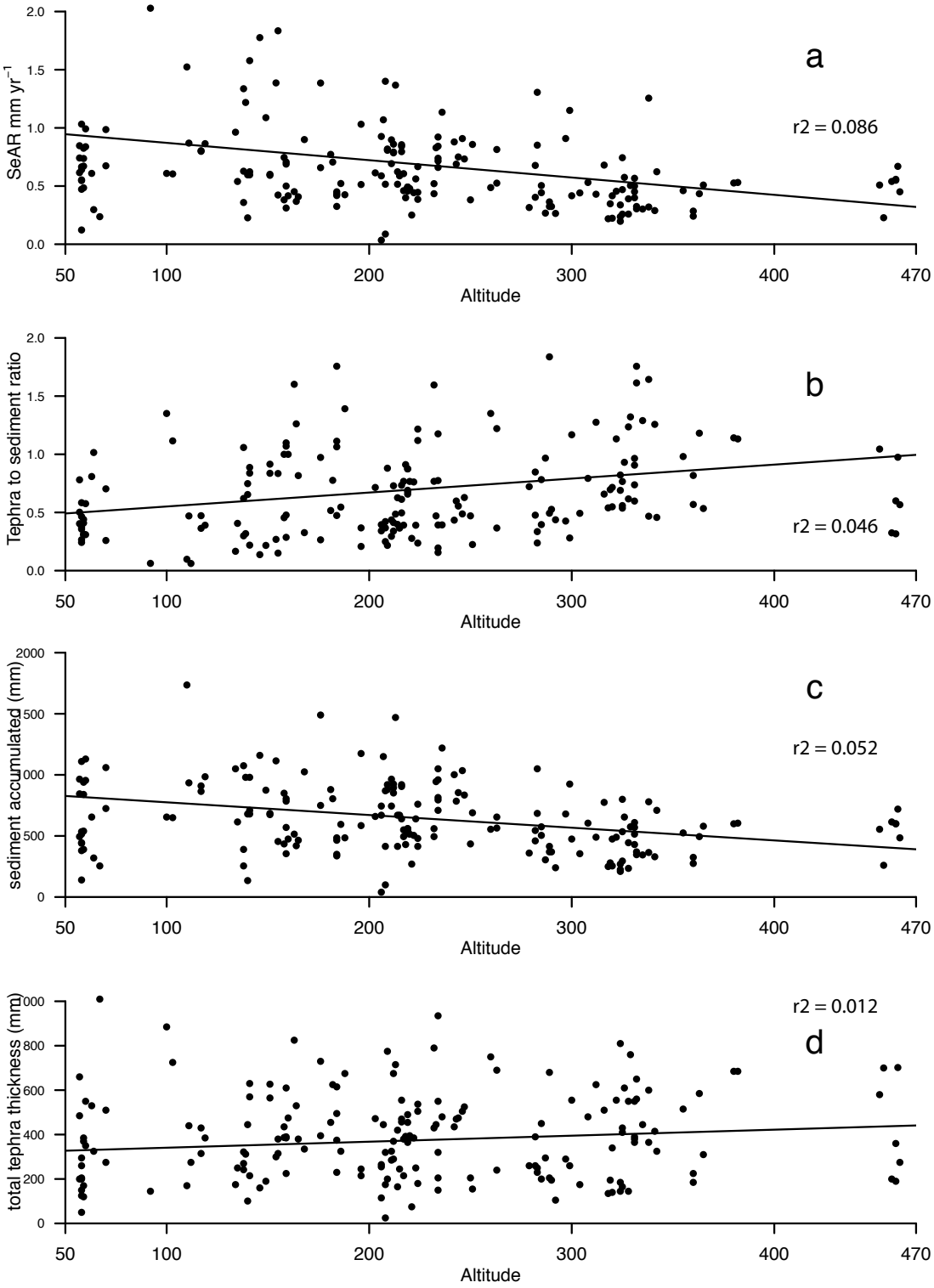

Figure 5.16: Summary of variations in (a) SeAR rates, (b) ratio of tephra to sediment, (c) total sediment accumulated and (d) total tephra accumulated against altitude. Linear best fit lines are also plotted. Profiles recorded to less than 500 years were not included.

Mean SeAR is 0.27 mm yr^{-1}, and the maximum SeAR 0.35 mm yr^{-1}, which is 0.3 mm yr^{-1} lower than the post-Landnám mean. There is no significant difference in SeAR through time with the period between SILK-LN (^{14}C 3139±40 BP, Larsen *et al.*, 2001) and SILK-UN (^{14}C 2660±50 BP, Larsen *et al.*, 2001) which has a SeAR of 0.24 mm yr^{-1} and SILK-UN to Landnám which has a SeAR of 0.28 mm yr^{-1}.

Sections above 300 m

Sections found above 300 m tended to have similar stratigraphic features. 300 m is probably above the altitudinal limit for continuous forest birch, but below the limit of shrub growth, based on modern measurements at Skaftafell 100 km east of Skaftártunga (Wöll, 2008). Total accumulation post-Landnám was 414 mm of tephra and 471 mm of sediment giving a total depth of $\sim$ 90 cm to the Landnám tephra, and a maximum depth of $\sim$ 110 cm. Profiles at this altitude were mainly recorded in the north of Skaftártunga, which means that E 935 was thicker, on average 295 mm. More profiles here has signs of cryoturbation such as thufur (Figure 5.17).

In some sequences there is instability immediately after the Landnám tephra, with high SeAR levels. These sites are at altitudes which were likely to have once been near continuous woodland cover. The highest SeAR levels through the post-Landnám period are immediately after settlement (for example in profiles 77–79, Figure 5.43 and 5.18), and these decline rapidly, mostly by AD 935. Later in historical time SeAR generally are in the range 0.3–0.6 mm yr^{-1} . There is a slight increase after AD 1625 in some profiles but much less than seen in lower areas.

Sections below 300 m

Many profiles below 300 m show stability though the entire settlement period, with a narrow range of SeAR variation observed, although SeAR is generally 0.2–0.3 mm yr^{-1} above rates observed prior to Landnám. However a subset of sections differed substantially from this pattern, therefore stratigraphic sections below 300 are classified into two types (Figure 5.18, b and c). Mean total accumulation since Landnám is $\sim$ 707 mm of aeolian sediment and $\sim$ 358 mm of tephra, however the maximum accumulation was $>$ 4.5 m of accumulated tephra and sediment since Landnám.

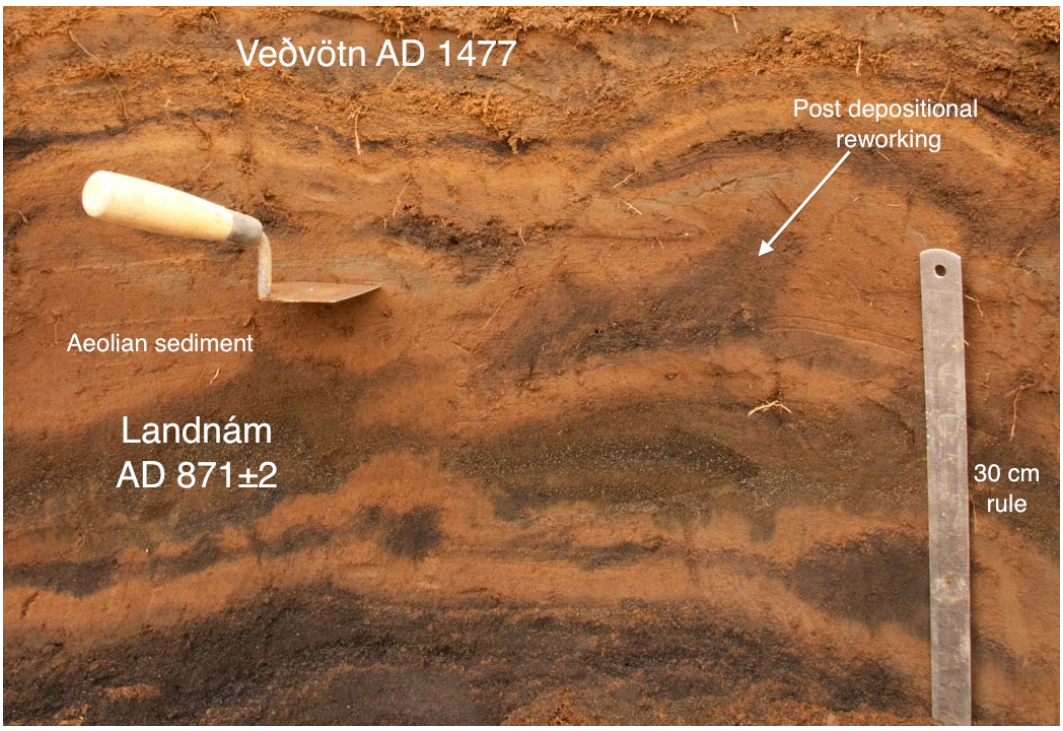

Figure 5.17: Profile 178, 324 m shows signs of post-depostional reworking due to cryoturbation, and the E 935-940 tephra is not continuous

Sections below 300 m, type A

A key feature is a trend of increasing SeAR rates, most usually seen after AD 1625. SeAR rates were high — 2 mm yr^{-1} was typical. This did not reflect early SeAR rates which were near the regional mean.

Three main trends in SeAR were common in this type of profile.

(1) High levels of accumulation and frequent instability in the early period (most commonly starting after AD 935)

(2) Lower levels of accumulation from AD 1262–1600

(3) Increasing SeAR rates from AD 1625 to the present day reaching very high levels of $\sim$ 2 mm yr^{-1}.

Sections below 300 m, type B

Rofabard erosion escarpments are less common below 150 m, therefore profiles are less influenced by local ($<$ 250 m, Dugmore & Erskine, 1994) sediment signals. 14 profiles recorded on the edge the Holmsá river do not show increasing SeAR rates after AD 1625 (Figure 5.22). The course of the river changed in the 1970's after the glacial fed river Leirá was diverted into the

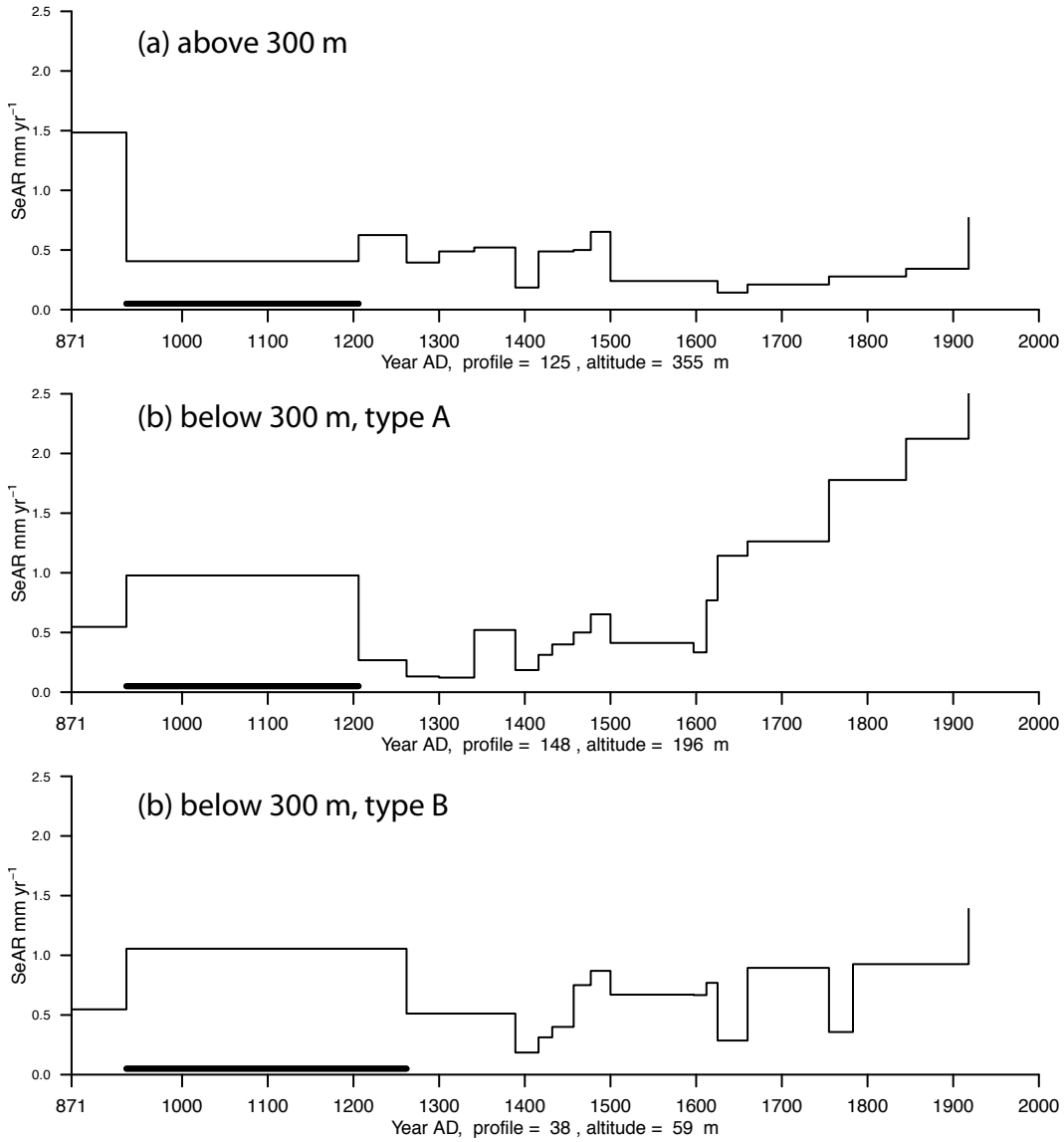

Figure 5.18: Representative profiles from (a) above 300 m, (b) below 300 m, type A and (c) below 300 m, type B. Black bars indicate periods with indicators of fluvial reworking. Further examples of each profiles types is in Appendix D

Holmsá river 3 km upstream for road construction (personal communication, Hrífunes landowner). This erosion of the river bank is therefore very recent. The implication is that these profiles reflect accumulations at the regional level. The SeAR does not increase at these sites after K 1625 unlike type A profiles, supporting the idea that the large increase in SeAR seen after K 1625 in type A is partially due to proximity to the eroding front (i.e. local signals), as opposed to regional increases in sediment flux.

Lowland redeposition profiles

An additional type of profile was recorded, which was < 500 mm in depth to bed rock material or glacial diamict, and contained two tephra layers. The earliest tephra found in these sequences is H 1845. These profiles were located on areas between areas of Holocene accumulated sediment sequences, that are interpreted as paleo-rofabard sequences. Rofabards at the edge of these sequences are vegetated on the erosion face and are not judged to be actively eroding. There are two possible interpretations — either these are the refilling in of areas eroded a recently (perhaps associated with lowland rofabard development after AD 1500), or these areas periodically erode and then are redeposited, of which the latest phase of stability started some time in the early 19^{th} century. Examples are profiles 88–90 in Figure 5.26 and profiles 93 and 94 in Figure 5.24.

5.4 Presentation of stratigraphic sections

The stratigraphic sections are presented here and are divided into groups of 2–14. Skaftártunga was divided into four areas, which are shown in Figure 5.20, and within these areas there are further subdivisions based on profile groupings. Detailed maps provide locations of the profiles and illustrate the groupings in which the profile have been drawn. Diagrams of the complete stratigraphic sections are linked by field identified tephra layers. A key to the stratigraphic symbols used is in Figure 5.19. The symbology was based on that used by Þórarinsson (1958) and by Dugmore (1987). In addition to stratigraphic sections rates of sediment accumulation are presented for all profiles in Appendix D. Sections are drawn relative to the location of the H 1206 tephra, as this was found in most sections.

Maps are provided of key areas. To determine the level of current vegetation cover LANDSAT 7 imagery for 21^{st} June 2004 (File: LE72180152004173EDC01) was obtained from http://glovis.usgs.gov/. This file was converted into a Normalized Difference Vegetation Index (NDVI) using the formula

$$NDVI = \frac{Band4 - Band3}{Band4 + Band3}$$

by Edward Mitchard using ENVI 4.4 (ITT Systems) . This was then used to categorise land cover into four basic vegetation cover classes, for NDVI values of: -1–0, 0–0.1, 0.1–0.3 and 0.3–1. The lowest values are areas of no vegetation cover, then areas with little (< 50%) vegetation cover, then grass or heath vegetation and the highest values are trees or improved grassland. The results of this classification are displayed on the relevant detailed maps. Areas of

existing erosion with bare soil cover can be seen on the tops of many hills and more generally in areas above 300 m, with zones of partial erosion and more vegetation cover in the zone 150–200 m, while many lowland areas are fully vegetated, with the exception of sandur plains or lava flows. The sections are split according to limitations of page size, and the groupings are presented in Figure 5.20.

5.4.1 Area 1 — Hrífunes and Flaga landholdings

Area 1 contains Hrífunes and Flaga landholdings, and goes from 57–266 m a.s.l. In total 55 sections were collected here (Figure 5.21), and the total area of covered by these sections is 35 km^2.

Altaey

Three profiles were recorded here (Figure 5.28) in order to confirm the chronology and to match chronology of the area to sections recorded here by (Óladóttir *et al.*, 2008).

5.4.2 Area 2 — Snæblýi and Borgarfell landholdings

Sections were collected from the landholdings of Snæblýi and Borgarfell, as well as 7 profiles from the hill of Hussafell and 2 recorded in the home field of Hilð. Profiles were recorded in several locations around the farm. Profiles 109–112 were recorded from a recent ditch, within the current infield area. The sections are in located in the map in Figure 5.29.

Hilð and Hussafell

Two profiles were collected from ditches on the landholding of Hilð (Figure 5.32).

Figure 5.19: A key to stratigraphic symbols used.

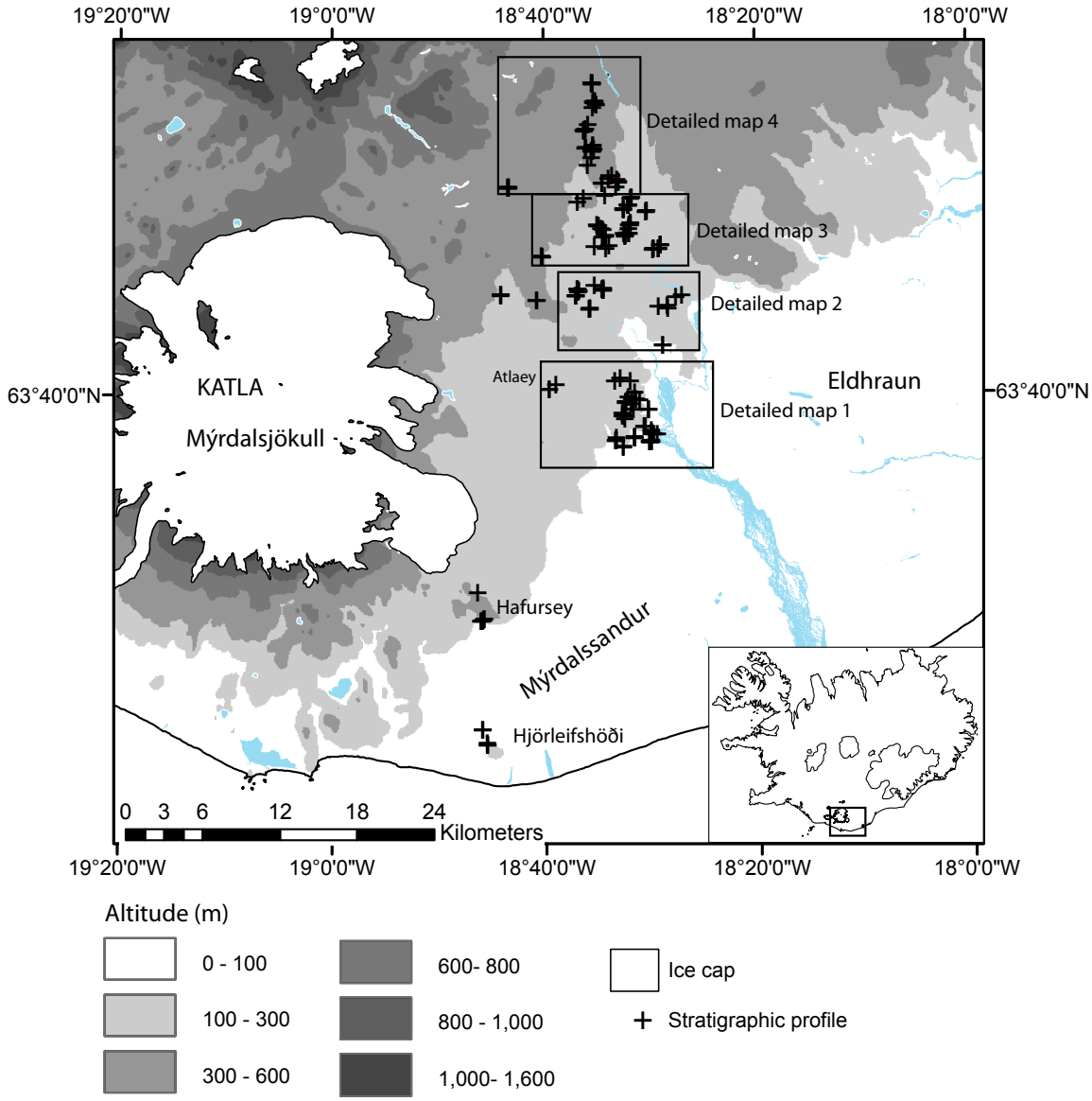

Figure 5.20: Profile locations in this study. Detailed maps are shown for four areas.

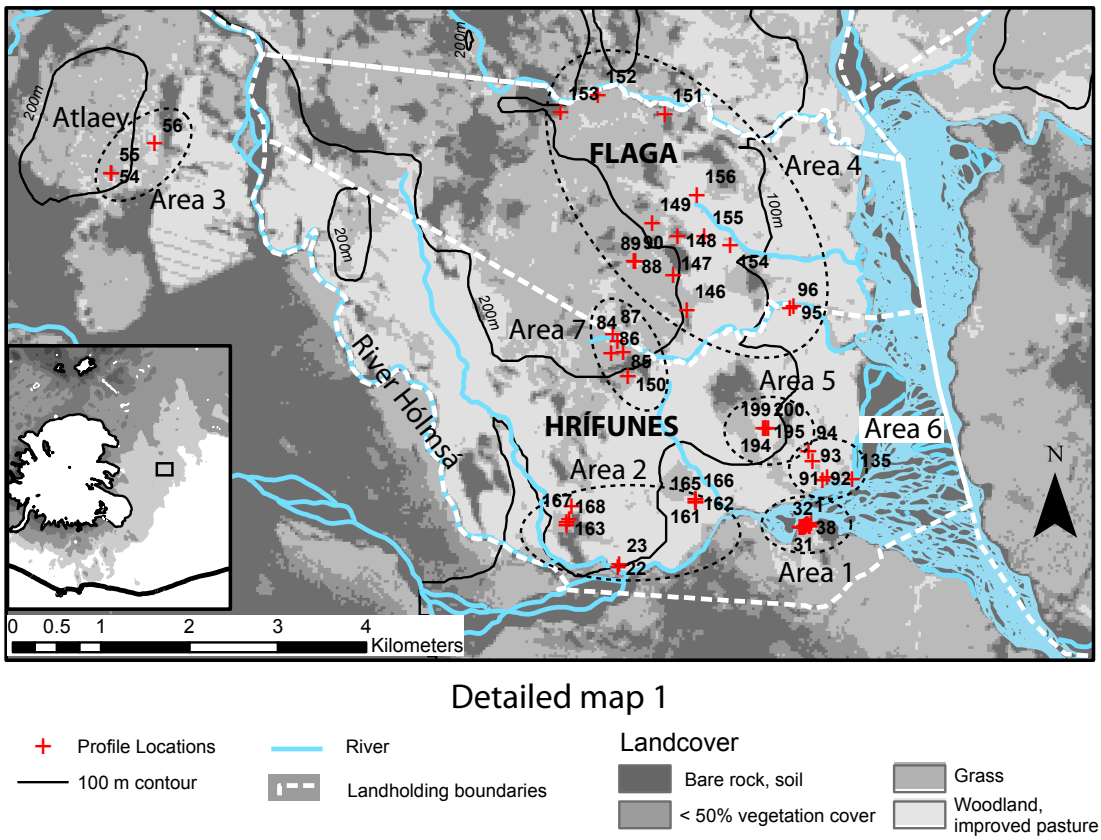

Figure 5.21: Area 1 — Hrífunes and Flaga landholdings profile location map. Shading represents NDVI vegetation cover in 2004.

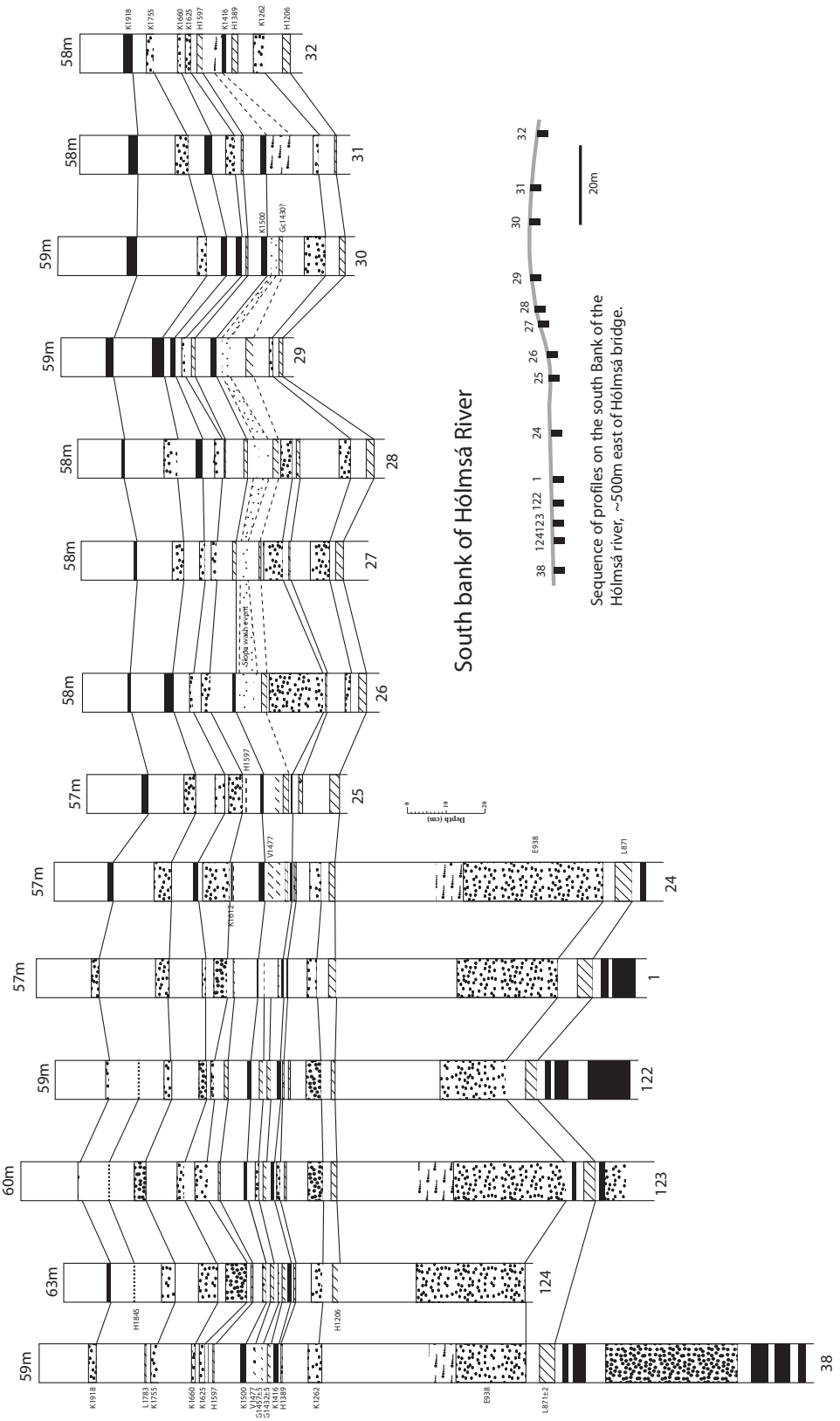

Figure 5.22: Area 1, site 1 —Stratigraphic sections recorded on a 150 m long section on the south Bank of the river Hólmsá

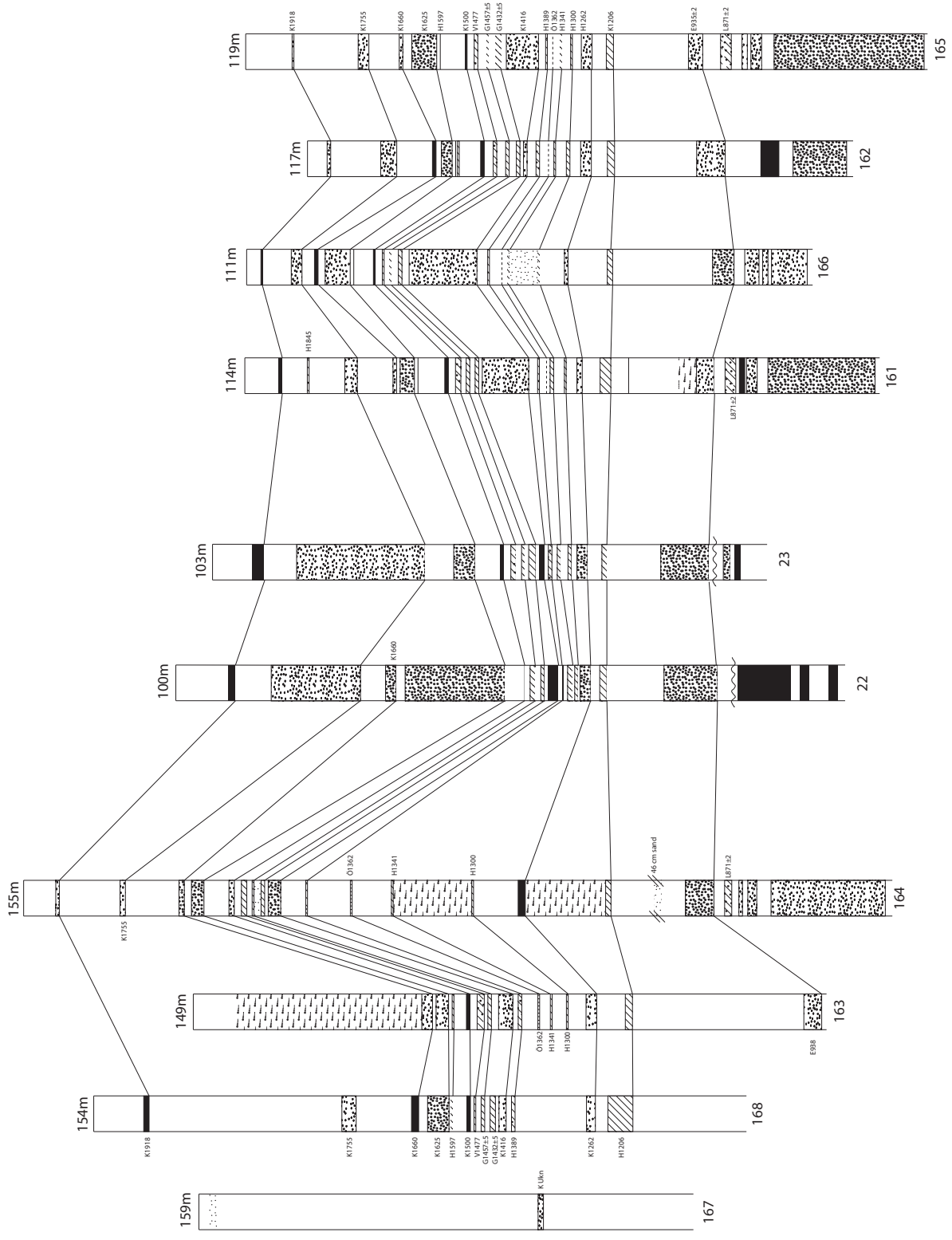

Figure 5.23: Area 1, site 2 — Sections west of Hómlsá bridge

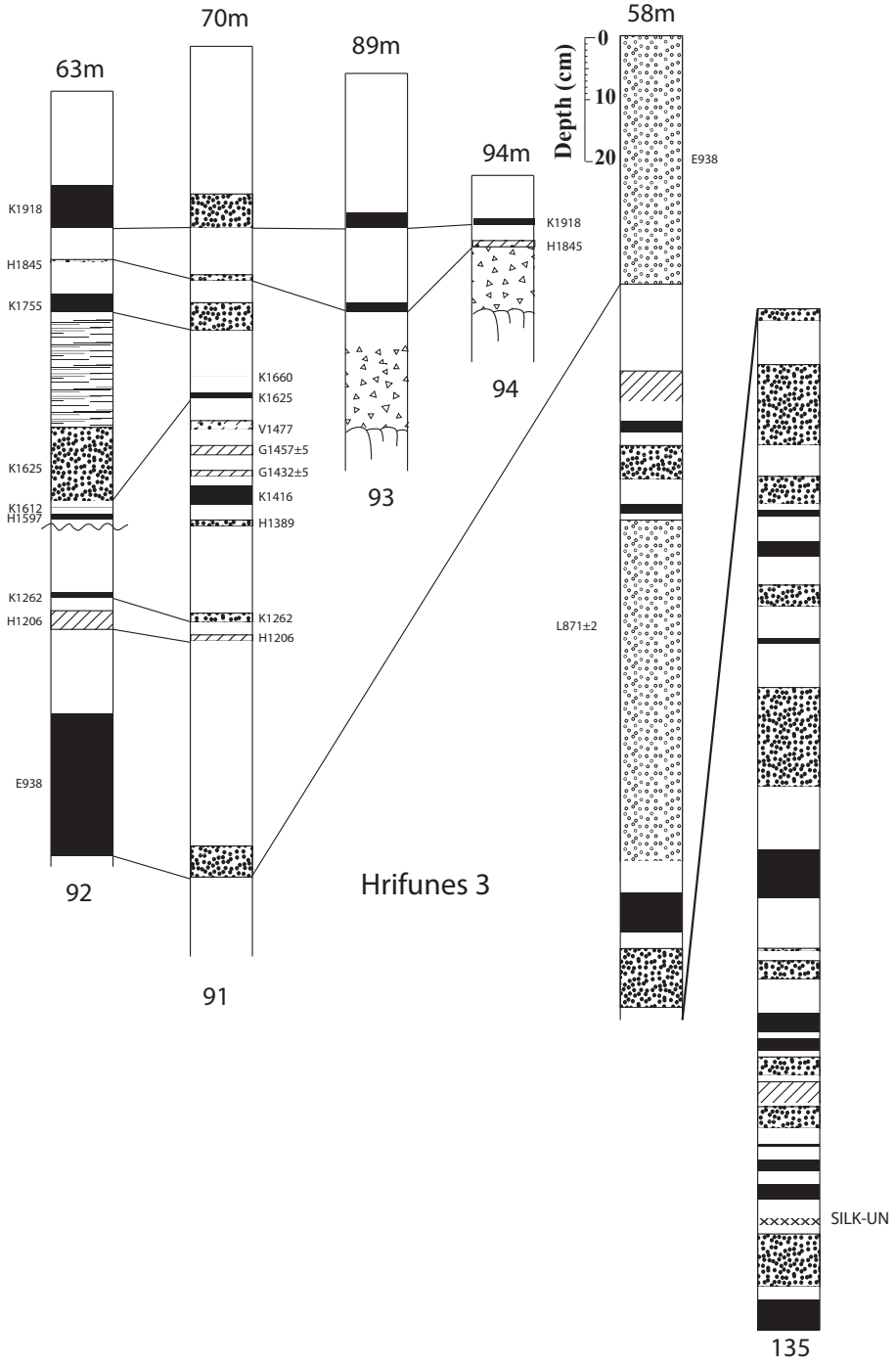

Figure 5.24: Area 1, site 6

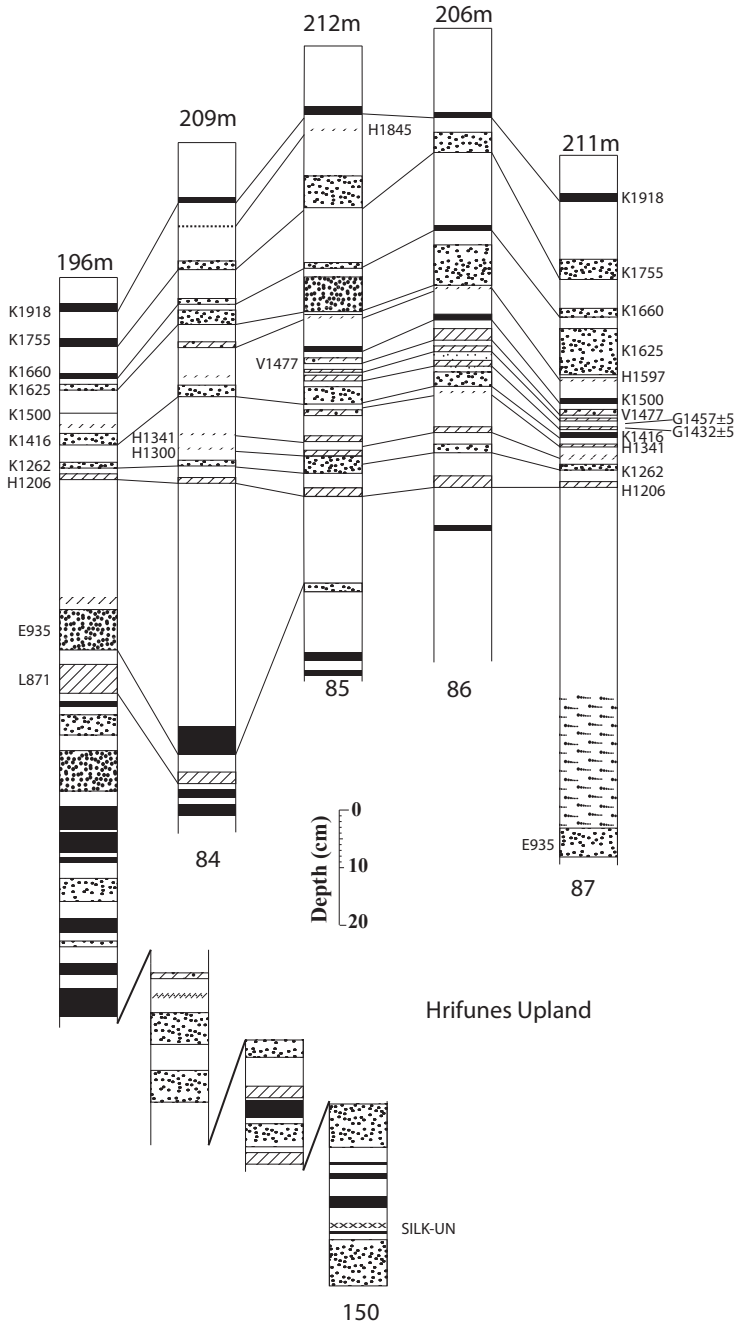

Figure 5.25: Area 1, site 7

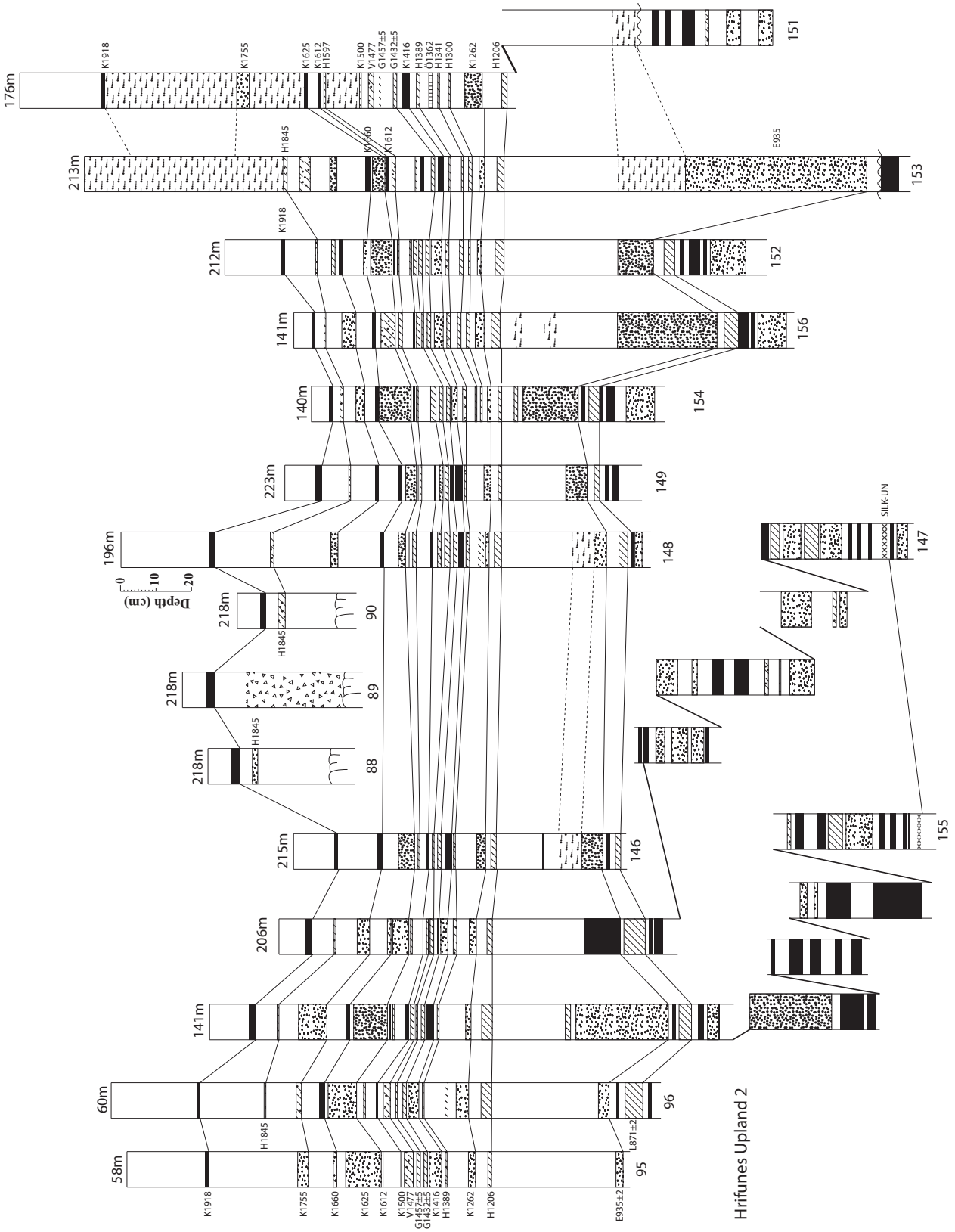

Figure 5.26: Area 1, site 4

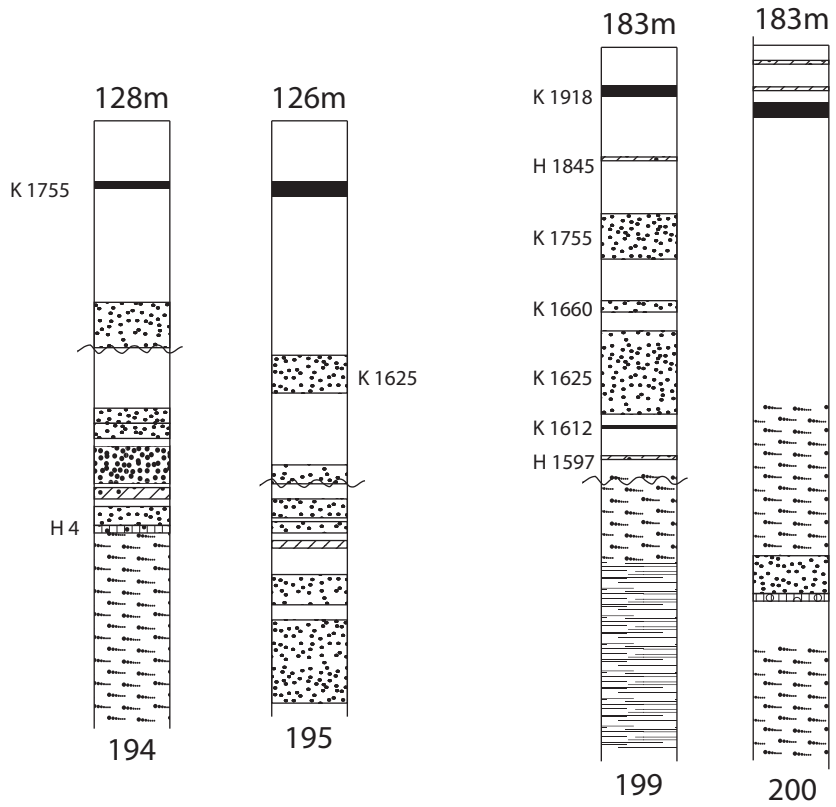

Figure 5.27: Area 1, site 5

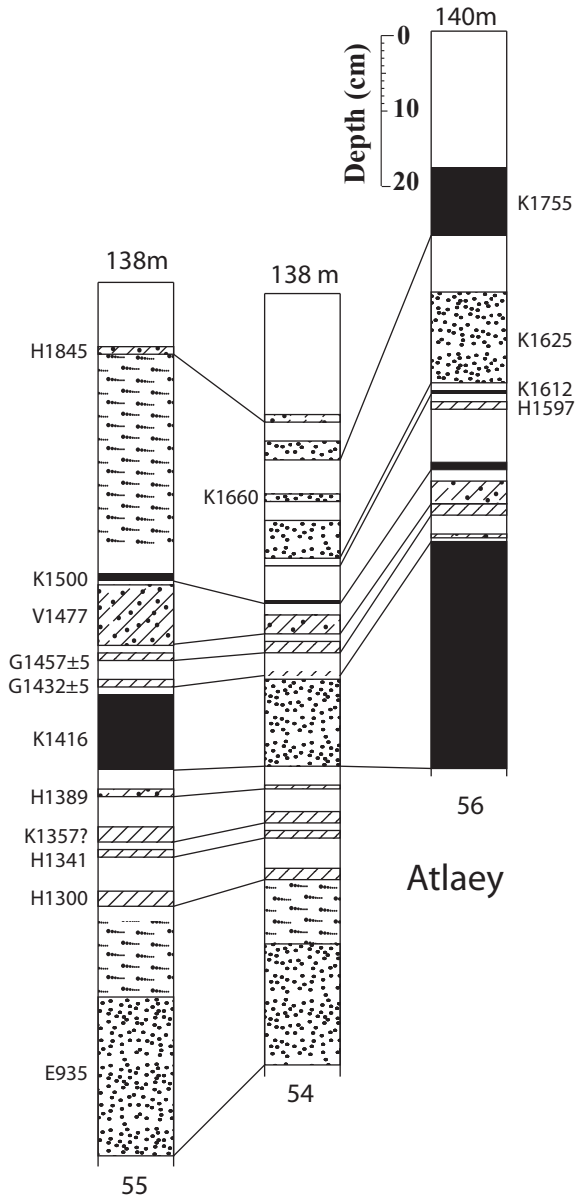

Figure 5.28: Area 1, site 3 — Atlaey Profiles

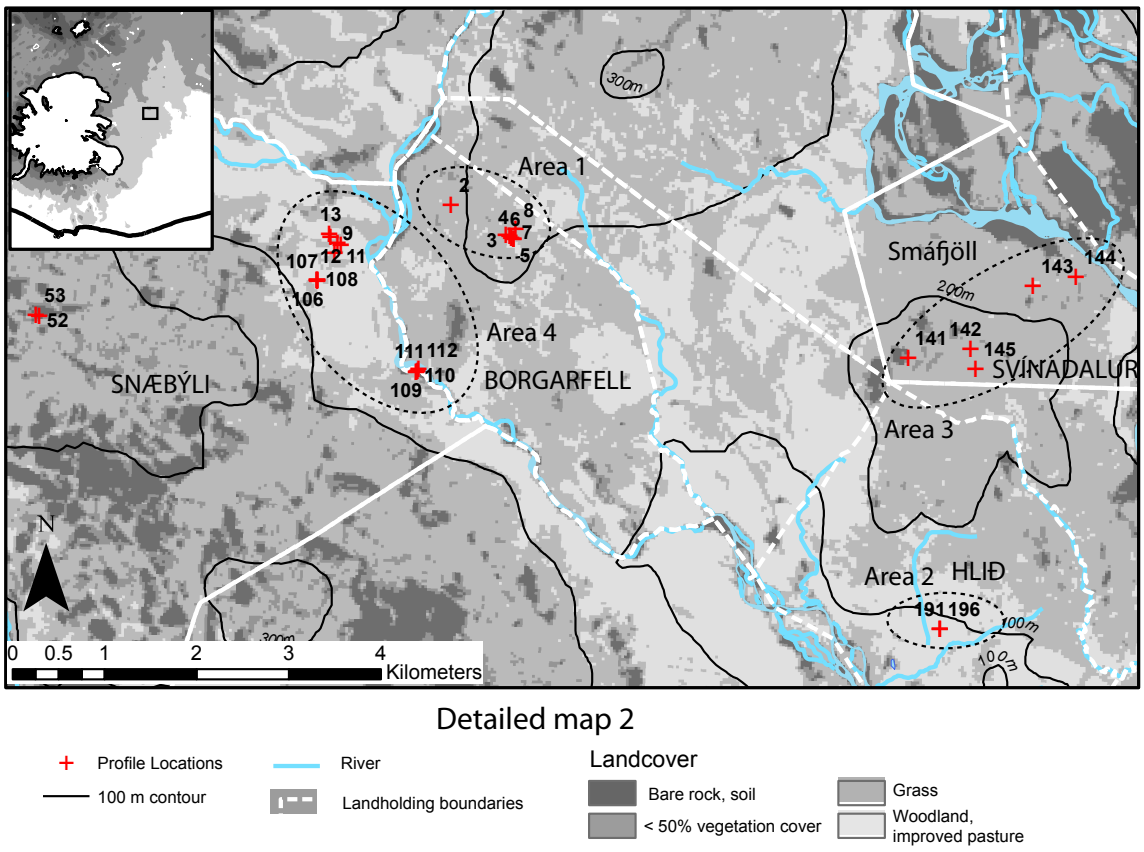

Figure 5.29: Area 2 — Snæblyí, Borgarfell profile location map. Shading represents NDVI vegetation cover in 2004

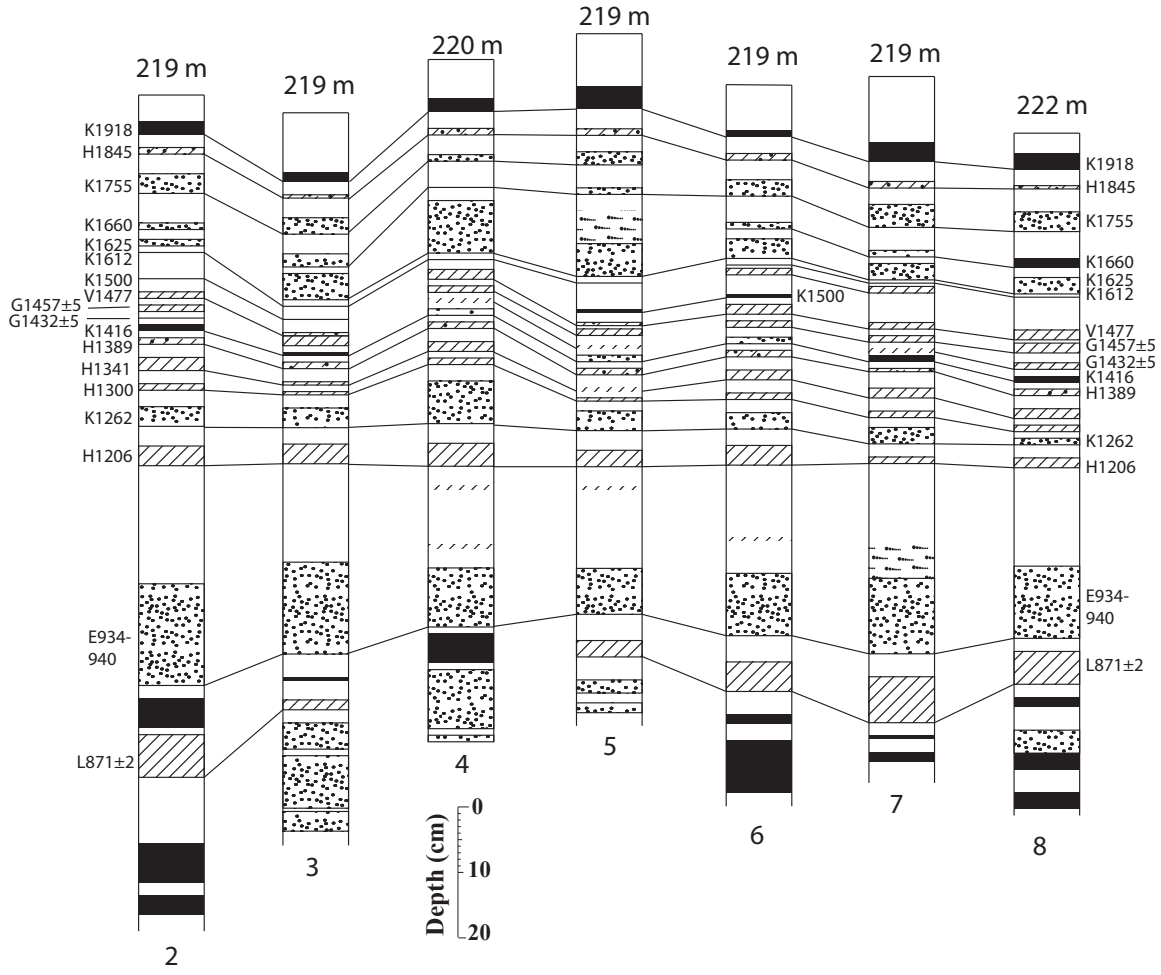

Figure 5.30: Area 2, site 1 — Borgarfell

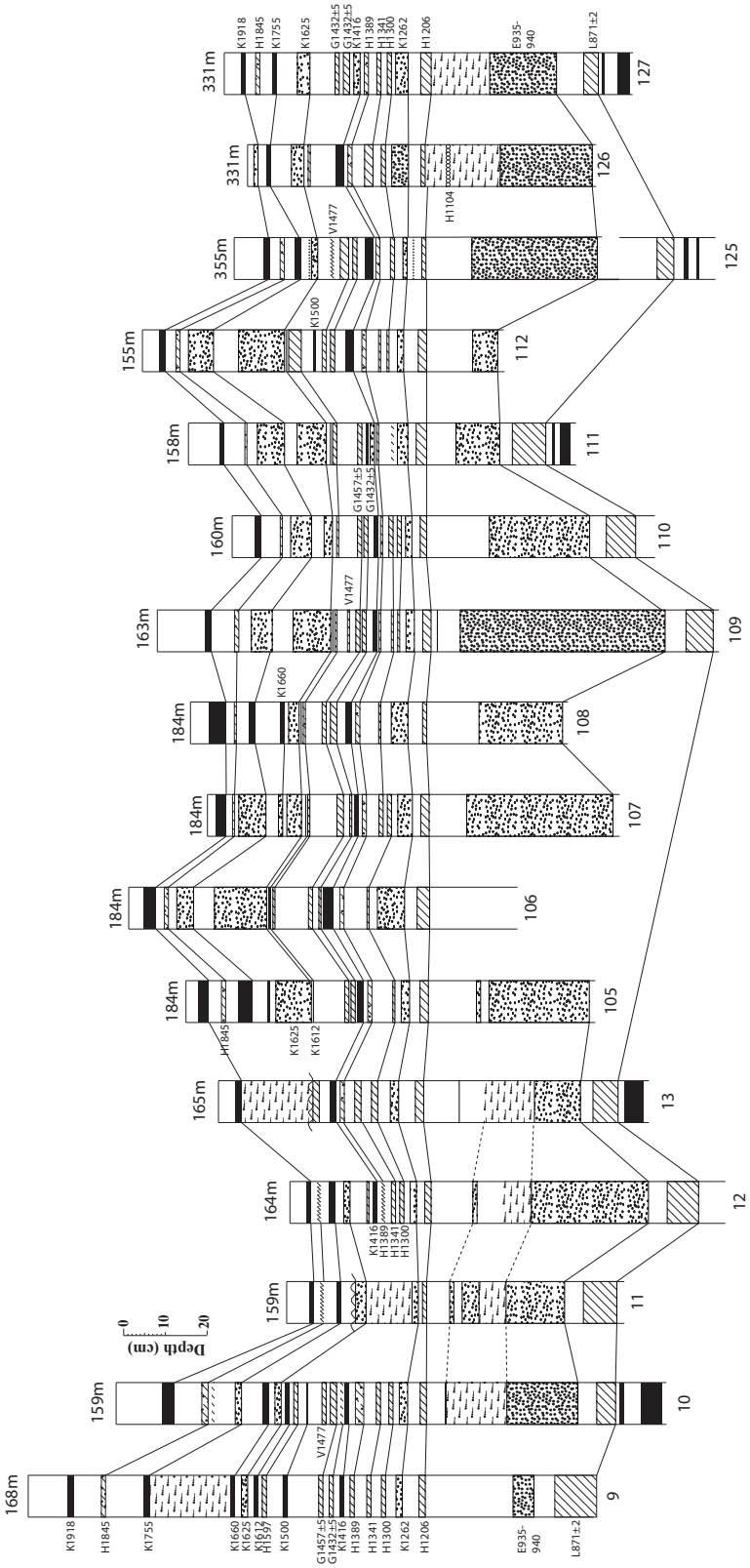

Figure 5.31: Area 4, site 4 — Snæblyí

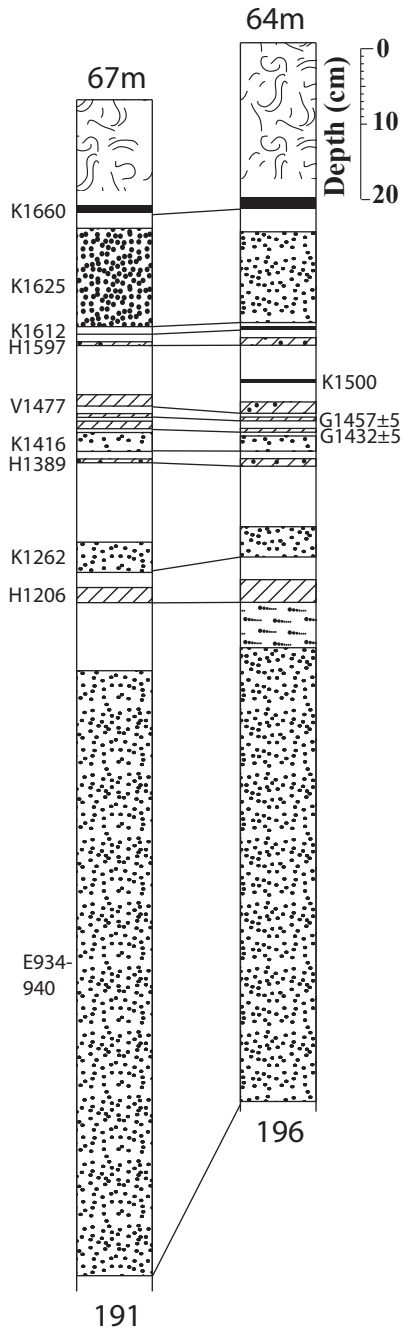

Figure 5.32: Area 2, site 2 — Hilð

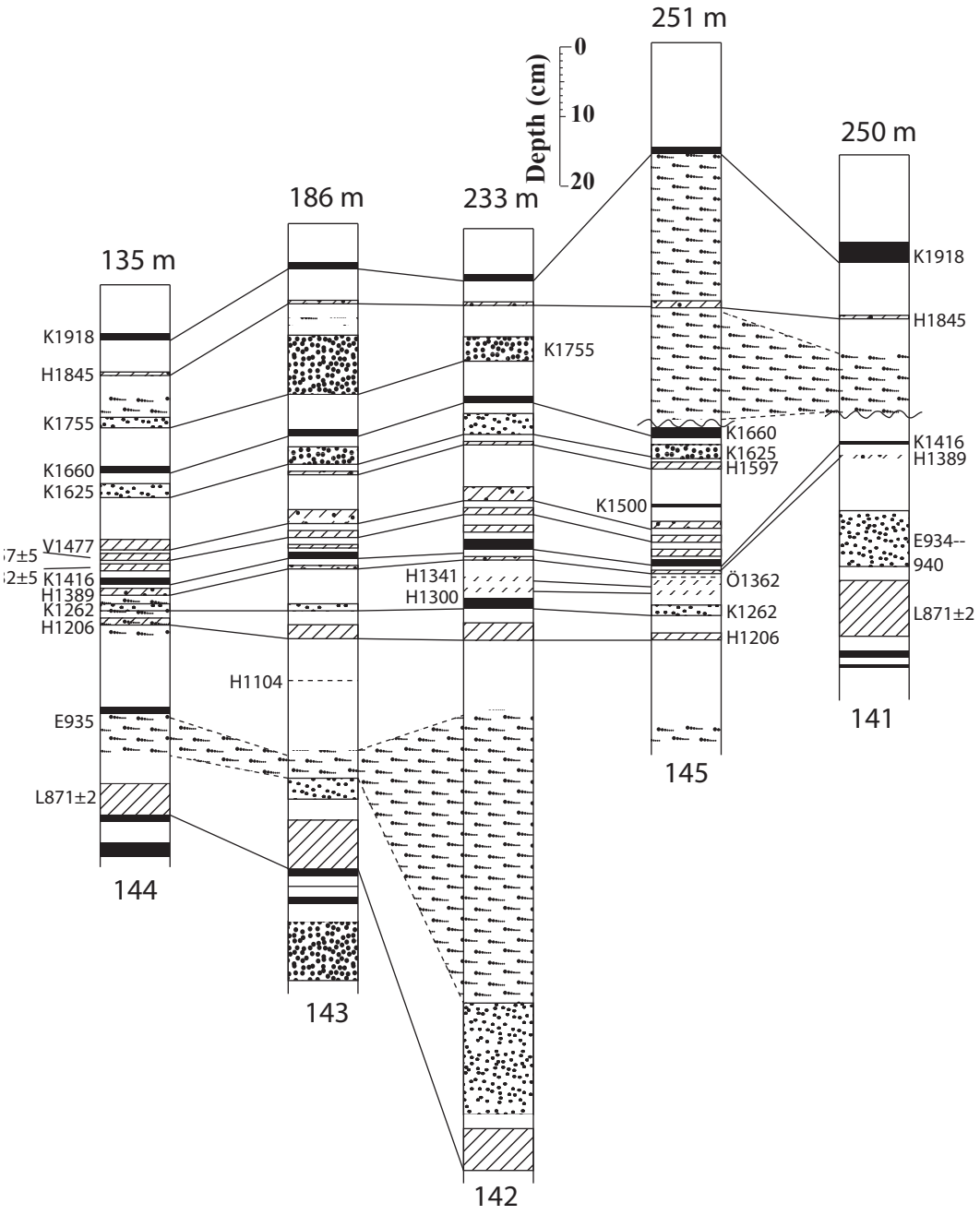

Figure 5.33: Area 2, site 3 — Hussafell

5.4.3 Area 3 — Búland and areas of communal grazing

The farm of Búland is located at the altitude of 280 m. The location of sections from here is indicated in Figure 5.34. This area has two abandoned farms marked on current maps. The name of Bulandssel suggests is was a sheiling site, and there is no record of it before AD 1845 (personal communication, Hildur Gestsdóttir). Svartinúpur does appear on the Jarðabok AD 1703 census (Census, 1703), but it is not clear when it was abandoned.

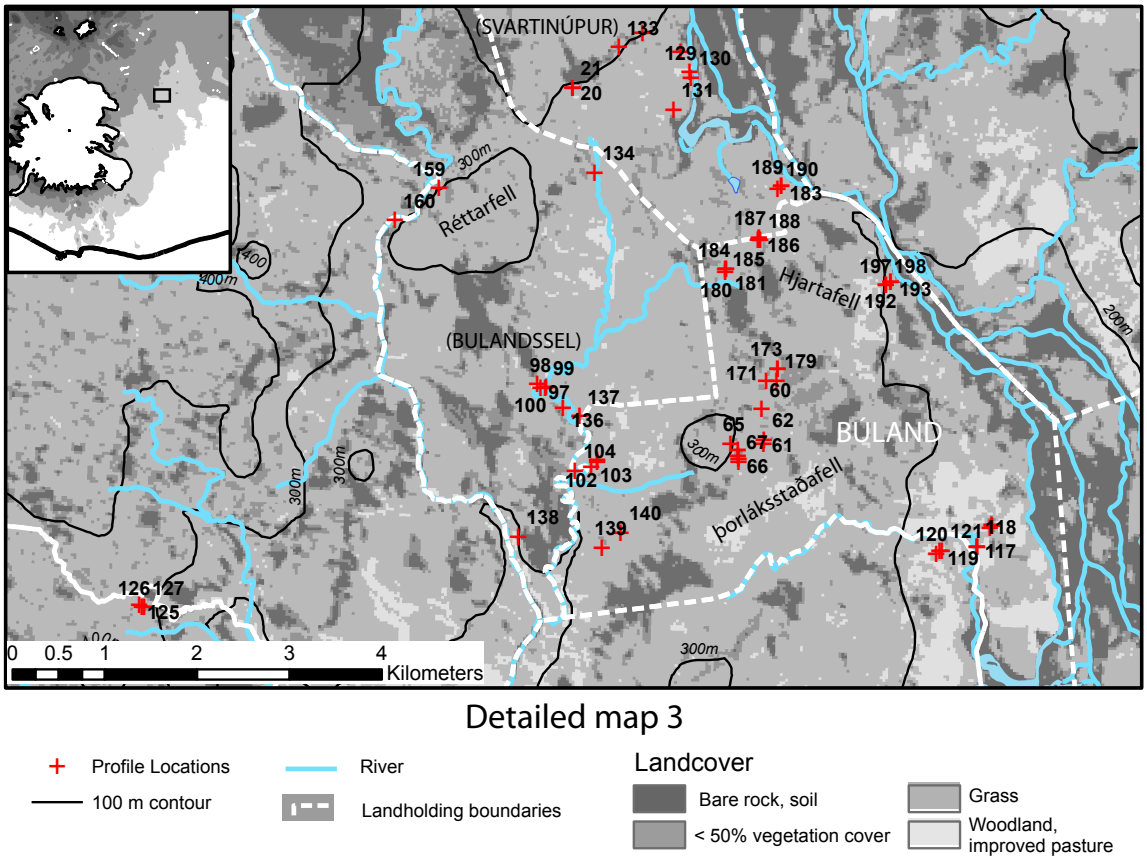

Figure 5.34: Area 3 — Búland profile location map. Shading represents NDVI vegetation cover in 2004

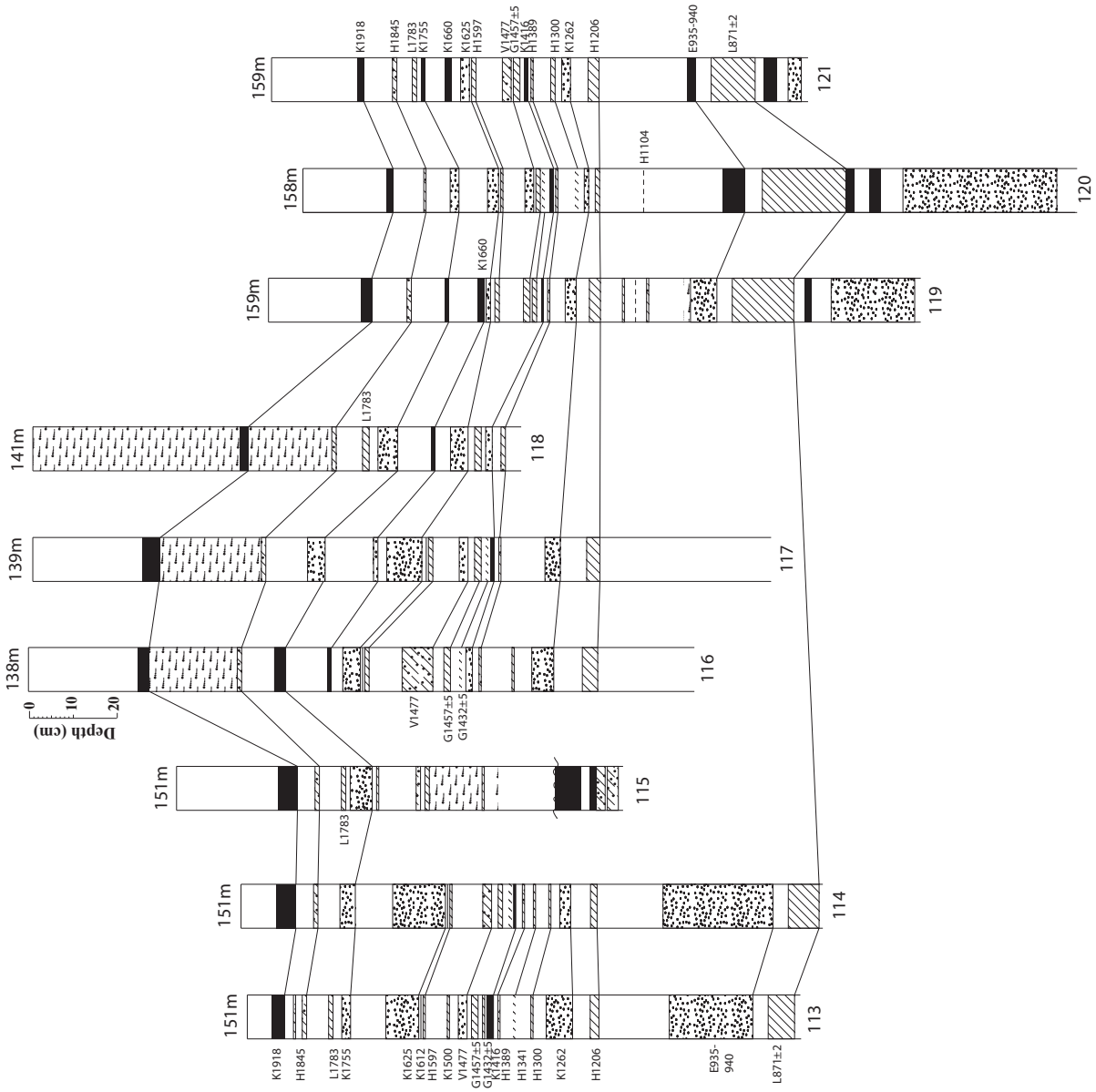

Figure 5.35: Area 3, site 1 Búland

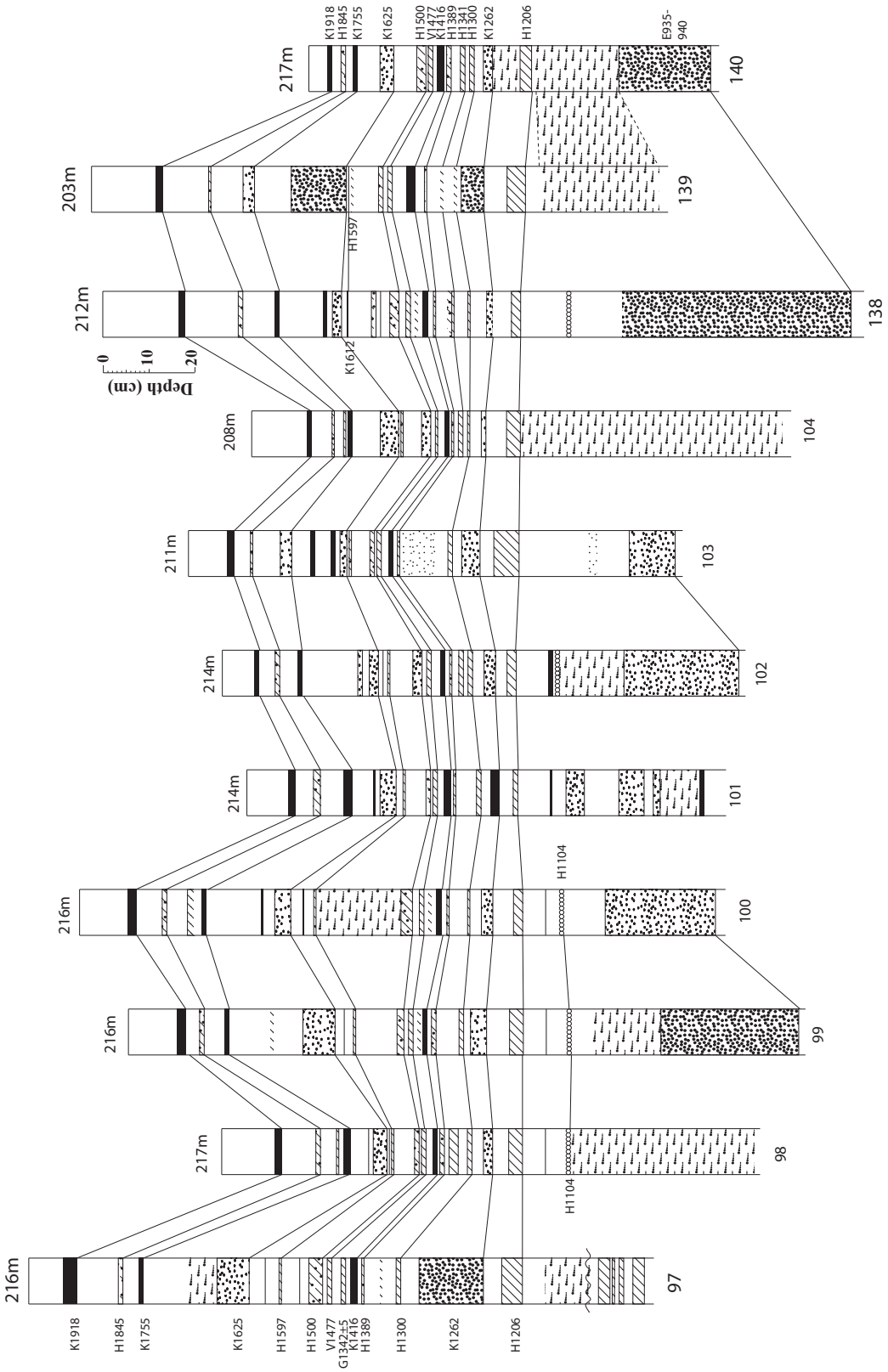

Figure 5.36: Area 3, site 2 — Bulandssel

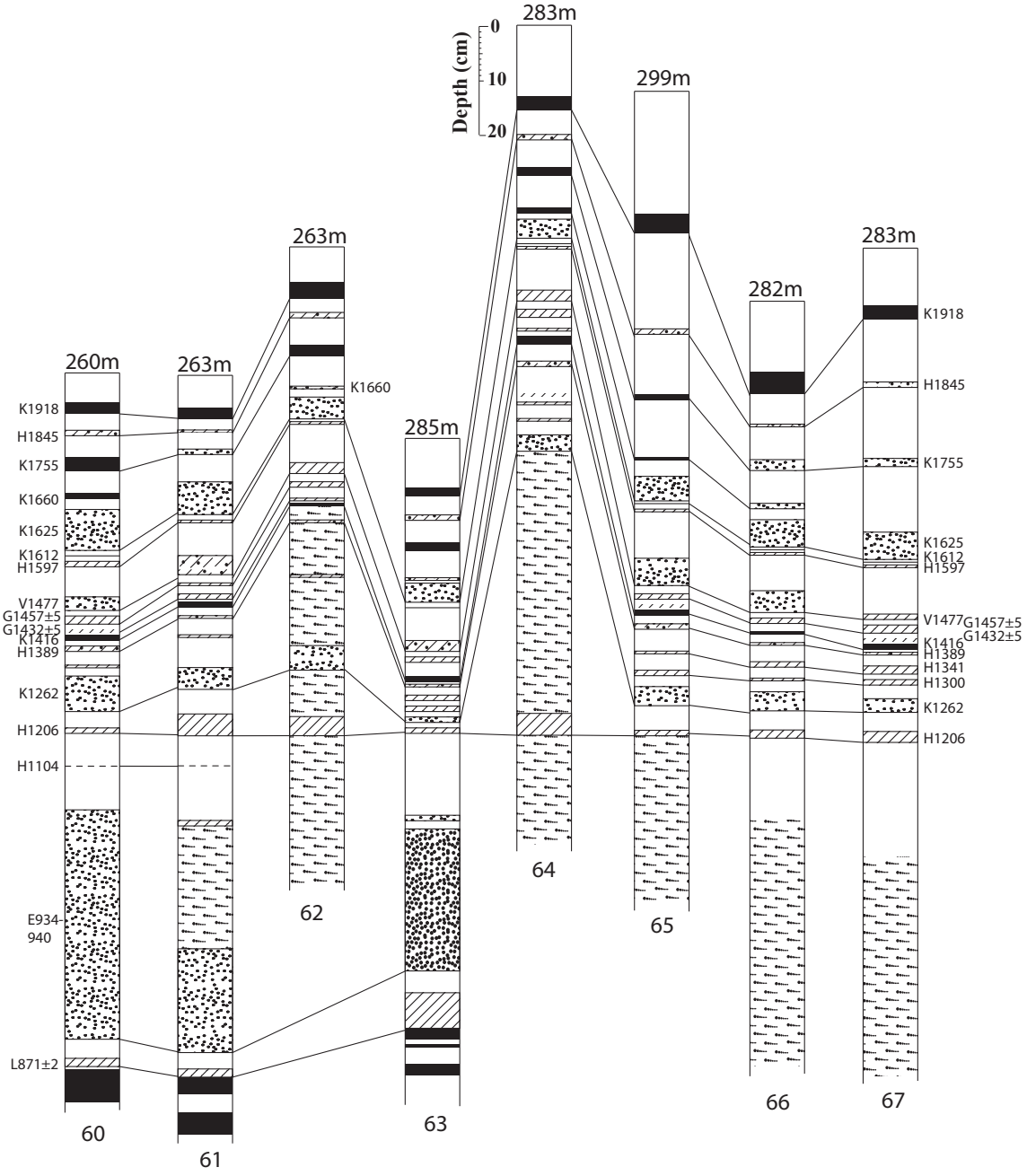

Figure 5.37: Area 3, site 3 —Þorlásstaðafell

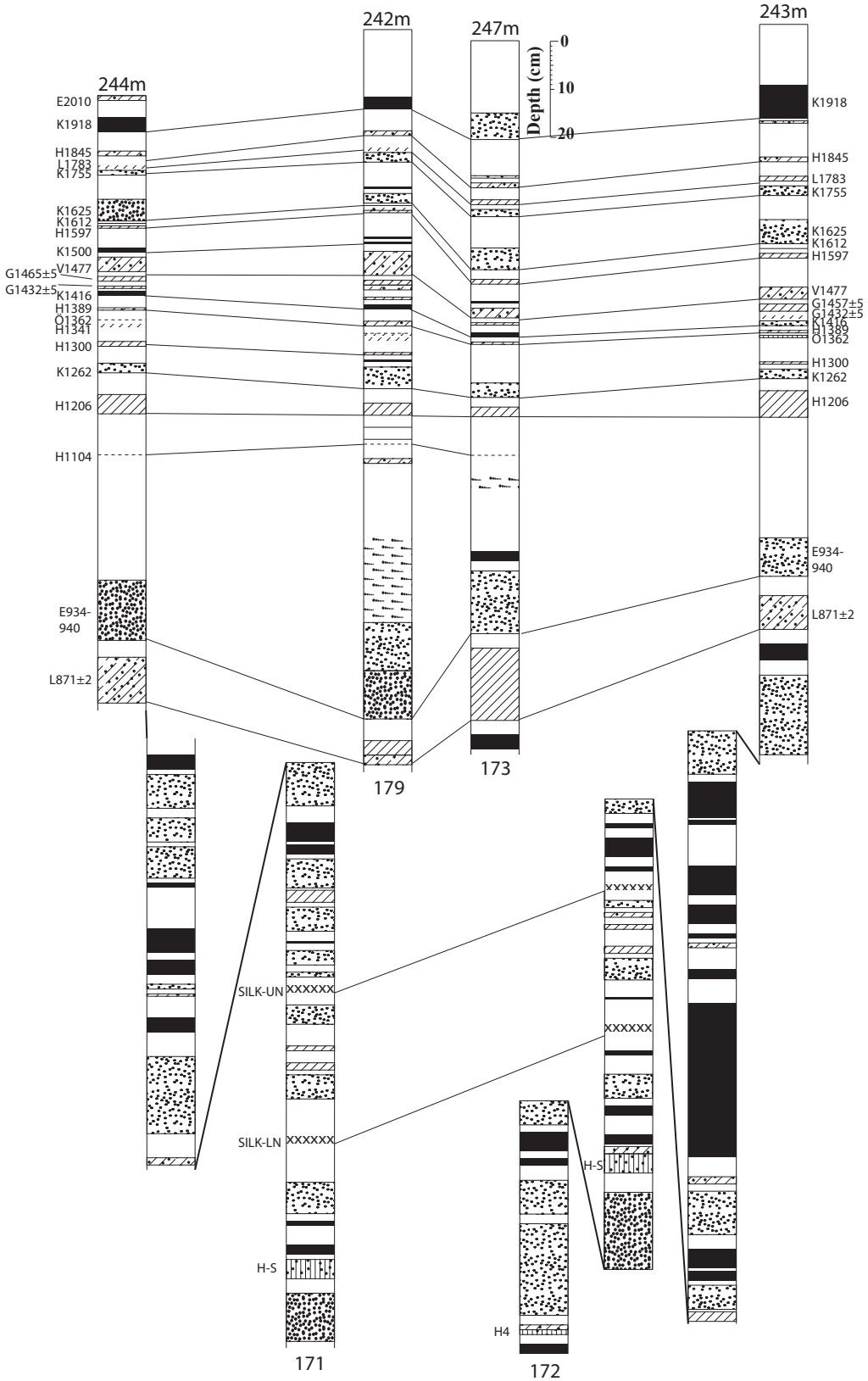

Figure 5.38: Area 3, site 4 —Þorlásstaðafell

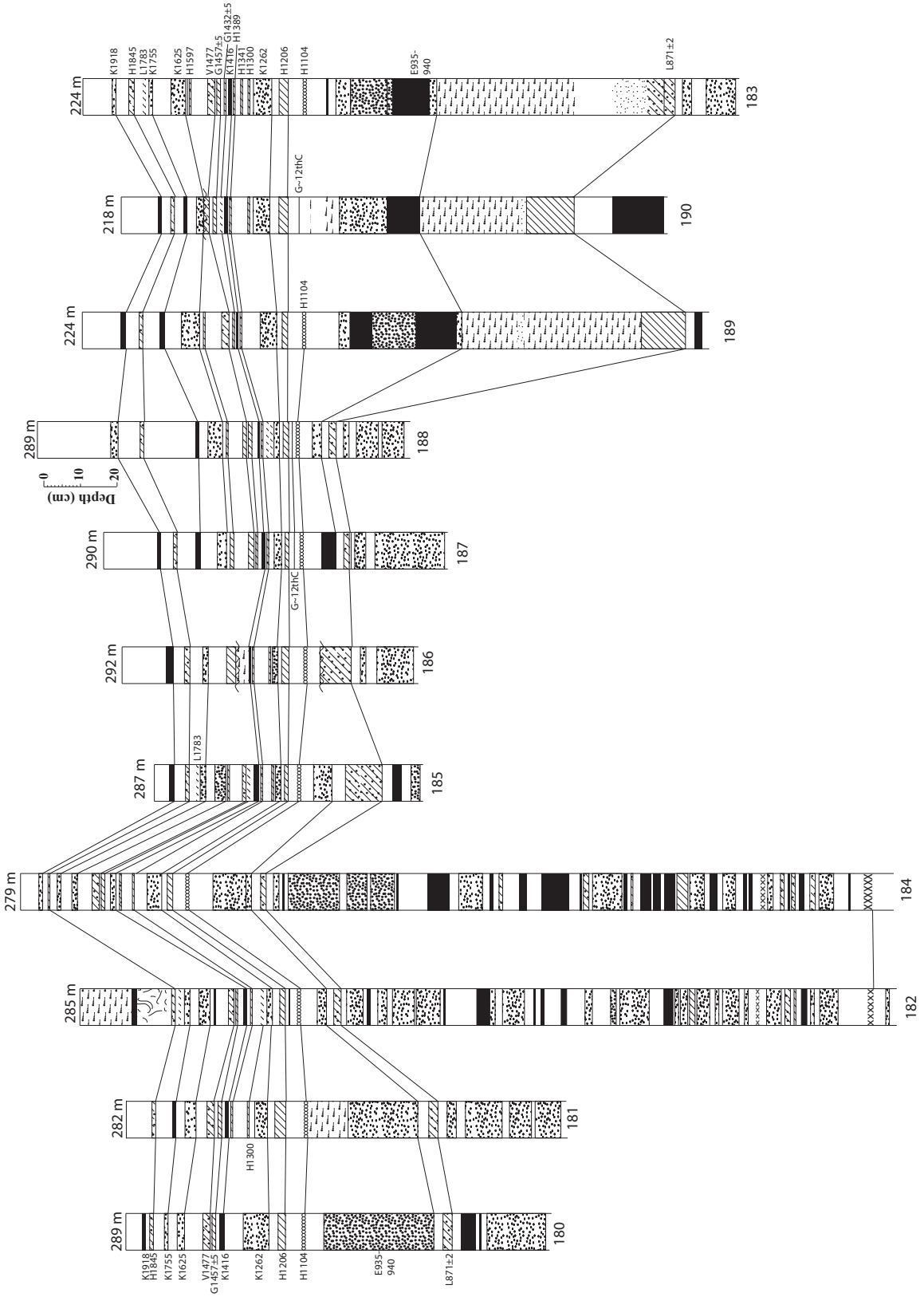

Figure 5.39: Area 3, site 5 —Hjartafell

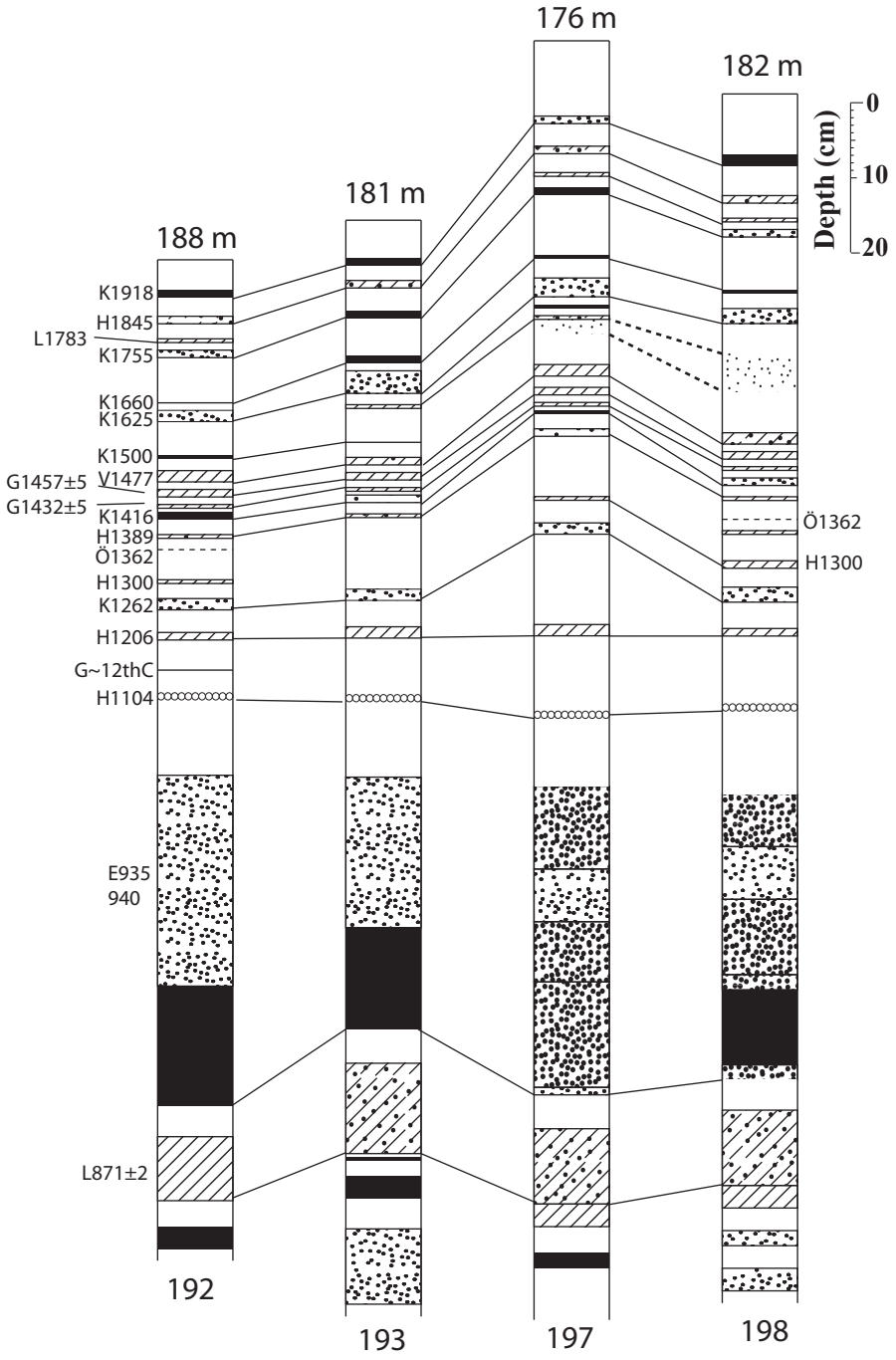

Figure 5.40: Area 3, site 6 — Hjartafell

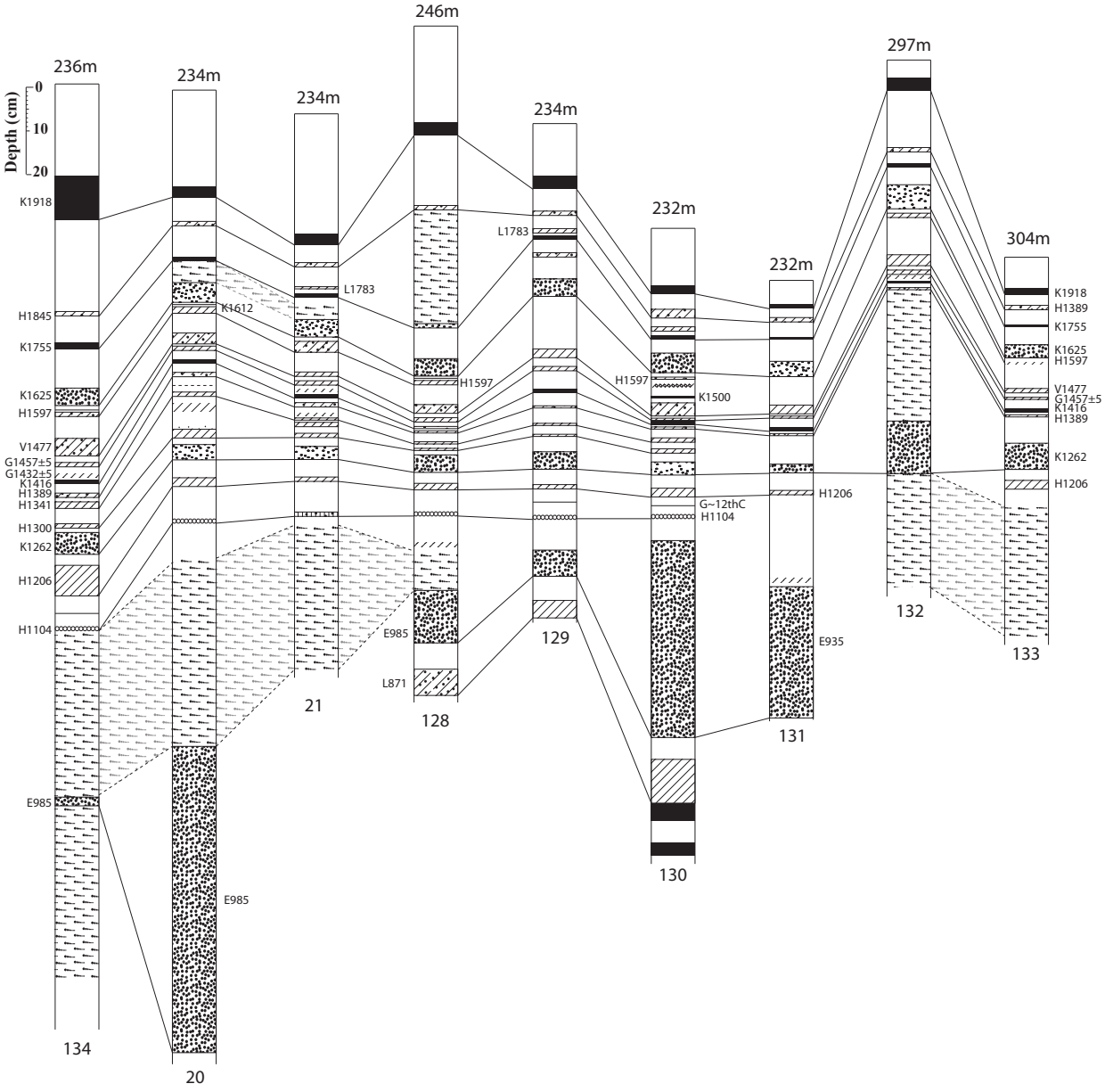

Figure 5.41: Area 3, site 7 — Nupshethi

5.4.4 Area 4 — Communal grazing areas

Sections from areas of communal grazing are recorded. The following sections are shown in the detailed map in Figure 5.42.

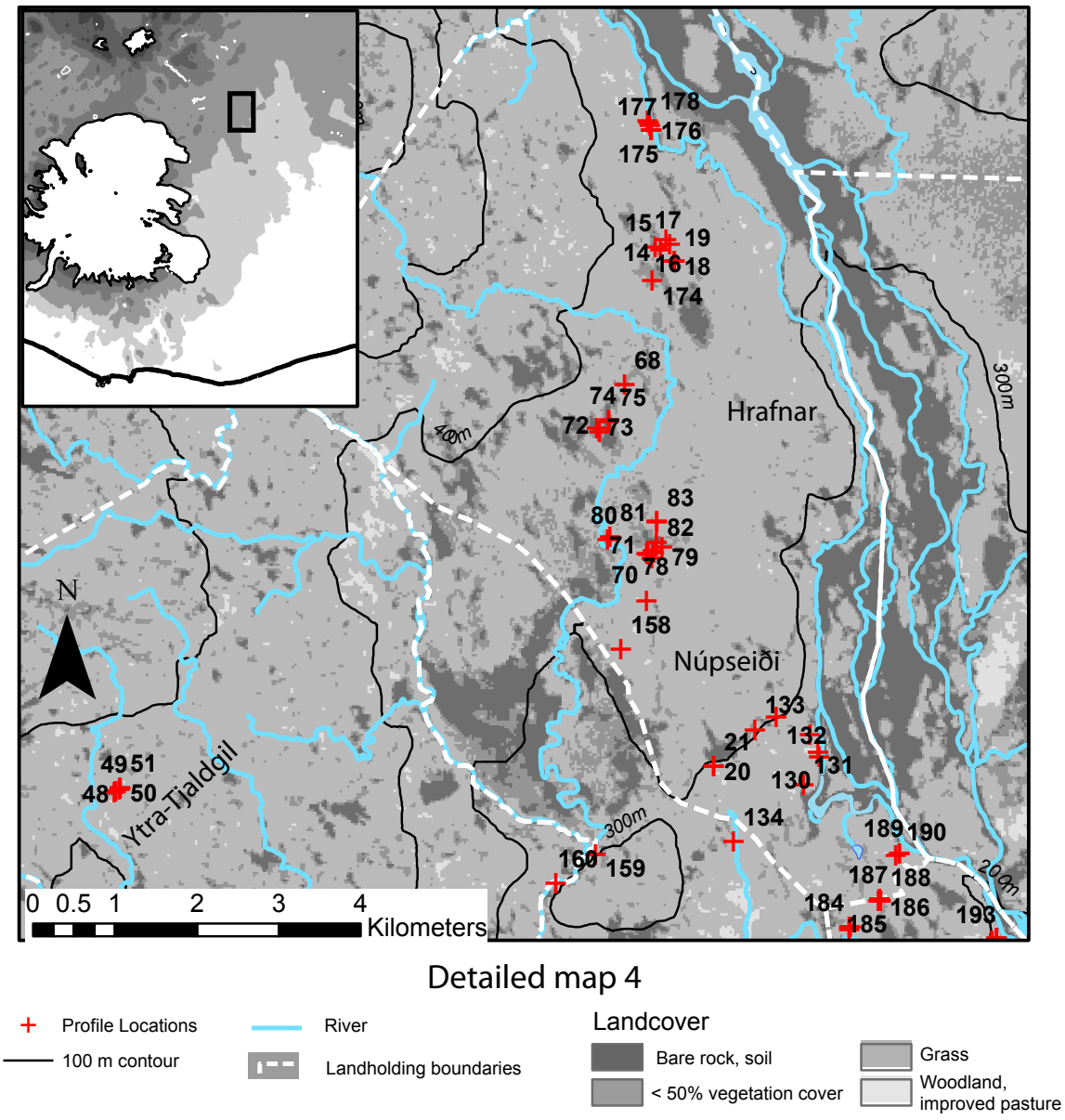

Figure 5.42: Area 4 - Communal grazing, 200 to 368 m. Shading represents NDVI vegetation cover from 2004

5.4.5 Ytra-tjaldsheil and Holmsarfoss

The following stratigraphic profiles were located in areas that were not associated with any particular landholdings, but that may still have been grazed. Sections from Figure 5.47 are located in Figure 5.42.

Figure 5.43: Area 4, site 1

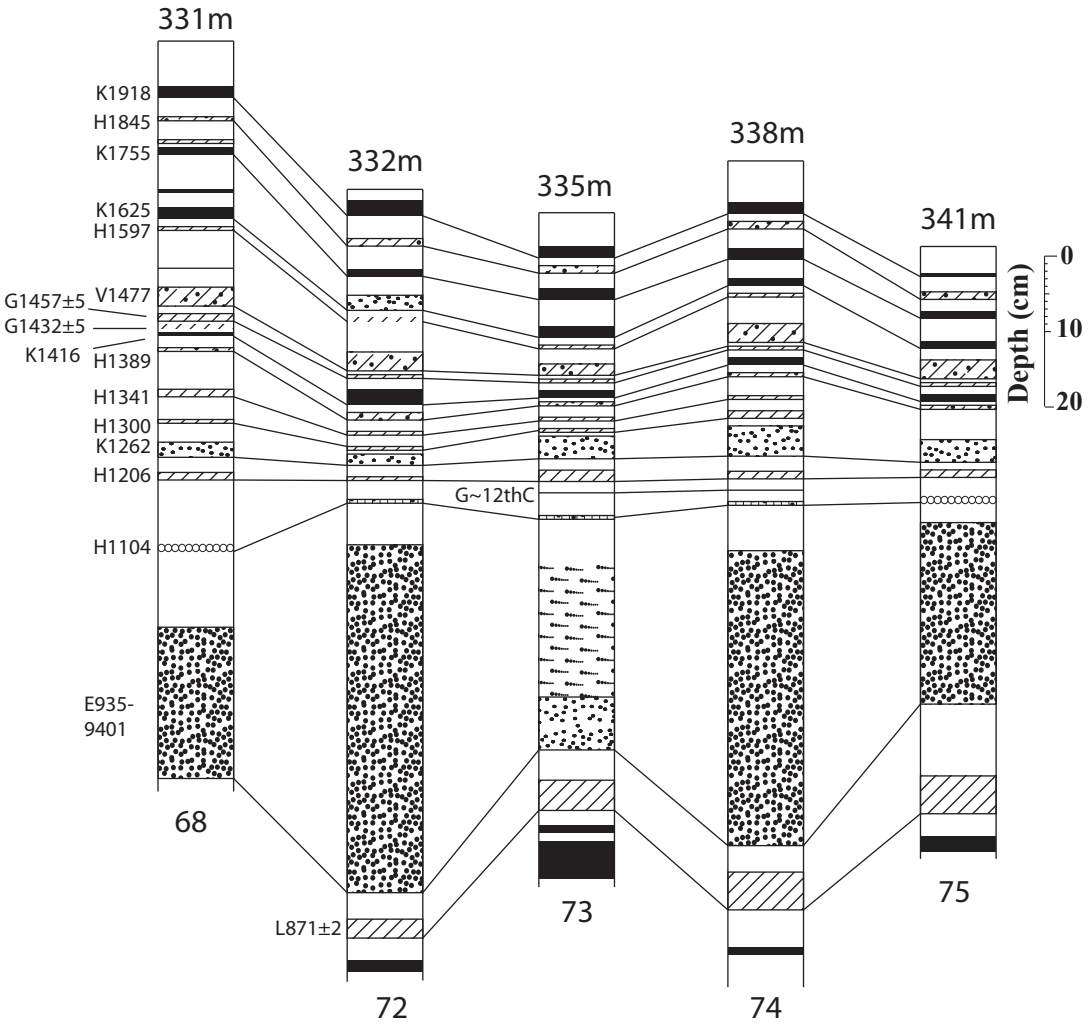

Figure 5.44: Area 4, site 2

5.4.6 Mýrdalssandur

In order to expand the chronology 11 sections were dug on Mýrdalssandur. Five were collected from Hjörleifshöðí. The chronology was similar to that found in Skaftártunga, with the addition of the Katla AD 1357 tephra, however tephra preservation was not as good. The main feature observed was widespread instability starting immediately after the K 1416 tephra, which continued through until K 1918. This produced exceptional SeAR rates of > 6 mm yr^{-1} as active slope wash deposited material. Despite this instability the sites were still vegetated. Sections on Harfursey (Figure 5.50 and 5.20) were short and located on steep slopes. Their proximity to the Katla mean they pick up additional tephra layers, K 1357 and K 1721.

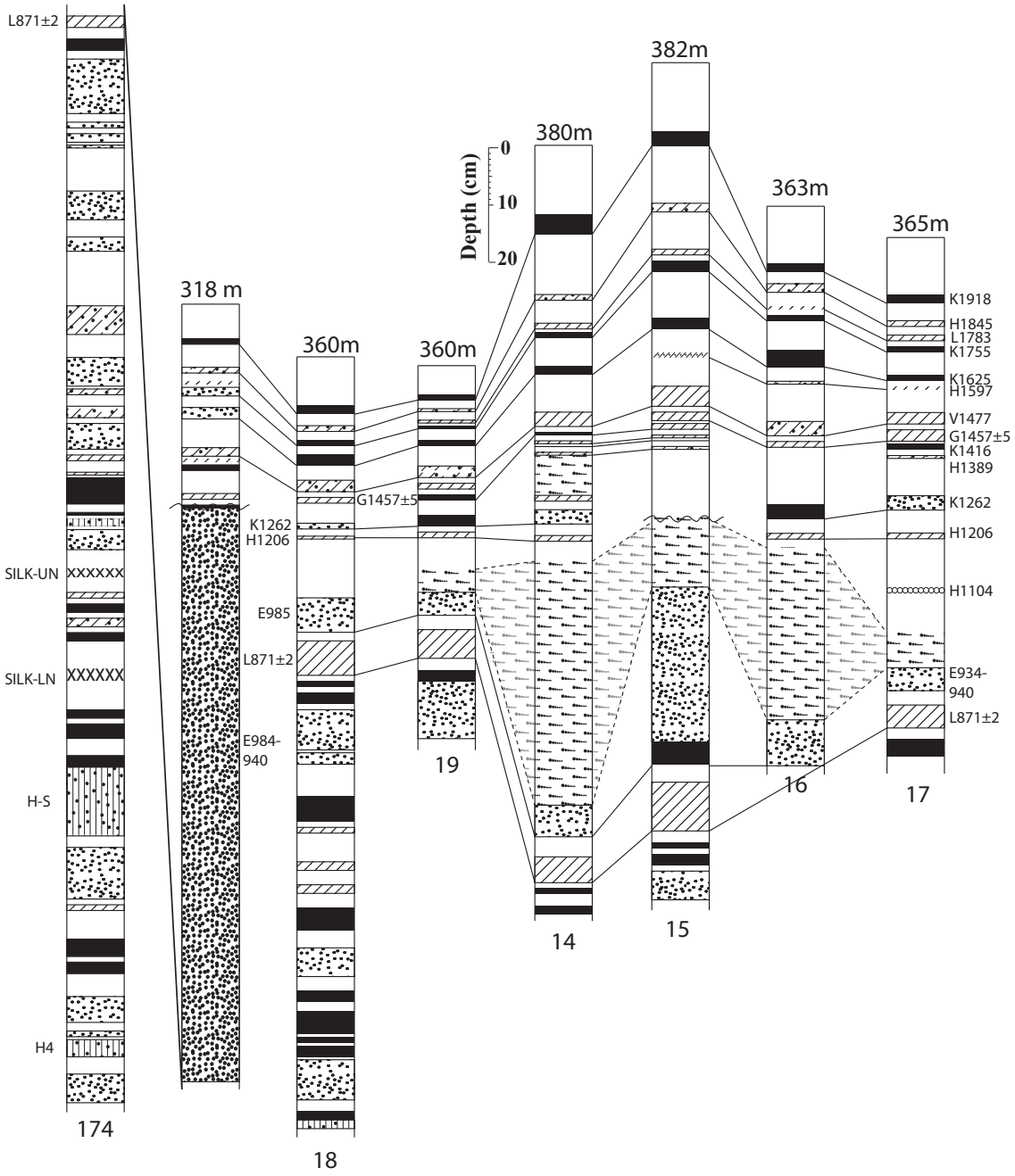

Figure 5.45: Area 4, site 3

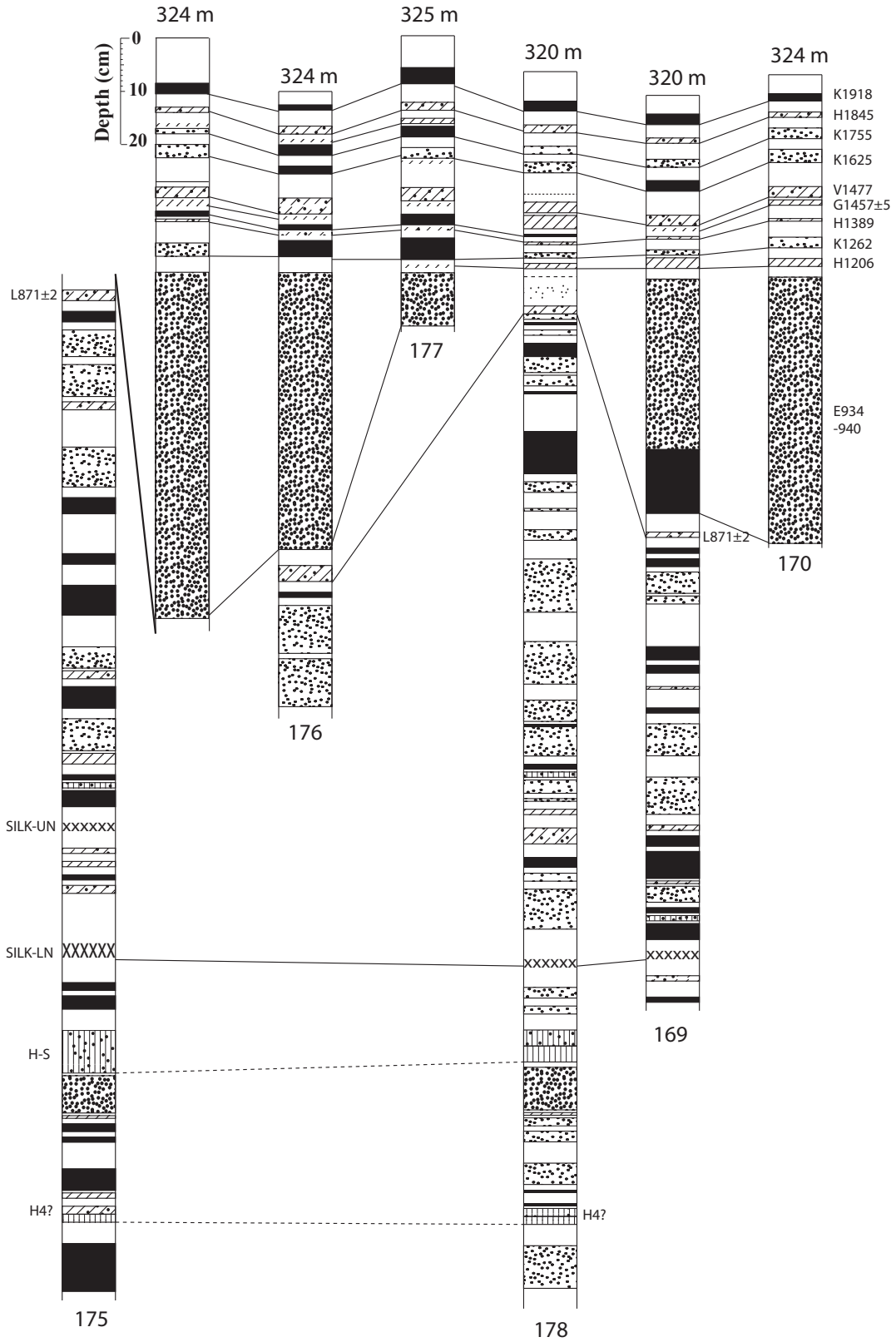

Figure 5.46: Area 4, site 4

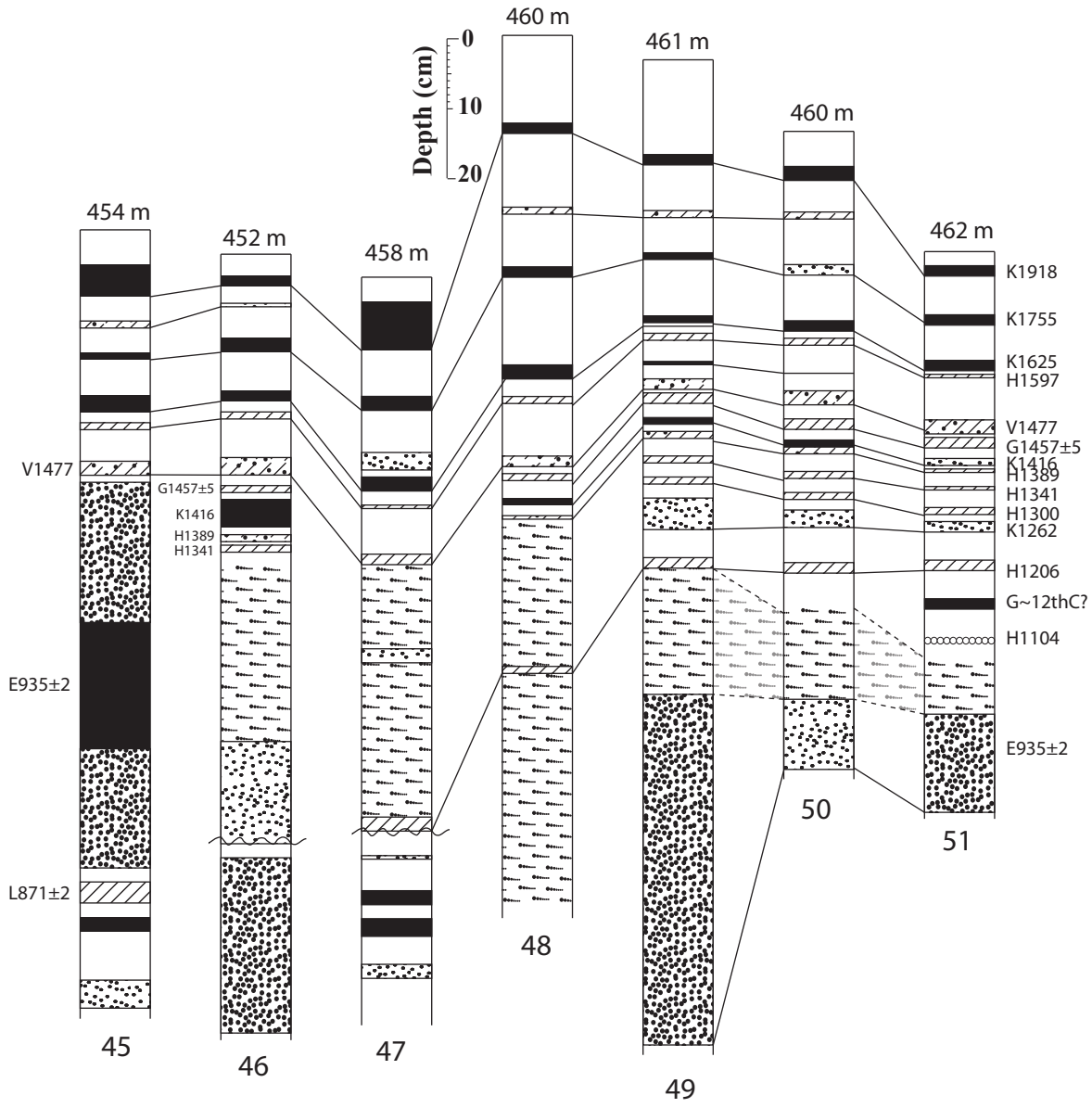

Figure 5.47: Area 4, site 3 — Ytra-Tjaldgil

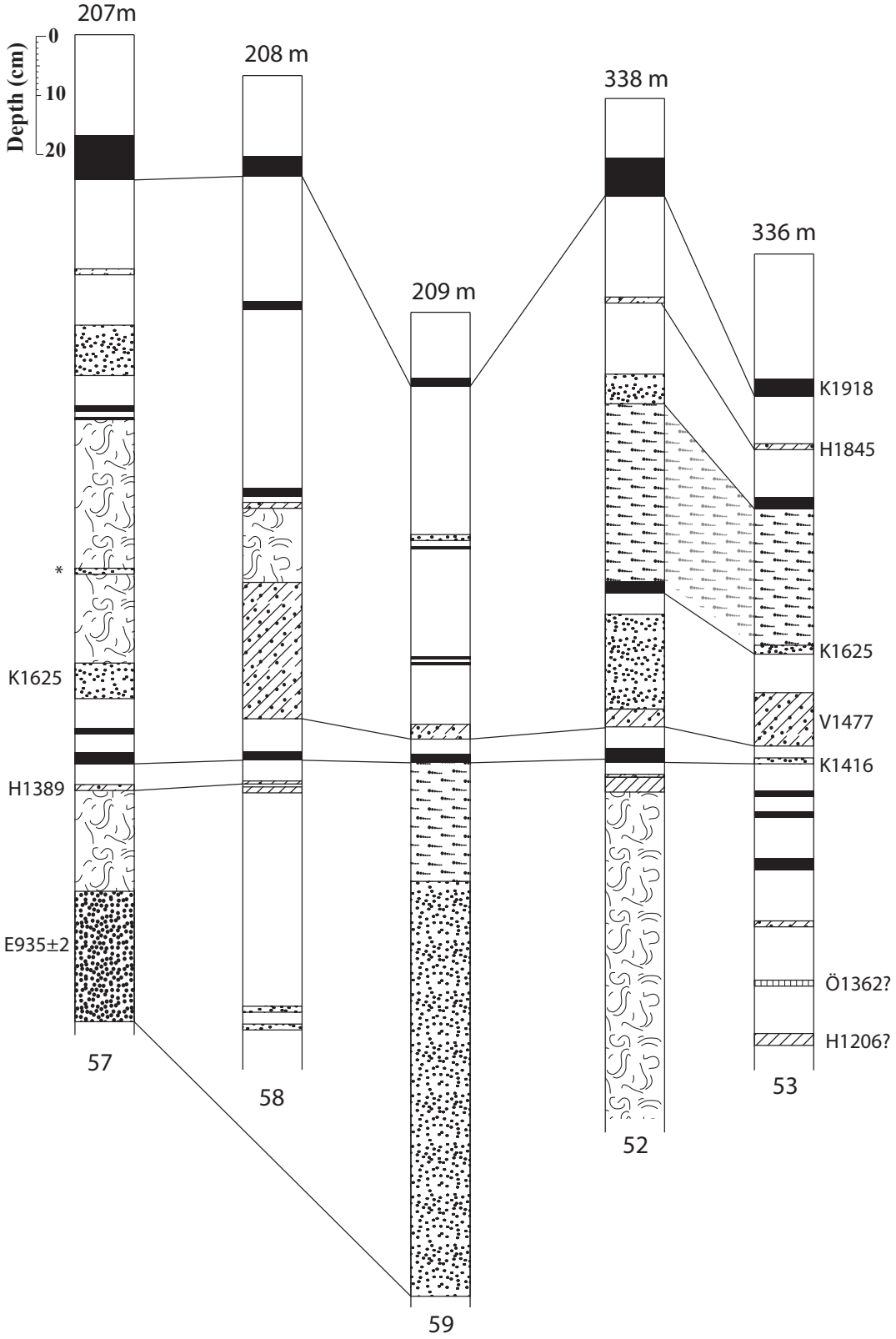

Figure 5.48: Sections from Loðnugil

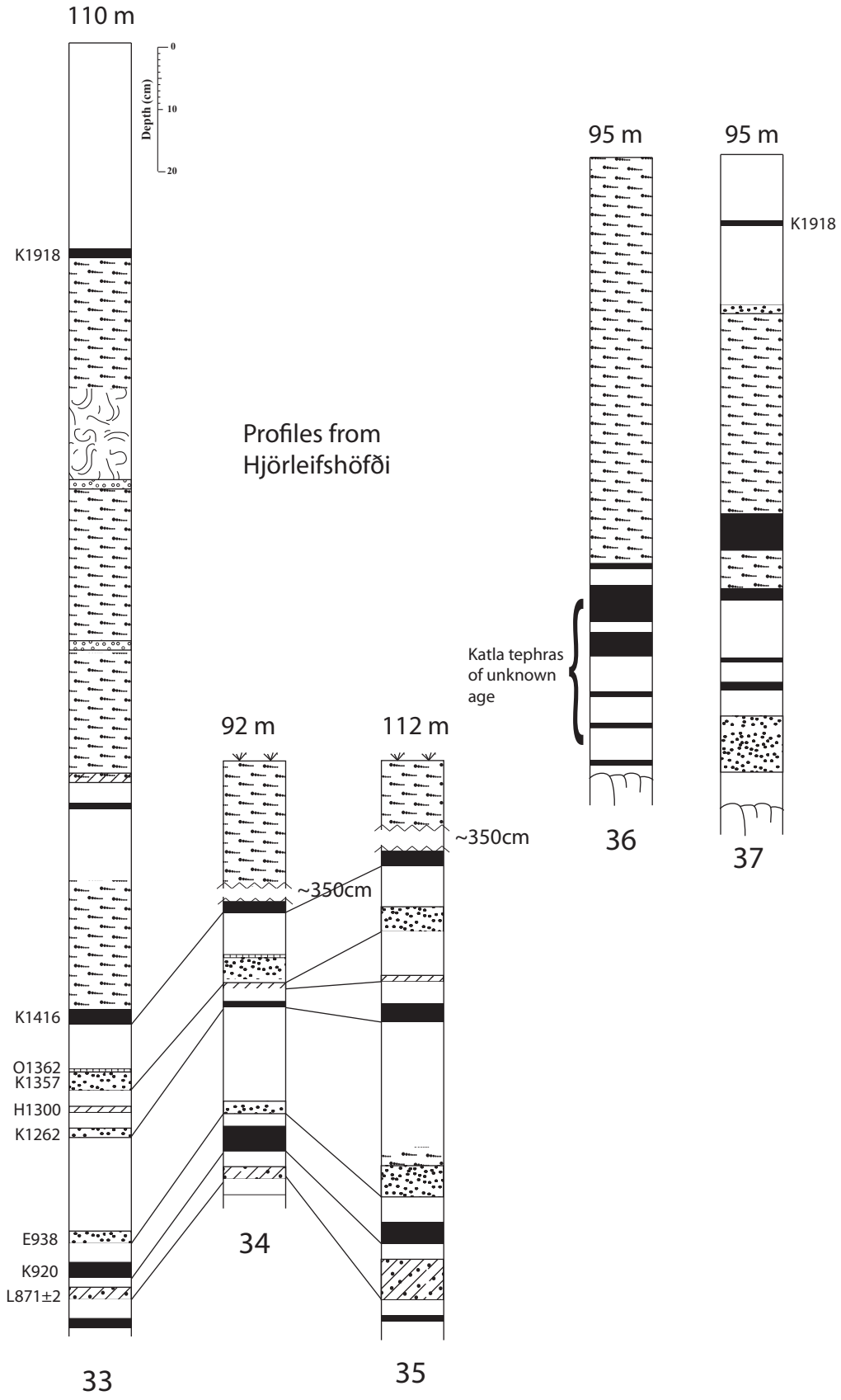

Figure 5.49: Sections from Hjörleifshófði, Mýrdalssandur

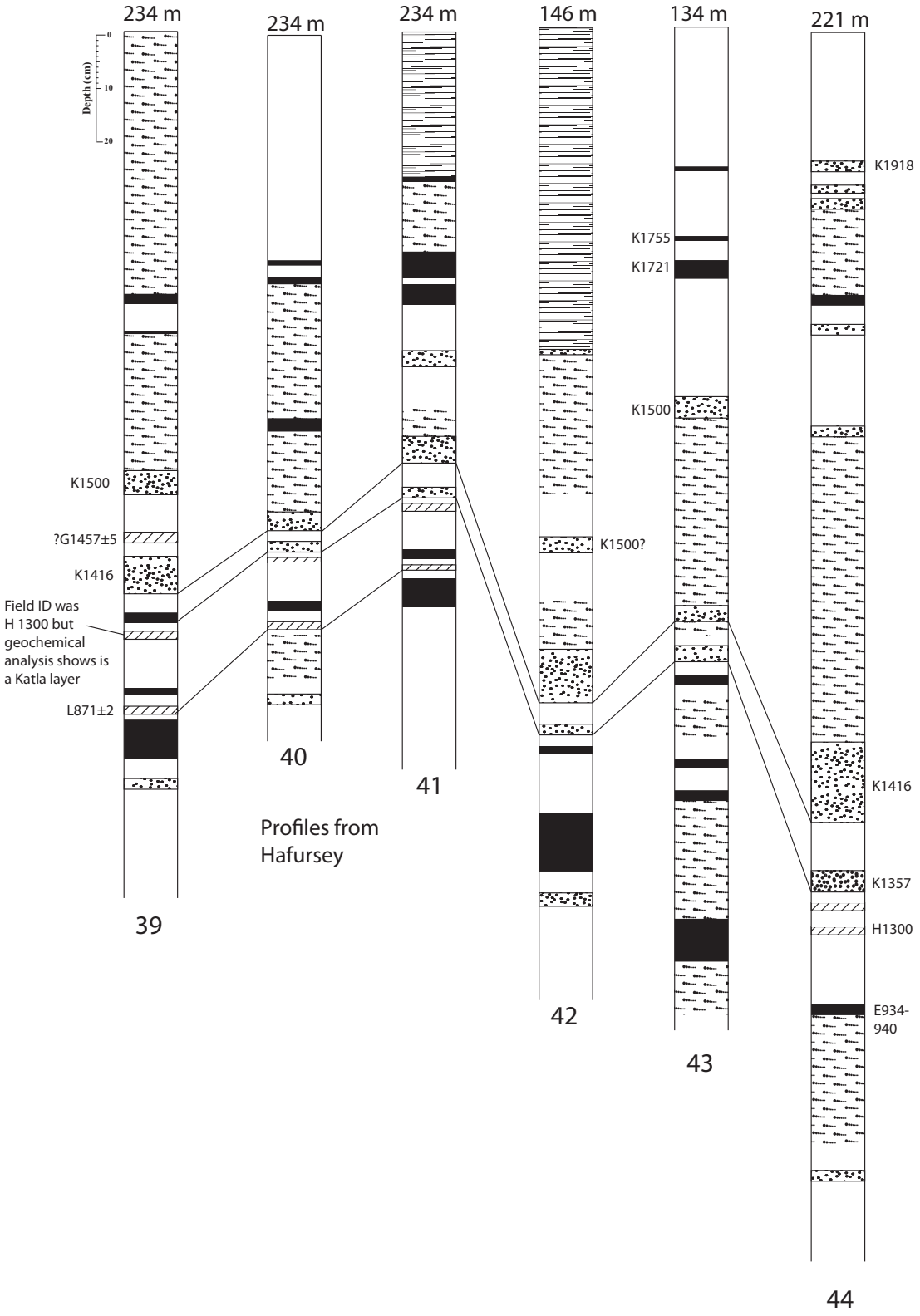

Figure 5.50: Sections from Harfusey, Mýrdalssandur

5.5 Key points

- The chronology of Skaftártunga is described with the identification of four dated tephra prior to Landnám and 20 tephra layers identified in the period after Landnám. H 1104 is found in 56 profiles and a Grímsvötn tephra from the 12^{th} century is identified. The period of AD 1389–1500 contains 6 tephra providing a high resolution record of change over this period.

- Geochemical analysis confirms the presence of two tephra layers from Grímsvötn in the 15^{th} century, and these layers are mapped across 400 km^2. Age estimates of the tephra based on SeAR are AD 1432±5 and AD 1457±5. These layers were identified in 89 and 140 sections respectively.

- Key geomorphic features are identified. These are; instability related to tephra fall, and increases in SeAR due to proximity to active rofabards.

- Stratigraphic sections above 300 m generally shave high SeAR rates directly after Landnám, then relatively low SeAR to the present, sections below 300 m exhibit greater variability and can be categorised into profiles (type A) that see increasing rates of SeAR after AD 1600 to levels more than double the regional mean SeAR and profiles (type B) which see a generally flat trend of SeAR with comparatively minor fluctuations.

- 200 stratigraphic profiles, of which 189 are from Skaftártunga and 11 from Mýrdalssandur are presented and contain 2625 identified tephra. These are from 6 landholdings and an area of communal grazing land and from altitudes of 57 to 468 m.

Chapter 6

Discussion: Plague and landscape change

6.1 Introduction

This chapter takes the chronological framework and geomorphology presented in Chapter 5 and uses it to test the hypothesis that there is a geomorphic signal as a result of population reduction after episodes of plague in AD 1402–1404 and AD 1494. A 200 year period of reduced SeAR and increased landscape stability which ends by AD 1597 is consistent with reduced grazing pressure due to population decline. This change comes after a period where SeAR levels are already declining and the changes identified are small deviations from the mean SeAR rate, therefore this reduction must be placed in the context of overall trends in SeAR and erosion identified in Section 3.5.3.

Firstly new data is evaluated against existing spatio-temporal models of landscape change; the landscape impact of settlement, woodland clearance, rangeland management, climate change, proximity to eroding slopes, and variations in eroding soil depth. Then landscape change during the period AD 1389-1597 is evaluated at three scales (Section 1.3.3), changes over Skaftártunga, changes over individual landholdings and changes within individual profiles. The longer term geomorphic impact of a period of reduced grazing pressure is then considered — it is argued that population decline may have delayed the onset of severe erosion that started in the early AD 1600s and took place under similar climatic conditions to the period of landscape stability seen from AD 1389–1597.

6.2 General trends in SeAR and erosion

Previous studies (e.g. Dugmore & Buckland, 1991; Simpson *et al.*, 2001; Mairs *et al.*, 2006; Dugmore *et al.*, 2009) have identified five main trends in land degradation and SeAR in Iceland over the last 1500 years (Section 3.5.3). Aggregate SeAR for Skaftártunga is presented and evaluated against a new integrated spatio-temporal model of erosion and an new model of landscape change related to population decline is presented (Figure 6.1).

6.2.1 Changes at the regional scale

At the scale of Skaftártunga ($\sim$400km^2) there is a stepwise change in SeARs after settlement. Prior to Landnám sediment accumulation was low and varied little in absolute terms across the landscape and after Landnám mean SeAR doubles and increased variability indicates a more heterogeneous landscape (Figure 6.2). While the regional change is homogeneous after Landnám, at the level of the individual profile this change is time transgressive with distinct spatial gradients.

6.2.2 Altitudinal model of erosion

A key feature of the altitudinal model of landscape degradation proposed by Dugmore & Buckland (1991) is that erosion begins soon after Landnám at higher altitudes and progressively encroaches on lower elevations. Initial breaches in vegetation cover start in marginal uplands above areas of continuous tree cover. Erosion spots then propagate downslope through time, initiating erosion on lower slopes. In Skaftártunga for the first 60 years after settlement the highest SeARs are recorded above 300 m, which supports this model (Figure 6.3, (a)). Erosion in upland areas has been thought to have been because inland sites were preferentially settled because they had thin woodland cover — however there is increasing evidence that early farm sites were distributed widely across the landscape, and not just in upland areas (Vesteinsson *et al.*, 2002; McGovern *et al.*, 2007). Increases in erosion at early periods are therefore most likely due to the higher vulnerability of upland areas.

6.2.3 Woodland clearance

The transformation of the Icelandic environment from $\sim$25% woodland cover to $<$ 1% woodland cover probably occurred progressively, with the first major contraction occurring over a period of 300–400 years after settlement (Church *et al.*, 2007; Lawson *et al.*, 2007). Apparent inconstancies in the pollen record

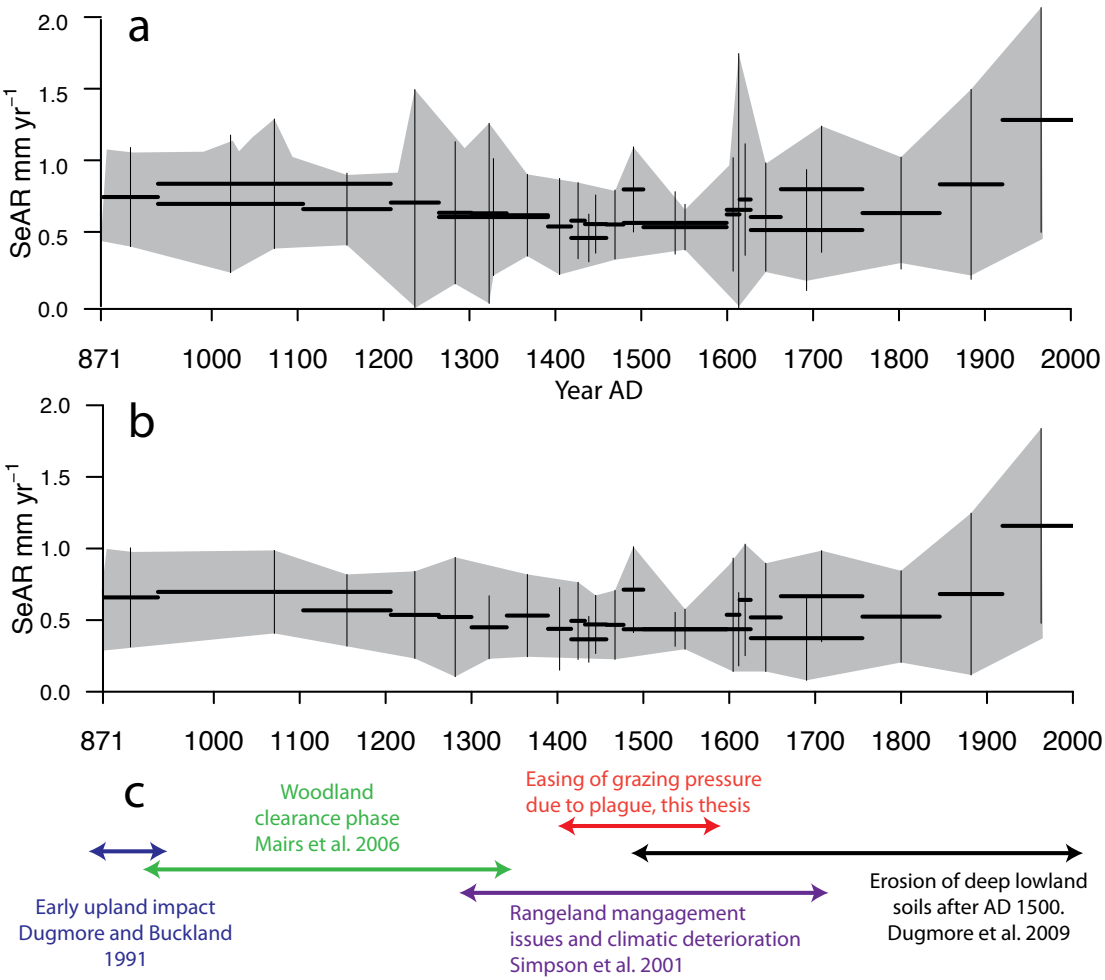

Figure 6.1: Aggregate SeARs for Skaftártunga. Bar indicates mean SeAR and vertical bars and grey band highlights range of results based on 1σ from the mean. (a) Shows data from all profiles including profiles where there was indication of slope wash (gravel or mixing of aeolian sediment and tephra). (B) presents just aeolian accumulation rates which reflect sediment changes within 250 m of individual profiles site (Dugmore & Erskine, 1994). (c) summarises general models of landscape change, with the additional models tested in this thesis, for further details see section 3.5.3.

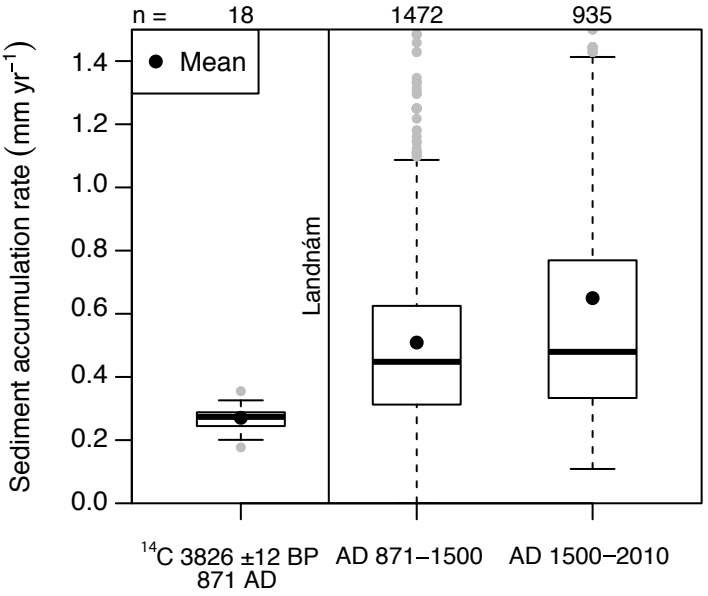

Figure 6.2: Aggregate sediment accumulation rates for three periods, pre-Landnám (3390 BP – 871 ± 2 AD), the AD 871–1500 (the medieval warm period) and AD 1500–2000 (the Little Ice age and 20^{th} century) for all measurements of SeAR. The outliers extend to maximum accumulation rates of 3.7 mm yr^{-1} and 2.9 mm yr $^{-1}$ for the MWP and LIA. Mean pre-Landnám SeARs of 0.3 mm yr^{-1} match measurements of 0.2–0.3 mm yr^{-1} around Eyjafjallajökull from Dugmore *et al.*, 2000.

would appear to be a consequence of site selection; early clearance within 50 years of Landnám occurs around farm sites (Hallsdóttir, 1987; Mairs *et al.*, 2006), but surrounding woodlands are cleared progressively over the period of 500 years. Areas that had substantial forest cover experienced larger SeARs than areas with little or no tree cover in the period after Landnám (AD 900–1200, Mairs *et al.*, 2006). The altitudinal limit for tree growth in Skaftártunga is probably ∼250–300 m for forest cover (trees $>$ 2 m height) and ∼400 m for scrub, based on modern measurements at Skaftafellsheiði (Wöll, 2008). There is a significant difference in mean SeAR rates in the period AD 935–1262 ($<$ 250 m 0.58 mm yr^{-1} , 95% CI 0.52–0.64; $>$250 m 0.42 mm yr^{-1}, 95% CI 0.36–0.48) which corresponds with areas of expected woodland cover prior to Landnám (Figure 6.3) — this difference can be explained by the difference in the change from

Betula spp. woodland (height $>$ 2 m) $\longrightarrow$ open grassland

which generates landscape instability and higher SeAR levels because of the time taken to establish a dense turf sward which is resilient to grazing. In contrast the change from

Betula spp. and *Salix* scrub (height < 2 m) $\longrightarrow$ open grassland

does not seem to produce landscape instability and does not elevate SeAR levels as a well established grass sward could coexist with the more widely spread trees/ shrubs. By AD 1300 SeAR declines to mean post-Landnám levels in areas below 300 m and there is no altitudinal trend in SeAR, which coincides with other indicators of woodland contracting (Church *et al.*, 2007; Lawson *et al.*, 2007). This decline in SeAR at low levels is consistent with an 'open' landscape where grass sward which is relatively resistant to grazing is established in all areas.

6.2.4 Climate response and rangeland management

Unpredictable climatic shifts of increasing magnitude drive changes in SeAR from AD 1300 onwards as a consequence of the failure of rangeland management to react to climatic changes (Simpson *et al.*, 2001). Problems of climate prediction could have been compounded by additional distractions and impairments to effective rangeland management, related to the *Sturlungaöld* period of civil war, the loss of independence to Norway and changes in law codes. There is archaeological and historical evidence for a changing ratio of sheep to cattle in North Iceland from AD 1100 onwards (McGovern *et al.*, 2007), but this change may not have been uniform across Iceland. The implication of this would have been to increase pressure on rangeland grazing away from home fields and farms. From AD 1262–1389 erosion in upland areas over 300 m increases slightly and erosion in lowland areas declines significantly. This decline in erosion in lowland areas is interpreted as reflecting that the transition from wooded landscape to open landscape is completed (Figure 6.4).

6.2.5 Changing patterns of lowland erosion

Regional scale changes

Dugmore *et al.,* (2009) argue that the difference between increasing rates of sediment accumulation seen after AD 1500 and apparent declining overall rates of soil cover loss is due to the difference in the depth of soil being eroded. Altitudes above 400 m where the soil depth is thin (< 1 m) could see rapid rates of land cover loss due to the development of closely spaced erosion spots that

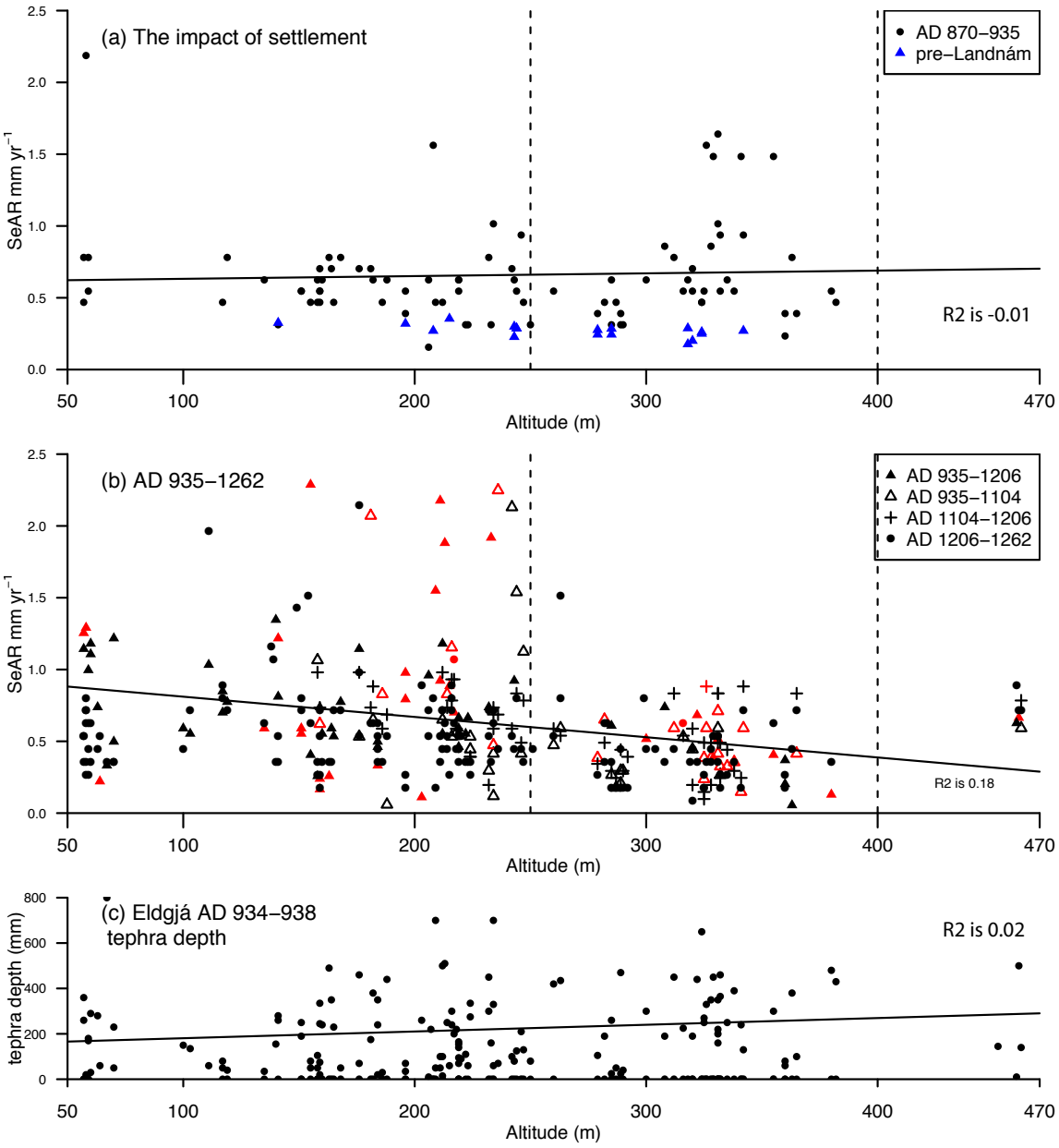

Figure 6.3: SeARs plotted by altitude for, (a) prior to settlement and the initial settlement period and (b) AD 935–1262 (the woodland clearance phase). Altitudinal limits of growth for > 2m height woodland *Betula* forest at ∼250 m and the limit of individual shrub growth at ∼400 m are indicated (broken lines). A linear best fit line for SeAR rates with no fluvial reworking has been added. Red data points are stratigraphic sections that showed signs of reworking. All areas see an increase in SeAR after Landnám, with the largest increase in areas above the tree line (a). 70–280 years after settlement areas below the woodland tree line experience higher rates of SeAR. The frequency of slope wash occurrence is similar (17% vs 27%) — this is probably related to the thick tephra from Eldgjá. The differences in SeAR cannot be explained by variations in the the thickness of tephra from the eruption of Eldgjá in AD 934–940 (c).

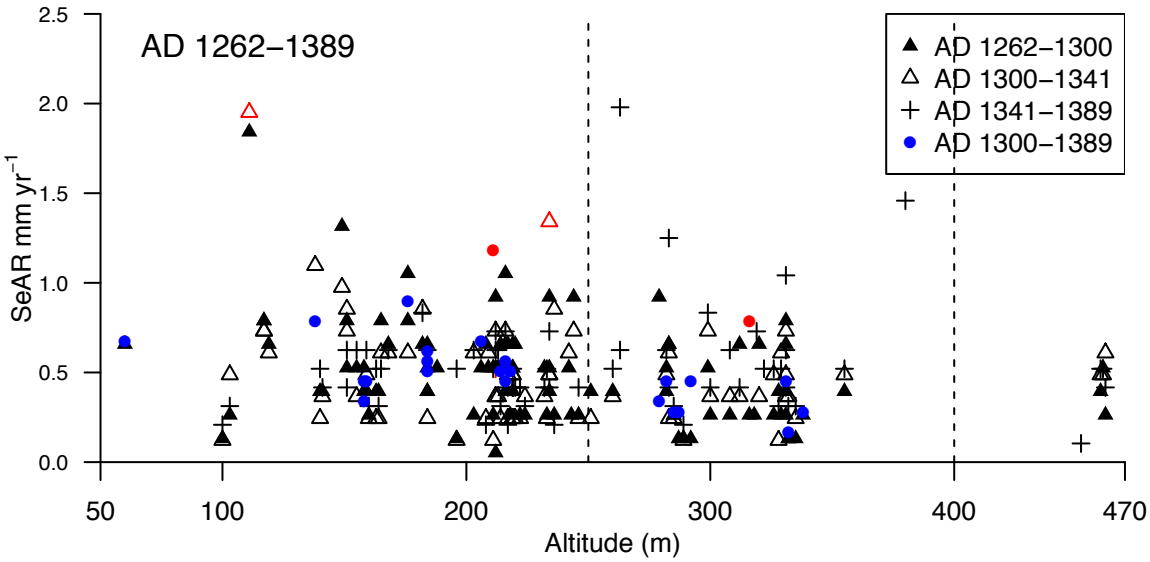

Figure 6.4: Sediment accumulation rates by altitude for the period AD 1262–1389 showing little altitudinal variation as SeAR levels in lowland areas decline. Periods of slope wash are indicated in red. SeAR in upland areas is slightly higher (0.47 mm yr^{-1}, 95%CI 0.39–0.56) than in the previous three centuries (0.42 mm yr^{-1}, 95%CI 0.36–0.47) but this difference is not significant.

rapidly combine. Declining rates of land cover loss in lower, less ecologically marginal areas could be related to higher SeAR because of the presence of deep soils which may be $>$ 6 m thick. In Skaftártunga SeAR and instability increases from around AD 1600 onwards especially in areas below 250 m (Figure 6.5).

Local scale change

In contrast to 'spot' erosion in the highlands where there may be many low intensity sources of sediment scattered across the landscape, 'rofabard' erosion in the lowlands may have large persistent local sources of sediment. Where rofabard erosion takes place in deep soils persistent and localised high intensity sources of sediment have significant effect on the visible rates of SeAR as the rofabard migrates across the landscape (Figure 6.5, the contrast between profile 148 and 24). This is illustrated with the contrast with the SeAR record from a single profile (148) which shows after K 1625 SeAR rates progressively increase from 0.33 mm yr^{-1} to 2.74 mm yr $^{-1}$. This profile was located on the edge of a large rofabard which had eroded $\sim$5 m of Holocene sediments to bedrock. Prior to this point SeARs at these two sections show a similar pattern. From the record at profile 148 the vegetation breach can be inferred to have started in the early 17th century — indicating a threshold was crossed whereas after earlier periods of increased erosion (AD 935–1206, AD 1300–1341, AD 1416–1500)

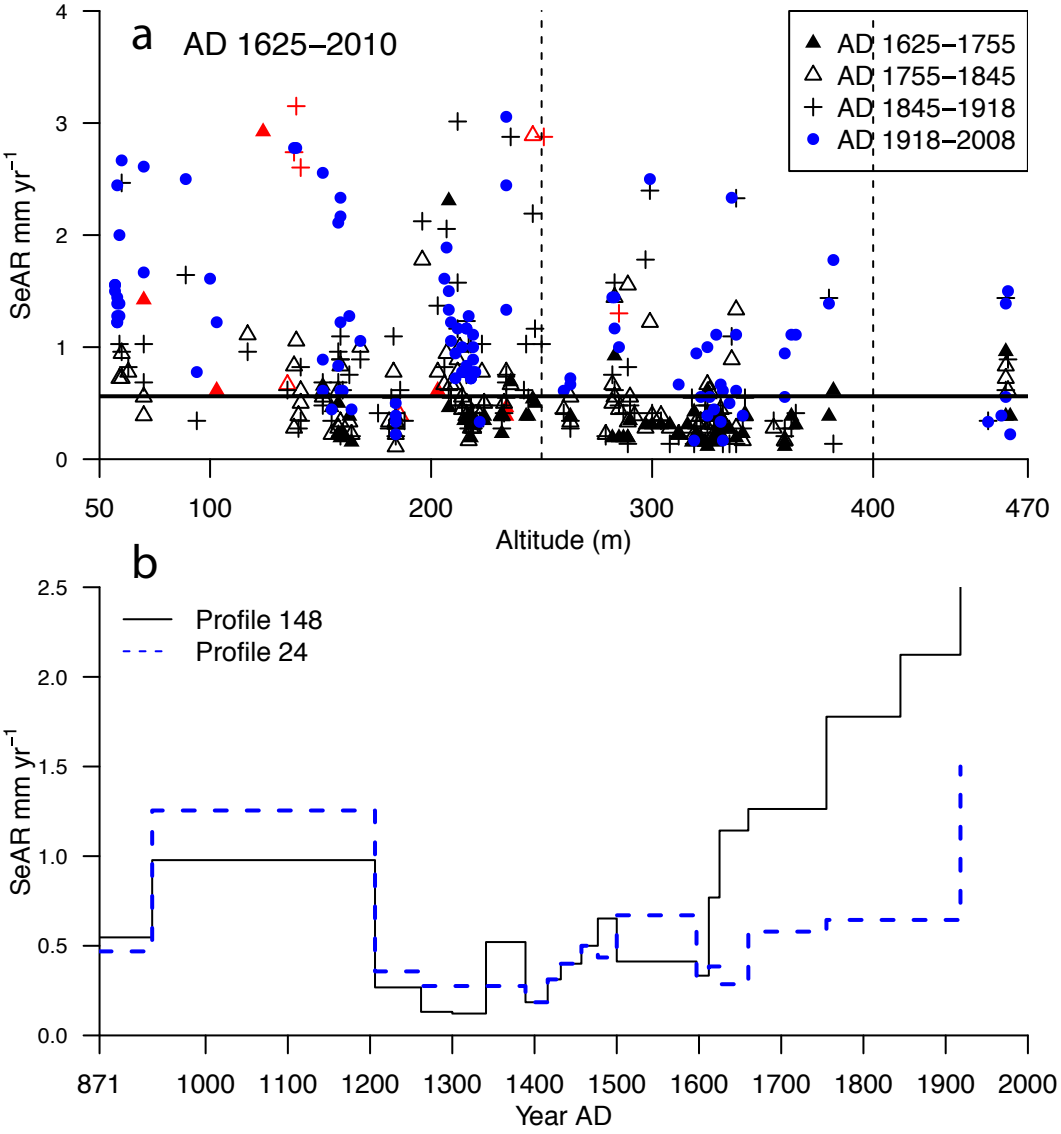

Figure 6.5: At the regional scale after K 1625 SeAR rates increase and many profiles have rates of SeAR > 2mm yr^{-1}. 32% of profiles have SeARs of more than double the post-Landnám average (thick line). Red signifies sections with fluvial reworking. (b) illustrates the difference proximity to rofabard erosion fronts makes at the local scale, by showing type A and B profiles (Section 5.3.2. Further examples of this difference are in Appendix D

SeARs returned to lower levels. In contrast profile 24, located 2.5 km away from profile 148, is located on a edge of a river bank which eroded within the last 50 years (Figure 5.22) and does not see systematic increases in SeAR until after K 1918, where apparent SeARs are higher because they contain the turf as well as aeolian accumulation. Local patterns of SeAR after AD 1625 indicate how proximity to active erosion fronts elevates SeAR levels but does not necessarily correlate with increasing areal erosion. Further examples of this contrast seen in profiles below 300 m are shown in Appendix D.

6.3 Population decline

6.3.1 Regional scale change

While there is no difference in aggregate mean SeARs before, during or after periods of plague (Figure 6.1, Figure 6.6) additional alternative indicators of landscape stability show that the period AD 1389–1597 experienced lower than average landscape instability, which is consistent with a reduction in grazing pressure due to population decline. Aggregate SeAR rates alone cannot capture all indicators of landscape stability. This is because the standard deviation of SeAR for the period AD 1389–1416 is 74% of the mean — change at individual sites relative to SeAR rates previously will be masked by the differences between sites.

To quantify landscape instability three alternative measurements were used (Figure 6.7). SeAR rates are compared against the mean post-Landnám SeAR within the section they were recorded in rather than the regional mean (Figure 6.7). Calculating the percentage of profiles where an age period (a stratigraphic unit defined by dated tephra) has the first or second lowest SeAR post-Landnám gives an indication of especially low periods of accumulation. Two age periods were more likely to be the lowest in any given profile than could be explained by chance. These periods were AD 1206–1341 and AD 1389–1477. The period AD 1500–1755 has some indicators of this (i.e. not all tephra age periods were significantly above percentages which could be expected by chance) (Figure 6.7). These signals together show that the period AD 1389–1457 and to a lesser extent AD 1477–1597 have the lowest signals of instability and landscape degradation in the post-Landnám record (Figure 6.7).

These indicators show there is increased landscape stability starting after AD 1389 and lasting until AD 1597. This is seen in

(a) A higher than randomly expected percentage of profiles (25% vs 6%) record their lowest or second lowest post-Landnám SeAR rates during AD

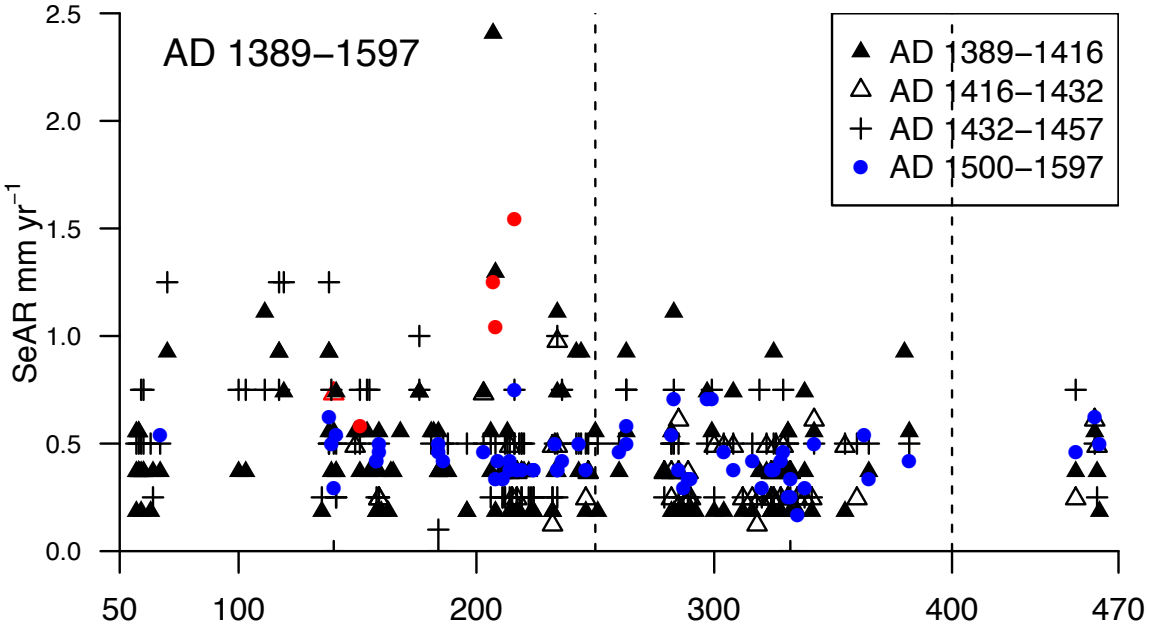

Figure 6.6: SeAR plotted against altitude for the period encompassing population decline shows no significant altitudinal trends.

1389–1416

(b) Variability (SD as % of SeAR mean) is average in AD 1389–1416, and reduces to below average for AD 1416–1597.

(c) Deviations from the mean SeAR per profile is low (0.18 mm yr^{-1}).

It is the presence of all these indicators that differentiate it from other periods which have similar low SeAR totals (i.e. AD 1597–1625 and AD 1206–1341). The period H 1300–1341 has high variability in accumulation rates (120%) compared with the post-plague period. The elevated SeARs in the period H 1341–1389 could be explained by a series of severe cold years and heavy sea ice around this period (Ogilvie, 1984). The period H1597–1660 is different because variability increases in the landscape indicating instability and although some low totals for SeAR are found, in general erosion rates are increasing (Figure 6.1). The period from V 1477–K 1500–H 1597 does have some indicators which are consistent with a lower grazing impact after a plague in AD 1494, but these are not as clear as for AD 1389–1416 (Figure 6.7). There are three reasons why any geomorphic signal from this event would be smaller than that of the plague in AD 1402. They are that

The death rate was lower (Karlsson, 1996) , therefore any reduction in grazing could be expected to be smaller.

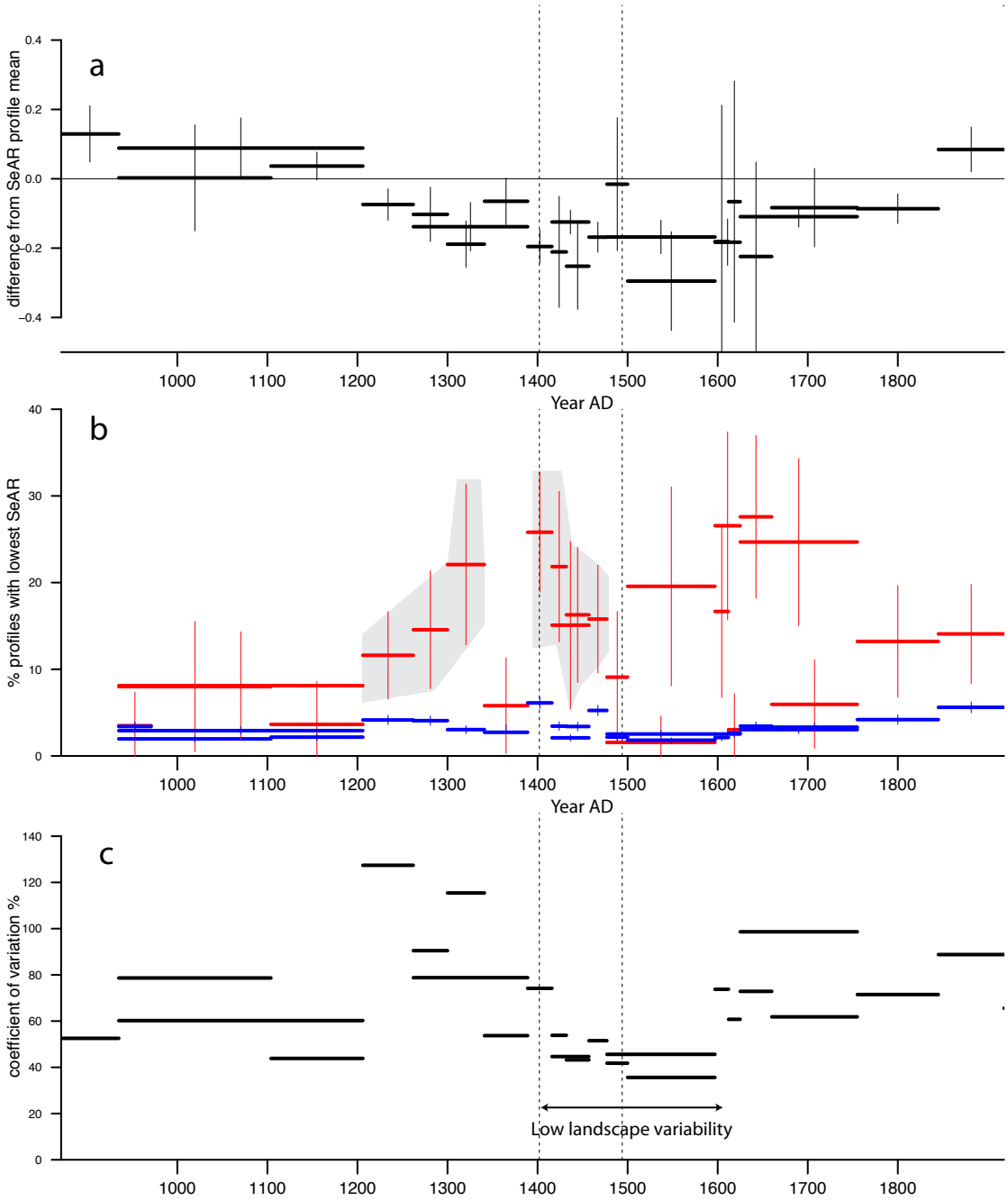

Figure 6.7: Alternative indicators of landscape stability. Broken vertical lines indicate the dates of the two plagues. The deviation in SeAR for each time period from the profile mean (as opposed to the regional mean) is shown in (a). (b) shows the percentage of profiles which recorded the lowest or second lowest SeAR in the post-Landnám period, divided by age period (n=> 40). The red bars indicate the percentage and 95% CI, while the blue bars indicate the expected random percentage based on the proportion of age periods as a proportion of total age periods identified, with 95% CI. Areas shaded in grey show where all the age periods have significantly more low SeAR rates than could be expected by chance (c) indicates the coefficient of variation (% variance of standard deviation of mean) which shows low variability from AD 1416–1597.

The configuration of tephras Only a relatively small number of sections (55) could constrain the period AD 1477-1500 and of this period only the last 6 years would be affected by the AD 1494 plague, — this effectively 'smears' (Baillie, 1991; Blaauw, 2011) any change between the periods of AD 1477–1500 and AD 1500–1597.

Deteriorating climatic conditions In the AD 1420s a long term decline in storminess in the North Atlantic is reversed so by AD 1494 mean storminess is higher (Dawson *et al.*, 2004; Dugmore *et al.*, 2007b) and temperatures are cooler (Mann *et al.*, 2009). A higher intensity of erosive processes mean that pre-existing erosion fronts produce more sediment even if reduced grazing prevents the formation of new erosion spots (Dugmore *et al.*, 2009).

6.3.2 Changes at the scale of landholdings

This section describes and presents data on change at the resolution of individual landholdings. Differences between landholdings can be explained as being related to the underlying geography of the landholdings (such as altitude and vegetation cover), and differences in management, wealth and influence (Mairs *et al.*, 2006). Here difference between five landholdings, and areas of high altitude communal grazing are compared (Figure 6.8).

Trends identified at the regional scale can also be seen at this scale — early upland impact after Landnám is seen in areas of higher altitude (c, d), and high SeARs are seen from AD 935–1206 in areas expected to have had more woodland cover (a, b). Changes in the period from AD 1389 reflect two patterns, either a period of no or little change in SeAR (b, c, d) or increasing SeAR rates during the 15^{th} century (a). This pattern of increased erosion in lowland areas during a period of low population is consistent with two hypotheses. Firstly, lowland areas would probably not be abandoned at all, so the pattern seen may be driven by climatic change rather than any change in grazing intensity over this period. Alternatively it may reflect changes or increases in more damaging land use practices such as grazing outside the growing season (Simpson *et al.*, 2001), as a response to a reduced labour force in general. The first hypothsis is considered most likely because of climatic deterioration during this period (Section 6.4).

The period from AD 1500–1600 shows little difference between areas. After AD 1625 there is a trend of increasing SeAR seen in all areas.

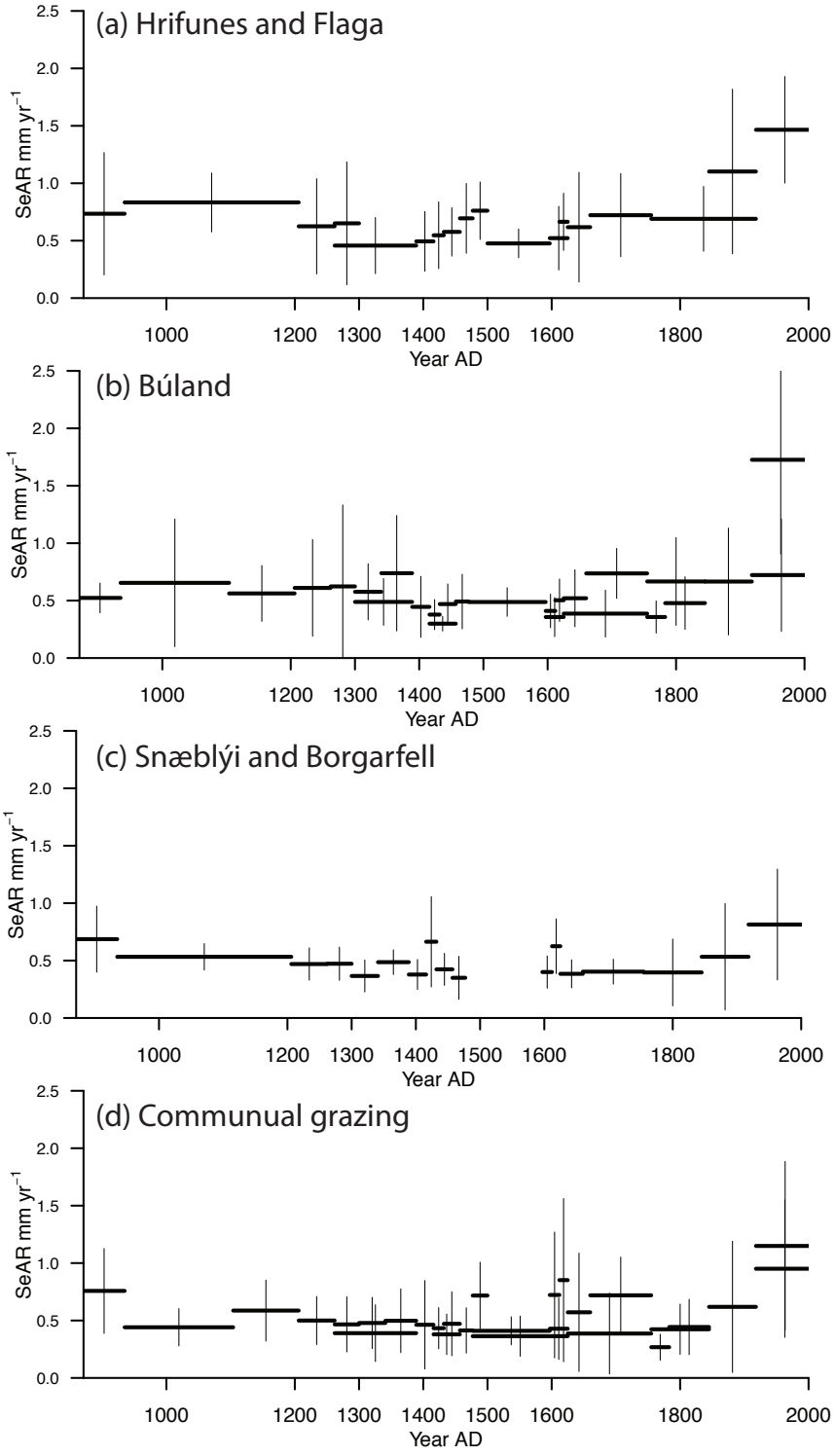

Figure 6.8: SeAR measurements from five land holdings (a, b and c) and communal grazing areas (d). Vertical bars show 1σ standard deviation for the mean (horizontal bar) of a minimum of 10 sections. Sections with signs of fluvial reworking were excluded.

6.3.3 Local scale change

Photogrammetric records from 27 profiles (Section 4.3.4) improve the resolution of change at the level of an individual profile, allowing detailed comparisons to be made between individual sites rather than between multiple profiles where changes at individual sites may be masked by the variability between sites. The resolution of these measurements is significant because the typical separation between the H 1389 tephra and K 1416 tephra is 12 mm, at these distances measurements to ±2.5 mm have a measurement error of ±20%.

The period of AD 1389–1416 has the lowest SeAR in the post-settlement period in 63% of profiles recorded to high resolution. These measurements confirm the pattern seen from large numbers of lower resolution measurements (Figure 6.9). In profile 179 the H 1389–K 1416 SeAR of 0.4 mm yr^{-1} is lower than the pre-Landnám figure of 0.42 mm yr^{-1} and is the lowest sedimentation rate over the last 2600 years. The landscape returned to average post-Landnám SeAR in the period AD 1416–1477. There is no apparent SeAR change related to the second plague in AD 1494.

6.4 Changing climate and degradation AD 1300–1600

By the time of the first plague the landscape was cleared of woodland, had been settled for 500 years, and this was prior to the stripping of deep lowland sediments. Can the patterns of SeAR in the period AD 1300–1600 be explained by changes in climate alone?

To test this hypothesis two areas were compared with proxies of climatic change (Figure 6.10). The lowland landholdings (55–225 m a.s.l) of Hrífunes and Flaga (Figure 6.10, part c) have good grazing, and given that demographic decline would have produced heterogenous impact grazing pressure with better areas experiencing limited or no decline (Lagerås, 2007) it is not surprising there is no reduction in SeAR in AD 1402 and AD 1494. There is a correlation between SeAR and declining temperature and increasing storminess through the AD 1400s (Figure 6.10 part a and b). Its sensitivity to climatic perturbations may indicate that there was regular grazing outside the growing season (Simpson *et al.*, 2001; 2004), a possible response to a reduced labour force, although it seems more likely that SeAR was responding to climatic deterioration. However increasing rates of SeAR seen from AD 1400–1500 stop after the second plague in AD 1494, although change during this period is not as well constrained by tephra.

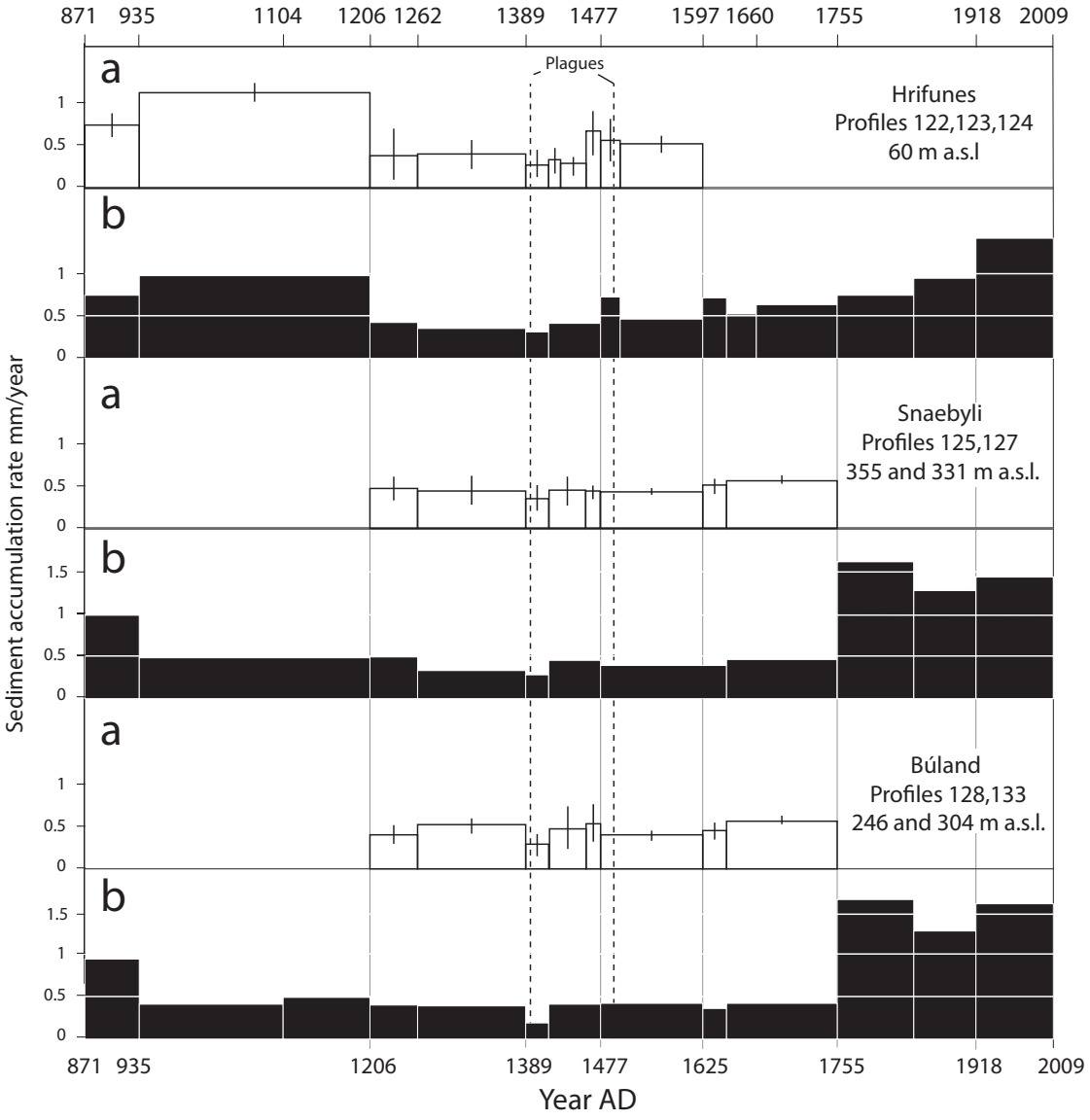

Figure 6.9: (a) Photogrammetric measurements of SeAR in three different landholdings, vertical bars show 1σ deviation and the timing of plagues is indicated by broken vertical lines. (b) shows standard measurements of the same stratigraphic sections. The period AD 1389–1416 has the lowest rates of SeAR post-Landnám.

The pattern of instability at Hrífunes is different from upland areas (Figure 6.10, part d). There is no increase in SeAR during 15^{th} century. This could because upland areas experienced reduced grazing pressure as the population retreated to core areas. Reducing the grazing in these areas would reduce landscape sensitivity to climatic impacts as grazing opens erosion spots which provide sediment.

6.4.1 Long term geomorphic impacts of population decline

Climate proxies in the period AD 1420–1500 and AD 1590–1660 indicate that these periods were similar (frequent sea ice, large negative temperature deviations from the mean, high storminess indicators, Figure 3.9), however one period experienced widespread threshold crossing geomorphic change and the erosion of deep lowland sediments, and the other saw limited increases in erosion in lowland areas which declined when climate ameliorated. Why does the erosion of lowland sediments not occur when climate deteriorates in the mid-14^{th} century, but does occur in a similar phase of climatic deterioration from AD 1590–1630?

Different population regimes could explain why the impact of deteriorating climate in AD 1420–1500 pushed lowland areas close to, but not over a geomorphic threshold whereas deteriorating climate around AD 1600 marks the start of widespread landscape instability and increasing SeAR in all areas. Separating the factors that *trigger* erosion which are primarily grazing, and the factors that control the *propagation* of erosion, which are primarily the intensity of physical climatic processes (Dugmore *et al.*, 2009), the different responses to climatic deterioration may be understood. The earlier period had a lower than average population due to disease whereas the later period probably had a population above the 50,000 level seen at the start of the 18^{th} century (Thórarinsson, 1961; Karlsson, 2000). This could explain why the geomorphic signal is spatially differentiated in AD 1400–1500 (because it is partially driven by variations in grazing pressure), whereas the transition at ∼AD 1600 occurs in all areas below 250 m (Figure 6.1, a), suggesting that climate is the primary driver. A similar period of instability around Eyjafjallajökull is identified by Dugmore *et al.* (2009) as starting after AD 1510 but before AD 1721. These periods of instability could be contemporaneous. In the AD 1400s climatic change would have increased the intensity of processes of erosion but a lower grazing regime would have reduced the likelihood of erosion being triggered. By AD 1600 increased grazing could provide erosion triggering factors and climatic deterioration propagates vegetation breaches leading to widespread mobilisation

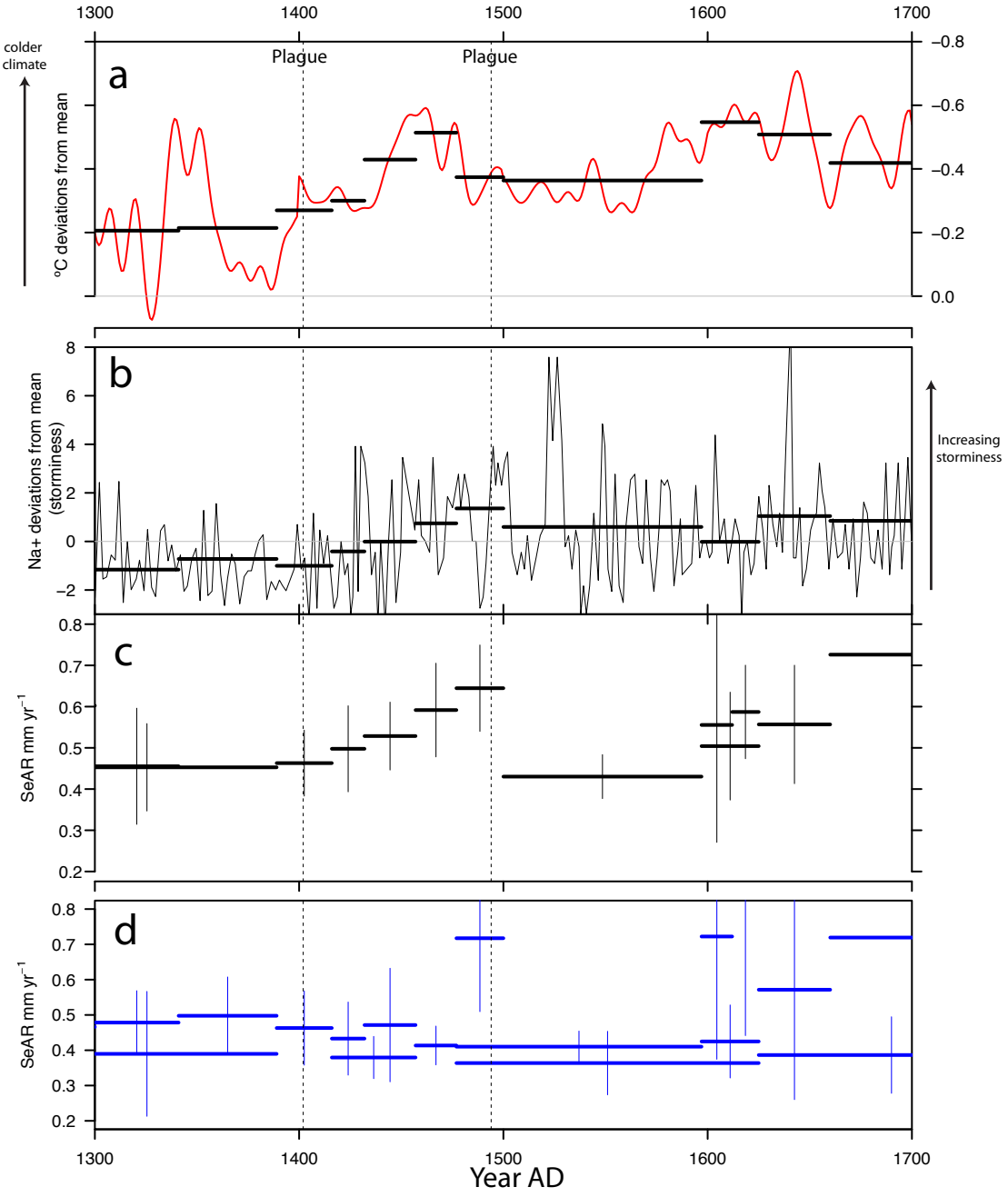

Figure 6.10: The period AD 1300-1700 sees substantial climatic changes in Iceland. (a) shows the multi-proxy reconstructed temperature curve (Mann *et al.*, 2009), with averages over the periods bounded by tephra indicated by black bars. (b) shows deviations from the mean in Na^+ from the GISP ice core, a proxy for storminess (Meeker and Mayskwi, 2002). (c) shows SeAR (error bars show 95% CI) from profiles at Hrífunes and Flaga (n=55) landholdings (50–230 m asl) which shows SeAR rates correlating closely with temperature. (d) shows SeAR from profiles above 250 m (n=64), which shows poor correlation with climatic signals.

of deep lowland sediments.

6.4.2 The 18^{th} century — a comparison

The 18^{th} century had three periods of significant population decline of which we have good historical records (Section 3.3.1). However the chronological resolution provided by tephra over this period is not as well resolved as AD 1389–1500, with 95 years separating the tephras of K 1660 and 90 years between K 1755 and H 1845, and the L 1783 tephra is recorded in only 34 profiles. Additionally the erosion of deep lowland sediments by this period enhances SeAR rates in all areas generally which may mask trends caused by changes in land use intensity. (Figure 6.1).

6.5 Key Points

- Long term trends in sediment flux in Skaftártunga can be related to existing models of landscape change.
- Population decline can be an explanation for a period of increased landscape stability AD 1389–1597 at the scale of the region, which cannot be explained by existing models of landscape change, and is consistent with reductions in grazing caused by population decline.
- The pattern of change in the period AD 1389–1597 varies, with lower altitude areas experiencing increasing SeAR, reflecting deteriorating climate, and higher altitude areas seeing no change in SeAR over this period. This can be interpreted as reflecting declining pressure on rangeland grazing, but no or little change in grazing in lower altitude areas .
- Population decline may have delayed the onset of extensive erosion of lowland soils which starts after AD 1625, in a period of similar climatic deterioration to AD 1450–1500.

Chapter 7

Conclusions

7.1 Introduction

This thesis examines the role that sudden declines in population have on landscapes in pastoral farming systems. This chapter summaries the key findings of this study. Two main research objectives have been tackled: firstly to enhance methodologies for assessing landscape change using tephrochronology, and secondly a critical assessment of population and geomorphological change over the past 1200 years in Skaftártunga. This chapter reflects on how this study has achieved these aims and evaluates wider implications arising from the work in this thesis.

7.2 Tephrochronology and landscape change

The resolution of existing models of landscape change has typically been that of decades to centuries, and existing measurement techniques have been sufficient for observing large scale changes such as the widespread increase in SeARs after AD 1500 (Dugmore & Buckland, 1991; Dugmore & Erskine, 1994). The focus of this study is on changes over years and decades within a period of 150 years so higher resolution measurements of sequences were required. In addition alternative indicators of overall landscape stability were considered. These enhancements and their implications are summarised below.

7.2.1 Methodological improvements

Improved measurement of sedimentary sequences A novel application of photogrammetric techniques to the 2D measurement of stratigraphic sequences of tephra and sediment was presented in Section 4.3.4. Systematic errors caused by the internal camera geometry were $<1\pm$ mm,

and in total the error was ±1 mm for the measurement of sequences 2 m away from the camera. These results were verified by comparing multiple manual measurements of sediment with photogrammetric measurements. Greater numbers of manual measurements produced values closer to that achieved by photogrammetric measurement, which indicates photogrammetric measurement produces figure close to the actual sediment depth.

In addition to improved resolution of measurement this technique improves the frequency of measurements. This is significant because of the spatial variability at mm to cm scales in the thickness of tephra. This variability means that although single measurements can be representative, comparisons of photogrammetric and manual measurements show that ∼20% of single measurements are not representative of the actual sediment depth. Based on the variability in thickness in stratigraphic units around 20 measurements are needed to give mean measures of depth with an an error of ±2.5 mm (to a 95% confidence interval).

The value of this new approach is that statistical techniques can be applied rigorously to measurements of stratigraphic sequences.

Improved dating of tephra using SeAR models SeAR has been used to estimate the age of tephra in both pre-Landnám and post-Landnám sequences. In pre-Landnám sequences, small numbers of measurements combined with uncertainties in the radiocarbon dating of bounding layers can limit the accuracy multiple decades or to century time-scales (to ±250 years (e.g. Óladóttir *et al.*, 2005). Where stratigraphic units are well bounded (for instance in post-Landnám sequences where tephra have been matched to historical eruptions) the accuracy of dating has been routinely limited because of the small number of measurements taken.

This study dates tephra layers to ±5 years ($\pm 1\sigma$), based on hundreds of measures of sediment accumulation from two profiles (Section 4.2.3). These measurements were shown to be robust because they were replicated by dating the same tephra using lower resolution measurements from 75 profiles. This resolution of dating using SeAR is dependant on two criteria; a high sedimentation rate, which separates chronologically close tephra, and a small time period between tephras of known age (in this case 61 years). Lower sediment accumulation rates and a larger age separation between securely dated tephra would increase the error of age estimates. Where the dates of tephra used to bound SeAR calculations have uncertainties themselves (for example they were dated by

radiocarbon dating of associated organic material) the application of this technique in a Bayesian framework (see Church *et al.*, 2007) could be used.

The dating resolution of these tephra is of suitable precision to make a worthwhile contribution to understanding rapid (sub decadal) change, so the improved techniques of SeAR dating aids the investigation and assessment of human-ecodynamics and coupled socio-ecological systems.

Alternative indicators of landscape stability Sediment accumulation rates have been frequently used to identify past episodes of landscape change (e.g. Dugmore & Buckland, 1991; Simpson *et al.*, 2001; Dugmore *et al.*, 2009). This study quantifies variation across the landscape and uses it to identify periods of enhanced landscape stability. Deviations in SeAR rates from the profile mean as opposed to regional mean to are used to successfully identify changes otherwise obscured by the large variations in SeAR which are seen across the landscape.

These indicators can be used in addition to straightforward changes in SeAR to gain a better understanding of landscape stability.

7.2.2 Data presented

This thesis identifies 2625 separate tephra deposits from 200 stratigraphic sections. Highlights of new tephrochronological insights gained in this thesis are:

Mapping two little known Grímsvötn tephra This study maps for the first time the extent of two 15^{th} century tephra layers from Grímsvötn over $\sim$400 km^2 (Section 5.2.3), and correlates the G 1457$\pm$5 layer with two published stratigraphic sections; a profile closer to Grímsvtötn (Óladóttir *et al.*, 2011b), and a Grímsvötn tephra in Mýrdaur (Erlendsson *et al.*, 2009), 45 km to the south west of Skaftártunga.

This data could be combined with a more extensive program out with Skaftártunga to better the constrain the volume of total tephra erupted, determine eruption dynamics and map the full fallout extent.

Dating of two 15^{th} century Grímsvötn tephra This study dated two tephra layers from Grímsvötn to AD 1432$\pm$5 and AD 1457$\pm$5 (Section 5.2.3).

This dating of two tephra enhances the chronology of the poorly known 15^{th} century and permits a finer scale investigation of landscape changes in a crucial period in Icelandic history, when modern economies

developed, climate changes of the Little Ice Age developed and the world stood on the threshold of a period of European dominance.

Improved post-Landnám tephrochronology of Skaftártunga Composite chronologies for Skaftártunga from Larsen, 2000; Larsen *et al.*, 2001; Óladóttir *et al.*, 2005 were used to identify tephra tephra in the field. In addition to tephra layers previously found in this area deposits from the H 1104 eruption have been recorded for the first time, as well as an undated Grímsvötn tephra from the 12^{th} century.

In addition to landscape applications considered here this enhanced tephrochronology is ready for new applications in archaeological, geological and paleo-environmental studies.

7.3 The landscape impact of population decline

The second research goal of the thesis was to investigate landscape change after two 15^{th} century plagues in Skaftártunga. Contrasting possible impacts of population change were tested, namely; decreased impact, no impact, increased impact and changes in spatial patterns of impact. To establish pre- and post-plague trajectories of change contrasting scales of research were undertaken to examine both detailed SeARs over the 1200 years of settlement and lower resolution studies for ∼1400 years prior to Landnám. The main findings of this research can be summarised as:

A period of landscape stability AD 1389–1597 There was a period of landscape stability from AD 1389–1597 in the Skaftártunga. This stability is consistent with a reduction in grazing pressure as a result of population decline. This period of landscape stability occurs at the same time as a period of climatic deterioration (where other periods of climatic deterioration of comparable magnitude show increases in erosion) suggesting that there was a reduction in intensity of land use over this period.

There are no increases in impact that can be related to population decline.

Spatial patterns of impact related to population decline Lowland landholdings show a decline in SeAR after AD 1389 for 26 years, then increases in SeAR over the rest of the 15^{th} century, while higher altitude grazing areas generally see no systematic change in this period. This is interpreted as a result of continued use of lowland areas combined with reduced use in upland areas. There is little evidence that increases of

SeAR in lowland areas were due to less effective land management techniques, a possible response to reduced labour, as increases in SeAR can be explained by climatic deterioration in the period AD 1450–1500.

Change at individual sites High resolution photogrammetric measurements from 27 stratigraphic sections match the pattern of change seen in aggregate measures of accumulation, with more than 50% of profiles recorded using this technique having the lowest SeAR rates during the period AD 1389–1416, suggesting that this was a period of lower than usual grazing impact.

Integrated spatio-temporal model of landscape change Data from this study was evaluated against a new synthesis of existing models of landscape change (Dugmore & Buckland, 1991; Simpson *et al.*, 2001; Mairs *et al.*, 2006; Dugmore *et al.*, 2009). Records of landscape change in Skaftártunga can be explained by these models with the addition of reduced grazing impact related to demographic decline. Initial landscape impact (AD 870–935) is larger in marginal upland areas (Dugmore & Buckland, 1991), areas which would have had woodland cover see increases in SeARs over the period of woodland clearance (AD 935–1262, Mairs *et al.*, 2006). Erosion increases again in higher altitude areas of rangeland grazing after AD 1300 probably due to difficulties in managing an increasingly unpredictable climate (Simpson *et al.*, 2001). Increases in sediment flux which start after AD 1500 around Eyjafjallajökull, and have been related to the encroachment of erosion fronts onto deep lowland sediments (Dugmore *et al.*, 2009) start in Skaftártunga around AD 1600. A possible explanation for this 100 year difference is the generally lower altitude of grazing areas found in Skaftártunga which could make them less vulnerable to the impact of climatic deterioration.

Possible century scale consequences of population decline SeAR and variability increase in all areas after AD 1625 during a period of similar climate to AD 1420–1500, which does not generally see increases in indicators of erosion. This is explained by a loss of resilience in the 17^{th} century. Increases in resilience in the 15^{th} century are consistent with a lower grazing impact.

Based on the evidence presented it is possible to evaluate the hypothesis proposed in Chapter 1. The hypothesis that best matches the geomorphic consequences of population decline is: (i) there is a decline in erosion. The hypothesis that landscape impact increases as a result of feral or unmanaged

sheep grazing at damaging times can be rejected. There is no indication that there was a systematic change in land use, but instead it seems most likely there was a proportional decline in the intensity of existing patterns of land use.

The second hypothesis tested was that declining population affected landscape resilience, either increasing resilience, decreasing resilience or having no effect. Differing impacts of climate in the period of AD 1420–1500 and AD 1600 onwards are consistent with an increase of landscape resilience as a result of a scaling back of landscape use, therefore this thesis accepts the hypothesis that the plague did increase landscape resilience. The final hypothesis tested was, at what scales are patterns of landscape change as a result of population decline visible? This thesis found that landscape change indicating declining landscape pressure was found at all the scales tested (regional, landholdings and slopes).

7.4 Wider Implications

There are implications for both tephrochronology and human eco-dynamics.

7.4.1 Improved measurement of sequences

Reconstructions of the volume of tephra production are based commonly based on isopachs of terrestrial fallout and therefore dependant on representative measures of tephra thickness. Where tephra thickness is variable increasing the number of measurements within sections could create more representative measures of mean thickness.

This technique provides a way to start realising the full potential of tephrochronology for '3-D' reconstructions of landscape, over the scales of cm to metre and years to centuries that are vital for understanding human-ecodynamics (Dugmore *et al.*, 2004). There is considerable potential for GIS applications within tephrochronology (Newton *et al.*, 2007; Lowe, 2011), and it is planned that data from this project will be be analysed further to tackle other environmental and human eco-dynamic questions. For example key scales of variation within tephra layers and specific stratigraphic units (e.g. aeolian sediment) can be assessed: what ranges of variability occur on scales of 10^3 to $10^{-2}\mathrm{m}^2$?

High resolution measurement is key to understanding transformations of tephra layers themselves — from initial fallout, through surface re-working, the formation of a stratigraphic record to later transformations of the stratigraphic record. The taphonomy of tephra layers in stratigraphic sequences may reflect

both the environment at the time of deposition, for example the vegetation cover, and the post-depositional reworking of the tephra. Investigations of geomorphological features indicative of post-depositional reworking within stratigraphic sequences, such as thufur, solifluction lobes and other cryoturbation features (e.g. Kirkbride & Dugmore, 2005), direct anthropogenic re-working of the tephra (Erlendsson *et al.*, 2009) and shear zones within tephra sequences which may indicate earthquakes, all could benefit with the application of this technique.

Where archaeological features such as charcoal pits have been dated by a combination of radiocarbon and SeAR (e.g. Church *et al.*, 2007) this technique could be generally applied to produce more wide ranging environmental reconstructions of comparable resolution and scale. The application of tephrochronology to a wide range of academic disciplines such as archaeology is improved if more tephra can be dated, even when this is done by less accurate methods such as SeAR. However the dating using SeAR to within 10 years is of comparable or better resolution than radiocarbon dating. This scale is of great utility for archaeological and other paleo-environmental records.

7.4.2 Impact of population decline on landscapes

The spatial and temporal implications of population changes, including periods of population decline, need to be considered as events that can be recorded in environmental records. Changes in landscape stability suggest there was an overall decline in intensity of grazing, but that this varied spatially, with more marginal areas seeing bigger declines. These changes had a spatially variable effect on landscape resilience to later climatic change and human impact. There was no indication that impact increased.

One possible interpretation of the landscape-scale record through the plagues is that a cull of the human population simply eases environmental pressures, however this suggestion is too simplistic. The consequences of both the plague years and other periodic stressors of medieval to early modern Icelandic society are not only seen in the avoidance of collapse; they are also bound up with other possible outcomes that did not occur. In the aftermath of profound increases in mortality the Icelanders did not either panic or succumb to apathy, both of which would have resulted in large flocks of sheep becoming feral. This was a real possibility; in the AD 1860s a flock of 100 feral sheep were present in the highlands east of Skaftártunga, descendants of two ewes and a ram which had escaped in AD 1820 (Adalsteinsson, 1981). That this did not occur is probably related to the fact livestock in 15^{th} century Iceland were the

basis of individual wealth; for livestock to become a common resource would have torn apart the fabric of that society.

In addition, there is no evidence that Icelanders reacted opportunistically and abandoned or reduced the more labour intensive cattle raising in favour of keeping larger numbers of sheep, which in many ways would have been an ideal solution to an acute lack of manpower and the need to maintain food production. This is all the more remarkable because sheep ratios had been rising at least since the 12^{th} century, most noticeably in the smallest landholdings. The big change in sheep numbers in Skaftártunga did not come until early modern times. The history of this development is not known in detail but the main outlines are clear, and there are no indications that the ratio rose faster in the 15^{th} or early 16^{th} centuries than before or after (personal communication, Orri Vésteinsson). It is likely that in the aftermath of the plague, people acted to conserve the core functionality of the economy; despite the labour requirements they scaled back to more balanced ratios of cattle to sheep and preserved their cattle herds, which in Skaftártunga were maintained through into the early AD 1700s.

Skaftártunga's location between the coastal lowlands and sandur to the south, and the interior to north, the presence of *Betula spp.* and *Salix spp.* woodland prior to settlement and where winter grazing is possible even in the coldest decades means that the area is typical of the best agricultural land in Iceland. Therefore its response to population decline after the plagues can be considered representative of these areas elsewhere in Iceland.

7.5 Future research directions

Further work may seek to look for 'early warning signals' (Scheffer *et al.*, 2009) of threshold landscape changes, for example the initiation of erosion in deep lowland sediments. A possible forerunner to erosion in lowland sediments could be prolonged instability in freshly fallen tephra, which would produce a stratigraphic signal of increased variation in tephra thickness. One approach could be to characterise variability in tephra thickness due to post-depositional reworking (that is, thickness variability independent of variations due to differing fallout thickness) as being a signal of a system with reduced resilience and one that is close to or approaching a threshold of change (Section 2.4, Scheffer *et al.*, 2009). This could be linked to studies of variability in modern tephra falls, and determining how this variability is related to vegetation cover and current landscape stability. How much does the form of the tephra reflect the vegetation cover at the time of deposition, or is variability simply a

reflection of tephra depth?

A further question which this research raises is that we know relatively little about how livestock ratios changed prior to the AD 1700s in the south of Iceland. Analysis of archaeofauna could help to improve the understanding of how livestock ratios change after settlement, especially if it was done using the high resolution tephrochronological framework available. This data is needed in order to evaluate to what extent changes in landscape stability seen throughout the earlier settlement period may be explained by increasing proportions of ecologically damaging sheep.

This new data set has validated some of the existing theories of landscape change and soil erosion in post-Landnám Iceland, however it also identifies trends which currently are not well understood. The decline in SeAR and increasing indicators of landscape stability after AD 1206 are here tentatively linked with the end of a transition from woodland to open grassland. However without archaeological evidence of woodland management such as charcoal pits this hypothesis is still largely untested, and it is worthy of further investigation. An alternative explanation is simply that this is an artefact of the dating separation between tephras in AD 935 and AD 1206, which extends a relatively short lived period of landscape change associated with settlement over a period of 271 years. This is supported by the fact that where the H 1104 tephra is present (25% of stratigraphic sections) indications of landscape instability decline before AD 1206.

More work could be done on the geometry of erosion at the slope scale as the data here confirms earlier work showing that SeAR are increased greatly by proximity to active eroding slopes (Dugmore & Erskine, 1994) and is therefore crucial to interpreting aggregated changes in SeAR across many profiles. A better understanding of how erosion progressed at individual sites may allow for individual stratigraphic sections to be 'corrected' relative to the regional SeAR signal, and by doing so aggregate measures of SeAR could then be tested for correlations against wider climatic records.

7.6 Resilience of pastoral socio-natural systems to episodes of demographic decline

This thesis shows that periods of demographic decline can be detected in geomorphic records provided chronological control of high enough resolution is available. The ultimate impact of population decline and subsequent decline in grazing in pastoral environments is one of increasing landscape resilience.

However increased landscape resilience is only apparent in periods where human populations are low, increased landscape resilience does not persist longer than the period of human population decline.

Geomorphic thresholds of erosion in deeper lowland soils are known to have been crossed around Eyjafjallajökull after AD 1510 (Dugmore & Buckland, 1991) but here, with better chronological control they can be show to have taken place after AD 1597. This coincides with a period of climatic deterioration. Climatic conditions during the period AD 1450–1500 were similar, but are not associated with increases in erosion. The delayed onset of threshold-crossing soil erosion could be a result of lower grazing pressure due to the maintenance of cattle herds and limited development of sheep flocks. Despite large demographic changes the complex socio-ecological system of the farming communities of southern Iceland did not collapse or change significantly their farming methods, but the consequence was large scale, effectively irreversible transformation of landscapes.

In southern Iceland there are no indications that abrupt population decline precipitated enhanced environmental impact and so those episodes did not result in changes in the livestock mix, or badly managed or feral populations of sheep and goats. The plagues and resultant demographic shocks in 15^{th} century Iceland did not propagate into 'collapse' indicating that this social-ecological system was resilient.

Scaling back and conserving core-functionality was perhaps not a dynamic response, but it was also not the easy response to the crises of the 15^{th} century. It reveals both a functional resilience as well as an ideological one; in spite of calamity on such an enormous and unprecedented scale that it must have led to questioning about the viability of the socio-economic order, people seem to have maintained confidence in the basic soundness of their system and a belief that it would recover if its basic premises were not allowed to become derailed. Their belief proved them right even if one of the side-effects may have been reduced dynamism and further entrenching of the established order. Echoes of these choices can be heard today, as we face similar options of continuity or change and the potential trade-off both involve.

Appendices

Appendix A

Measuring sediment sequences with ImageJ

Firstly the photograph is loaded into the software ImageJ. ImageJ is an open source imaging software and is available from http://rsbweb.nih.gov/ij/index.html. Its inbuilt measurement tools are used to measure the plastic targets created for scale. The plug in *My Plugin.class* was selected by selecting Plugins — > Compile and Run and then navigating to the folder where the file is stored. For uneven tephra layers the Freehand line selection tool (selected by right clicking on the line selection toolbar button) was used. It is then possible to trace the tephra for measurement and the output of xy coordinates will appear in a Log window. These results can then be copied and analysed in a suitable program. In this thesis the LOOKUP function of MS Excel was used to ensure that only pairs of coordinates where the x coordinates matched were selected and used as measurements.

An example of the plugin being used is shown in Figure A.1

Figure A.1: Measuring sediment sequences with ImageJ

A.1 ImageJ plug in JAVA code

```
import ij.*;
import ij.plugin.filter.PlugInFilter;
import ij.process.*;
import ij.gui.*;
import java.awt.*;
import java.awt.event.*;
import java.util.*;

/**
Richard Streeter
September 2010

This JAVA plugin for the ImageJ software implements the
MouseListener and  MouseMotionListener interfaces and
listens for mouse events generated by the current image.
When the user traces a line on the image the xy
```

```
coordinates are recorded and stored in a Log dialogue box, these can
then be copied into another program or saved.
It extends already the existing classes mouseListener() and
MouseMotionListener() which are open source and
available at
http://rsbweb.nih.gov/ij/plugins/index.html
*/

public class My_Plugin implements PlugInFilter, MouseListener,
MouseMotionListener {
ImagePlus img;
ImageCanvas canvas;
static Vector images = new Vector();

public int setup(String arg, ImagePlus img) {
this.img = img;
IJ.register(Mouse_Listener.class);
return DOES_ALL+NO_CHANGES;
}

public void run(ImageProcessor ip) {
IJ.showMessage("My_Plugin","This plug in is for the measurement
 of tephra layers \n It records the xy coordinates as you drag the
 mouse along. \n");
Integer id = new Integer(img.getID());
if (images.contains(id)) {
IJ.log("Already listening to this image");
return;
} else {
ImageWindow win = img.getWindow();
canvas = win.getCanvas();
canvas.addMouseListener(this);
canvas.addMouseMotionListener(this);
//int tool = Toolbar.getInstance().addTool("Test Tool");
//Toolbar.getInstance().setTool(tool);
//images.addElement(id);
}
}

public void mousePressed(MouseEvent e) {
int x = e.getX();
```

```
int y = e.getY();
int offscreenX = canvas.offScreenX(x);
int offscreenY = canvas.offScreenY(y);
}

public void mouseReleased(MouseEvent e) {
// IJ.log("nothing ");
}

// Logs movement when the mouse is dragged

public void mouseDragged(MouseEvent e) {
int x = e.getX();
int y = e.getY();
int offscreenX = canvas.offScreenX(x);
int offscreenY = canvas.offScreenY(y);
IJ.log(offscreenX+","+offscreenY);
}
public static String modifiers(int flags) {
String s = " [ ";
if (flags == 0) return "";
if ((flags & Event.SHIFT_MASK) != 0) s += "Shift ";
if ((flags & Event.CTRL_MASK) != 0) s += "Control ";
if ((flags & Event.META_MASK) != 0) s += "Meta (right button) ";
if ((flags & Event.ALT_MASK) != 0) s += "Alt ";
s += "]";
if (s.equals(" [ ]"))
  s = " [no modifiers]";
return s;
}
public void mouseExited(MouseEvent e) {}
public void mouseClicked(MouseEvent e) {}
public void mouseEntered(MouseEvent e) {}
public void mouseMoved(MouseEvent e) {}
}
```

Appendix B

Profile locations

The GPS profile locations and altitudes for 200 stratigraphic profiles, as well as the year they were recorded.

Table B.1: GPS location and altitudes for stratigraphic profiles

Profile Number	Year recorded	Longitude	Latitude	Altitude (m)
1	2008	-18.501122	63.634628	57
2	2008	18.587917	63.743000	219
3	2008	-18.575904	63.740071	219
4	2008	-18.575007	63.739898	220
5	2008	-18.574646	63.739736	219
6	2008	-18.574169	63.739641	219
7	2008	-18.574169	63.739641	219
8	2008	-18.573733	63.740632	222
9	2008	-18.613534	63.738458	168
10	2008	-18.612169	63.739143	159
11	2008	-18.612808	63.739378	159
12	2008	-18.614379	63.739942	164
13	2008	18.614666	63.740315	165
14	2008	-18.587328	63.869972	380
15	2008	-18.588555	63.870349	382
16	2008	-18.585848	63.871089	363
17	2008	-18.585084	63.870611	365
18	2008	-18.583956	63.868773	360
19	2008	-18.583956	63.868773	360
20	2008	-18.574972	63.813556	234
21	2008	-18.574972	63.813556	234
22	2008	-18.544205	63.630437	100
23	2008	-18.543955	63.630678	103

Continued on next page ...

Continued ...

Profile Number	Year recorded	Longitude	Latitude	Altitude (m)
24	2008	-18.501250	63.634487	57
25	2008	-18.501411	63.634434	57
26	2008	-18.501599	63.634381	58
27	2008	-18.501746	63.634346	58
28	2008	-18.502027	63.634347	58
29	2008	-18.502174	63.634318	59
30	2008	-18.502321	63.634348	59
31	2008	-18.502494	63.634367	58
32	2008	-18.502668	63.634349	58
33	2008	-18.757914	63.423555	110
34	2008	-18.759065	63.423428	92
35	2008	-18.758766	63.424844	112
36	2008	-18.765505	63.434034	95
37	2008	-18.765546	63.434034	95
38	2008	-18.500800	63.634622	59
39	2008	-18.762742	63.510724	234
40	2008	-18.763616	63.510987	234
41	2008	-18.764301	63.510553	224
42	2008	-18.765480	63.509424	146
43	2008	-18.768399	63.509690	134
44	2008	-18.772914	63.529620	221
45	2008	-18.723051	63.811080	454
46	2008	-18.723306	63.811049	452
47	2008	-18.722895	63.811117	458
48	2008	-18.722073	63.811353	460
49	2008	-18.721959	63.811440	461
50	2008	-18.721945	63.811434	460
51	2008	-18.721958	63.811546	462
52	2008	-18.678607	63.732456	338
53	2008	-18.679300	63.732503	336
54	2008	-18.659380	63.670750	138
55	2008	-18.659390	63.670750	138
56	2008	-18.649525	63.673683	140
57	2008	-18.734800	63.736500	207
58	2008	-18.734900	63.736500	208
59	2008	-18.734900	63.736200	209
60	2008	-18.533889	63.782222	260
61	2008	-18.533510	63.778825	263

Continued on next page ...

Continued ...

Profile Number	Year recorded	Longitude	Latitude	Altitude (m)
62	2008	-18.533384	63.779220	263
63	2008	-18.539128	63.778262	285
64	2008	-18.539197	63.777708	283
65	2008	-18.540730	63.778848	299
66	2008	-18.539024	63.777364	282
67	2008	-18.539087	63.777127	283
68	2008	-18.596528	63.855333	331
69	2008	-18.589940	63.836274	332
70	2008	-18.590805	63.836738	328
71	2008	-18.591326	63.836801	325
72	2008	-18.602694	63.850167	332
73	2008	-18.603386	63.850530	335
74	2008	-18.600325	63.851478	338
75	2008	-18.600325	63.851278	341
76	2008	-18.589678	63.837188	325
77	2008	-18.589336	63.836881	331
78	2008	-18.588800	63.837951	326
79	2008	-18.587419	63.837564	329
80	2008	-18.600856	63.838417	312
81	2008	-18.600233	63.838672	322
82	2008	-18.588593	63.840246	319
83	2008	-18.588592	63.840323	320
84	2008	-18.543917	63.653333	209
85	2008	-18.542668	63.652194	212
86	2008	-18.545367	63.652094	206
87	2008	-18.545009	63.654018	211
88	2008	-18.540083	63.661416	218
89	2008	-18.539821	63.661400	218
90	2008	-18.539705	63.661410	218
91	2008	-18.496199	63.639330	70
92	2008	-18.497366	63.639037	70
93	2008	-18.499527	63.641012	89
94	2008	-18.500439	63.642010	94
95	2008	-18.503673	63.656690	58
96	2008	-18.504509	63.656566	60
97	2008	-18.582448	63.784499	216
98	2008	-18.583095	63.784789	217
99	2008	-18.581417	63.784484	216

Continued on next page ...

Continued ...

Profile Number	Year recorded	Longitude	Latitude	Altitude (m)
100	2008	-18.581227	63.784508	216
101	2008	-18.570048	63.777429	214
102	2008	-18.570078	63.777237	214
103	2008	-18.571361	63.776701	211
104	2008	-18.574947	63.776364	208
105	2008	-18.617472	63.735744	184
106	2008	-18.617419	63.735684	184
107	2008	-18.617473	63.735720	184
108	2008	-18.617310	63.735732	184
109	2008	-18.595770	63.726743	163
110	2008	-18.595771	63.726707	160
111	2008	-18.595497	63.726898	158
112	2008	-18.595225	63.727017	155
113	2008	-18.483567	63.770743	151
114	2008	-18.483480	63.770716	151
115	2008	-18.483952	63.770511	151
116	2008	-18.486886	63.768629	138
117	2008	-18.486827	63.768655	139
118	2008	-18.486797	63.768668	141
119	2008	-18.495089	63.768361	159
120	2008	-18.495768	63.768052	158
121	2009	-18.494503	63.768359	159
122	2009	-18.500000	63.634722	59
123	2009	-18.500278	63.634444	60
124	2009	-18.500556	63.634444	63
125	2009	-18.670833	63.763611	355
126	2009	-18.670278	63.763333	331
127	2009	-18.669722	63.763333	331
128	2009	-18.551111	63.816944	246
129	2009	-18.549167	63.815000	234
130	2009	-18.548889	63.814444	232
131	2009	-18.552778	63.811389	232
132	2009	-18.559444	63.818889	297
133	2009	-18.564722	63.817500	304
134	2009	-18.570278	63.805278	236
135	2009	-18.490556	63.639167	58
136	2009	-18.577500	63.782500	208
137	2009	-18.573889	63.781667	206

Continued on next page ...

Continued ...

Profile Number	Year recorded	Longitude	Latitude	Altitude (m)
138	2009	-18.587500	63.770000	212
139	2009	-18.569167	63.768889	203
140	2009	-18.565000	63.770278	217
141	2009	-18.487500	63.727778	250
142	2009	-18.473889	63.728611	233
143	2009	-18.460000	63.734722	186
144	2009	-18.450556	63.735556	135
145	2009	-18.472778	63.726667	251
146	2009	-18.528056	63.656389	206
147	2009	-18.531111	63.660000	215
148	2009	-18.530000	63.663889	196
149	2009	-18.535833	63.665278	223
150	2009	-18.541667	63.649722	196
151	2009	-18.532778	63.676389	176
152	2009	-18.548056	63.678333	212
153	2009	-18.556667	63.676667	213
154	2009	-18.518056	63.663056	140
155	2009	-18.523889	63.663889	141
156	2009	-18.525556	63.668056	141
157	2009	-18.591389	63.831667	342
158	2009	-18.597778	63.826389	316
159	2009	-18.604444	63.803889	308
160	2009	-18.614167	63.800833	300
161	2010	-18.526390	63.637220	114
162	2010	-18.526390	63.636940	117
163	2010	-18.555830	63.635000	149
164	2010	-18.554720	63.636670	155
165	2010	-18.526390	63.636940	119
166	2010	-18.526390	63.637220	111
167	2010	-18.555280	63.635280	159
168	2010	-18.555830	63.634720	154
169	2010	-18.590000	63.883890	320
170	2010	-18.590280	63.884170	328
171	2010	-18.532780	63.785000	244
172	2010	-18.530280	63.786110	243
173	2010	-18.530280	63.786110	247
174	2010	-18.589440	63.866670	318
175	2010	-18.589440	63.883060	324

Continued on next page ...

Continued ...

Profile Number	Year recorded	Longitude	Latitude	Altitude (m)
176	2010	-18.589440	63.883060	324
177	2010	-18.589440	63.883060	324
178	2010	-18.589720	63.883610	325
179	2010	-18.530560	63.785000	242
180	2010	-18.541670	63.795560	289
181	2010	18.541390	63.795830	282
182	2010	-18.534440	63.798610	285
183	2010	-18.529170	63.803890	224
184	2010	-18.541670	63.795830	279
185	2010	-18.534170	63.798610	287
186	2010	-18.534170	63.798890	292
187	2010	-18.534170	63.798890	290
188	2010	-18.533890	63.798610	289
189	2010	-18.529170	63.803890	224
190	2010	-18.530000	63.803610	218
191	2010	-18.481110	63.701390	67
192	2010	-18.505280	63.794440	188
193	2010	-18.505280	63.794440	181
194	2010	-18.510830	63.644440	128
195	2010	-18.510280	63.644440	126
196	2010	-18.481110	63.701390	64
197	2010	-18.506390	63.794170	176
198	2010	-18.506390	63.794170	182
199	2010	-18.509720	63.644440	183
200	2010	-18.510280	63.644440	124

Appendix C

Geochemical analysis results

Full geochemical analysis results for analysis on the EMPA microprobe at the NERC Tephra analytical unit at the University of Edinburgh. Standards analysed are indicated by the Tables C.1 and C.2.

Table C.1: Standards used for analyses

Element	Standard Name :
Na	Jadeite-BL7
Mg	Spinel-BL8
Al	BIR1G-BLG1
K , K	Orthoclase-BL7
Ca, Ca, Si	Wollast-BL8
Fe	Fayalite
P , P	P K4
Ti, Ti	Rutile-BL8
Mn	PuMn -BL8

Full results of analysis. Sample numbers are based on the name of the profile recorded, and the identification of the tephra layer provided in Table 5.2. The sample name is guided by the original field identification of the tephra, and is not necessarily the actual identification, i.e. two samples were field identified as H 1300, but were actually Katla tephra. This is made clear in the table.

Firstly tephras dating before AD 1400 are presented (Table C.3), then AD 1400–1500, including the Grímsvötn tephra (Table C.4, page 183), then tephras sampled in the period after AD 1500 (Table C.5, page 185).

Table C.2: Composition of standards

Standard name	Composition
Jadeite-BL7	Na : 11.34%, Al : 13.23%, Si : 27.78%, Fe : 0.17%, O : 47.65%
Spinel-BL8	Mg : 17.084%, Al : 37.9306%, O : 44.9854%
BIR1G-BLG1	O : 44.6498%, Na : 1.82%, Mg : 5.8491%, Al : 8.1995%, Si : 22.2973%, P : 0.0092%, K : 0.0249%, Ca : 9.9095%, Ti : 0.575%, Cr : 0.05%, Mn : 0.1355%, Fe : 6.4802%, Sr : 0.%
Orthoclase-BL7	Na : 1.65%, Al : 9.69%, Si : 30.27%, K : 12.6%, O : 45.87%
Wollast-BL8	Mg : 0.17%, Al : 0.03%, Si : 24.%, Ca : 34.32%, Mn : 0.05%, Fe : 0.28%, O : 41.37%
Fayalite	Fe : 54.8113%, Si : 13.7823%, O : 31.4064%
P K4	O : 38.77%, F : 3.53%, Na : 0.17%, Si : 0.16%, P : 17.8%, Cl : 0.41%, Ca : 38.61%, Sr : 0.06%, Ce : 0.85%
Rutile-BL8	Ti : 59.34%, O : 39.89%, Mg : 0.01%, Fe : 0.59%, Nb : 0.17%
PuMn -BL8	Mn : 100.%

Table C.3: Results of geochemical analyses for tephras prior to AD 1400

SiO_2	TiO_2	Al_2O_3	FeO	MnO	MgO	CaO	Na_2O	K_2O	P_2O_5	Total
SILK-UN, Profile 135										
64.18	1.42	13.99	6.32	0.20	1.30	3.51	4.72	2.55	0.27	98.45
64.82	1.42	14.00	5.77	0.21	1.32	3.35	4.77	2.65	0.26	98.58
64.48	1.41	14.06	5.90	0.20	1.39	3.54	4.56	2.58	0.27	98.42
65.14	1.43	13.80	6.18	0.19	1.27	3.17	4.73	2.64	0.27	98.82
64.71	1.42	13.56	6.07	0.20	1.37	3.32	4.76	2.62	0.27	98.3
65.42	1.40	13.82	5.64	0.21	1.34	3.48	4.70	2.58	0.26	98.85
64.61	1.43	13.90	5.90	0.22	1.29	3.52	4.60	2.60	0.26	98.35
64.55	1.41	13.94	6.13	0.22	1.30	3.43	4.61	2.64	0.26	98.48
64.50	1.42	13.78	5.85	0.21	1.36	3.45	4.48	2.67	0.26	97.97
65.11	1.41	14.02	6.24	0.21	1.42	3.64	4.59	2.62	0.28	99.54
SILK-UN, Profile 147										
65.26	1.44	13.78	5.99	0.22	1.36	3.59	4.82	2.47	0.26	99.17
64.27	1.42	13.85	6.20	0.20	1.26	3.51	4.87	2.56	0.28	98.42
64.76	1.41	13.65	6.23	0.21	1.26	3.30	4.61	2.62	0.26	98.33
65.74	1.40	14.09	5.97	0.22	1.32	3.52	4.67	2.73	0.24	99.91

Continued on next page ...

Continued ...

SiO_2	TiO_2	Al_2O_3	FeO	MnO	MgO	CaO	Na_2O	K_2O	P_2O_5	Total
64.29	1.42	13.84	5.83	0.19	1.31	3.48	4.56	2.64	0.27	97.83
64.34	1.40	13.59	6.19	0.20	1.37	3.44	4.45	2.56	0.27	97.82
64.86	1.41	13.72	6.05	0.22	1.31	3.50	4.63	2.64	0.26	98.61
64.33	1.41	14.13	5.77	0.20	1.31	3.35	4.87	2.61	0.27	98.24
65.23	1.42	14.08	6.17	0.22	1.41	3.44	4.49	2.64	0.26	99.35
64.34	1.40	13.96	6.48	0.21	1.45	3.56	4.54	2.50	0.25	98.69
Landnám, Profile 17										
49.57	1.82	13.45	12.17	0.22	6.71	11.65	2.45	0.22	0.15	98.41
50.15	1.79	13.40	12.41	0.22	6.81	11.62	2.38	0.20	0.14	99.12
49.40	1.82	13.85	11.97	0.23	6.61	11.69	2.36	0.20	0.15	98.28
49.91	1.82	14.08	12.43	0.21	6.76	11.60	2.45	0.19	0.15	99.61
49.65	1.80	14.01	12.62	0.21	6.84	11.78	2.38	0.22	0.14	99.64
46.40	5.11	11.88	15.33	0.27	4.85	9.86	3.33	0.73	0.54	98.29
49.89	1.83	14.08	12.79	0.22	6.59	11.39	2.34	0.21	0.15	99.49
49.67	1.85	13.88	12.28	0.22	6.89	11.79	2.32	0.20	0.14	99.24
48.72	1.83	13.41	12.63	0.23	6.86	12.00	2.42	0.21	0.14	98.44
Grimsvotn 12thC, Profile 130										
48.54	2.91	13.15	12.99	0.23	5.70	9.97	2.78	0.43	0.29	97.00
49.97	2.68	13.70	13.27	0.22	5.49	9.73	2.93	0.47	0.29	98.76
48.73	2.81	13.43	13.46	0.23	5.82	10.35	2.91	0.44	0.27	98.43
48.76	2.76	13.35	13.61	0.22	5.77	10.04	2.75	0.39	0.27	97.92
47.96	2.82	13.28	13.44	0.23	5.78	10.24	2.85	0.34	0.27	97.21
48.29	2.82	13.09	13.89	0.23	5.73	10.14	2.86	0.44	0.28	97.77
47.88	2.89	13.23	13.68	0.22	5.47	9.79	2.80	0.39	0.29	96.64
49.40	2.83	13.25	13.82	0.22	5.92	9.99	2.84	0.37	0.27	98.90
49.71	2.75	13.43	13.30	0.22	5.48	10.05	2.92	0.47	0.28	98.62
48.63	2.82	13.15	13.72	0.24	5.77	10.23	2.64	0.40	0.28	97.88
Hekla 1104, Profile 17										
72.08	0.21	14.08	2.06	0.07	0.00	1.74	5.04	2.86	0.02	98.14
74.28	0.23	11.15	2.72	0.09	0.10	1.01	3.97	3.57	0.02	97.16
75.20	0.21	12.18	1.79	0.07	0.04	1.07	4.21	3.43	0.02	98.22
71.66	0.19	13.66	3.04	0.10	0.08	2.07	4.96	2.35	0.02	98.13
Hekla 1104, Profile 20										
72.00	0.21	13.94	3.31	0.11	0.11	1.97	4.97	2.85	0.01	99.48
72.10	0.21	14.84	2.86	0.09	0.08	2.18	5.15	2.49	0.01	99.99
70.04	0.17	15.42	2.52	0.08	0.08	2.53	5.77	2.40	0.02	99.04
71.93	0.22	13.37	3.33	0.13	0.08	1.90	4.64	2.78	0.02	98.39
Katla 1262, Profile 17										

Continued on next page ...

Continued ...

SiO_2	TiO_2	Al_2O_3	FeO	MnO	MgO	CaO	Na_2O	K_2O	P_2O_5	Total
46.68	4.66	12.61	15.00	0.26	4.85	9.02	3.17	0.84	0.71	97.79
46.71	4.66	12.40	14.25	0.25	4.84	9.39	3.39	0.78	0.71	97.37
46.93	4.67	12.76	14.67	0.25	4.91	9.24	3.43	0.81	0.70	98.37
45.12	4.64	12.40	14.57	0.23	4.60	9.42	3.14	0.83	0.72	95.67
45.75	4.66	12.80	14.53	0.22	4.75	9.06	3.16	0.77	0.73	96.41
47.39	4.66	12.80	15.17	0.24	4.83	9.29	3.25	0.80	0.69	99.12
47.06	4.67	12.68	14.42	0.24	4.85	9.19	3.23	0.81	0.72	97.87
46.39	4.67	12.54	14.62	0.24	4.65	9.40	3.25	0.90	0.72	97.39
46.08	4.35	13.20	14.72	0.22	5.10	9.93	2.93	0.68	0.46	97.66
47.42	4.70	12.57	14.47	0.25	4.88	9.44	3.08	0.76	0.75	98.33
Katla 1262, Profile 20										
46.97	4.78	12.45	14.92	0.23	4.75	9.30	3.25	0.85	0.53	98.05
46.36	4.77	13.04	14.75	0.24	4.97	9.37	3.09	0.89	0.53	97.99
47.60	4.71	12.92	14.07	0.25	4.73	9.34	3.20	0.89	0.54	98.24
47.03	4.76	12.28	14.80	0.23	4.87	9.44	3.21	0.85	0.54	98.01
46.98	4.78	12.43	14.47	0.24	4.91	9.45	3.12	0.81	0.50	97.69
46.92	4.79	12.74	14.58	0.26	4.94	9.10	3.12	0.85	0.52	97.82
46.78	4.80	12.70	14.51	0.23	4.91	9.44	3.30	0.80	0.52	97.98
47.20	4.79	12.65	14.87	0.23	4.87	9.59	3.09	0.79	0.52	98.60
47.01	4.78	12.82	14.26	0.25	4.86	9.22	3.31	0.84	0.52	97.87
48.03	4.76	12.53	13.94	0.24	4.93	9.29	3.17	0.87	0.51	98.28
Hekla 1300 Profile 39 (original sample name H 1300, Katla tephra)										
46.89	4.86	12.50	14.93	0.24	4.93	9.51	3.31	0.69	0.66	98.51
46.77	4.84	12.42	15.19	0.24	4.88	9.73	3.12	0.72	0.62	98.54
66.74	0.87	13.65	6.78	0.20	0.65	2.88	4.72	2.85	0.16	99.50
46.75	4.84	12.31	14.82	0.23	4.97	9.69	3.11	0.76	0.66	98.15
47.32	4.84	12.70	14.83	0.24	4.92	9.67	3.16	0.79	0.66	99.15
46.26	4.82	12.29	15.11	0.25	5.05	9.53	3.12	0.72	0.64	97.78
46.68	4.85	12.75	15.36	0.23	5.09	9.46	3.04	0.70	0.64	98.82
47.49	4.85	12.34	15.22	0.24	4.97	9.66	3.16	0.75	0.68	99.36
Hekla 1300 Profile 44										
46.87	4.59	12.88	14.98	0.24	4.83	9.51	3.11	0.77	0.53	98.32
60.59	1.27	15.06	9.09	0.27	1.65	4.92	4.14	1.53	0.51	99.02
59.53	1.29	15.02	9.69	0.26	1.77	5.07	4.45	1.52	0.49	99.08
46.53	4.82	12.42	14.83	0.23	4.89	9.40	3.13	0.72	0.63	97.6
46.87	4.59	12.88	14.98	0.24	4.83	9.51	3.11	0.77	0.53	98.32
60.59	1.27	15.06	9.09	0.27	1.65	4.92	4.14	1.53	0.51	99.02

Continued on next page ...

Continued ...

SiO_2	TiO_2	Al_2O_3	FeO	MnO	MgO	CaO	Na_2O	K_2O	P_2O_5	Total
59.53	1.29	15.02	9.69	0.26	1.77	5.07	4.45	1.52	0.49	99.08
46.53	4.82	12.42	14.83	0.23	4.89	9.40	3.13	0.72	0.63	97.6
Katla 1357, Profile 44										
47.29	4.79	12.36	15.06	0.24	4.95	9.52	3.11	0.69	0.74	98.74
46.13	4.78	12.82	14.90	0.23	4.94	9.67	3.19	0.72	0.73	98.12
46.54	4.74	12.42	14.81	0.23	4.86	9.42	3.21	0.77	0.74	97.74
46.21	4.73	12.58	15.31	0.24	4.74	9.63	3.14	0.78	0.73	98.08
47.99	4.78	12.52	14.78	0.24	5.05	9.67	3.22	0.80	0.72	99.77
46.36	4.78	12.60	14.98	0.25	5.07	9.45	3.18	0.70	0.71	98.08
47.09	4.78	12.53	14.54	0.23	4.92	9.56	3.16	0.79	0.72	98.32
47.39	4.74	12.55	14.78	0.24	4.99	9.51	3.11	0.77	0.78	98.84
46.14	4.72	12.61	14.92	0.24	4.91	9.65	3.14	0.77	0.73	97.84
46.54	4.76	12.60	14.99	0.24	4.91	9.48	3.08	0.78	0.72	98.09
Hekla 1389, Profile 179										
58.13	1.89	13.14	11.44	0.33	2.19	5.35	4.13	1.70	0.82	99.11
58.40	1.90	13.23	11.74	0.31	1.97	5.21	3.50	1.75	0.80	98.81
57.49	1.78	13.74	10.86	0.30	2.35	5.5	3.43	1.56	0.74	97.75
49.22	1.92	13.42	12.65	0.22	6.73	11.48	2.29	0.24	0.17	98.34
57.52	1.78	13.98	11.44	0.33	2.51	5.56	3.77	1.65	0.76	99.3
57.61	1.82	13.33	11.70	0.32	2.42	5.55	3.46	1.62	0.76	98.6

Table C.4: Results of geochemical analyses for tephras AD 1400–1500

SiO_2	TiO_2	Al_2O_3	FeO	MnO	MgO	CaO	Na_2O	K_2O	P_2O_5	Total
Katla 1416, Profile 20										
48.11	4.82	12.43	15.27	0.25	4.70	9.59	3.27	0.80	0.66	99.90
47.24	4.76	12.72	15.24	0.25	4.68	9.30	3.10	0.79	0.66	98.74
47.24	4.76	12.25	14.42	0.25	4.94	9.51	3.15	0.80	0.64	97.96
47.99	4.80	12.83	15.12	0.24	4.84	9.34	3.23	0.79	0.64	99.81
47.51	4.77	12.52	15.01	0.25	4.78	9.57	3.33	0.73	0.62	99.09
47.96	4.81	12.34	14.98	0.25	4.75	9.18	3.23	0.77	0.63	98.92
47.14	4.79	12.25	14.79	0.24	4.73	9.39	3.20	0.84	0.68	98.06
46.55	4.79	12.70	15.19	0.24	4.65	9.39	3.25	0.81	0.63	98.21
47.09	4.79	12.68	14.65	0.24	4.75	9.47	3.22	0.79	0.64	98.31
47.04	4.81	12.55	14.65	0.23	4.78	9.47	3.29	0.83	0.65	98.29
Katla 1416, Profile 49										
46.58	4.69	11.75	14.62	0.26	4.61	9.15	3.07	0.73	0.75	96.20
48.74	3.14	12.86	14.37	0.22	5.31	9.64	2.83	0.45	0.36	97.91

Continued on next page ...

Continued ...

SiO_2	TiO_2	Al_2O_3	FeO	MnO	MgO	CaO	Na_2O	K_2O	P_2O_5	Total
46.76	4.72	12.47	14.35	0.25	4.79	9.21	3.12	0.75	0.71	97.13
46.43	4.72	12.48	14.62	0.25	4.75	9.50	3.14	0.77	0.71	97.37
46.68	4.41	13.12	14.81	0.21	5.50	10.22	2.84	0.63	0.44	98.87
47.60	4.72	12.49	14.33	0.25	4.72	9.18	3.13	0.70	0.74	97.85
47.98	4.77	12.39	14.76	0.24	4.63	9.48	3.14	0.74	0.73	98.88
47.94	4.61	12.56	14.85	0.25	4.65	9.31	3.23	0.86	0.79	99.05
46.51	4.88	12.49	15.04	0.24	4.77	9.84	3.29	0.71	0.62	98.39
47.79	4.72	12.67	15.02	0.24	4.75	9.38	3.16	0.74	0.74	99.21
Katla 1416, Profile 112										
47.60	4.75	13.20	14.66	0.23	4.90	9.58	3.20	0.77	0.74	99.63
47.20	4.74	12.54	14.86	0.25	4.70	9.45	3.21	0.80	0.73	98.49
46.94	4.72	12.33	15.17	0.24	4.70	9.60	3.04	0.74	0.74	98.21
47.49	4.73	12.36	14.81	0.26	4.74	9.27	3.04	0.69	0.76	98.15
46.92	4.70	12.24	15.23	0.24	4.79	9.34	3.25	0.84	0.75	98.30
47.86	4.81	12.48	14.80	0.23	4.79	9.64	3.18	0.82	0.77	99.38
47.00	4.75	12.49	15.14	0.23	4.75	9.40	3.33	0.80	0.74	98.63
46.88	4.78	12.81	15.40	0.26	4.72	9.60	3.44	0.74	0.76	99.39
47.53	4.81	12.60	14.70	0.24	4.70	9.51	3.39	0.78	0.78	99.03
47.72	4.78	12.38	14.60	0.25	4.67	9.25	3.17	0.81	0.78	98.42
Katla 1416, Profile 179										
46.80	4.88	12.63	14.49	0.25	4.94	9.26	3.17	0.85	0.52	97.78
47.24	4.84	12.70	14.35	0.26	4.73	9.31	3.16	0.83	0.53	97.94
46.60	4.88	12.41	14.74	0.25	4.91	9.46	3.19	0.83	0.50	97.77
47.47	4.88	12.61	14.28	0.26	4.74	9.51	3.16	0.86	0.52	98.27
46.94	4.88	12.46	14.71	0.27	4.92	9.43	3.12	0.81	0.53	98.07
47.19	4.87	12.07	14.54	0.24	4.95	9.81	3.16	0.75	0.52	98.09
47.20	4.87	12.55	14.70	0.23	4.78	9.53	3.16	0.82	0.51	98.37
46.63	4.88	12.39	14.69	0.24	4.87	9.52	3.25	0.80	0.52	97.78
47.07	4.85	12.60	14.65	0.26	4.81	9.47	3.21	0.76	0.51	98.18
47.17	4.87	12.26	14.67	0.25	4.96	9.40	3.29	0.79	0.54	98.18
Grímsvötn 1432±5, Profile 152										
48.34	2.64	13.88	12.79	0.21	6.03	10.64	2.86	0.42	0.25	98.04
48.34	2.64	13.64	12.97	0.22	6.07	10.35	2.76	0.44	0.26	97.68
48.32	2.60	13.54	13.12	0.21	6.06	10.54	2.90	0.41	0.24	97.94
50.18	2.67	13.48	13.35	0.23	5.78	10.11	2.93	0.40	0.26	99.38
48.80	2.61	13.86	13.01	0.21	5.98	10.51	2.85	0.37	0.26	98.47
48.62	2.62	13.56	13.13	0.21	5.88	10.31	2.81	0.41	0.27	97.82
48.64	2.62	13.55	12.95	0.22	6.01	10.48	2.74	0.33	0.26	97.81

Continued on next page ...

Continued ...

SiO_2	TiO_2	Al_2O_3	FeO	MnO	MgO	CaO	Na_2O	K_2O	P_2O_5	Total
Grímsvötn 1432±5, Profile 87										
50.13	2.65	13.35	12.77	0.21	6.12	10.23	2.81	0.40	0.29	98.95
49.89	2.76	13.18	13.08	0.23	5.82	10.39	2.84	0.36	0.28	98.82
49.11	2.61	13.27	12.49	0.21	6.10	10.44	2.86	0.32	0.27	97.66
49.25	2.61	13.19	12.99	0.21	5.75	10.49	2.80	0.33	0.26	97.87
49.33	2.66	13.31	12.63	0.21	5.82	10.47	2.75	0.34	0.27	97.80
49.82	2.66	13.41	12.90	0.22	6.06	10.31	2.74	0.34	0.27	98.72
49.73	2.65	13.17	12.90	0.22	6.03	10.80	2.64	0.33	0.28	98.76
49.45	2.64	13.64	12.74	0.21	6.04	10.51	2.75	0.38	0.25	98.62
50.02	2.63	13.70	12.71	0.22	5.90	10.50	2.71	0.35	0.27	99.03
49.98	2.66	13.47	12.66	0.23	6.03	10.28	2.56	0.38	0.27	98.52
Grímsvötn 1432±5, Profile 179										
49.18	2.71	13.46	12.88	0.23	6.19	10.51	2.74	0.38	0.17	98.44
49.55	2.67	13.30	12.97	0.22	6.09	10.34	2.69	0.38	0.19	98.39
49.45	2.68	13.51	13.19	0.22	6.09	10.57	2.74	0.31	0.18	98.95
48.80	2.70	13.49	13.14	0.22	6.05	10.42	2.70	0.39	0.19	98.10
49.46	2.68	13.37	12.65	0.21	6.20	10.49	2.65	0.38	0.18	98.27
49.22	2.62	13.47	12.55	0.21	6.13	10.59	2.72	0.35	0.18	98.03
49.00	2.68	13.33	12.83	0.22	5.97	10.75	2.80	0.36	0.19	98.14
49.21	2.69	12.85	12.69	0.21	6.19	10.35	2.88	0.40	0.19	97.67
49.49	2.69	13.33	12.43	0.23	5.83	10.75	2.80	0.40	0.18	98.12
Grímsvötn 1457±5, Profile 152										
50.06	2.99	13.11	14.60	0.25	5.64	10.03	2.93	0.45	0.26	100.32
50.68	2.58	13.27	13.00	0.21	5.72	10.05	2.74	0.49	0.25	98.99
49.19	2.95	12.60	13.90	0.24	5.39	9.41	2.79	0.42	0.28	97.18
49.49	2.77	13.14	13.23	0.21	5.85	9.95	2.81	0.46	0.26	98.19
49.51	2.76	12.63	13.63	0.23	5.76	9.94	2.91	0.42	0.27	98.05
49.11	2.66	13.13	12.80	0.22	5.84	10.36	2.79	0.34	0.25	97.52
49.12	2.63	13.53	13.01	0.21	5.91	10.42	2.57	0.41	0.23	98.04
49.50	2.78	12.79	13.92	0.22	5.64	10.19	2.77	0.41	0.26	98.48
49.28	2.63	13.08	12.66	0.22	5.94	10.08	2.88	0.42	0.23	97.42
49.57	2.60	12.85	13.07	0.23	5.97	10.19	2.66	0.36	0.24	97.75
Grímsvötn 1457±5, Profile 49										
49.89	2.85	13.32	13.94	0.23	5.80	10.17	2.96	0.43	0.27	99.87
49.53	2.90	12.95	14.19	0.23	5.63	9.99	2.68	0.36	0.28	98.73
49.75	2.93	13.29	13.34	0.23	5.49	9.86	2.87	0.42	0.28	98.47
50.09	2.99	13.21	13.80	0.23	5.52	9.82	2.78	0.47	0.31	99.23
49.75	2.83	13.18	13.75	0.22	5.66	10.24	2.80	0.39	0.28	99.10

Continued on next page ...

Continued ...

SiO_2	TiO_2	Al_2O_3	FeO	MnO	MgO	CaO	Na_2O	K_2O	P_2O_5	Total
49.83	2.82	13.32	13.12	0.24	5.66	10.44	2.80	0.40	0.27	98.91
49.09	2.86	13.70	13.29	0.22	5.83	9.96	2.84	0.44	0.28	98.52
50.51	2.68	13.49	12.69	0.22	5.83	10.51	2.65	0.38	0.26	99.23
49.68	2.84	13.38	13.47	0.23	5.82	10.02	2.92	0.44	0.29	99.09
49.79	2.86	13.32	13.51	0.23	5.70	10.11	2.81	0.42	0.28	99.02
Grímsvötn 1457±5, Profile 20										
49.27	2.64	13.24	12.63	0.22	5.87	10.40	2.73	0.41	0.26	97.68
49.14	2.67	13.60	13.31	0.23	5.94	10.47	2.73	0.37	0.28	98.75
49.39	2.58	13.54	12.77	0.22	6.14	10.46	2.91	0.34	0.26	98.62
48.92	2.65	13.28	12.95	0.22	5.96	10.42	2.79	0.39	0.27	97.85
48.93	2.91	13.44	14.00	0.22	5.67	10.02	2.95	0.50	0.29	98.94
48.80	2.85	13.23	13.18	0.24	5.53	10.12	2.81	0.41	0.29	97.47
48.75	2.94	13.07	13.85	0.23	5.59	9.90	2.82	0.44	0.31	97.90
50.11	3.07	13.19	14.21	0.23	5.34	9.78	3.03	0.39	0.32	99.68
Grímsvötn 1457±5, Profile 27										
49.07	2.60	13.54	12.84	0.21	6.03	10.54	2.90	0.39	0.25	98.38
49.45	2.63	12.79	12.95	0.20	5.92	10.38	2.81	0.41	0.27	97.81
49.86	2.66	13.47	13.26	0.22	6.09	10.55	2.80	0.34	0.26	99.52
49.45	2.63	13.48	13.07	0.23	6.08	10.41	2.82	0.31	0.27	98.74
49.51	2.63	13.15	13.07	0.22	6.25	10.46	2.93	0.41	0.27	98.92
49.35	2.64	13.58	12.47	0.23	6.01	10.46	2.99	0.36	0.27	98.35
49.17	2.65	13.53	12.68	0.22	6.07	10.35	2.63	0.34	0.27	97.92
49.40	2.66	13.57	13.10	0.20	5.95	10.37	2.73	0.36	0.27	98.61
49.46	2.63	13.22	12.86	0.23	5.91	10.44	2.79	0.38	0.28	98.20
49.86	2.63	13.66	13.18	0.22	5.88	10.39	2.74	0.35	0.26	99.17
Grímsvötn 1457±5, Profile 56										
49.49	2.89	12.96	13.67	0.22	5.67	10.33	2.80	0.39	0.30	98.72
50.09	2.83	13.03	13.45	0.22	5.75	10.22	2.83	0.43	0.28	99.13
48.74	2.66	13.07	12.97	0.21	6.10	10.61	2.90	0.37	0.29	97.92
49.18	2.79	13.67	13.49	0.23	5.72	10.38	2.80	0.38	0.28	98.90
50.04	3.06	13.18	14.27	0.23	5.29	9.84	2.88	0.44	0.33	99.54
50.59	2.68	13.35	12.42	0.21	5.88	10.62	2.73	0.30	0.28	99.07
50.03	2.63	13.32	12.70	0.20	5.48	10.14	2.95	0.48	0.29	98.22
49.84	2.70	13.30	12.82	0.22	5.73	10.33	2.74	0.35	0.30	98.32
49.77	2.85	13.00	13.99	0.23	5.48	10.15	2.76	0.44	0.32	98.98
49.52	2.68	13.20	12.99	0.23	5.89	10.39	2.90	0.40	0.27	98.48
Grímsvötn 1457±5, Profile112										
49.35	1.80	15.26	10.50	0.18	7.84	11.97	2.32	0.21	0.16	99.58

Continued on next page ...

Continued ...

SiO_2	TiO_2	Al_2O_3	FeO	MnO	MgO	CaO	Na_2O	K_2O	P_2O_5	Total
49.66	2.67	13.79	12.90	0.22	5.98	10.37	2.81	0.36	0.29	99.05
49.23	2.96	13.12	14.09	0.26	5.49	9.96	2.89	0.45	0.32	98.76
49.98	2.75	13.21	13.11	0.23	5.91	10.41	2.88	0.42	0.29	99.18
50.31	2.67	13.36	13.09	0.22	5.87	10.36	2.79	0.34	0.28	99.28
49.85	2.69	13.28	12.94	0.20	6.00	10.32	2.75	0.44	0.28	98.74
49.72	2.98	13.12	13.74	0.24	5.43	9.93	2.78	0.44	0.32	98.69
49.36	2.66	13.57	13.06	0.22	5.92	10.37	2.70	0.39	0.28	98.53
50.04	2.83	13.66	13.65	0.23	5.68	10.12	2.88	0.35	0.28	99.71
49.94	2.68	13.51	13.10	0.22	5.99	10.45	2.79	0.34	0.27	99.28
Grímsvötn 1457±5, Profile 17										
48.13	2.76	13.26	13.75	0.24	5.98	10.30	2.88	0.41	0.28	98.00
49.43	2.87	13.04	13.55	0.22	5.53	10.03	2.75	0.40	0.30	98.11
49.57	2.67	13.61	12.97	0.22	5.85	10.32	2.90	0.45	0.28	98.81
48.78	2.63	13.68	13.15	0.22	6.00	10.32	2.65	0.41	0.27	98.11
49.87	2.84	13.23	13.18	0.22	5.65	10.23	2.90	0.39	0.31	98.84
48.96	2.85	12.97	13.64	0.22	5.61	9.73	2.90	0.39	0.30	97.56
48.83	2.80	13.10	13.04	0.23	5.72	10.15	2.83	0.36	0.29	97.36
48.40	2.64	13.57	12.93	0.20	6.04	10.54	2.71	0.34	0.27	97.64
Grímsvötn 1457±5, Profile 87										
49.15	2.65	13.39	13.17	0.22	6.09	10.29	2.83	0.41	0.26	98.47
49.49	2.78	13.28	13.43	0.23	5.93	10.37	2.67	0.38	0.28	98.83
48.47	2.99	12.86	14.34	0.26	5.44	9.54	2.84	0.45	0.32	97.5
48.14	2.59	13.13	12.58	0.21	6.04	10.55	2.73	0.36	0.27	96.60
49.66	2.88	13.35	13.89	0.22	5.42	10.35	2.90	0.42	0.31	99.39
49.32	2.80	12.81	12.95	0.24	5.64	10.34	2.86	0.38	0.30	97.66
50.53	2.67	13.61	12.73	0.20	5.87	10.44	2.84	0.40	0.25	99.56
49.39	2.70	13.16	13.12	0.21	5.84	10.72	2.73	0.34	0.27	98.47
50.16	2.65	13.14	12.86	0.23	6.04	10.51	2.81	0.38	0.27	99.03
49.80	2.66	13.61	13.12	0.22	5.91	10.46	2.74	0.37	0.25	99.14
49.63	2.81	13.27	13.18	0.23	5.88	10.38	2.82	0.36	0.24	98.79
49.36	2.92	13.02	13.46	0.22	5.69	10.13	2.84	0.41	0.29	98.35
Grimsvotn 1457±5, Profile 179										
48.90	2.94	12.95	13.63	0.25	5.61	10.04	2.90	0.42	0.24	97.88
49.44	2.47	13.64	11.82	0.20	6.55	11.16	2.57	0.30	0.21	98.37
49.53	2.70	13.41	13.18	0.22	6.16	10.40	2.83	0.36	0.24	99.02
49.19	2.72	13.31	13.13	0.22	5.94	10.50	3.03	0.38	0.25	98.68
48.67	2.70	13.60	13.19	0.23	6.07	10.56	2.69	0.39	0.23	98.34
50.03	2.75	13.44	13.14	0.22	5.93	10.32	2.84	0.41	0.25	99.33

Continued on next page ...

Continued ...

SiO_2	TiO_2	Al_2O_3	FeO	MnO	MgO	CaO	Na_2O	K_2O	P_2O_5	Total
49.09	3.11	12.81	13.96	0.24	5.35	9.99	2.96	0.46	0.28	98.24
49.12	2.70	13.22	13.03	0.22	6.04	10.50	2.79	0.34	0.25	98.20
Veiðivötn 1477, Profile 17										
49.53	2.11	12.76	13.63	0.24	6.16	11.22	2.46	0.23	0.16	98.49
49.39	2.19	12.86	13.89	0.25	6.27	11.10	2.47	0.22	0.18	98.84
49.69	2.17	12.85	13.51	0.24	6.04	10.90	2.59	0.23	0.17	98.39
50.26	2.15	13.10	13.46	0.24	6.12	11.42	2.53	0.25	0.16	99.69
50.60	2.12	13.11	13.50	0.24	6.07	11.23	2.46	0.26	0.16	99.75
Veiðivötn 1477, Profile 20										
48.90	2.17	12.82	13.86	0.25	5.92	10.57	2.60	0.28	0.18	97.54
48.14	1.80	13.37	12.53	0.23	6.79	11.52	2.52	0.21	0.14	97.24
48.21	1.96	13.66	12.98	0.23	6.22	10.92	2.61	0.26	0.16	97.21
49.19	1.81	13.57	12.39	0.23	6.72	11.89	2.39	0.22	0.15	98.57
49.53	2.37	13.21	13.59	0.24	5.95	10.42	2.66	0.32	0.20	98.47
Veiðivötn 1477, Profile 179										
49.12	1.90	13.69	12.61	0.24	6.50	11.43	2.45	0.23	0.16	98.34
48.90	1.92	13.65	12.72	0.22	6.50	11.46	2.41	0.23	0.15	98.16
49.05	2.02	13.59	12.86	0.24	6.13	11.15	2.51	0.20	0.15	97.92
48.90	1.44	14.02	11.64	0.22	7.46	12.65	2.16	0.14	0.10	98.71
49.38	1.89	13.65	12.37	0.22	6.64	11.42	2.48	0.22	0.15	98.41
49.75	1.89	13.18	12.82	0.24	6.53	11.17	2.49	0.24	0.15	98.46
49.26	2.01	12.92	13.28	0.23	6.19	11.00	2.42	0.25	0.16	97.72
49.57	1.74	14.51	11.40	0.18	7.68	12.39	2.31	0.19	0.15	100.12
50.13	2.14	12.44	14.38	0.25	6.01	10.81	2.55	0.34	0.17	99.21
50.15	1.94	13.52	13.13	0.22	6.27	11.07	2.48	0.23	0.17	99.20
49.33	1.85	13.53	12.30	0.22	6.61	11.28	2.41	0.22	0.16	97.93
Katla 1500, Profile 112										
47.19	4.92	12.73	15.23	0.23	4.98	9.82	3.07	0.77	0.65	99.59
46.50	4.90	12.72	14.70	0.23	4.99	9.71	3.11	0.75	0.60	98.20
49.42	4.07	13.14	13.57	0.22	4.57	8.80	3.31	1.07	0.48	98.65
46.85	4.86	12.23	14.89	0.25	4.90	9.53	3.13	0.73	0.69	98.05
46.72	5.03	12.42	15.58	0.23	5.07	9.73	3.17	0.73	0.65	99.33
46.60	4.90	12.21	14.92	0.23	5.03	9.80	3.18	0.75	0.60	98.21
46.86	4.98	12.48	15.17	0.25	5.07	9.98	3.22	0.69	0.61	99.31
46.92	4.88	12.59	15.03	0.25	5.13	10.11	2.97	0.77	0.63	99.28
50.33	4.04	12.80	13.83	0.22	4.48	8.82	3.36	1.00	0.47	99.35
Katla 1500, Profile 152										
45.82	5.03	12.51	15.42	0.26	4.90	9.87	3.09	0.68	0.66	98.24

Continued on next page ...

Continued ...										
SiO_2	TiO_2	Al_2O_3	FeO	MnO	MgO	CaO	Na_2O	K_2O	P_2O_5	Total
47.38	4.87	12.50	15.06	0.24	5.08	9.92	3.05	0.69	0.61	99.40
46.87	4.89	12.21	15.39	0.26	4.57	9.41	3.19	0.86	0.75	98.41
46.93	4.87	12.78	14.97	0.25	5.09	9.69	3.17	0.72	0.69	99.16
46.40	4.91	12.88	14.82	0.25	5.29	9.63	3.14	0.70	0.64	98.65
46.70	5.03	12.30	15.72	0.26	4.83	9.52	3.06	0.73	0.66	98.82
46.31	4.84	12.60	15.25	0.24	5.11	9.46	3.06	0.74	0.69	98.29
47.06	4.92	12.35	15.06	0.24	5.06	9.88	2.88	0.71	0.66	98.82
46.33	4.93	12.42	15.04	0.24	5.02	9.94	2.95	0.70	0.64	98.20
46.95	5.05	12.34	15.59	0.24	5.02	9.69	3.12	0.76	0.62	99.39
Katla 1500, Profile 179										
46.27	4.94	12.31	15.10	0.24	5.11	9.96	3.11	0.69	0.58	98.31
45.96	5.09	11.99	15.37	0.24	5.11	9.99	2.90	0.71	0.54	97.91
46.25	5.13	12.39	15.36	0.27	5.08	9.90	2.81	0.76	0.55	98.50
46.28	5.01	12.33	14.85	0.24	5.06	10.11	3.10	0.72	0.59	98.28
46.75	4.92	12.28	14.67	0.25	5.08	9.54	3.06	0.76	0.57	97.89
46.06	5.02	12.38	14.99	0.24	5.21	10.04	3.00	0.78	0.56	98.28
45.75	4.92	12.67	15.11	0.24	5.07	9.92	2.99	0.68	0.55	97.90
46.59	4.96	12.09	15.05	0.24	5.09	9.86	3.01	0.68	0.56	98.13
46.68	5.07	12.17	15.15	0.27	5.18	10.02	3.28	0.74	0.59	99.14
46.20	5.06	12.45	15.44	0.24	4.96	9.90	3.03	0.71	0.56	98.53

Table C.5: Results of geochemical analyses for tephras AD 1500–1918

SiO_2	TiO_2	Al_2O_3	FeO	MnO	MgO	CaO	Na_2O	K_2O	P_2O_5	Total
Hekla 1597, Profile 20										
49.38	1.90	13.56	13.02	0.21	6.54	11.28	2.59	0.20	0.16	98.84
47.47	4.37	12.69	13.91	0.23	4.55	8.98	3.34	0.92	0.51	96.97
62.83	1.08	15.57	8.36	0.26	1.23	4.63	4.61	1.86	0.35	100.78
62.28	1.06	15.01	9.00	0.26	1.39	4.67	4.42	1.79	0.34	100.22
49.57	3.73	12.85	14.94	0.26	4.42	8.67	3.02	0.57	0.38	98.41
61.36	1.04	15.23	8.89	0.26	1.35	4.71	4.47	1.70	0.32	99.31
60.99	1.08	14.76	9.13	0.26	1.44	4.80	4.61	1.74	0.35	99.17
Hekla 1597, Profile 56 (Katla tephra)										
47.13	4.72	13.18	14.62	0.22	4.89	9.74	3.26	0.71	0.77	99.24
47.14	4.73	12.69	15.25	0.22	4.99	9.67	3.13	0.73	0.79	99.33
47.37	4.83	12.31	14.63	0.25	4.85	9.62	3.11	0.85	0.80	98.62
47.59	4.75	12.34	14.59	0.24	4.76	9.51	3.13	0.66	0.75	98.30
47.83	4.73	12.53	14.82	0.24	4.96	9.42	3.36	0.70	0.77	99.35

Continued on next page ...

Continued ...

SiO_2	TiO_2	Al_2O_3	FeO	MnO	MgO	CaO	Na_2O	K_2O	P_2O_5	Total
46.57	4.73	12.22	14.67	0.24	4.99	9.27	3.07	0.70	0.75	97.20
46.86	4.73	12.80	14.81	0.25	4.90	9.56	3.19	0.82	0.79	98.71
46.92	4.73	12.84	14.25	0.25	4.88	9.67	3.21	0.78	0.80	98.33
46.83	4.68	12.61	14.90	0.25	4.83	9.43	3.12	0.81	0.79	98.24
47.12	4.71	12.43	14.88	0.24	4.87	9.65	3.10	0.82	0.79	98.62
Hekla 1597, Profile 179										
45.80	4.70	12.70	14.43	0.23	5.15	10.35	2.90	0.63	0.40	97.29
59.95	1.23	15.25	8.51	0.26	1.56	5.23	4.72	1.43	0.43	98.57
59.49	1.32	14.53	9.59	0.25	1.71	4.98	4.15	1.77	0.47	98.25
59.35	1.38	13.83	9.80	0.27	1.84	4.87	4.09	1.74	0.52	97.70
59.03	1.35	14.62	10.01	0.28	1.89	5.00	4.23	1.89	0.50	98.79
61.63	1.06	15.48	8.62	0.25	1.33	4.79	4.43	1.78	0.33	99.70
59.76	1.28	15.11	9.31	0.27	1.63	5.45	4.53	1.36	0.47	99.18
60.21	1.34	14.63	9.44	0.29	1.83	5.04	4.24	1.70	0.50	99.24
Katla 1625, Profile 20										
45.66	4.76	12.25	15.05	0.24	4.99	9.58	3.38	0.82	0.84	97.57
46.57	4.75	12.46	14.78	0.24	4.87	9.61	3.08	0.67	0.78	97.83
46.21	4.77	12.71	14.85	0.25	4.97	9.82	3.17	0.75	0.82	98.32
47.27	4.74	12.47	14.52	0.24	5.09	9.68	3.21	0.80	0.81	98.82
46.17	4.76	12.49	15.37	0.26	4.96	9.60	3.21	0.75	0.78	98.34
45.97	4.74	12.70	14.55	0.25	4.94	9.55	3.20	0.72	0.82	97.44
47.03	4.84	12.29	14.89	0.25	4.90	9.69	3.05	0.73	0.68	98.35
47.21	4.74	12.85	14.97	0.23	4.94	9.62	3.06	0.78	0.80	99.20
47.04	4.71	12.29	14.91	0.23	4.91	9.76	3.00	0.72	0.86	98.42
47.05	4.77	12.40	15.17	0.23	4.85	9.43	3.25	0.72	0.77	98.64
Katla 1755, Profile 20										
46.89	4.72	12.46	15.05	0.24	4.98	9.57	3.03	0.76	0.66	98.37
46.58	4.71	12.46	14.94	0.25	5.06	9.46	3.21	0.70	0.64	98.00
45.14	4.68	12.51	14.74	0.25	5.00	9.37	3.11	0.70	0.65	96.15
46.28	4.69	12.79	14.96	0.24	4.97	9.60	3.19	0.68	0.63	98.04
45.21	4.69	12.57	14.26	0.23	4.97	9.56	3.11	0.69	0.67	95.96
45.62	4.66	12.63	15.13	0.26	5.04	9.13	3.17	0.67	0.65	96.95
45.62	4.63	12.88	14.61	0.24	4.91	9.52	3.16	0.75	0.63	96.95
45.52	4.67	12.49	15.00	0.24	4.90	9.39	3.14	0.72	0.67	96.73
46.42	4.66	13.04	14.61	0.24	4.98	9.65	3.06	0.79	0.65	98.10
46.24	4.69	12.55	14.41	0.23	4.92	9.67	3.14	0.79	0.61	97.25
Hekla 1845, Profile 17										
59.06	1.26	14.71	9.35	0.26	1.76	5.18	4.35	1.61	0.54	98.09

Continued on next page ...

Continued ...

SiO_2	TiO_2	Al_2O_3	FeO	MnO	MgO	CaO	Na_2O	K_2O	P_2O_5	Total
60.44	1.19	14.98	8.96	0.25	1.64	5.25	4.44	1.53	0.46	99.13
61.11	1.18	15.40	8.87	0.25	1.68	5.07	4.39	1.54	0.46	99.94
48.8	1.89	13.34	12.57	0.23	6.76	11.34	2.44	0.23	0.18	97.77
59.73	1.22	15.46	9.09	0.25	1.71	5.31	4.39	1.52	0.50	99.18
Hekla 1845, Profile 20										
49.10	1.80	14.01	12.38	0.21	6.60	11.51	2.50	0.18	0.17	98.46
48.69	1.97	13.23	13.59	0.21	6.27	11.21	2.40	0.23	0.18	97.98
49.61	1.82	13.88	12.38	0.22	6.58	11.58	2.49	0.21	0.17	98.94
48.81	1.79	14.02	12.30	0.21	6.64	11.29	2.34	0.20	0.15	97.76
49.73	1.91	13.75	12.84	0.22	6.46	11.26	2.33	0.23	0.19	98.93
60.73	1.18	15.36	8.87	0.25	1.56	5.19	4.52	1.84	0.45	99.95
61.04	1.12	15.28	8.68	0.24	1.51	4.93	4.38	1.54	0.43	99.15
Katla 1918, Profile 20										
46.55	4.78	12.33	14.97	0.23	4.95	9.46	2.97	0.79	0.51	97.55
47.27	4.64	12.74	14.80	0.22	4.78	9.50	3.15	0.78	0.54	98.42
47.43	4.68	12.70	14.78	0.24	4.96	9.21	3.22	0.81	0.73	98.74
46.86	4.65	12.65	14.50	0.23	4.86	9.61	3.19	0.74	0.53	97.84
47.11	4.68	12.65	14.90	0.24	4.86	9.62	3.18	0.75	0.70	98.70
47.50	4.62	12.52	14.98	0.25	4.85	9.68	3.07	0.70	0.66	98.83
46.46	4.66	12.69	14.42	0.24	4.70	9.44	3.30	0.81	0.72	97.45
47.54	4.73	13.04	14.87	0.23	4.81	9.55	3.16	0.78	0.51	99.22
47.31	4.63	13.23	14.96	0.23	4.97	9.64	2.64	0.81	0.68	99.10
46.41	4.58	13.00	14.83	0.23	4.86	9.37	3.16	0.81	0.71	97.96

Appendix D

Sediment accumulation data for profiles

Full sediment accumulation data for profiles is provided here. Profiles are grouped as they are presented in Chapter 5. Black bars along the x axis indicates periods where there was indication of reworking in the profiles

Section 5.3.2, on page 92 identified three major 'types' of stratigraphic section. Here further examples of each type are identified, Table D.1

Table D.1: Examples of different stratigraphic sections types

Section characteristics	Profile Numbers
(a) Upland sections, above altitude of 300 m. SeAR rates are highest immediately after Landnám, before declining	72, 73, 74, 75, 77, 79, 78, 83, 80, 81
(b) Sections below 300 m, type A. These sections have high SeAR prior to AD 1262, before declining to post-Landnám mean levels. The, from around AD 1625 onwards SeARs increase, often to above 2 mm yr^{-1}. This is interpreted as being close to active erosion fronts.	145, 151, 152, 148, 155, 95, 139, 138, 197, 128, 165, 119, 121, 120, 65, 57
(c) Sections below 300 m, type B. These have the same pattern of SeAR as type A until the after AD 1625. These profiles have no systematic increase in SeAR, and show variations around the mean value until K 1918. Many of these sections were	180, 181, 184, 185, 187, 189, 190, 183, 197, 198, 192, 193,

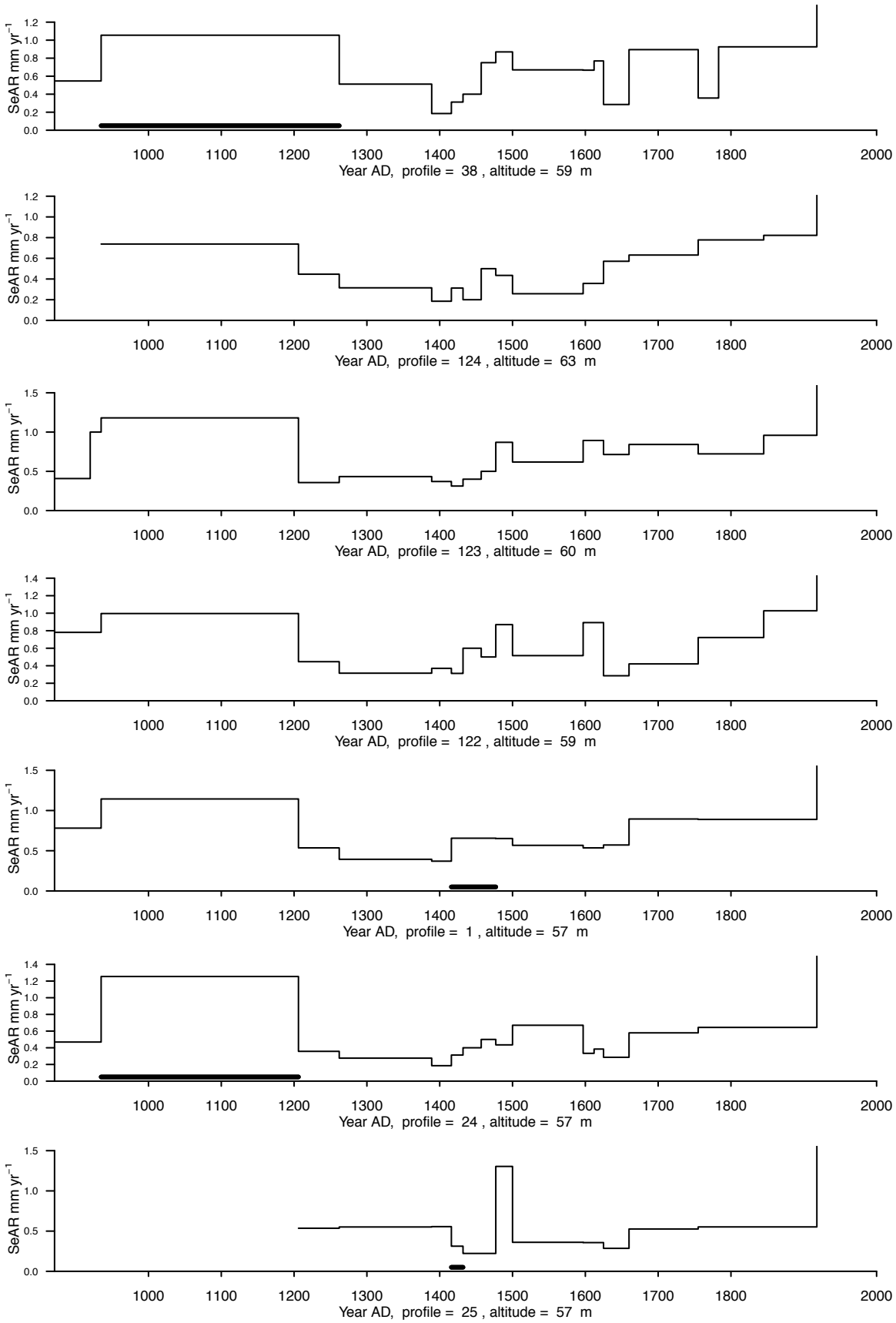

Figure D.1: Area 1 Profiles

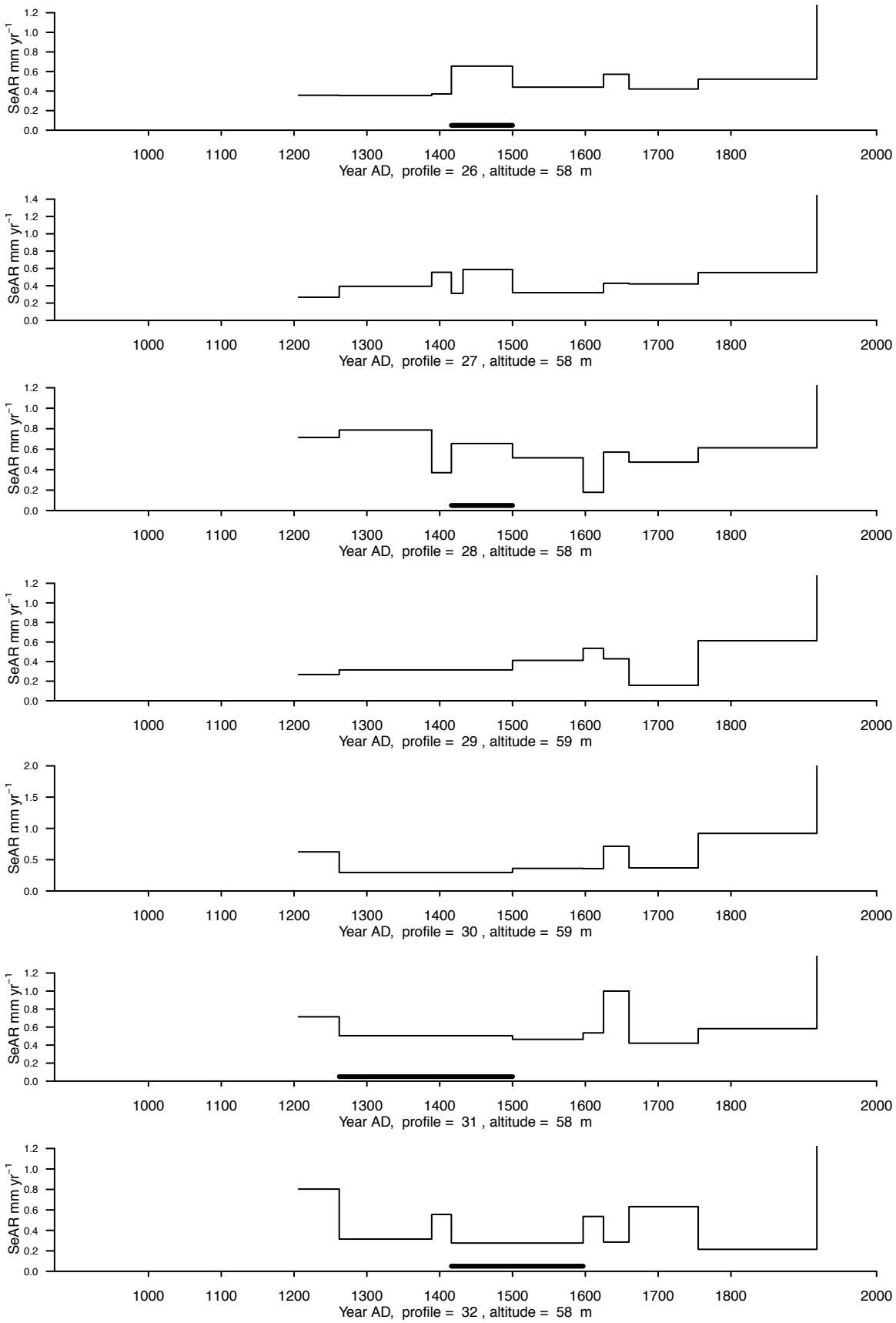

Figure D.2: Area 1 Profiles

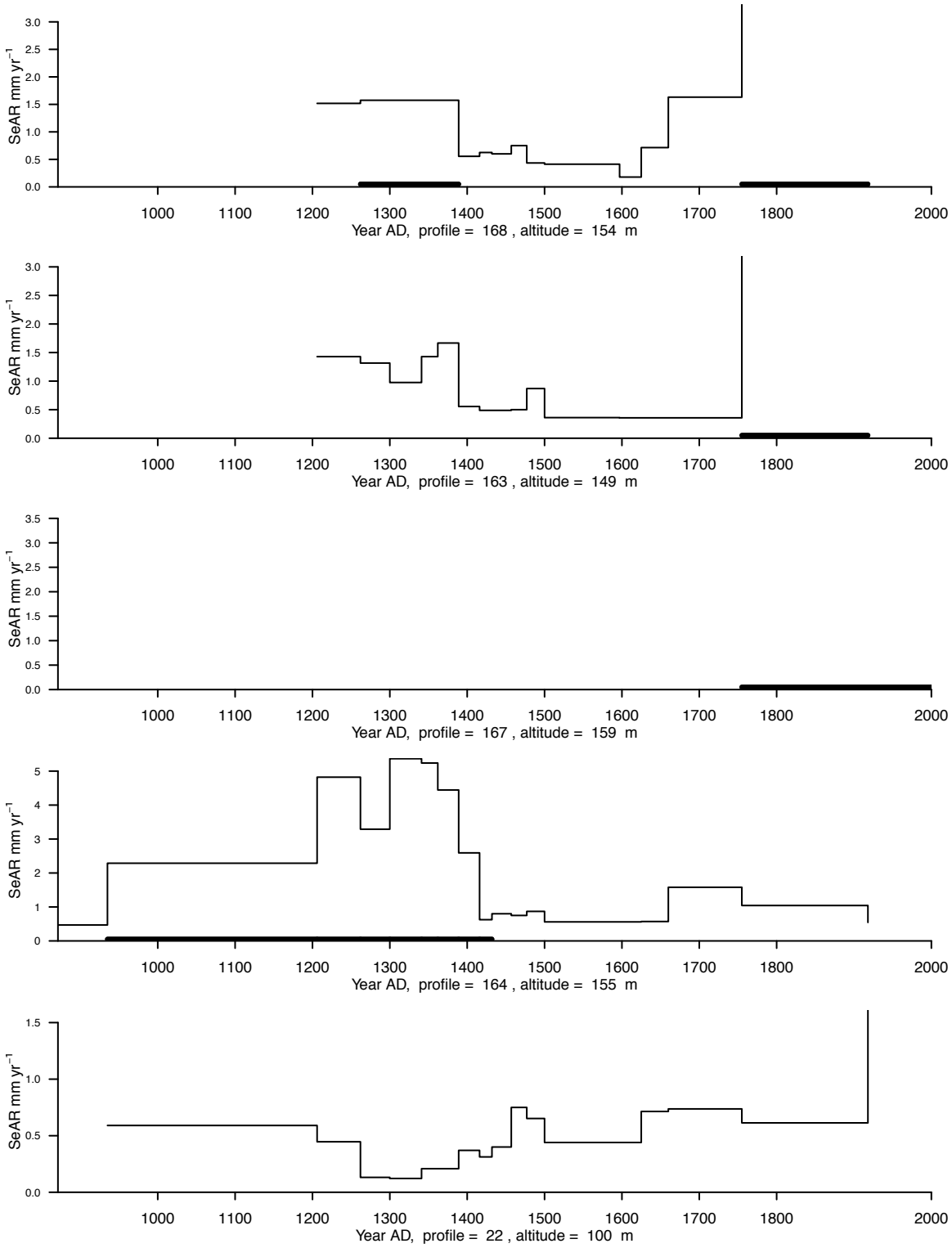

Figure D.3: Area 1 Profiles

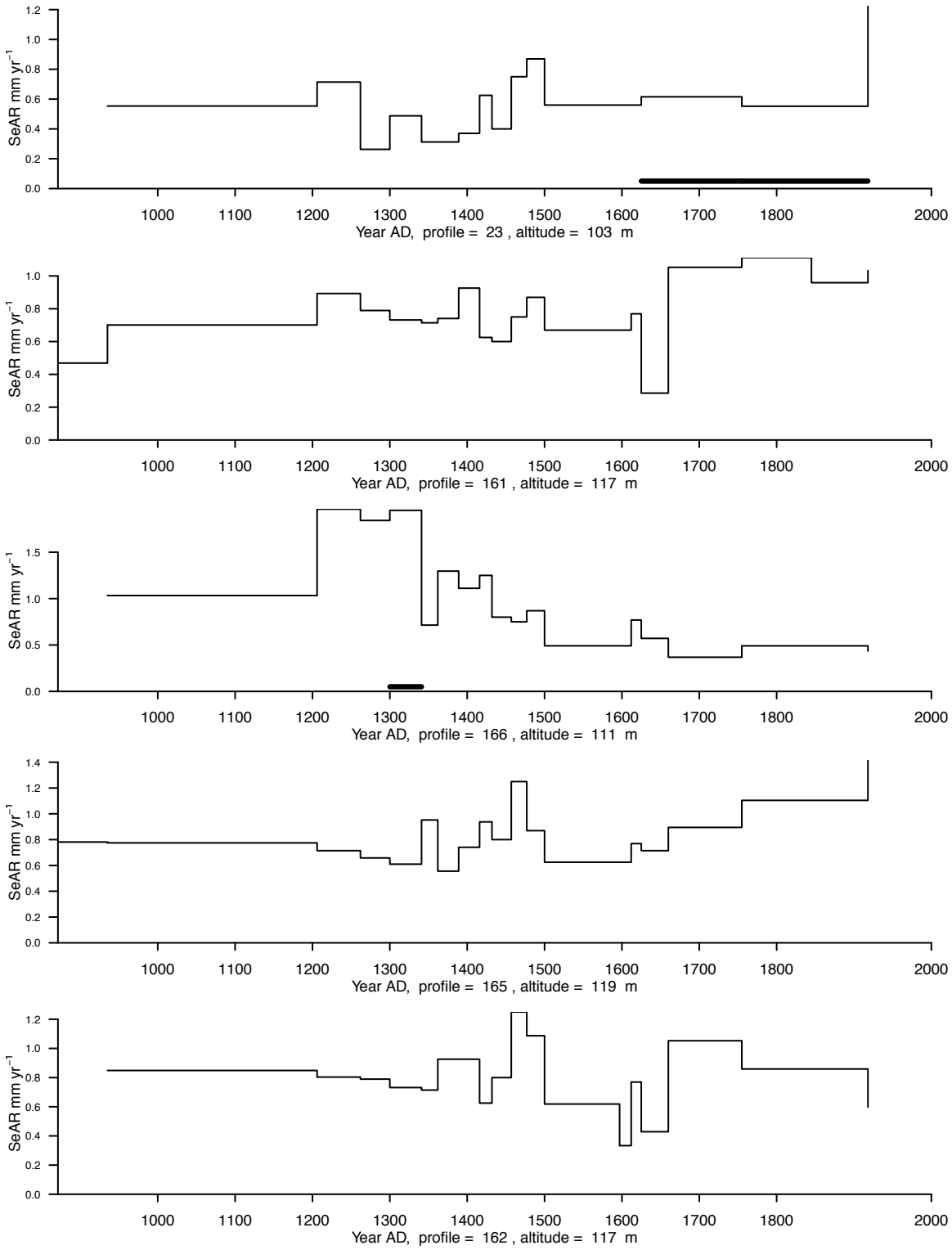

Figure D.4: Area 1 Profiles

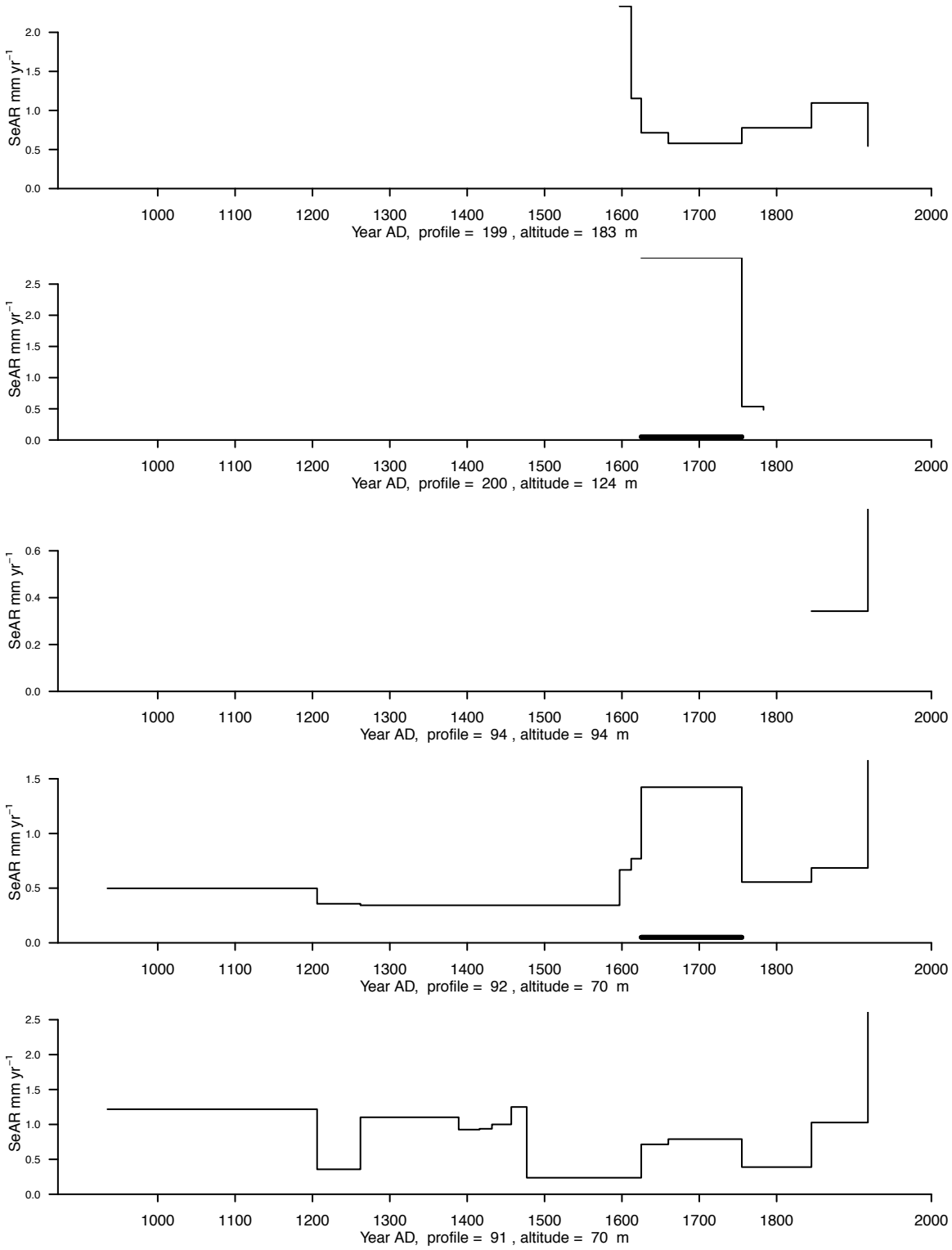

Figure D.5: Area 1 Profiles

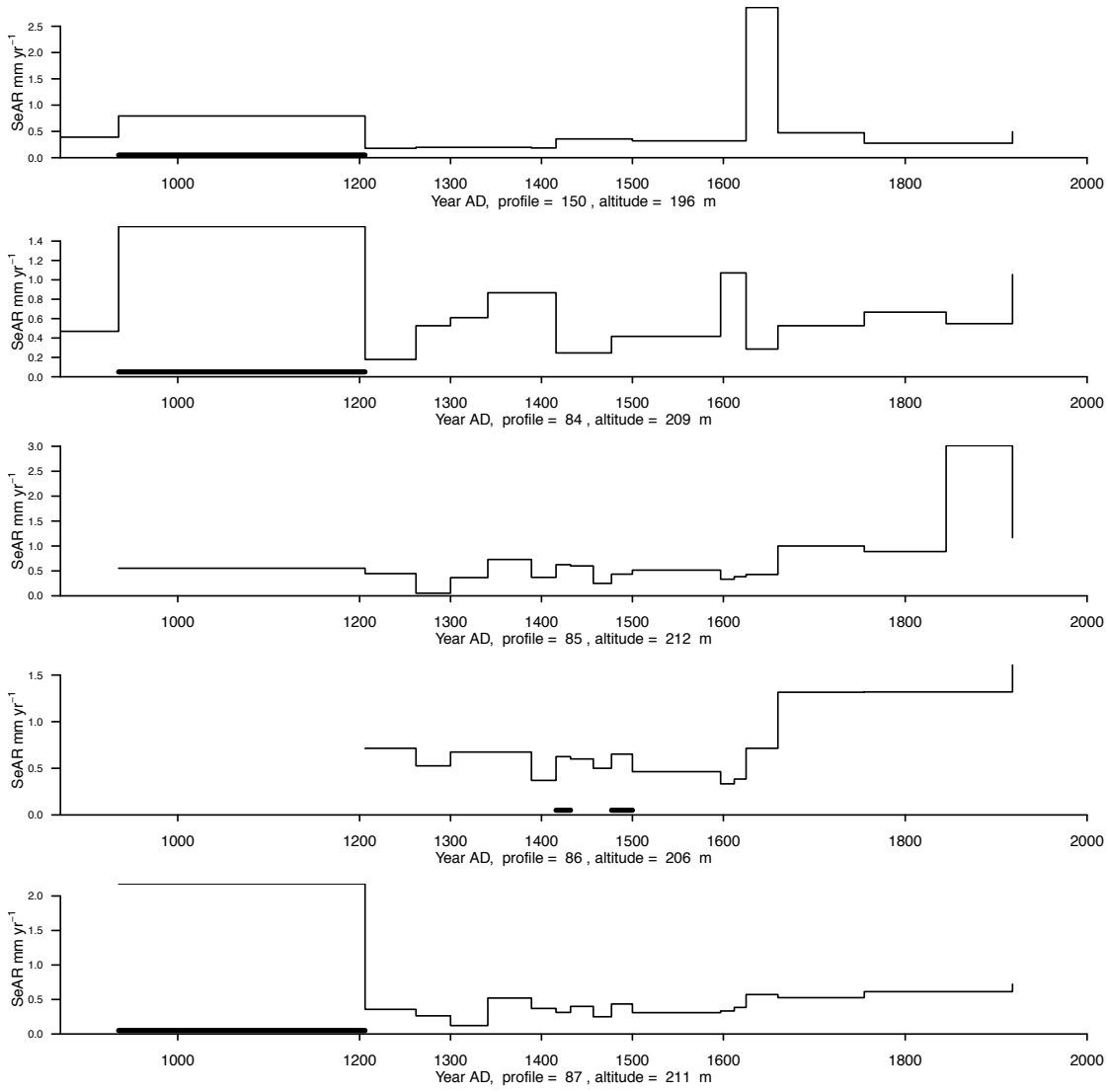

Figure D.6: Area 1 Profiles

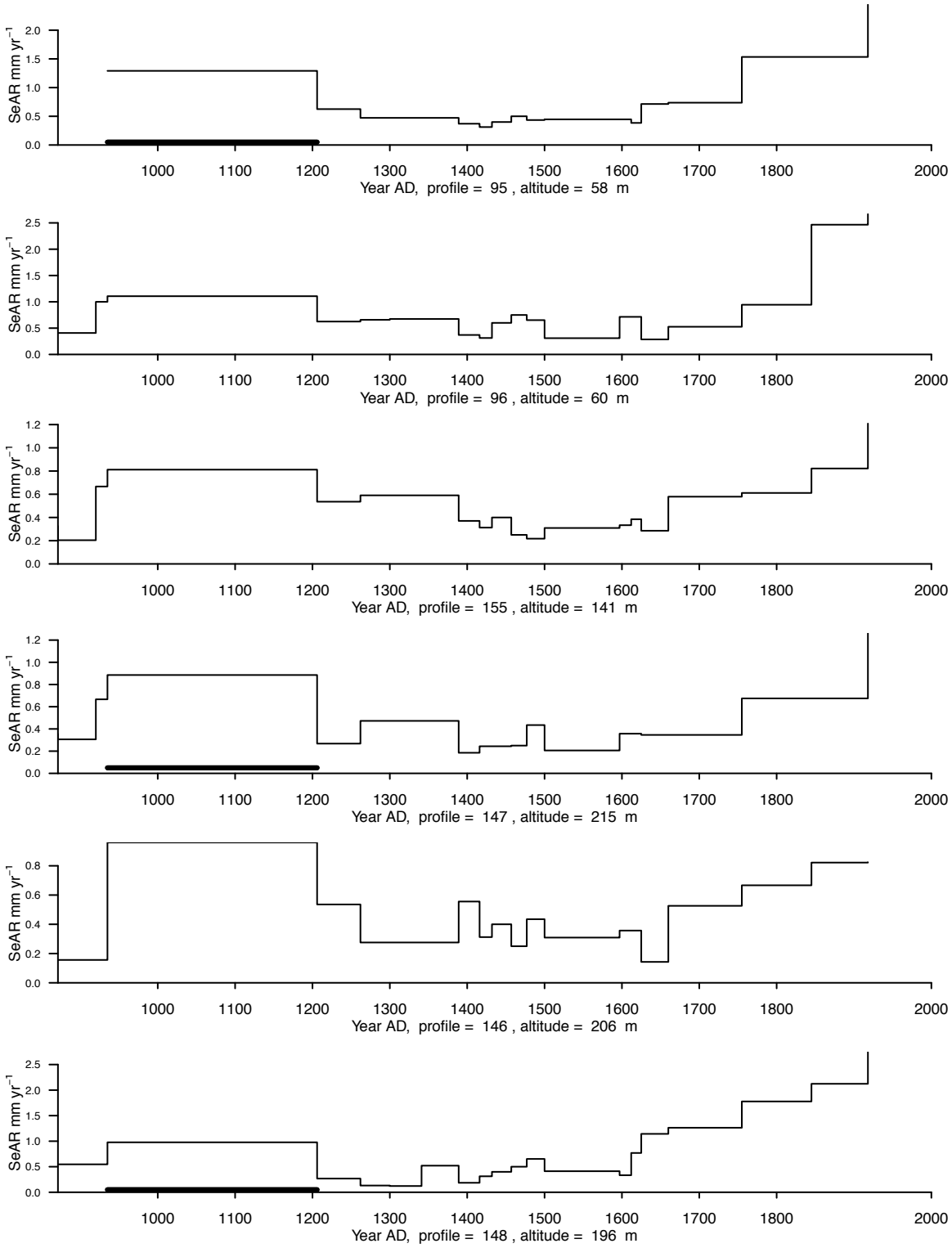

Figure D.7: Area 1 Profiles

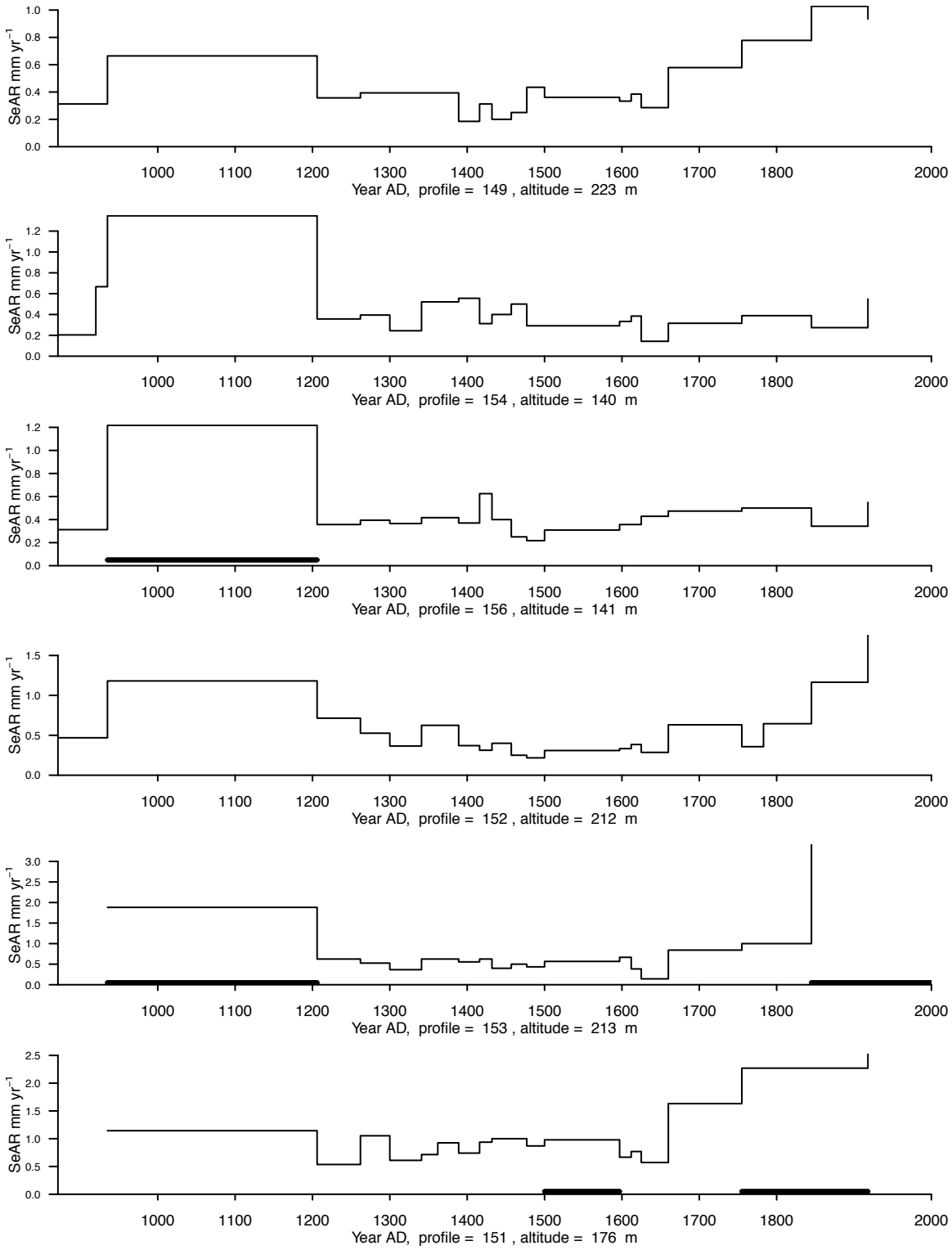

Figure D.8: Area 1 Profiles

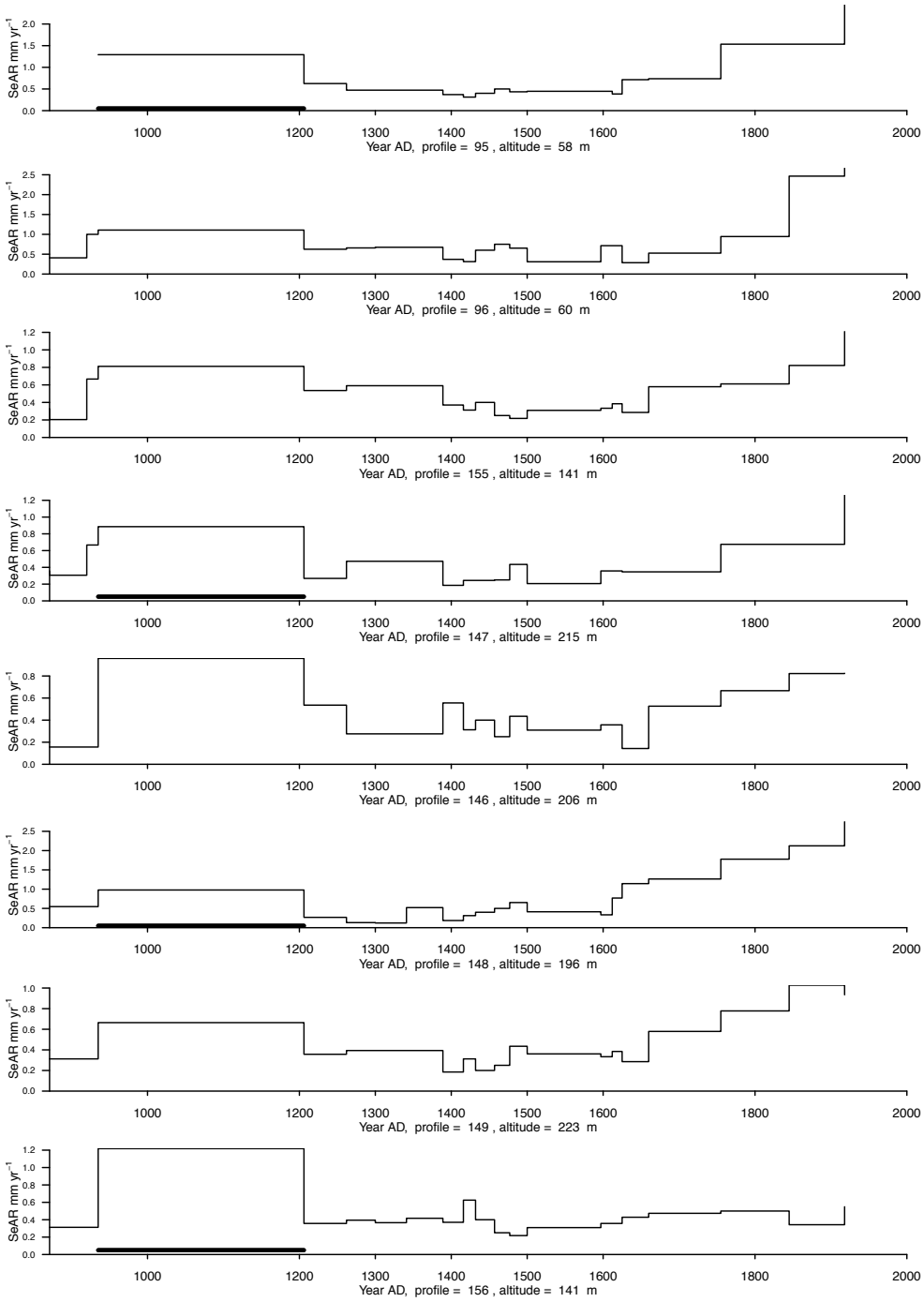

Figure D.9: Area 1 Profiles

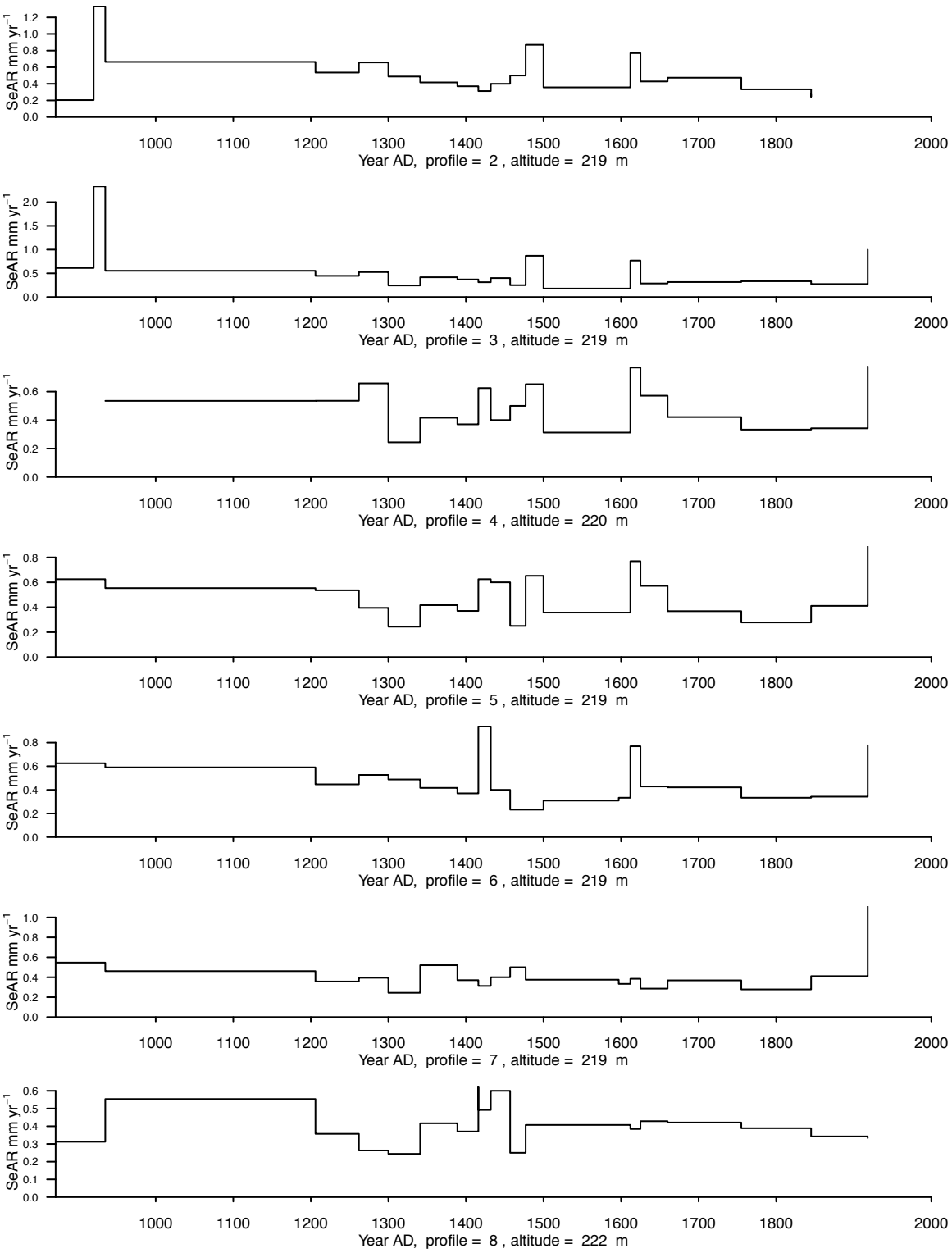

Figure D.10: Area 2 Profiles

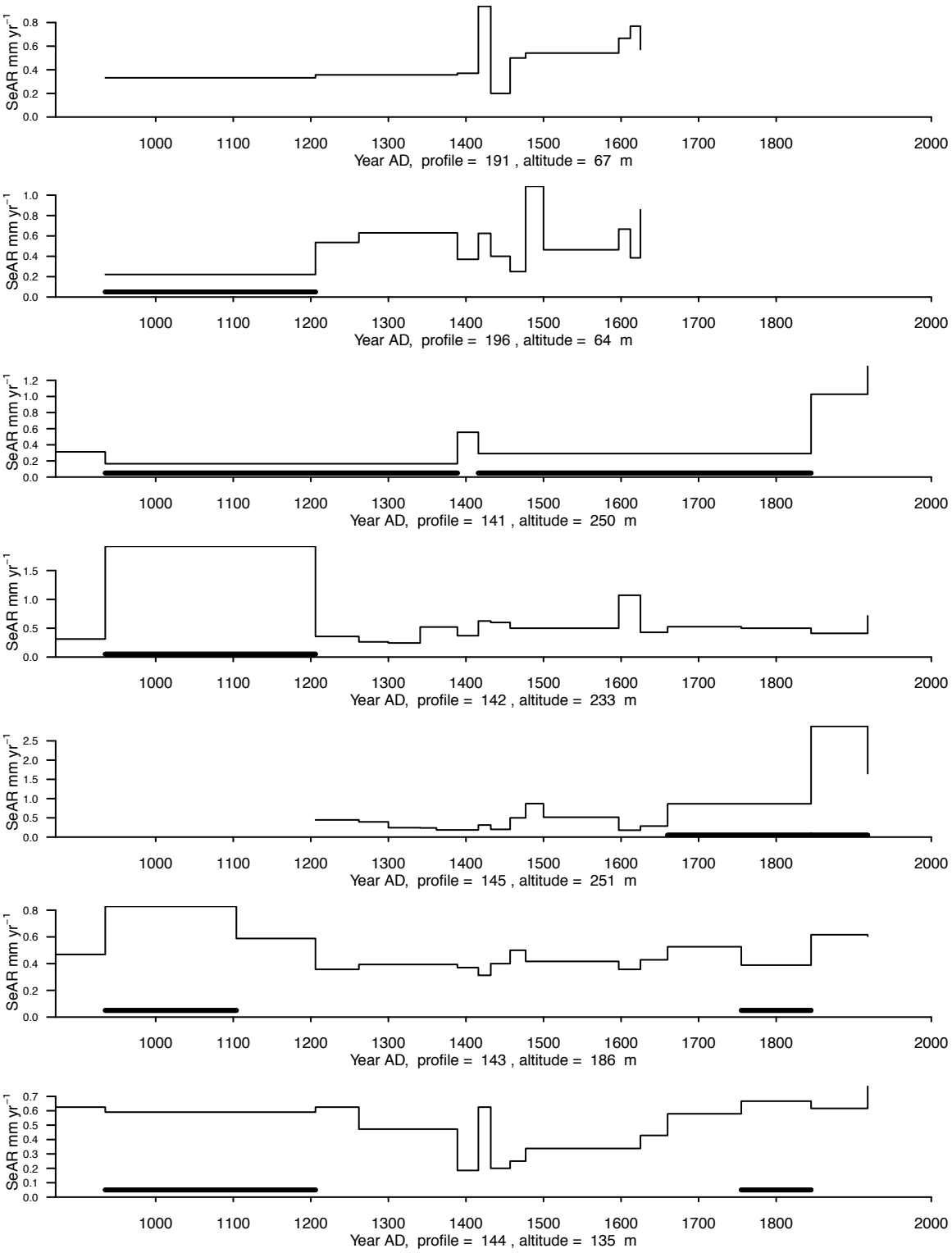

Figure D.11: Area 2 Profiles

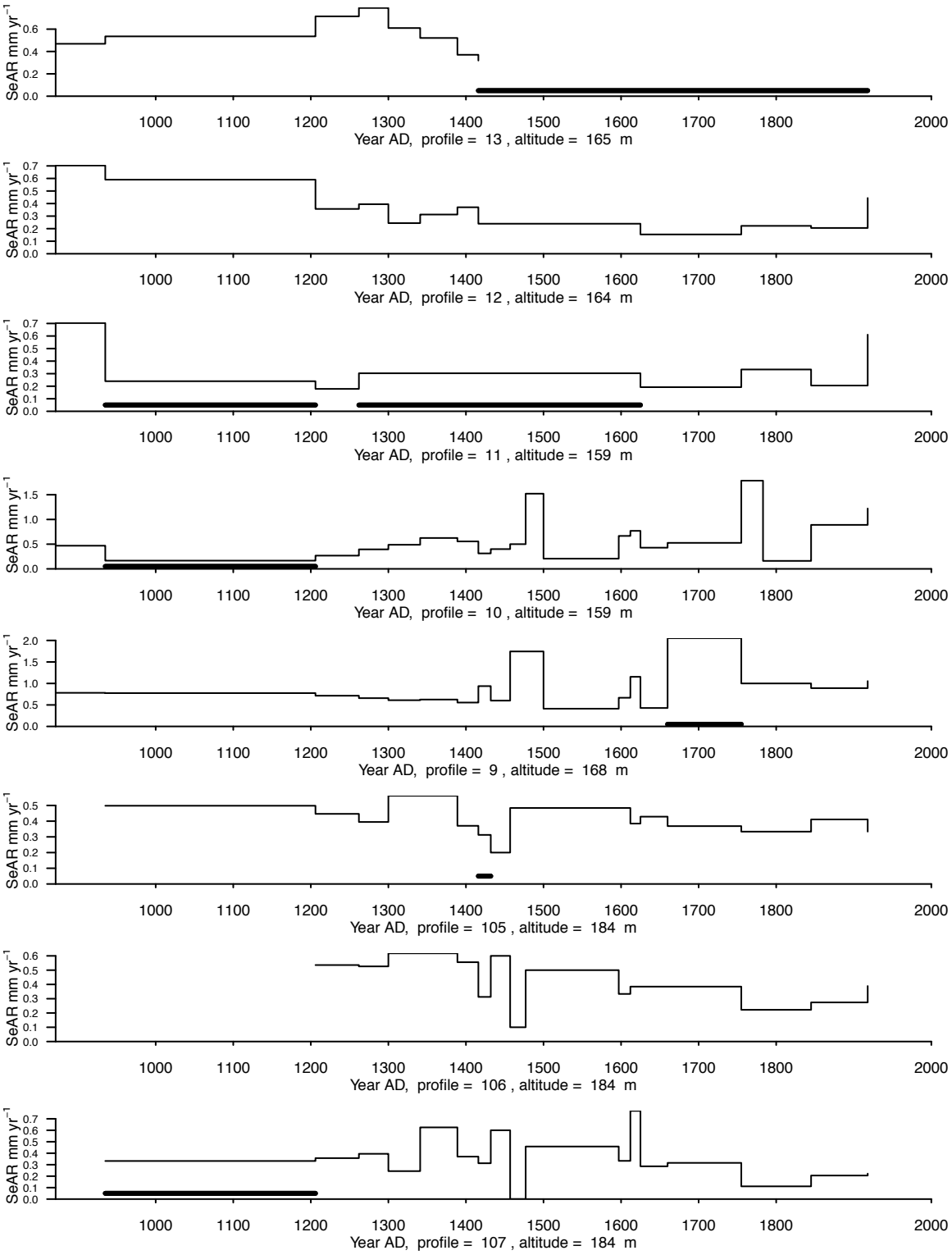

Figure D.12: Area 2 Profiles

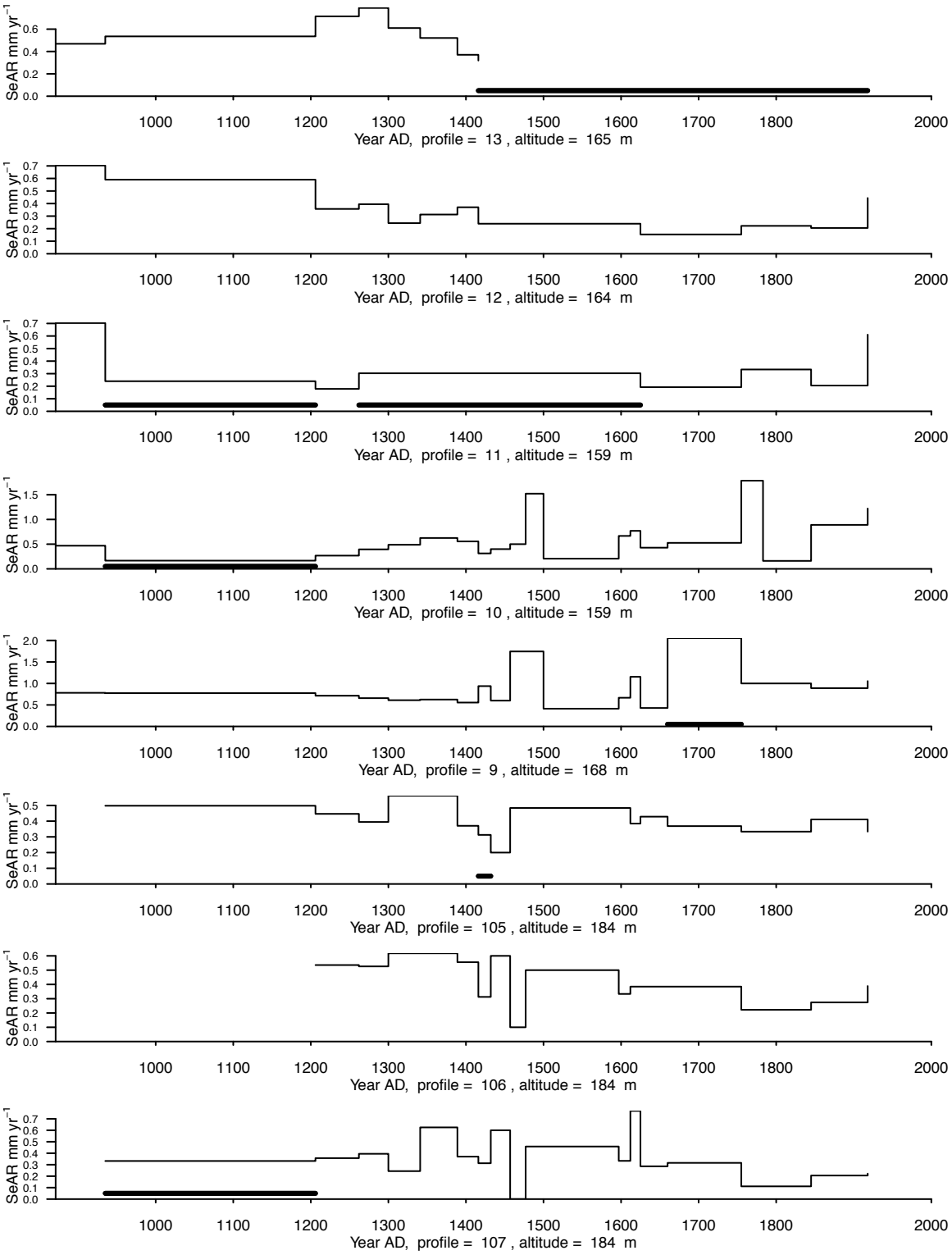

Figure D.13: Area 2 Profiles

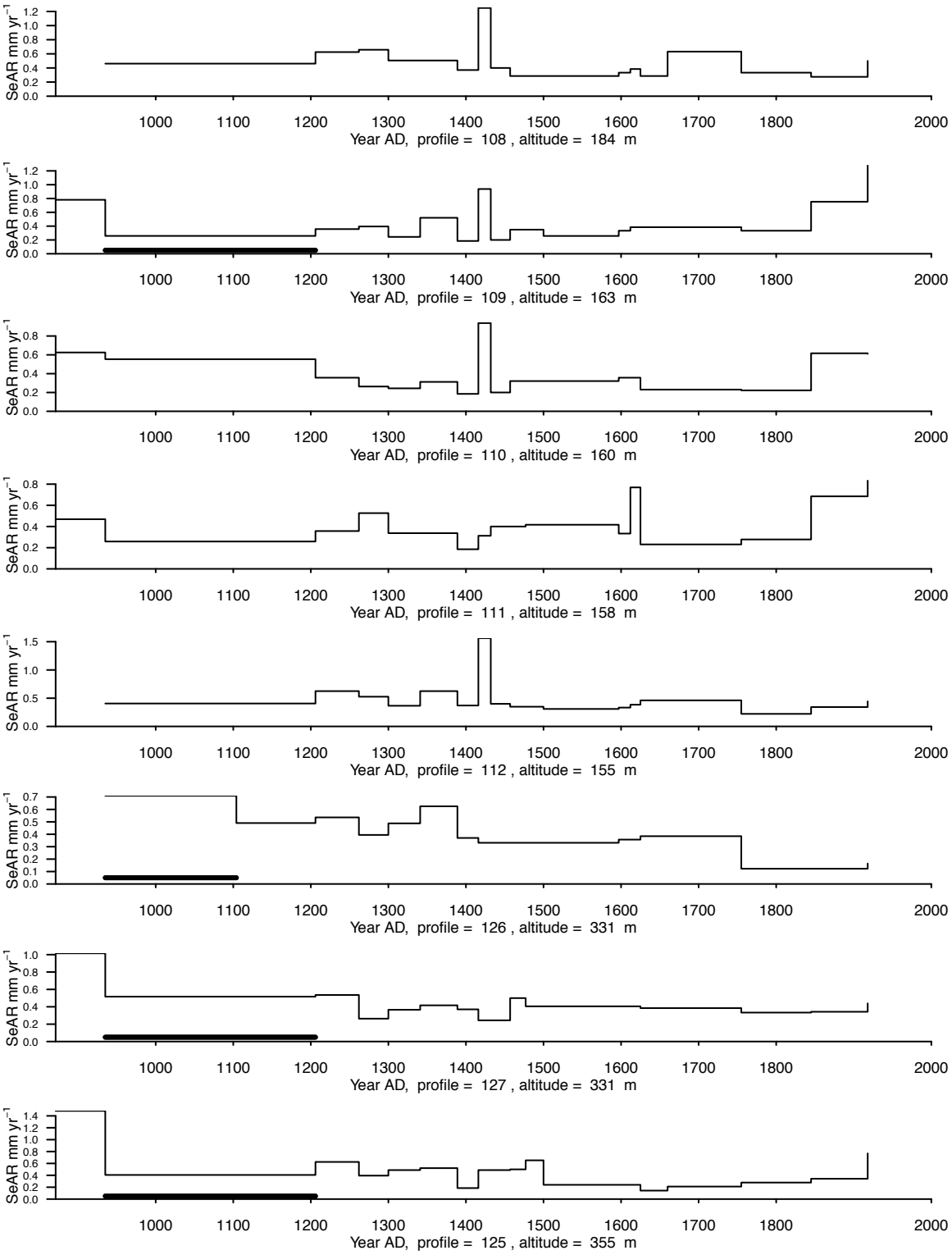

Figure D.14: Area 2 Profiles

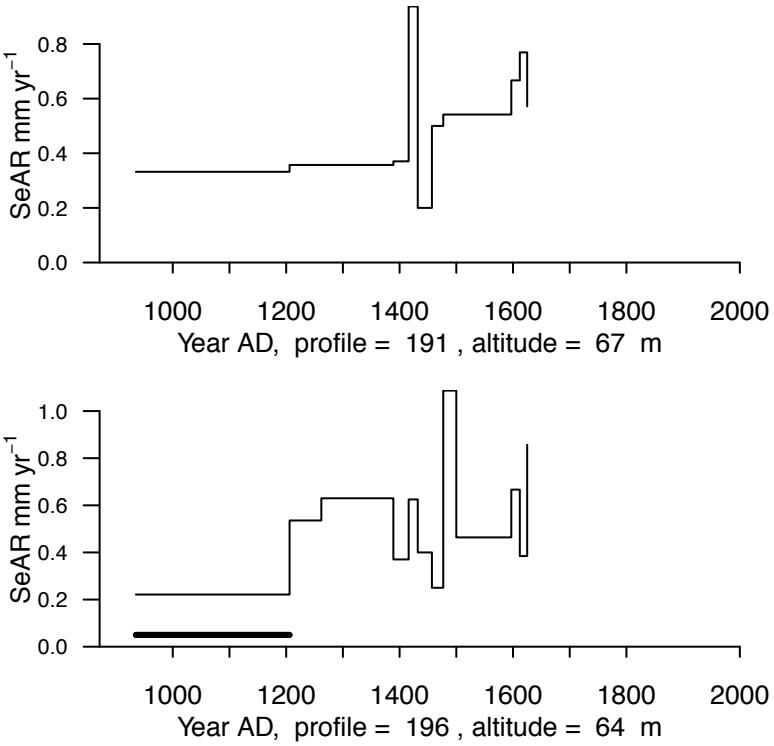

Figure D.15: Area 2 Profiles

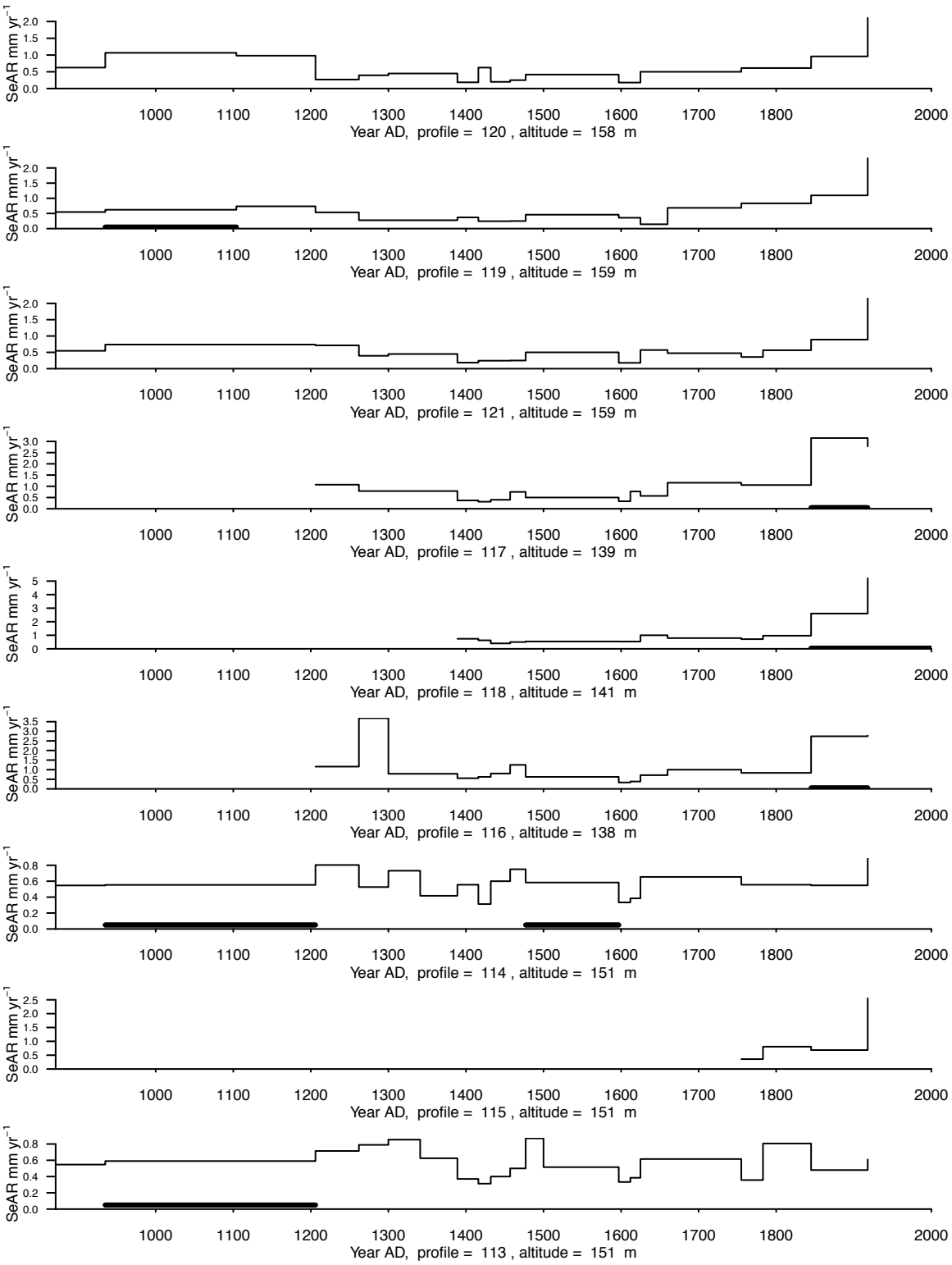

Figure D.16: Area 3 Profiles

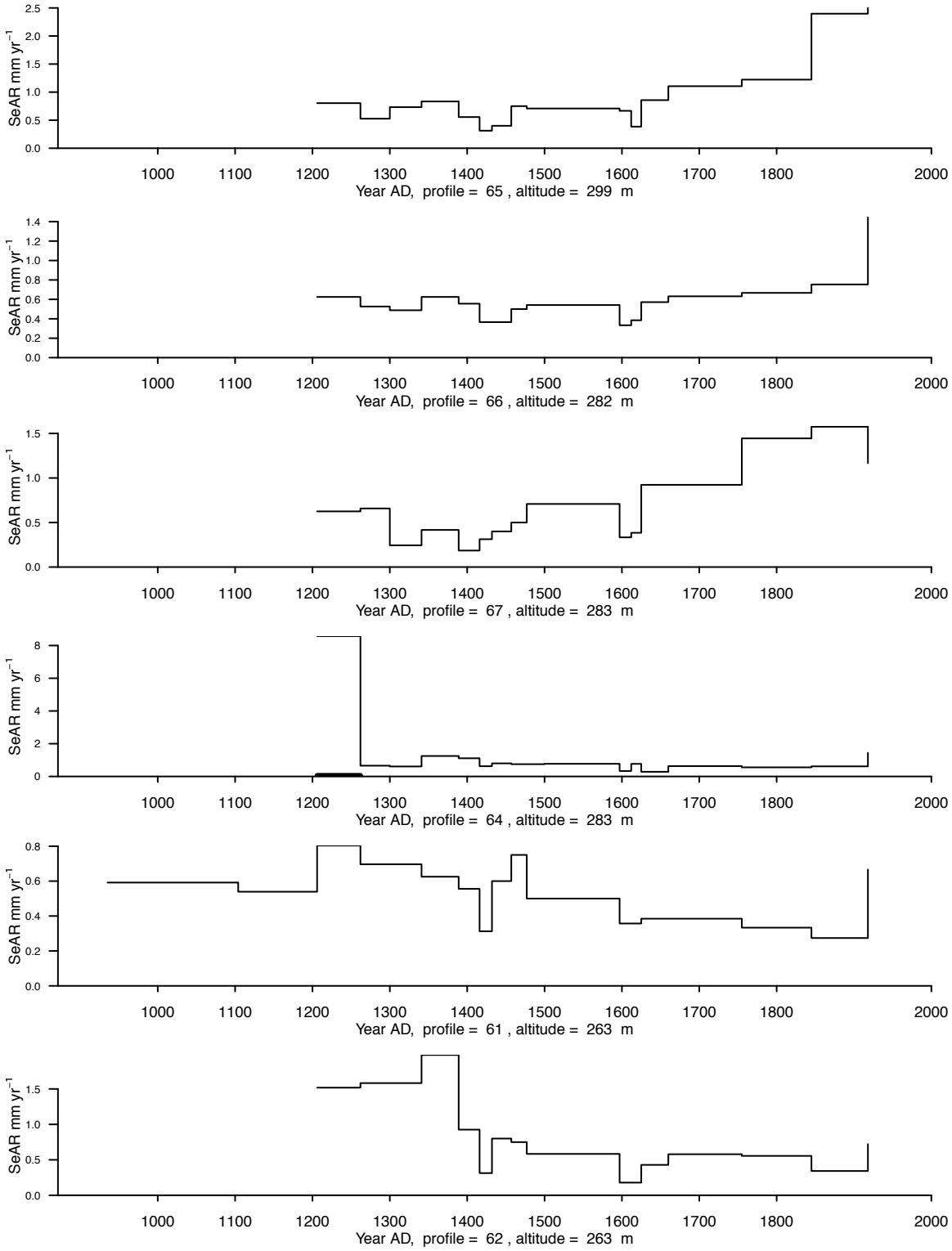

Figure D.17: Area 3 Profiles

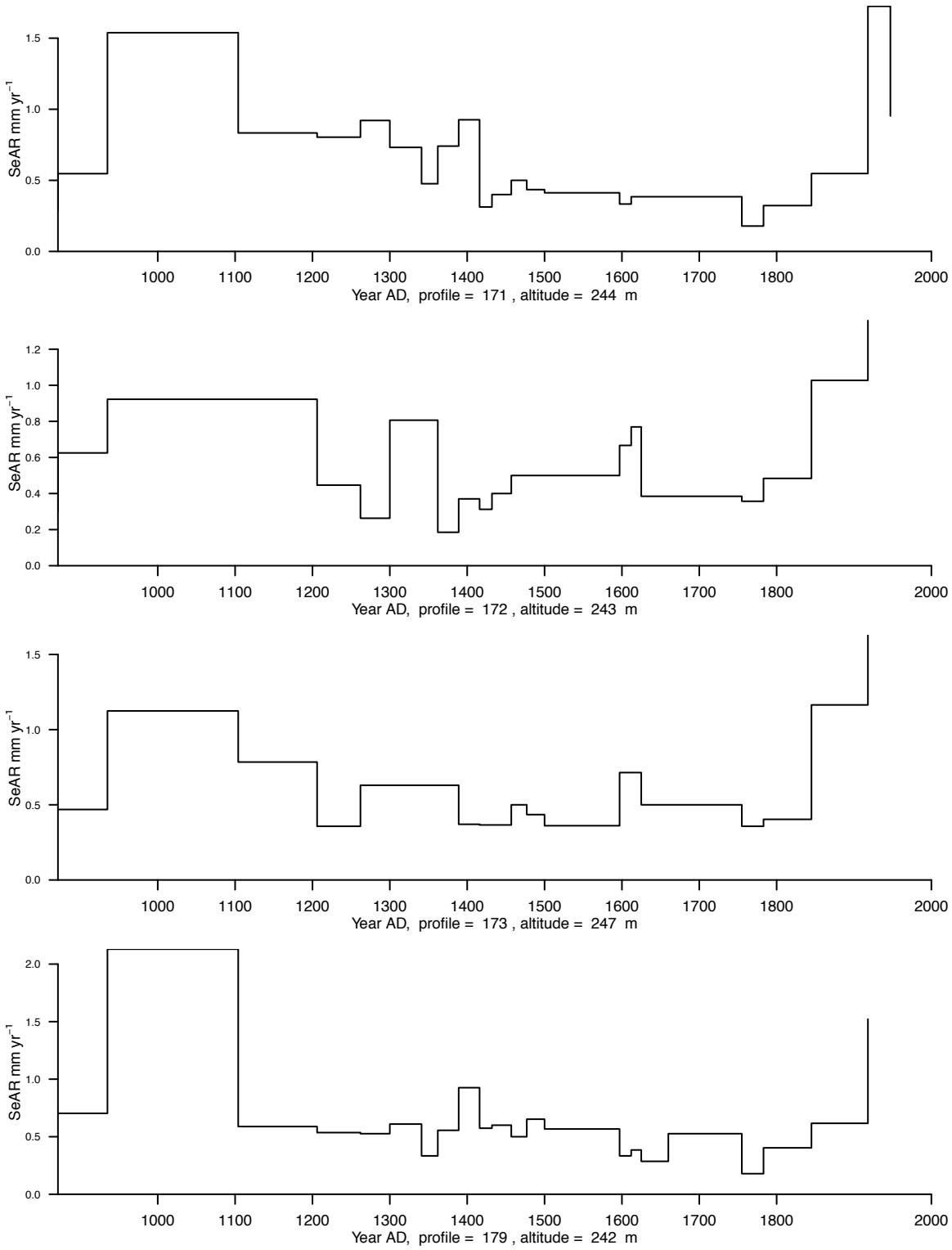

Figure D.18: Area 3 Profiles

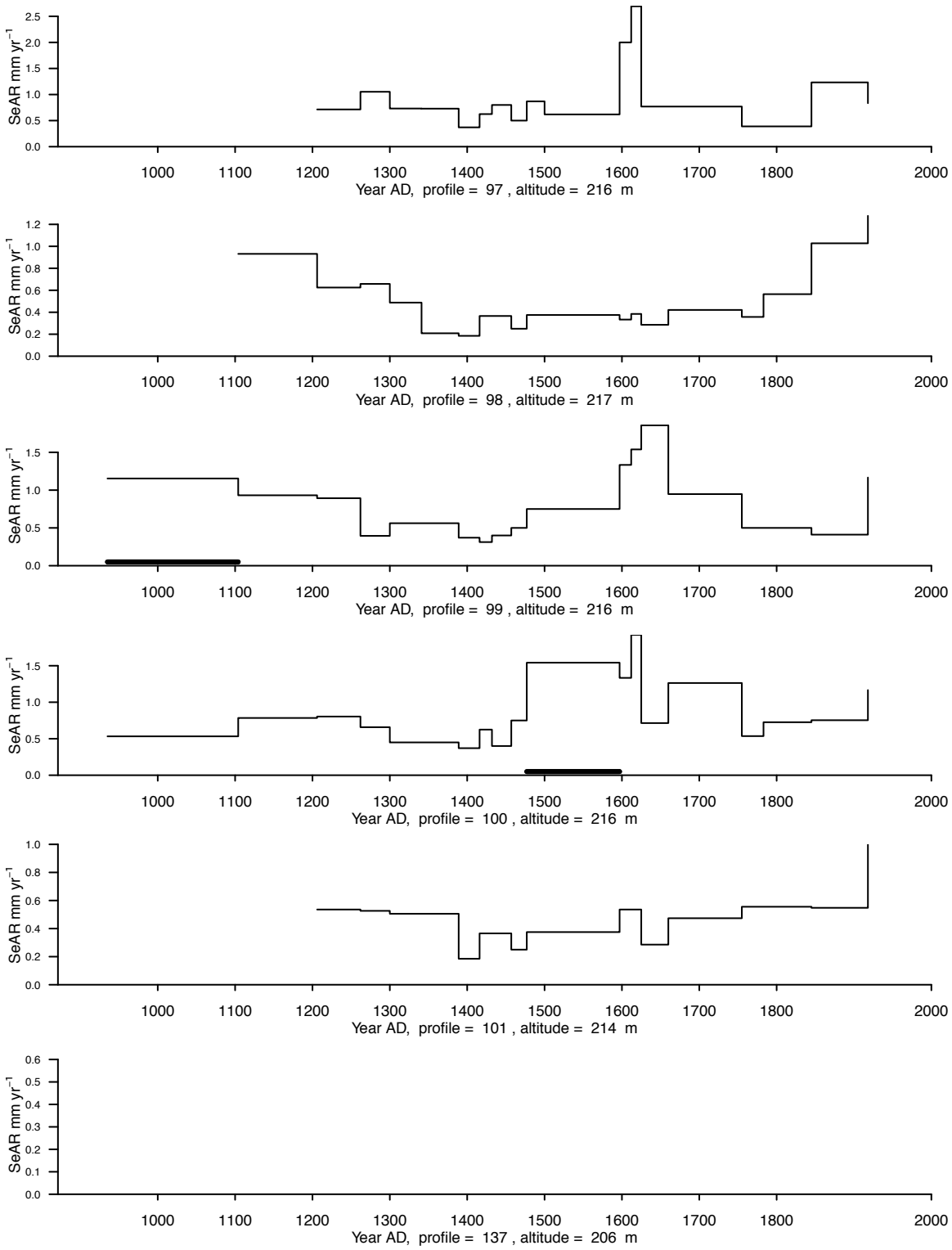

Figure D.19: Area 3 Profiles

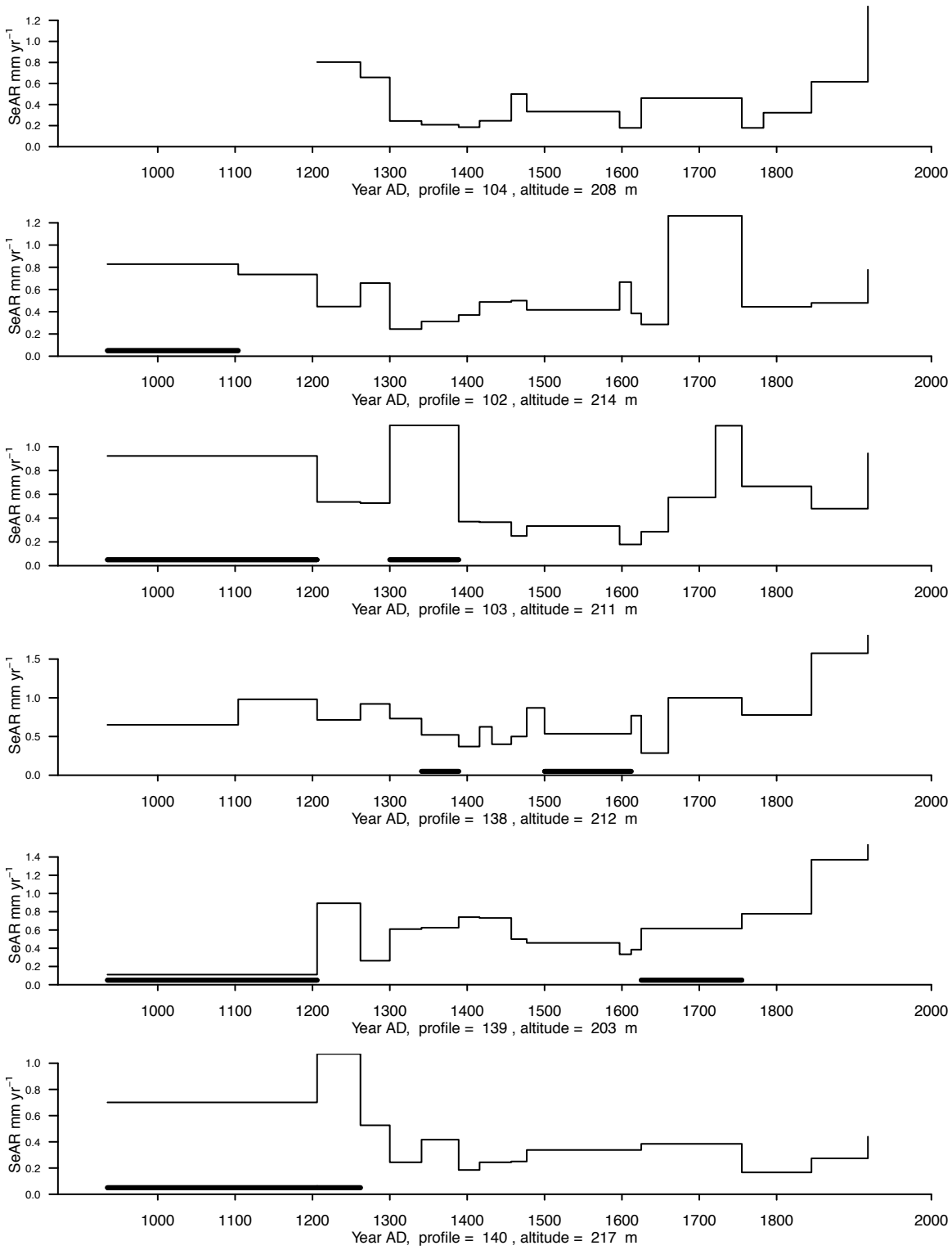

Figure D.20: Area 3 Profiles

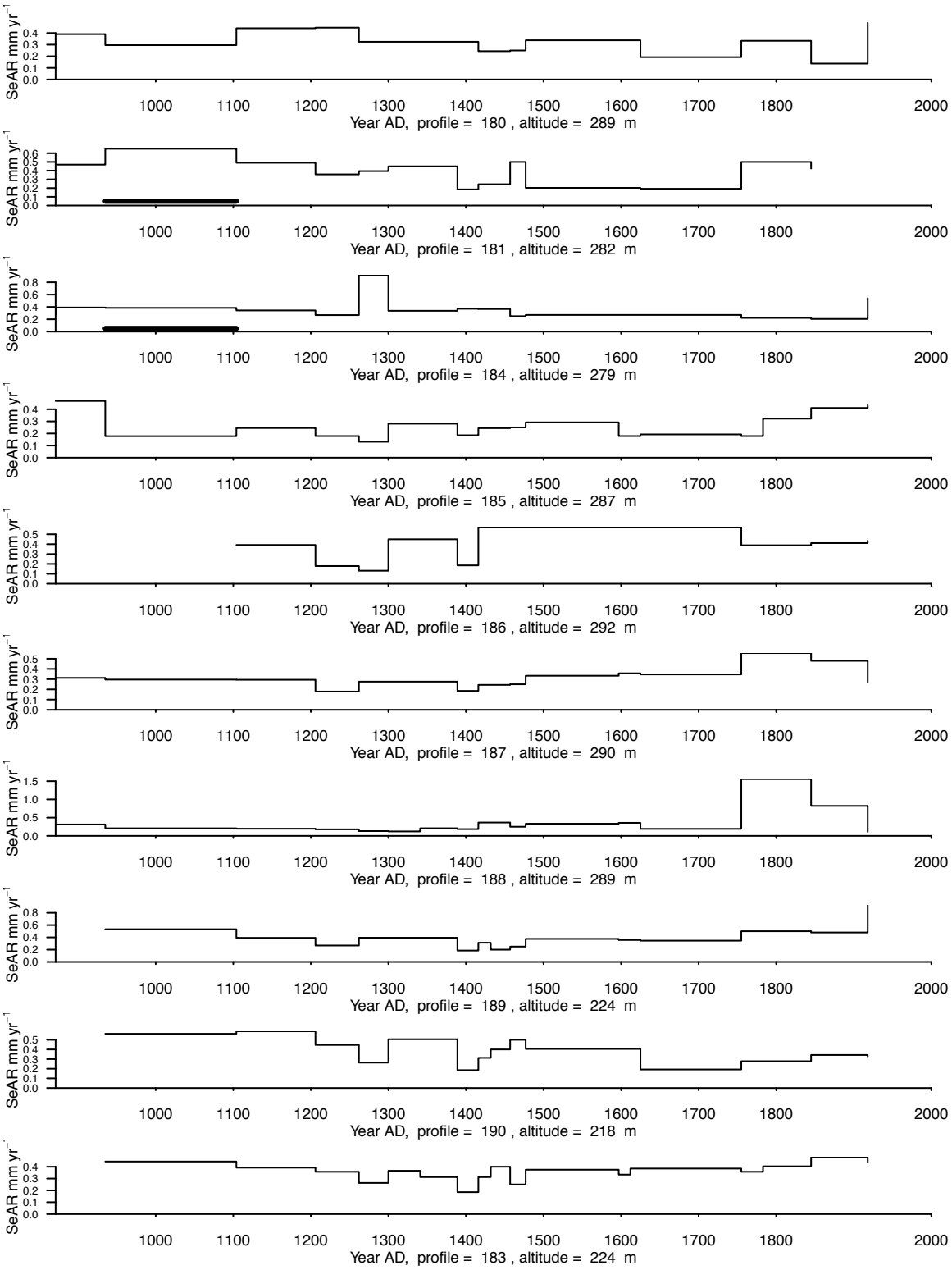

Figure D.21: Area 3 Profiles

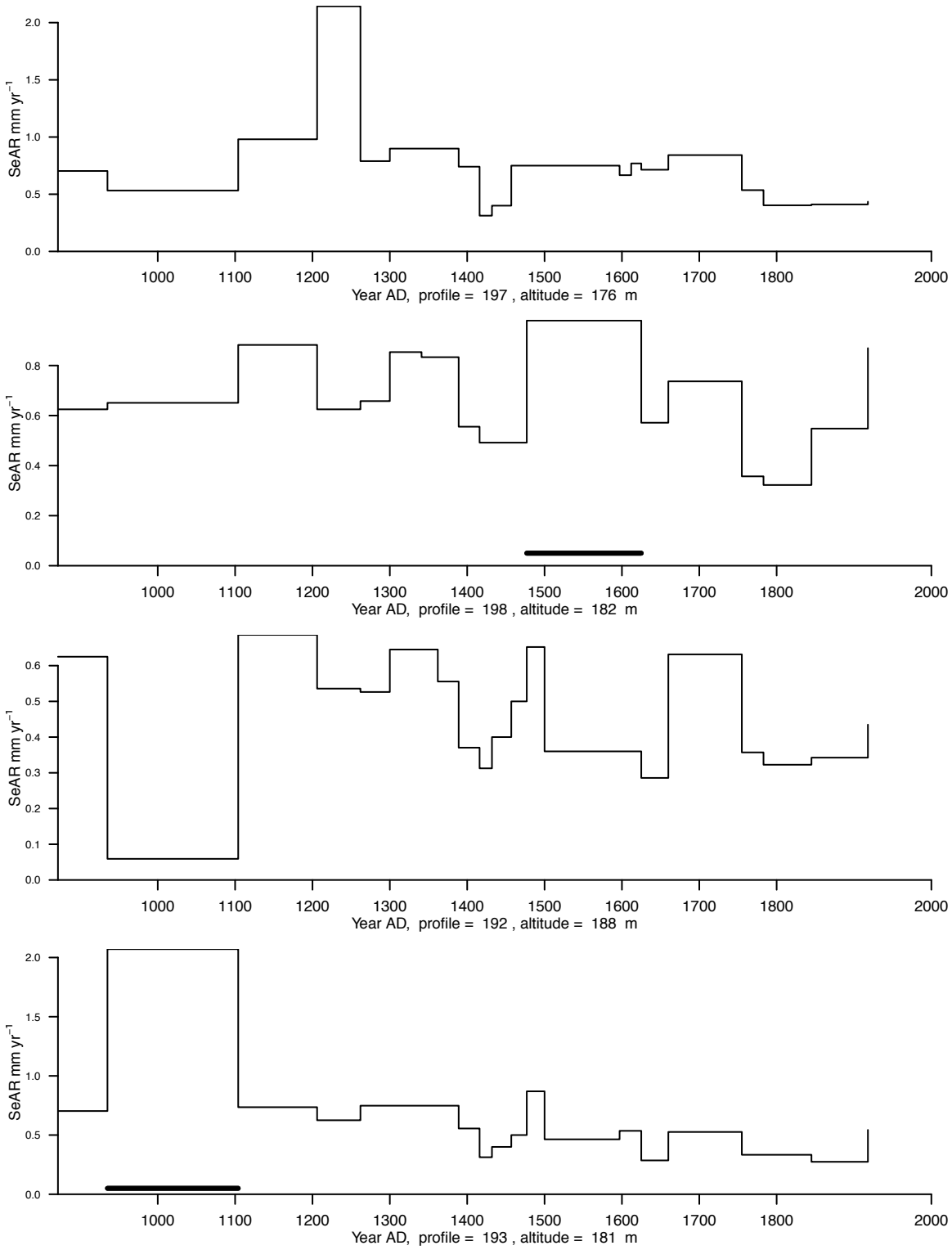

Figure D.22: Area 3 Profiles

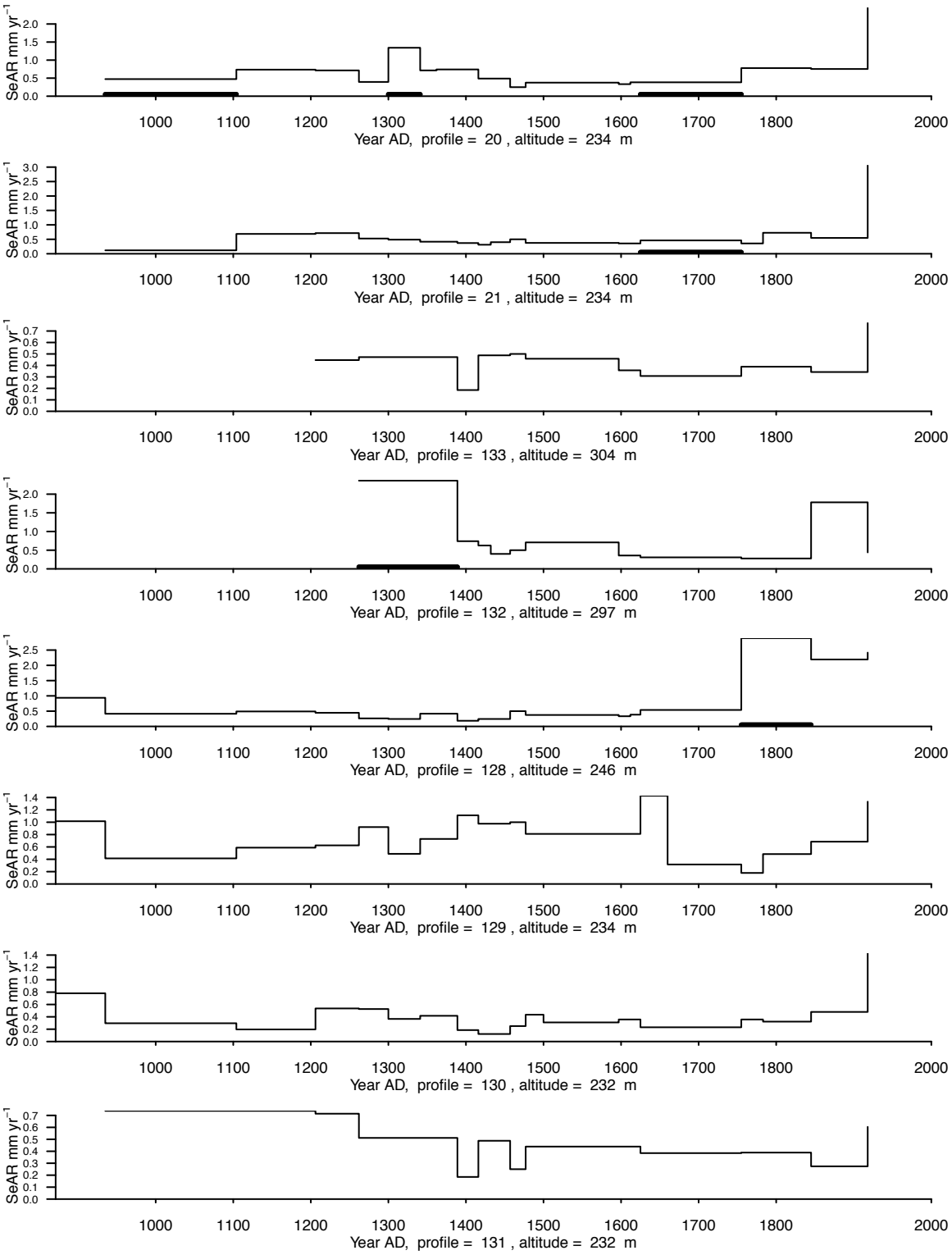

Figure D.23: Area 3 Profiles

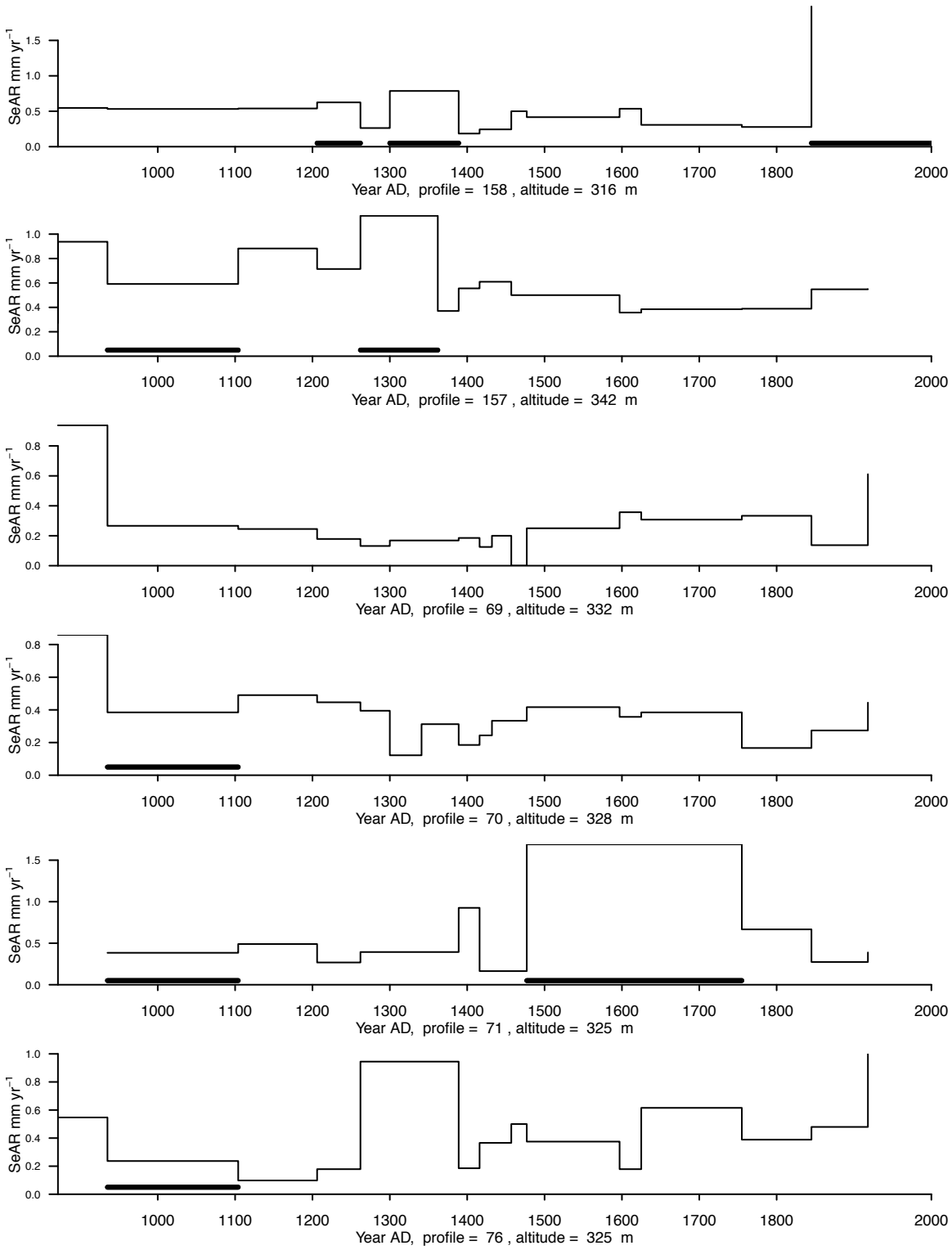

Figure D.24: Area 4 Profiles

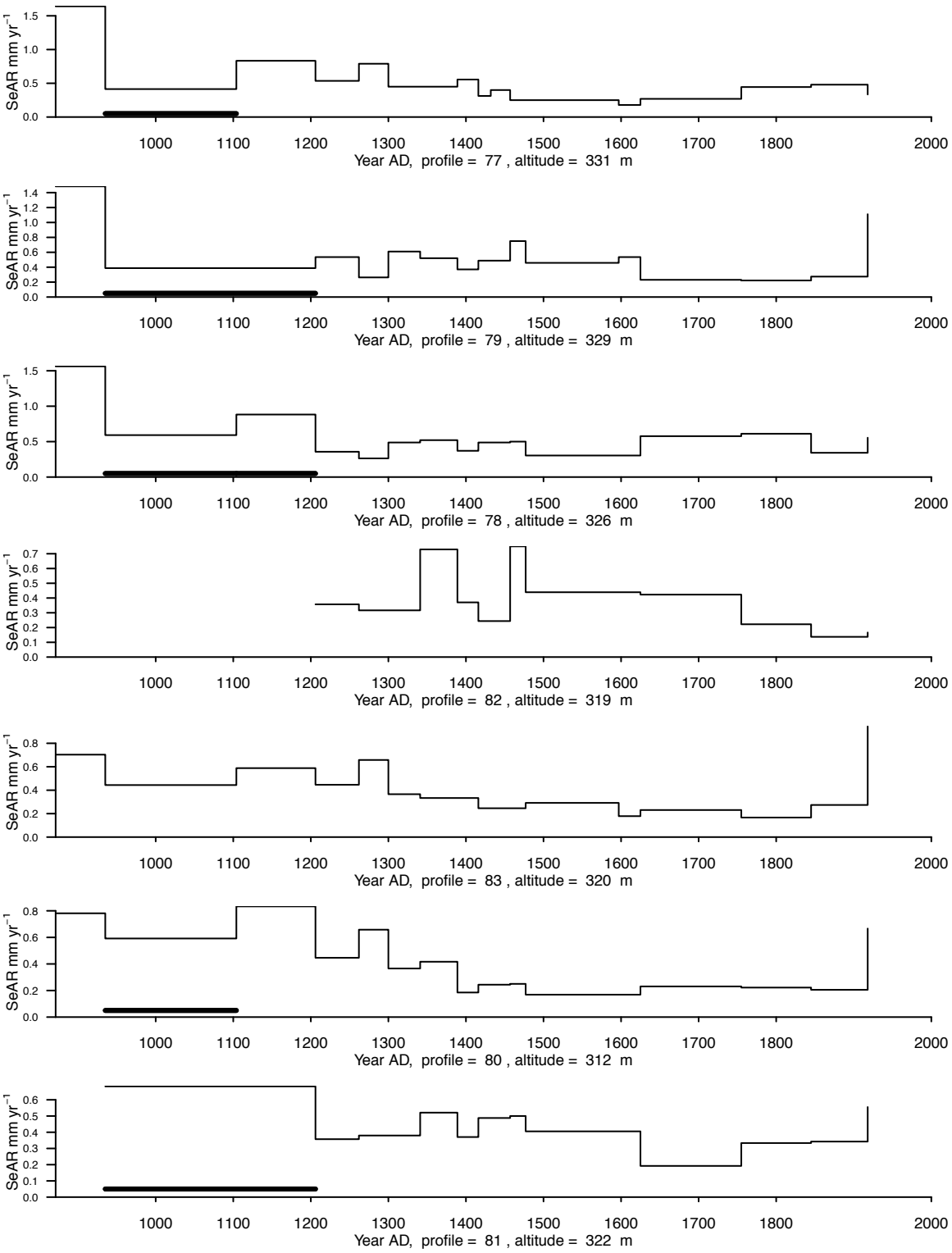

Figure D.25: Area 4 Profiles

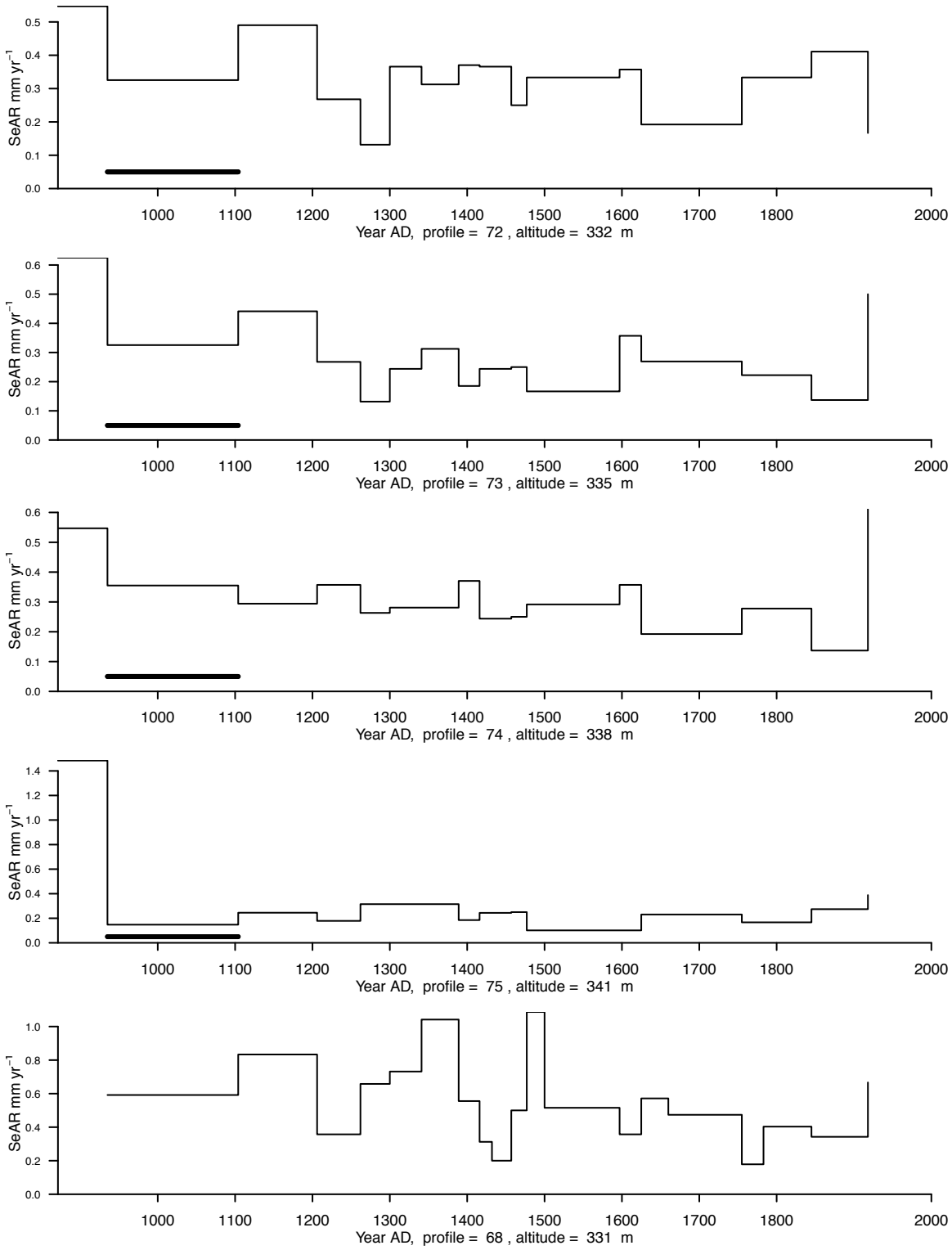

Figure D.26: Area 4 Profiles

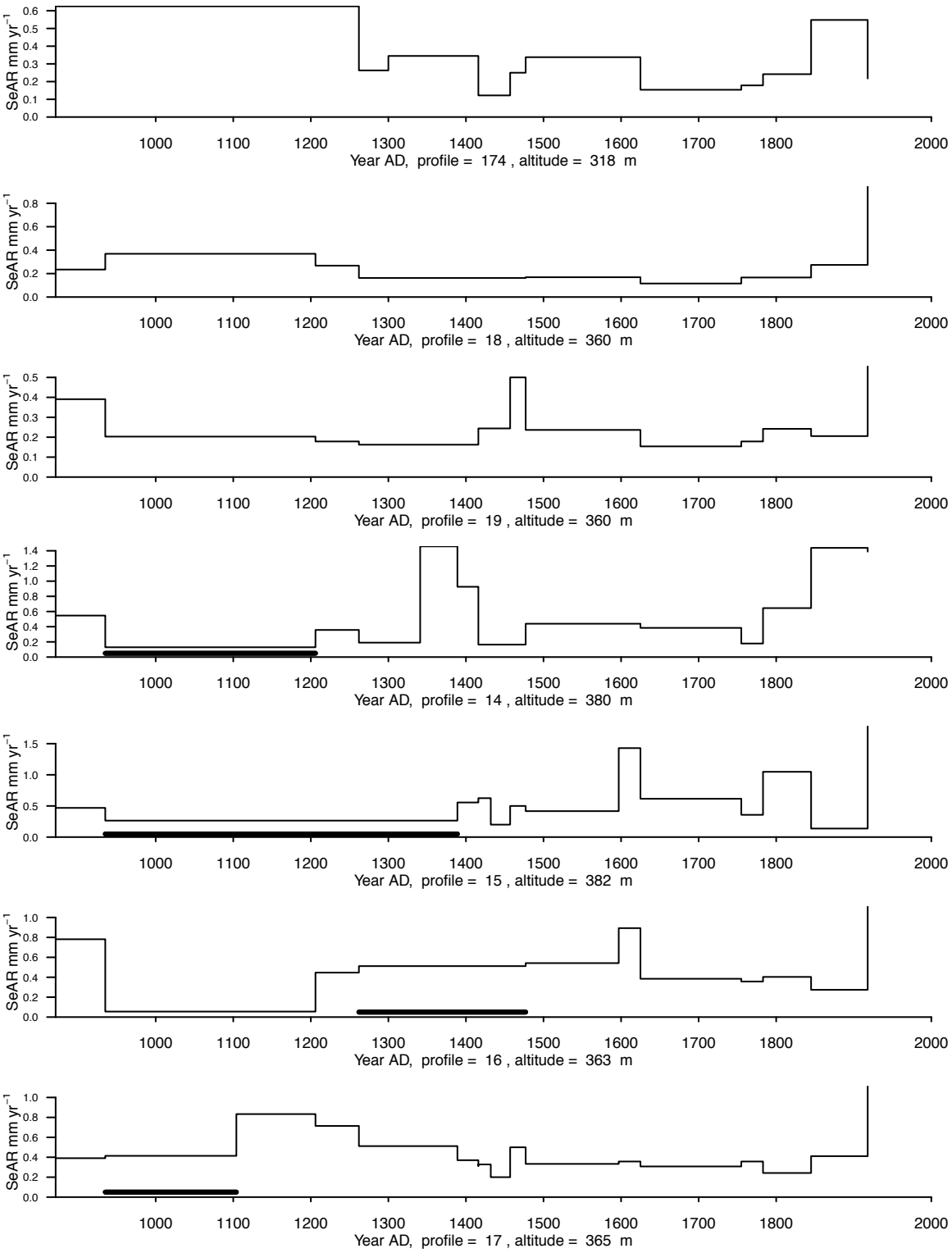

Figure D.27: Area 4 Profiles

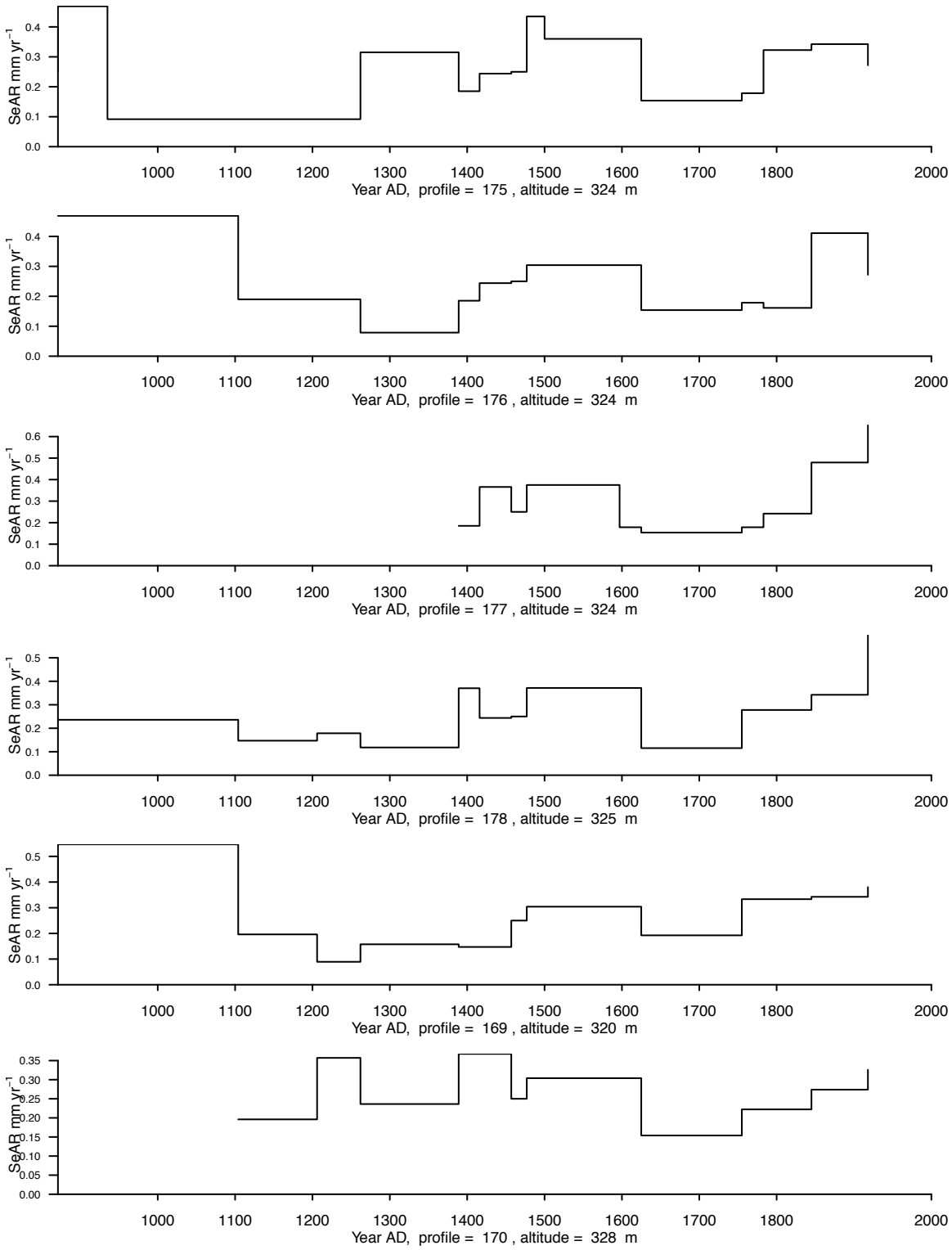

Figure D.28: Area 4 Profiles

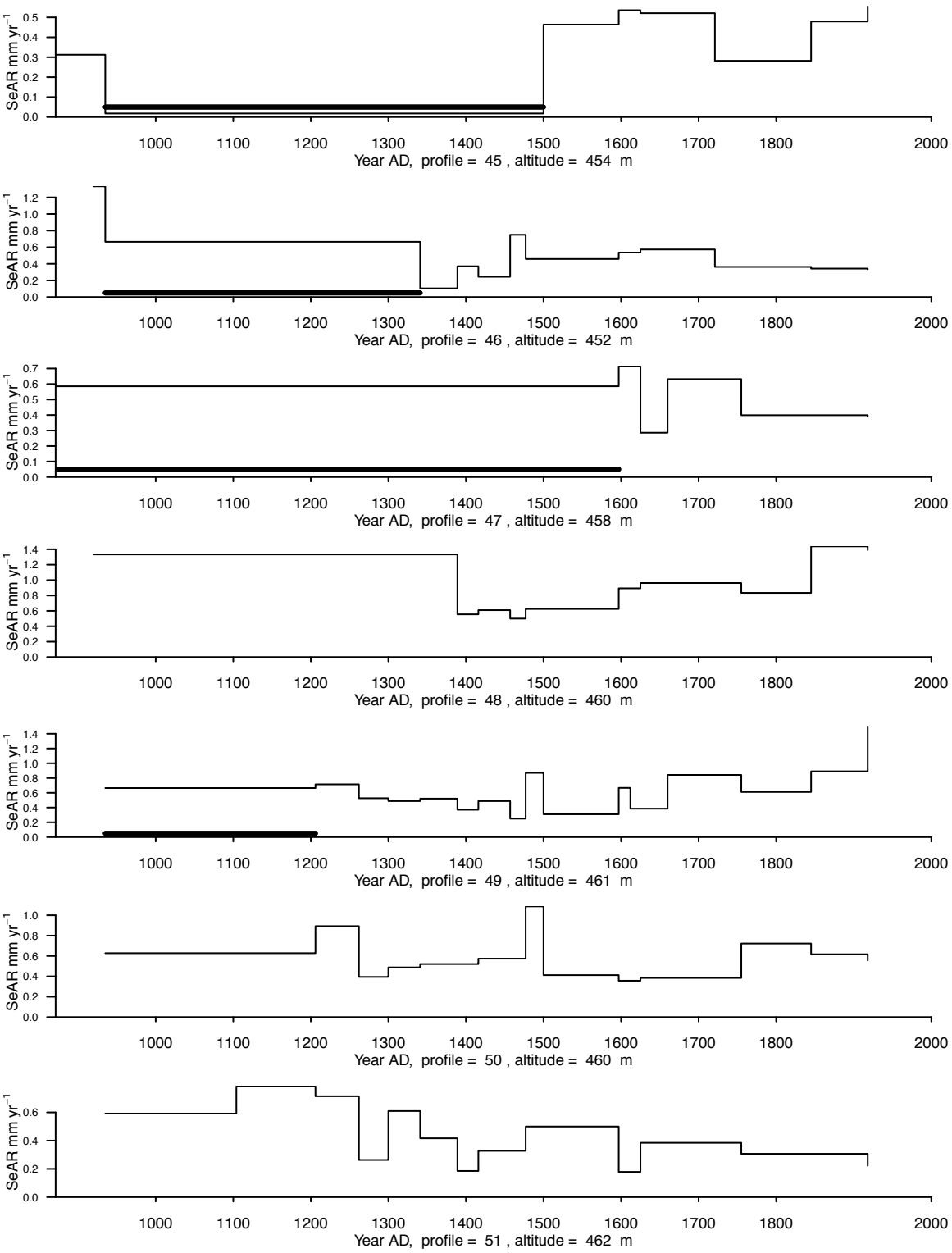

Figure D.29: Area 4 Profiles

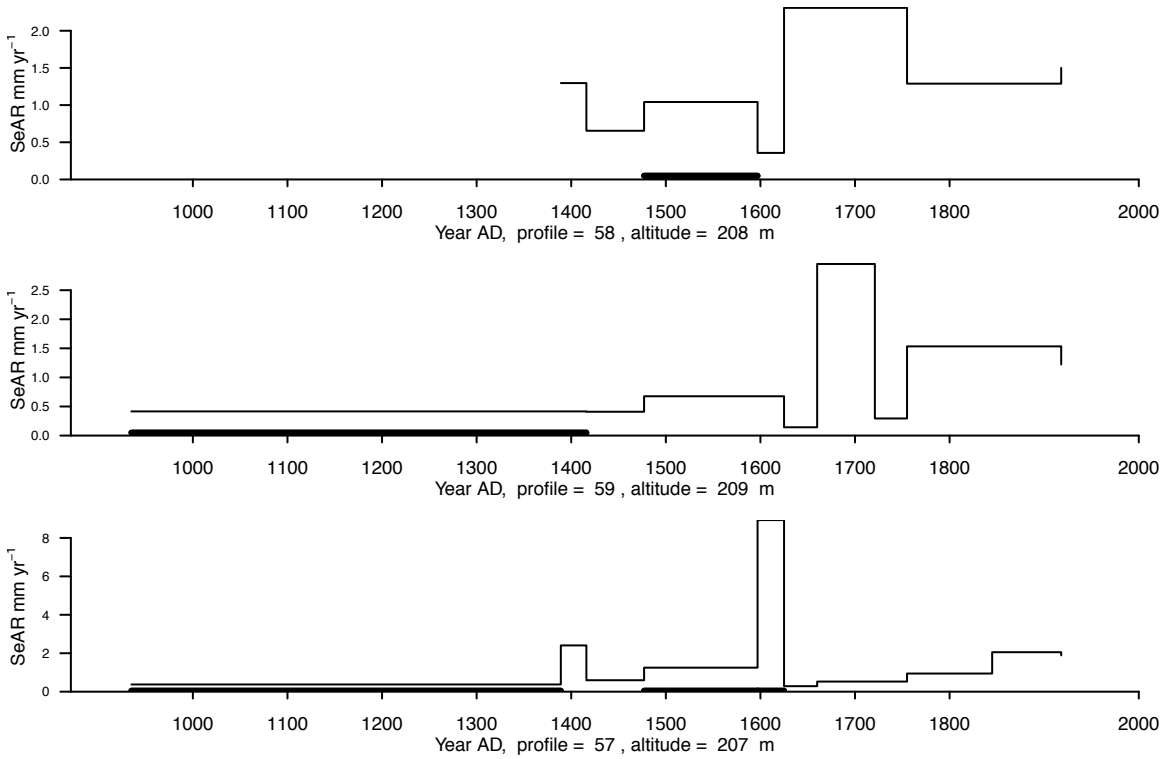

Figure D.30: Area 4 Profiles

References

Aberth, J. 2001. *From the brink of the apocalypse : confronting famine, war, plague*. Routledge, New York; London.

Adalsteinsson, S. 1981. *Sauþkindin landiþ of Þjóþin*. Bjallin, Reykjavik.

Adalsteinsson, S. 1990. Importance of Sheep in eary Icelandic Agriculture. *Acta Archaeologica*, **61**, 285–291.

Ahmad A, C. J. 1999. Photogrammetric Capabilities of the Kodak DC40, DCS420 and DCS460 Digital Cameras. *The Photogrammetric Record*, **16(94)**, 601–615.

Amorosi, T., Buckland, P., Dugmore, A., Ingimundarson, J. H., & McGovern, T. H. 1997. Raiding the landscape: Human impact in the Scandinavian North Atlantic. *Human Ecology*, **25**(3), 491–518.

Andrews, J. T., Caseldine, C., Weiner, N. J., & Hatton, J. 2001. Late Holocene (ca. 4 ka) marine and terrestrial environmental change in Reykjarfjordur, north Iceland: climate and/or settlement? *Journal of Quaternary Science*, **16(2)**, 133–143.

Arnalds, Ó. 1990. *Characterization and erosion of andisols in Iceland*. Ph.D. thesis, Texas A&M University, Unpublished PhD thesis.

Arnalds, O. 2000. The icelandic 'rofabard' soil erosion features. *Earth Surface Processes and Landforms*, **25**(1), 17–28. 276KJ Times Cited:14 Cited References Count:33.

Arnalds, O. 2004. Volcanic soils of Iceland. *Catena*, **56**(1-3), 3–20.

Arnalds, Ó. 2008. Soils of Iceland. *Jökull*, **58**, 409–421.

Arnalds, O., Thorarinsdottir, E., Metusalemsson, S., Jonsson, A., Gretarsson, E., & Arnason, A. 2001. *Soil erosion in Iceland*. Tech. rept. (English translation of original Icelandic publication from 1997.) Soil Conservation Service and Agricultural Research Institute, Reykjavik,Iceland 121 pp.

Bailey, M. 1996. Demographic decline in late medieval England: some thoughts on recent research. *Economic History Review*, **159(1)**, 1–19.

Baillie, M. G. L. 1991. Suck in and smear: two related chronological problems for the 90s. *Journal of Theoretical Archaeology*, **2**, 12–16.

Benedictow, O. J. 2004. *The Black Death 1346-1353: The complete History*. Woodbridge, Boydell Press.

Bergthorsson, P. 1985. Sensitivity of Icelandic Agriculture to Climatic Variations. *Climatic Change*, **7**(1), 111–127.

Blaauw, M. 2011. Out of tune: the dangers of aligning proxy archives. *Quaternary Science Reviews*, **in press**, 1–12.

Blaauw, M., Wohlfarth, B., Christen, J. A., Ampel, L., Veres, D., Hughen, K. A., Preusser, F., & Svensson, A. 2010. Were last glacial

climate events simultaneous between Greenland and France? A quantitative comparison using non-tuned chronologies. *Journal of Quaternary Science*, **25(3)**, 387–394.

Boeserup, E. 1965. *The conditions of agricultural growth: The Economics of Agrerian change under population pressure*. Allen & Unwin.

Bolender, D. J. 2006. *The Creation of a Propertied Landscape:Land Tenure and Agricultural Investment in Medieval Iceland*. Unpublished, Evanston, Illinois.

Bolton, J. 1996. *'The World Upside Down' Plague as an Agent of Economic and Social Change*. Stamford, Eng.: Watkins. edited by Mark Ormrod and Phillip Lindley. Page 202.

Bouguet, J. 2000. *Camera calibration toolbox for Matlab*. Tech. rept. http://www. vision.caltech.edu/bouguetj/calib doc/index.html.

Boygle, J. 1999. Variability of tephra in lake and catchment sediments, Svínavatn, Iceland. *Global and Planetary Change*, **21**, 129–149.

Bradwell, T., Dugmore, A. J., & Sugden, D. E. 2006. The Little Ice Age glacier maximum in Iceland and the North Atlantic Oscillation: evidence from Lambatungnajokull, southeast Iceland. *Boreas*, **35**(1), 61–80.

Brander, J. A., & Taylor, M. S. 1998. The simple economics of Easter Island: A Ricardo-Malthus model of renewable resource use. *American Economic Review*, **88**(1), 119–138.

Brunk, G. G. 2002. Why Do Societies Collapse? A Theory Based on Self-Organized Criticality. *Journal of Theoretical Politics*, **14(2)**, 195–230.

Brunsden, D., & Thornes, J. B. 1979. Landscape sensitivity and change. *Transactions of the Institute of British Geographers*, **NS5**, 463–484.

Caseldine, C., & Turney, C. 2010. The bigger picture: towards integrating palaeoclimate and environmental data with a history of societal change. *Journal of Quaternary Science*, **25(1)**, 88–93.

Casely, A. F. 2006. *Medieval climate change and settlement in Iceland*. Unpublished PhD, University of Edinburgh.

Casely, A. F., & Dugmore, A. 2004. Climate change and 'anomalous' glacier fluctuations: the southwest outlets of Mýrdalsjökull, Iceland. *Boreas*, **33(2)**, 108–122.

Casely, A. F., & Dugmore, A. J. 2007. Good for glaciers, bad for people? Archaeologically relevant climate models developed from reconstructions of glacier mass balance. *Journal of Archaeological Science*, **34**(11), 1763–1773.

Census, J. A. . I. 1703. *Kvikfénaðarskýrslur 1703: Skaftafellssýsla*. Tech. rept. Þjóðskjalasafn Íslands. Skjalasafn Rentukammers D1, kassi 3, örk 3.

Chandler, J., Fryer, J., & A, J. 2005. Metric capabilities of low-cost digital cameras for close range surfact measurement. *Photogrammetric Record*, **20(109)**, 12–26.

Chandler, J. 1999. Effective Application of automated digital photogrammetry for geomorpholgical research. *Earth Surface Processes and Landforms*, **24**, 51–63.

Chiverrell, R. C., Harvey, A. M., & Foster, G. C. 2007. Hillslope gullying in the Solway Firth - Morecambe Bay region, Great Britain: Responses to human impact and/or climatic deterioration? *Geomorphology*, **84**, 317–314.

Church, M., Dugmore, A., Mairs, K. A., Millard, A., Cook, G., Sveinbjarnardottir, G., Ascough, P., & Roucoux, K. H. 2007. Charcoal Production during the Norse and Early Medieval periods in Eyjafjallahreppur, Southern Iceland. *Radiocarbon*, **49 (2)**, 659–672.

Cohn, S. K. 2002. *The black death transformed : disease and culture in early Renaissance Europe*. London: Arnold.

Coombes, P., & Barber, K. 2005. Environmental determinism in Holocene research: causality or coincidence? *Area*, **37**(3), 303–311.

Costanza, R., Graumlich, L., & Steffen, W. L. 2007a. *Sustainability or collapse? : an integrated history and future of people on earth*. Dahlem Workshop report. Cambridge, Mass. ; London: MIT Press in cooperation with Dahlem University Press.

Costanza, R., Graumlich, L., Steffan, W., Crumley, C., Dearing, J., Hibbard, K., Leemans, R., Redman, C., & Schimel, D. 2007b. Sustainability or Collapse: What Can We Learn from Integrating the History of Humans and the Rest of Nature? *AMBIO: A Journal of the Human Environment*, **36(7)**, 522–527.

Cowgill, G. L. 1998. A comment on: A theory of Preindustrial Dynamics. *Current Anthropology*, **39(1)**, 122.

Crumley, C. L. 1994. *Historical ecology : cultural knowledge and changing landscapes*. School of American Research advanced seminar series. Santa Fe, N.M.: School of American Research Press.

Cutter, S. L., Golledge, R., & Graf, W. L. 2002. The big questions in geography. *Professional Geographer*, **54**(3), 305–317.

Dakos, V., van Nes, E., Donangelo, R., Fort, H., & Scheffer, M. 2010. Spatial correlation as leading indicator of catastrophic shifts. *Theoretical Ecology*, **3**, 163–174.

Danielsen, R. 1995. *Norway : a history from the Vikings to our own times*. Oslo: Scandinavian University Press.

Dawson, A., Elliott, L., Noone, S., Hickey, K., Holt, T., Wadhams, P., & Foster, I. 2004. Historical storminess and climate 'see-saws' in North Atlantic region. *Marine Geology*, **210**(1-4), 247–259.

Dawson, A. G., Hickey, K., Mayewski, P. A., & Nesje, A. 2007. Greenland (GISP2) ice core and historical indicators of complex North Atlantic climate changes during the fourteenth century. *Holocene*, **17**(4), 427–434.

deMenocal, P. B. 2001. Cultural Responses to Climate Change During the Late Holocene. *Science*, **292**, 667–673.

Denevan, W. M. 1992. The Pristine Myth: The Landscape of the Americas in 1492. *Annals of the Association of American Geographers*, **82(3)**, 369–385.

Diamond, J., & Robinson, J. 2010. *Natural experiments of history*. Harvard University Press.

Diamond, J. M. 2005. *Collapse : how societies choose to fail or survive*. London: Allen Lane. Jared Diamond. ill., maps ; 24 cm. Includes bibliographical references and index.

Dugmore, A., Newton, A., Larsen, G., & Cook, G. 2000. Tephrochronology, Environmental Change and the Norse Settlement of Iceland. *Environmental Archaeology*, **5**, 21–34.

Dugmore, A., Church, M., Mairs, K. A., McGovern, T. H., Newton, A., & Sveinbjarnardottir, G. 2006. An Over-Optimistic Pioneer Fringe? Environmental Perpsectives on Medieval Settlement and Abandonment in Þrsmörk, South Iceland. *Pages 335–345 of:* Arneborg, J., & Grønnow, B. (eds), *Dynamics of Northern Societies: Proceedings of the SILA/NABO Conference on Arctic and North Atlantic Archaeology Copenhagen.* Publications from the National Museum, Studies in Archaeology and History. PNN.

Dugmore, A. J. 1987. *Holocene glacial fluctuations around Eyjafjallajökull, South Iceland*. Ph.D. thesis, University of Aberdeen.

Dugmore, A. J., & Buckland, P. 1991. Tephrochronology and late holocene soil erosion in Southern Iceland. *Pages 147–159 of:* Maizels, J. K., & Caseldine, C. (eds), *Environmental Change in Iceland: Past and Present*. Dordrecht ; London: Kluwer Academic.

Dugmore, A. J., Larsen, G., & Newton, A. J. 1995a. Seven Tephra Isochrones in Scotland. *Holocene*, **5(3)**, 257–266.

Dugmore, A. J., Church, M. J., Mairs, K. A., McGovern, T. H., Perdikaris, S., & Vesteinsson, O. 2007a. Abandoned farms, volcanic impacts, and woodland management: Revisiting Þjorsardalur, the "Pompeii of Iceland". *Arctic Anthropology*, **44**(1), 1–11.

Dugmore, A. J., Borthwick, D. M., Church, M. J., Dawson, A., Edwards, K. J., Keller, C., Mayewski, P., McGovern, T. H., Mairs, K. A., & Sveinbjarnardottir, G. 2007b. The role of climate in settlement and landscape change in the north Atlantic islands: An assessment of cumulative deviations in high-resolution proxy climate records. *Human Ecology*, **35**(2), 169–178.

Dugmore, A. J., Gisladottir, G., Simpson, I. A., & Newton, A. 2009. Conceptual models of 1200 years of Icelandic Soil Erosion Reconstructed Using Tephrochronology. *Journal of the North Atlantic*, **2**, 1–18.

Dugmore, A., & Erskine, C. C. 1994. *Environmental Change in Iceland*. Munchener Geographische Abhandlungen. Chap. Local and Regional Patterns of Soil Erosion in Southern Iceland, pages 63–78.

Dugmore, A., Cook, G., Shore, J., Newton, A., Edwards, K., & Larsen, G. 1995b. Radiocarbon dating tephra layers in Britain and Iceland. *Radiocarbon*, **37**(2), 379–388. 15th International Radiocarbon Conference, GLASGOW, SCOTLAND, AUG 15-19, 1994.

Dugmore, A., Larsen, L., , & Newton, A. 2004. *Tools for Constructing Chronologies*. Springer-Verlag, London. Chap. Tephrochronology and its application to Late Quaternary Environmental Reconstruction, with Special Reference to the North Atlantic Islands, pages 173–188.

Dull, R, A., Nevle, R, J., Woods, W, I., Bird, D, K., Avnery, S., & Denevan, W. 2010. The Columbian Encounter and the Little Ice Age: Abrupt Land Use Change, Fire, and Greenhouse Forcing. *Annals of the Association of American Geographers*, **100 (4)**, 755–771.

Duncan, C. J., & Scott, S. 2005. What caused the Black Death? *Postgraduate Medical Journal*, **81**(955), 315–320.

Edwards, K. J., Dugmore, A. J., & Blackford, J. J. 2004. Vegetational response to tephra deposition and land-use change in Iceland: a modern

analogue and multiple working hypothesis approach to tephropalynology. *Polar Record*, **40**(213), 113–120.

Einarsson, E. H., Larsen, G., & Thórarinsson, S. 1980. The Sólheimar tephra layer and the Katla eruption of c 1357. *Acta Naturalia Islandica*, **28**, 1–24.

Einarsson, M. Á. 1984. *World Survey of Climatology: 15: Climates of the Oceans*. Elsevier, Amsterdam. Chap. Climate of Iceland, pages 673–697.

Erlendsson, E., & Edwards, K. 2009. The timing and causes of the final pre-settlement expansion of Betula pubescens in Iceland. *The Holocene*, **19(7)**, 1083–1091.

Erlendsson, E., Edwards, K. J., & Buckland, P. C. 2009. Vegetational response to human colonisation of the coastal and volcanic environments of Ketilsstaðir, southern Iceland. *Quaternary Research*, **72**(2), 174 – 187.

Gathorne-Hardy, Freddy, J., Erlendsson, E., Langdon, Peter, G., & Edwards, Kevin, J. 2009. Lake sediment evidence for late Holocene climate change and landscape erosion in western Iceland. *Journal of Paleoliminology*, **42**, 413–426.

Geirsdottir, A., Miller, G. H., Thordarson, T., & Olafsdottir, K. B. 2009. A 2000 year record of climate variations reconstructed from Haukadalsvatn, West Iceland. *Journal of Paleolimnology*, **41**, 95–115.

Gísladóttir, G. 1998. *Environmental characterization and change in southwestern Iceland*. Ph.D. thesis, Department of Physical Geography, Stockholm., Disertation Series 10, Stockholm, Sweden.

Gísladóttir, G. 2001. *Land Degradation*. Kluwer Academic Publishers, Dordrecht, The Netherlands. Chap. Ecological disturbance and soil erosion on grazing land in southwest Iceland, pages 109–126.

Gissel, S., Jutikkala, E., Osterberg, E., Sandes, J., & Teitsson, B. 1981. *Desertion and Land Colonization in the Nordic Countries c. 1300-1600*. Stockholm, Sweden: Almqvist & Wiskell International.

Grattan, J., Rabartin, R., Self, S., & Thordarson, T. 1995. Volcanic air pollution and mortality in France. *Comptes rendus. Geoscience*, **337(7)**, 641–651.

Gronvöld, K., Oskarsson, N., Johnsen, S. J., Clausen, H., Hammer, C., Bond, G., & Bard, E. 1995. Ash layers from Iceland in the Greenland GRIP ice core correlated with oceanic and land based sediments. *Earth and Planetary Science Letters*, **54**, 238–246.

Grove, J. M. 2001. The initiation of the "Little Ice Age" in regions round the North Atlantic. *Climatic Change*, **48**(1), 53–82.

Grove, J. M. 2004. *Little ice ages : ancient and modern*. 2nd edn. Routledge studies in physical geography and environment ; 5. London: Routledge.

Gummer, B. 2009. *The Scourging Angel: The Black Death in the British Isles*. The Bodley Head Ltd.

Gunderson, L. H., & Holling, C. S. 2002. *Panarchy : understanding transformations in human and natural systems*. Washington, D.C. ; London: Island Press. edited by Lance H. Gunderson, C. S. Holling.

Gustavsson, G., Lemdahl, G., & Gaillard, M.-J. 2009. Abrupt forest ecosystem change in SW Sweden during the late Holocene. *The Holocene*, **19**, 691–702.

Haensch, S., Bianucci, R., Signoli, M., Rajerison, M., Schultz, M., Kacki, S., Vermunt, M., Weston, D. A., Hurst, D., Achtman, M., Carniel, E., & Bramanti, B. 2010. Distinct Clones of *Yersinia pestis* Caused the Black Death. *PLoS Pathog*, **6**(10), e1001134.

Hall, V. A. 2003. Vegetation history of mid- to western Ireland in the 2nd millennium AD; fresh evidence from tephra-dated palynological investigations. *Vegetation History and Archaeobotany*, **12**(1), 7–17.

Hallsdóttir, M. 1987. Pollen analytical studies of human influence on vegetation in relation to the Landnám tephra layerr in southwestern Iceland. *Lundqua Thesis*, **18**, 1–45.

Haraldsson, H. V., & Ólafsdóttir, R. 2006. A novel modelling approach for evaluating the preindustrial natural carrying capacity of human population in Iceland. *Science of the Total Environment*, **372**(1), 109–119.

Hatcher, J. 1977. *Plague, population, and the English economy, 1348-1530*. Macmillan (London).

Hays, J. 2005. *Epidemics and pandemics: their impacts on human history*. ABC-CLIO Inc.

Herlihy, D. 1997. *The Black Death and the Transformation of the West*. Cambridge, Massachusetts, and London, England: Harvard University Press.

Hunt, J., & Hill, P. G. 1993. Tephra geochemistry: a discussion of some persistent analytical problems. *Holocene*, **3(3)**, 271–278.

Jackson, M., Oskarsson, N., Tronnes, R., McManus, J., Oppo, D., Gronvöld, K., Hart, S., & Sachs, J. 2005. Holocene loess deposition in Iceland: Evidence for millennial-scale atmosphere-ocean coupling in the North Atlantic. *Geology*, **33**(6), 509–512.

Jakobsson, S. P. 1979. Petrology of Recent basalts of the Eastern Volcanic Zone, Iceland. *Acta Naturalia Islandica*, **26**, 1–103.

Jennings, A., Hagen, S., Harðardóttir, J., Stein, R., Ogilvie, A., & Jónsdóttir, I. 2001. Oceanographic Change and Terrestrial Human Impacts in a Post A.D. 1400 Sediment Record from the Southwest Iceland Shelf. *Climatic Change*, **48**, 83–100.

Jiang, H., Eirksson, J., Schulz, M., Knudsen, K.-L., & Seidenkrantz, M.-S. 2005. Evidence for solar forcing of sea-surface temperature on the North Icelandic Shelf during the late Holocene. *Geology*, **33**(1), 73–76.

Júlísson, Á, D. 1995. *Bonder i pestens tid; landbrug godsrift og social konflikt i smenmiddelalderens islandske bondesamfund [Farmers during epidemic times]*. Ph.D. thesis, University of Copenhagen. 597 p.

Kaplan, J. O., Krumhardt, K. M., & Zimmermann, N. 2009. The prehistoric and preindustrial deforestation of Europe. *Quaternary Science Reviews*, **28**, 3016–3034.

Karlsson, G. 1996. Plague without rats: The case of 15th-century Iceland. *Journal of Medieval History*, **22**(3), 263–284.

Karlsson, G. 2000. *Iceland's 1100 years : the history of a marginal society*. London: C. Hurst.

Kates, R. W., Clark, W. C., Corell, R., Hall, J. M., Jaeger, C. C., Lowe, I., McCarthy, J. J., Schellnhuber, H. J., Bolin, B., Dickson, N. M., Faucheux, S., Gallopin, G. C., Grübler, A., Huntley, B., Jäger, J., Jodha, N. S., Kasperson, R. E.,

Mabogunje, A., Matson, P., Mooney, H., III, B. M., O'Riordan, T., & Svedin, U. 2001. Sustainability Science. *Science*, **292(5517)**, 641–642.

Kershaw, I. 1973. The Great Famine and agrarian crisis in England 1315-1322. *Past and Present*, **59**, 3–50.

Kirch, P. V. 2007. Hawaii as a model system for human ecodynamics. *American Anthropologist*, **109**(1), 8–26.

Kirkbride, M., & Dugmore, A. 2006. Respones of mountain ice caps in central Iceland to Holocene climate change. *Quaternary Science Reviews*, **25(13-14)**, 1697–1707.

Kirkbride, M. P., & Dugmore, A. J. 2008. Two millennia of glacier advances from southern Iceland dated by tephrochronology. *Quaternary Research*, **70**(3), 398 – 411.

Kirkbride, M. P., & Dugmore, A. 2001. Timing and significance of mid-Holocene glacier advances in northern and central Iceland. *Journal of Quaternary Science*, **16**, 145–153.

Kirkbride, M. P., & Dugmore, A. J. 2005. Late Holocene solifluction history reconstructed using tephrochronology. *Pages 145–155 of:* HARMS, C. & MURTON, J. B. (ed), *Cryospheric Systems: Glaciers and Permafrost*, vol. 242. Geological Society, London.

Kitsikopoulos, H. 2002. The Impact of the Black Death on Peasant Economy in England, 1350-1500. *The Journal of Peasant Studies*, **29**, 71–90.

Lagerås, P. 2007. *The Ecology of Expansion and Abandonment: Medieval and Post-Medieval Land-use and Settlement Dynamics in a Landscape Perspective*. Stockholm: Riksantikvarieämbetet.

Lárasson, B. 1967. *The Old Icelandic Land Registers*. C.W.K. Gleerup.

Larsen, G. 1984. Recent volcanic history of the Veidivötn fissure swarm, southern Iceland - an approach to volcanic risk assessment. *Journal of Volcanology and Geothermal Research*, **22**, 33–58.

Larsen, G., Gudmundsson, Magnus, T., & Bjornsson, H. 1998. Eight centuries of periodic volcanism at the center of the Iceland hotspot revealed by glacier tephrostratigraphy. *Geology*, **26**, 943–946.

Larsen, G. 2000. Holocene eruptions within the Katla volcanic system, south Iceland: Characteristics and environmental impact. *Jökull*, **49**, 1–28.

Larsen, G., & Eiríksson, J. 2008a. Late Quaternary terrestrial tephrochronology of Iceland - frequency of explosive eruotions, type and volume of tephra deposits. *Journal of Quaternary Science*, **23(2)**, 109–120.

Larsen, G., & Eiríksson, J. 2008b. Holocene tephra archives and tephrochronology in Iceland - a brief overview. *Jökull*, **58**, 229–250.

Larsen, G., Dugmore, A., & Newton, A. 1999. Geochemistry of historical-age silicic tephras of Iceland. *The Holocene*, **9, 4**, 463–471.

Larsen, G., Newton, A., Dugmore, A., & Vilmundardottir, E. 2001. Geochemistry, dispersal, volumes and chronology of Holocene silicic tephra layers from the Katla volcanic system, Iceland. *Journal of Quaternary Science*, **16(2)**, 119–132.

Lawson, I. T., Gathorne-Hardy, F. J., Church, M. J., Newton, A. J., Edwards, K. J., Dugmore, A. J., & Einarsson, A. 2007. Environmental impacts of the Norse settlement: palaeoenvironmental data from Mývatnssveit, northern Iceland. *Boreas*, **36**(1), 1–19.

Lee, R. 1987. Population dynamics of humans and other animals. *Demography*, **24**, 443–465.

LMI, T. I. G. I. 1993. *Digital vegetation index map of Iceland*. Tech. rept. The Icelandic Geodetic Survey, Reykjavík, Iceland.

Lovell, W. G. 1992. "Heavy shadows and black night": Disease and depopulation in Colonial Spanish America. *Annals of the Association of American Geographers*, **82(3)**, 426–443.

Lowe, D, J. 2011. Tephrochronology and its application: A review. *Quaternary Geochronology*, **6(2)**, 107–153.

Mairs, K. A., Church, M., Dugmore, A., & Sveinbjarnardottir, G. 2006. Degrees of Success: Evaluating the Environmental Impacts of Long Term Settlement in South Iceland. *Pages 365–373 of:* Arneborg, J., & Grønnow, B. (eds), *Dynamics of Northern Societies: Proceedings of the SILA/NABO Conference on Arctic and North Atlantic Archaeology Copenhagen.* Publications from the National Museum, Studies in Archaeology and History. PNN.

Mann, M. E., Zhang, Z., Rutherford, S., Bradley, R. S., Hughes, Malcom, K., Shindell, D., Ammann, C., Faluvegi, G., & Ni, F. 2009. Global Signatures and Dynamical Origins of the Little Ice Age and Medieval Climate Anomaly. *Science*, **326**, 1256–1260.

Marlon, J. R., Bartlein, P. J., Carcaillet, C., Gavin, D. G., Harrison, S. P., Higuera, P. E., Joos, F., Power, M. J., & Prentice, I. C. 2008. Climate and human influences on global biomass burning over the past two millennia. *Nature Geoscience*, **1**, 697–702.

Massé, G., Rowland, Steven, J., Scicre, M.-A., Jacob, J., Jansen, E., & Belt, S. T. 2008. Abrupt climate changes for Iceland during the last millennium: Evidence from high resolution sea ice reconstructions. *Earth and Planetary Science Letters*, **269**, 565–569.

McGovern, T. H., Vesteinsson, O., Fridriksson, A., Church, M., Lawson, I., Simpson, I. A., Einarsson, A., Dugmore, A., Cook, G., Perdikaris, S., Edwards, K. J., Thomson, A. M., Adderley, W. P., Newton, A., Lucas, G., Edvardsson, R., Aldred, O., & Dunbar, E. 2007. Landscapes of settlement in Northern Iceland: Historical ecology of human impact and climate fluctuation on the millennial scale. *American Anthropologist*, **109**(1), 27–51.

McKinzey, K. M., Olafsdottir, R., & Dugmore, A. J. 2005. Perception, history, and science: coherence or disparity in the timing of the Little Ice Age maximum in southeast Iceland? *Polar Record*, **41**(219), 319–334.

Meeker, L. D., & Mayewski, P. A. 2002. A 1400-year high-resolution record of atmospheric circulation over the North Atlantic and Asia. *Holocene*, **12**(3), 257–266.

Naeser, C. W., Briggs, N. D., Obradovich, J. D., & A., I. G. 1981. Geochronology of Quaternary Tephra Deposits. *Pages 13–47 of:* S, S., & J., S. R. S. (eds), *Tephra Studies*. C, vol. Proceedings of the NATO Advanced study Institute 'Tephra studies as a Tool in Quaternary Research', no. 75.

Nevle, R. J., & Bird, Dennis, K. 2008. Effects of syn-pandemic fire reduction and reforestation in the tropical Americas on atmospheric CO2 during European conquest. *Palaeogeography Palaeoclimatology Palaeoecology*,

264(1-2), 25–38.

Newton, A., Dugmore, A., & Gittings, B. 2007. Tephrabase: tephrochronology and the development of a centralised European database. *Journal of Quaternary Science*, **22(7)**, 737–743.

Ogilvie, A. 1992. *Climate since A.D. 1500.* London, Routledge. Chap. Doccumentary evidence for changes in the climate of Iceland, AD 1500 to 1800, pages 92–117.

Ogilvie, A. E. J. 1984. The Past Climate and Sea-Ice Record from Iceland, .1. Data to Ad 1780. *Climatic Change*, **6**(2), 131–152.

Ogilvie, A. E. J. 1986. The climate of Iceland, 1701-1784. *Jökull*, **36**, 57–73.

Ogilvie, A. E. J., & Jonsson, T. 2001. "Little Ice Age" research: A perspective from Iceland. *Climatic Change*, **48**, 9–52.

Óladóttir, B, A., Sigmarsson, O., Larsen, G., & Devidal, J.-L. 2011a. Provenenance of basaltic tephra from Vatnajokull subglacial volcanos, Iceland, as determined by major- and trace-element analyses. *The Holocene*, **in press**.

Óladóttir, B., Larsen, G., Thordarson, T., & O., S. 2005. The Katla volcano S-Iceland: Holocene tephra stratigraphy and eruption frequency. *Jökull*, **55**, 53–74.

Óladóttir, B., O., S., Larsen, G., & Thordarson, T. 2008. Katla volcano, Iceland: magma composition, dynamics and eruption frequency as recorded by Holocene tephra layers. *Bulletin of Volcanology*, **70**, 475–493.

Óladóttir, B., Larsen, G., & Sigmarsson, O. 2011b. Holocene volcanic activity at Grimsvötn, Bardarbunga and Kverkfjoll subglacial centres beneath Vatnajokull, Iceland. *Bulletin of Volcanology*, **in press**.

Óladóttir, B. A., Thordarson, T., Larsen, G., & Sigmarsson, O. 2007. Survival of the Myrdalsjokull ice cap through the Holocene thermal maximum: evidence from sulphur contents in Katla tephra layers (Iceland) from the last 8400 years. *Annals of Glaciology*, **45**, 183–188(6).

Ólafsdóttir, R. 2001. *Land degradation and climate in Iceland: a spatial and temporal assessment.* Meddelanden fran Lunds Universtets Geografiska Insitutioner. Avhandlingar 143. Lund. 128pp.

Olafsdóttir, R., & Guómundsson, H. J. 2002. Holocene land degradation and climatic change in northeastern Iceland. *Holocene*, **12**(2), 159–167.

Ólafsdóttir, R., P, S., & H, H. 2001. Simulating Icelandic vegetation cover during the Holocene. Implications for long-term land degradation. *Geografiska Annaler*, **83A:4**, 203–215.

Oldfield, F., & Alverson, K. 2003. The societal relevance of Paleoenvironmental Research. *Pages 143–62 of:* Averson, K. D., Bradley, R., & Pederson, T. F. (eds), *Paleoclimate, global change and the future.* Springer.

O'Sullivan, P. 2008. The 'collapse' of civilizations: what palaeoenvironmental reconstruction cannot tell us, but anthropology can. *The Holocene*, **18**(1), 45–55.

Parry, M, L. 1981. Climatic change and the agricultural frontier: a research strategy. *In:* Wigley, T. M. L., Ingram, M. J., & Farmer, G. (eds), *Climate and history : studies in past climates and their impact on man.* Cambridge: Cambridge University Press.

Patterson, W. P., Dietrich, Kristin, A., Holmden, C., & Andrews,

J. T. 2010. Two millennia of North Atlantic seasonality and implications for Norse colonies. *Proceedings of the National Academy of Sciences of the United States of America*, **107(12)**, 5306–5310.

Phillips, J. D. 2003. Sources of nonlinearity and complexity in geomorphic systems. *Progress in Physical Geography*, **27(1)**, 1–23.

Pike, R. 2000. Geomorphometry: diversity in quantitative surface analysis. *Progress in Physical Geography*, **24(1)**, 1–20.

Platt, C. 1996. *King Death : The Black Death and is aftermath in late-medieval England*. 1st edn. Guildford: UCL Press Limited.

Poos, L. R. 1991. *A rural society after the Black Death : Essex, 1350-1525*. Cambridge studies in population, economy and society in past time ; 18. Cambridge: Cambridge University Press.

Ran, L., Jiang, H., Knudsen, K. L., & Eiríksson, J. 2011. Diatom-based reconstruction of palaeoceanographic changes on the North Icelandic shelf during the last millennium. *Palaeogeography, Palaeoclimatology, Palaeoecology*, **302**(1-2), 109 – 119.

Reed, S. J. B. 1993. *Electronic Microprobe Analysis and Scanning Electronic Microscopy in Geology*. Cambridge University Press, Cambridge.

Rieke-Zapp, D. H., Rosenbauer, R., & Schlunegger, F. 2009. A Photogrammetric Surveying Method for field applications. *The Photogrammetric Record*, **24(125)**, 5–22.

Ruddiman, W. F. 2003. The anthropogenic greenhouse era began thousands of years ago. *Climatic Change*, **61(3)**, 261–293.

Ruddiman, W. F. 2005. *Plows, plagues, and petroleum : how humans took control of climate*. Princeton, N.J. ; Oxford: Princeton University Press.

Ruddiman, W. F., & Ellis, E. C. 2009. Effect of per-capita land use change on Holocene forest clearance and CO2 emissions. *Quaternary Science Reviews*, **28**, 3011–3015.

Russell, J. C. 1948. *British Medieval Population*. Albuquerque: University of New Mexico Press.

Scheffer, M. J., Bascompte, W., Brock, V., Brovkin, S., Carpenter, V., Dakos, H., Held, EH van Nes, M., Rietkerk, & Sugihara, G. 2009. Early warning signals for critical transitions. *Nature*, **461**, 53–59.

Schumm, S. A. 1979. Geomorphic thresholds: the concept and its applications. *Transactions of the Institute of British Geographers*, **NS4**, 485–515.

Simon, J. 1996. *The Ultimate Resource II*. Princeton University Press.

Simpson, I. A., Dugmore, A. J., Thomson, A., & Vesteinsson, O. 2001. Crossing the thresholds: human ecology and historical patterns of landscape degradation. *Catena*, **42**(2-4), 175–192.

Simpson, I. A., Adderley, W. P., Gumundsson, G., Hallsdottir, M., Sigurgeirsson, M. A., & Snaesdottir, M. 2002. Soil limitations to agrarian land production in premodern Iceland. *Human Ecology*, **30**(4), 423–443.

Simpson, I. A., Guomundsson, G., Thomson, A. M., & Cluett, J. 2004. Assessing the role of winter grazing in historic land degradation, Myvatnssveit, northeast Iceland. *Geoarchaeology-an International Journal*, **19**(5), 471–502.

Smith, K. T., & Dugmore, A. J. 2006. Jökulhlaups circa Landnam: Mid- to

late first millennium AD floods in South Iceland and their implications for landscapes of settlement. *Geografiska Annaler Series a-Physical Geography*, **88A**(2), 165–176.

Spinage, C. A. 2003. *Cattle Plague: A History*. Kluwer Academic, New York.

Steinthorsson, S. 1977. Tephra Layers in a Drill Core from the Vatnajökull Ice cap. *Jökull*, **27**, 2–27.

Sveinbjarnardottir, G., Erlendsson, E., Vickers, K., H., M. T., Milek, Karen, B., Edwards, K. J., A, S. I., & G, C. 2007. The palaeoecology of a high status Icelandic farm. *Environmental Archaeology*, **12**(2), 187–206.

Thomson, A. 2003. *A modelling approach to farm management and vegetation degradation in pre-modern Iceland*. PhD, Unpublished, University of Stirling.

Thomson, Amanda, M., & Simpson, I. A. 2007. Modeling Historic Rangeland Management and Grazing Pressures in Landscapes of Settlement. *Human Ecology*, **35**, 151–168.

Thórarinsson. 1975. *Katla og annáll Kötlugosa*. Árbók Ferðafélags Íslands.

Thórarinsson, S. 1944. Tefrokronoliska studier pa Island (Tephrochronological studies in Iceland). *Geografiska Annaler*, **26**, 1–217.

Thórarinsson, S. 1958. *The Öræfajökull eruption of 1362*. Vol. II. Acta Naturalia islandica.

Thórarinsson, S. 1967. *The Eruptions of Hekla in historical times. The Eruption of Hekla 1947-1948*. 1.

Thórarinsson, S. 1961. Population Changes in Iceland. *Geographical Review*, **51(4)**, 519–533.

Thordarson, T., & Self, S. 1993. The Laki (Skaftár Fires) and Grímsvötn eruptions in 1783-1785. *Bulletin of Volcanology*, **55**, 233–263.

Thordarson, T., & Self, S. 2003. Atmospheric and environmental effects of the 1783-1784 Laki eruption: a review and reassessment. *Journal of Geophysical Research: Atmospheres*, **108(D1)**, 4011.

Thoroddsen, Þ. 1914. Islands Klima i Oldtiden. *Geografisk Tidskrift*, **22**, 204–216.

Twigg, G. 1984. *The Black Death : a biological reappraisal*. Batsford.

van Hoof, T. B., Bunnik, F. P. M., Waucomont, J. G. M., Kurschner, W. M., & Visscher, H. 2006. Forest re-growth on medieval farmland after the Black Death pandemic - Implications for atmospheric CO2 levels. *Palaeogeography Palaeoclimatology Palaeoecology*, **237**(2-4), 396–411.

Vasey, D. E. 1996. Population regulation, ecology, and political economy in preindustrial Iceland. *American Ethnologist*, **23**(2), 366–392.

Vesteinsson, O., McGovern, T. H., & Keller, C. 2002. Enduring impacts: social and environmental aspects of Viking Age settlement in Iceland and Greenland. *Archaeologica Islandica*, **2**, 98–136.

Vinther, B. M., Clausen, H., B., Johnsen, S. J., Rasmussen, S. O., Anderson, K. K. andBuchardt, S. L., Dahl-Jensen, D., Seierstad, I. K., Siggaard-Andereson, M. L., Steffensen, J. P., Svensson, A., Olsen, J., & Heinemeier, J. 2006. A synchronized dating of three Greenland ice cores throughout the Holocene. *Journal of Geophysical Reseach*, **111**, 1–11.

Wackrow, R., Chandler, J. H., & Bryan, P. 2007. Geometric consistency

and stability of consumer-grade digital cameras for accurate spatial measurement. *The Photogrammetric Record*, **22(118)**, 121–134.

Wada, R. 1985. The distinctive properties of andosols. *Advances in Soil Sciences*, **2**, 173–229.

Walker, B., S, H. C., R, C. S., & A, K. 2004. Resilience, adaptability and transformability in social-ecological systems. *Ecology and Society*, **9(2)**, [online].

Weiss, H., Courty, M. A., Wetterstrom, W., Guichard, F., Senoir, L., Meadow, R., & Curnow, A. 1993. The Genesis and Collapse of Third Millennium North Mesopotamian Civilization. *Science*, **261(5124)**, 995–1004.

Westgate, J. A., & Gorton, M. P. 1981. Correlation techniques in tephra studies. *Pages 73–94 of:* Sefl, S., & Sparks, R. (eds), *Tephra Studies*. C, vol. Proceedings of the NATO Advanced study Institute 'Tephra studies as a Tool in Quaternary Research', no. 75.

Wöll, C. 2008. *Treeline of mountain birch (Betula pubescens Ehrh.) in Iceland and its relationship to temperature*. M.Phil. thesis, Technical University Dresden, Department of Forestry, diploma thesis in Forest Botany.

Wood, J. W. 1998. A theory of preindustrial population dynamics - Demography, economy, and well-being in malthusian systems. *Current Anthropology*, **39**(1), 99–135.

Wrigley, T., & Schofield, R. S. 1981. *The population history of England, 1541-1871: a reconstruction*. Harvard University Press (Cambridge, Mass).

Yeloff, D., & van Geel, B. 2007. Abandonment of farmland and vegetation succession following the Eurasian plague pandemic of AD 1347-52. *Journal of Biogeography*, **34**(4), 575–582.

Yeloff, D., van Geel, B., Broekens, P., Bakker, J., & Mauquoy, D. 2007. Mid- to late-Holocene vegetation and land-use history in the Hadrian's Wall region of northern England: the record from Butterburn Flow. *Holocene*, **17**(4), 527–538.

Zielinski, G. A., Germani, M. S., Larsen, G., Baillie, M. G., Whitlow, S., Twickler, M. S., & Taylor, K. 1995. Evidence of the Eldgjá (Iceland) eruption in the GISP2 Greenland ice core: relationship to eruption proceses and climatic conditions in the tenth century. *The Holocene*, **5(2)**, 129–140.

THE UNIVERSITY *of* EDINBURGH